

Characterization of Three-phase Flow and WAG Injection in Oil Reservoirs

By:

HAMIDREZA SHAHVERDI

BSc., MSc.

Submitted for the Degree of Doctor of Philosophy
in Petroleum Engineering

Department of Petroleum Engineering
Heriot-Watt University
Edinburgh, UK

February 2012

This copy of the thesis has been supplied on condition that anyone who consults it is understood to recognise that the copyright rests with its author and that no quotation from the thesis and no information derived from it may be published without prior written consent of the author or the University (as may be appropriate)

Abstract

Large quantities of oil usually remain in oil reservoirs after conventional water floods. A significant part of this remaining oil can still be economically recovered by Water-Alternating-Gas (WAG) injection. WAG injection involves drainage and imbibition processes taking place sequentially, hence the numerical simulation of the WAG process requires reliable knowledge of three-phase relative permeability (k_r) accounting for cyclic hysteresis effects.

In this study, the results of a series of unsteady-state two-phase displacements and WAG coreflood experiments were employed to investigate the behaviour of three-phase k_r and hysteresis effects in the WAG process. The experiments were carried out on two different cores with different characteristics and wettability conditions, using a low IFT (interfacial tension) gas–oil system.

The first part of this study, evaluates the current approach used in the oil industry for simulation of the WAG process, in which the two-phase relative permeability data are employed to generate three-phase k_r values using correlations (e.g. Stone, Baker). The performance of each of the existing three-phase relative permeability models was assessed against the experimental data. The results showed that choosing inappropriate three-phase k_r model in simulation of the WAG experiments can lead to large errors in prediction of fluid production and differential pressure. While some models perform better than others, all of the three-phase k_r models examined in this study failed to adequately predict the fluid production behaviour observed in the experiments. The continued production of oil after the breakthrough of the gas, which was one of the features of gas and WAG injection experiments at low gas-oil IFT, was not captured with these models.

The second aim of this research was to develop a method for obtaining the values of three-phase relative permeabilities directly from WAG core flood experiments. For this purpose, a new history matching method was devised based on a Genetic Algorithm to estimate three-phase k_r from unsteady-state coreflood experiments. Based on this methodology, a three-phase coreflood optimizer was developed that generates best k_r values by matching the experimentally obtained production and pressure data. First, the

integrity of the developed software was successfully verified by using two sets of experimental three-phase k_r data published in the literature. Then, the program was used to determine three-phase relative permeability of various cycles of the WAG experiments performed at different wettability conditions.

Two key parameters affecting the WAG performance, including the hysteresis phenomena occurring between k_r of the different WAG cycles and the impact of wettability of the rock, have been investigated. The data have been used to evaluate the existing hysteresis models published in the literature. Some of the shortcomings associated with the existing methods have been revealed and discussed.

In the latter part of the thesis, a new methodology is proposed for modelling of three-phase relative permeability for WAG injection. This approach addresses the hysteresis effects in the three-phase k_r taking place during the WAG process and attempts to reduce the inadequacies observed in the existing models. The integrity of this technique has been validated against the three-phase k_r data obtained from our WAG experiments.

تقدیم بہ، محترمہ عزیزم

Dedicated to my dear wife

Acknowledgments

I would like to express the earnest gratitude and respect to my dear supervisor Professor Mehran Sohrabi who provided the opportunity, financial support, an outstanding technical guidance which all were integral to this thesis. My second supervisor Dr. Mahmoud Jamiolahmady is gratefully acknowledged for his invaluable ideas and guidance during this research. My special thanks go to Professor Dabir Tehrani for his prominent practical comments and constructive assistance throughout this project. Much appreciation to Professor Ken Sorbie and Professor Willam Rossen for consenting to be the examiners. I also owe a great deal of debt to my dear friends Mr Mobeen Fatemi and Mr Shaun Ireland for conducting experimental work of the WAG project.

I am sincerely in debt to my dear friend Dr Masoud Riazi for encouraging me to apply for PhD at Heriot-Watt University and thanks for supporting me and my family once we arrived in Edinburgh. Special thanks go to my dear friends Norida Kechut, Olufemi Saliu, Hamidreza Hamdi, Alireza Emadi, Alireza Kazemi, Ali Maleki, Shahriar Bijani, Yousef Rafie, Hamid Bazargan and Seyed Mohammad Sadegh Emamian for the enjoyable and memorable time we had in Edinburgh.

Last but not the least, infinite reverence and gratitude go to my lovely wife for her endless patients and kind-heartedness during our life and I always feel so lucky being with her, also I wish to greatly acknowledge my parents for spending their life for me and bringing me up to this stage. I will never forget them.

Publications

Journal Papers:

1. Shahverdi, H., Sohrabi, M., Fatemi, M., and Jamiolahmady, M., 2011a, Three-phase relative permeability and hysteresis effect during WAG process in mixed wet and low IFT systems: *Journal of Petroleum Science and Engineering*, 78(3-4), p. 732-739.
2. Shahverdi, H., Sohrabi, M., and Jamiolahmady, M., 2011b, A New Algorithm for Estimating Three-Phase Relative Permeability from Unsteady-State Core Experiments: *Transport in Porous Media*, 90(3), p. 911-926.
3. Shahverdi, H., Sohrabi, M., Fatemi, M., and Jamiolahmady, M., Ireland, S., 2011c, A Three Phase Relative Permeability and Hysteresis Model for Simulation of Water Alternating Gas Injection: Submitted for SPE journal, Paper SPE 152218-PP.

Conference Papers:

4. Shahverdi, H., Sohrabi, M., Jamiolahmady, M., Fatemi, M., Ireland, S., Robertson, G.: "Investigation of Three-phase Relative Permeabilities and Hysteresis Effects Applicable to Water Alternating Gas Injection", SEP-EAGE IOR symposium in Cambridge, UK, April 2011.
5. Shahverdi, H., Sohrabi, M., Jamiolahmady, M., Fatemi, M., Ireland, S., Robertson, G.: "Evaluation Of Three-Phase Relative Permeability Models For WAG Injection Using Water-Wet And Mixed-Wet Core Flood Experiments", SEP (143030) Symposium in Vienna, Austria, May 2011.
6. Shahverdi, H., Sohrabi, M., Fatemi, M., and Jamiolahmady, M., Ireland, S., A Three Phase Relative Permeability and Hysteresis Model for Simulation of Water Alternating Gas Injection, Paper SPE 152218-PP, April 2012 SPE Symposium on Improved Oil Recovery, Tulsa, United States of America.
7. Shahverdi, H., Sohrabi, M., Jamiolahmady, M.: "A New Algorithm for Estimating Three-Phase Relative Permeability from Unsteady-State Core Experiments", Presented at the International Symposium of the Society of Core Analysts held in Halifax, Nova Scotia, Canada, 4-7 October, 2010.
8. Sohrabi, M., Shahverdi, H., Jamiolahmady, M., Fatemi, M., Ireland, S., Robertson, G.: "EXPERIMENTAL AND THEORETICAL THREE-PHASE RELATIVE PERMEABILITY FOR WAG INJECTION IN MIXED WET AND LOW IFT SYSTEMS", Presented at the International Symposium of the Society of Core Analysts held in Halifax, Canada, 4-7 October, 2010.
9. Sohrabi, M., Shahverdi, H., Jamiolahmady, M.: "Water Alternating Gas (WAG) Injection Studies in mixed wet and low IFT system", SPE DVEX, Aberdeen, May 2009.

10. Sohrabi, M., Shahverdi, Fatemi, M., H., Jamiolahmady. :”Determination of Three Phase Relative Permeability in Water-Alternating-Gas (WAG) Injection process -”, SPE DVEX, Aberdeen, May 2010.
11. Sohrabi, M., Shahverdi, H., Fatemi, M., Jamiolahmady. :”Theoretical and experimental investigation of WAG Injection -”, SPE DVEX, Aberdeen, May 2011.
12. Sohrabi, M., Jamiolahmady, M., Al-abri. M., Shahverdi, H., Ireland S. and Brown C.: “Experimental study of Water Alternating Gas (WAG) Injection”, Proceedings of the IEA - EOR Symposium, Beijing, China, November 3-5, 2008.
13. Sohrabi, M., Shahverdi, H., Jamiolahmady, M., :”New Developments in WAG Injection in near miscible system” , Proceedings of the IEA - EOR Symposium, Aberdeen, Scotland, October 18-20, 2010.

Table of Contents

1	Chapter 1: Introduction.....	1
1.1	Preface.....	1
1.2	Mechanism of Oil Recovery by WAG	2
1.3	WAG classification.....	4
1.3.1	Miscible WAG Injection (MWAG).....	5
1.3.2	Immiscible WAG Injection (IWAG).....	5
1.3.3	Simultaneous water and gas injection (SWAG).....	5
1.3.4	Hybrid WAG Injection	6
1.4	Effective parameters in WAG performance.....	6
1.4.1	Formation Heterogeneity	6
1.4.2	Injection Gas Characteristics.....	6
1.4.3	Injection Pattern	7
1.4.4	Tapering	7
1.4.5	Three-phase relative permeability	7
1.5	Review of three-phase relative permeability.....	9
1.6	Experimental and simulation review of WAG.....	14
1.7	Near-miscible flow	16
1.8	Scope of work.....	17
1.8.1	What is the problem?	17
1.8.2	Thesis content.....	19
1.9	References	22
2	Chapter 2: Coreflood Experiments.....	29
2.1	Coreflood Facility	29
2.2	Experimental Procedures	31
2.2.1	Core Preparation and Tracer Analysis.....	31
2.2.2	Establishing Connate Water Saturation.....	32
2.2.3	Test Fluids.....	33
2.2.4	Development of Mixed-Wettability.....	36
2.3	Coreflood experiments.....	38
2.3.1	Two-phase experiment.....	38
2.3.2	Three-phase experiments	42

2.4	References	45
3	Chapter 3: Evaluation of Three-Phase Relative Permeability Models	37
3.1	Three-Phase Relative Permeability Models	37
3.1.1	Saturation-Weighted interpolation model.....	39
3.1.2	Stone's first model:.....	40
3.1.3	Stone's Second Model:	40
3.1.4	Stone's first model exponent.....	41
3.1.5	IKU method.....	41
3.1.6	ODD3P Method.....	43
3.2	Hysteresis	45
3.2.1	Trapping Models	46
3.2.2	Two-phase hysteresis models.....	47
3.2.3	Three-phase (WAG) hysteresis model.....	49
3.3	Coreflood Simulation.....	53
3.3.1	Input data.....	53
3.3.2	Error analysis.....	54
3.3.3	Simulation results and discussion.....	55
3.4	Conclusions	66
3.5	Reference	68
4	Chapter 4: Determination of Three-Phase Relative Permeability from Unsteady-State Coreflood Experiment	70
4.1	Introduction	70
4.2	Theory	75
4.2.1	Mathematical model (Coreflood Simulator)	75
4.2.2	Relative permeability function	77
4.2.3	Estimation procedure	80
4.3	Verification of the algorithm.....	83
4.3.1	Results of first gas injection.....	84
4.3.2	Results of second gas injection	88
4.4	Conclusions	93
4.5	Reference	94
5	Chapter 5: Characterization of Three-Phase k_r and Hysteresis Effect in WAG Process	95

5.1	History matching results	95
5.1.1	1000mD-MW	96
5.1.2	65mD-WW	98
5.1.3	65mD-MW	100
5.2	Three-phase relative permeabilities.....	103
5.2.1	Hysteresis	103
5.2.2	Water-wet versus mixed-wet.....	121
5.2.3	Three-phase k_r versus two-phase k_r	124
5.3	Trapped gas and oil saturation	131
5.4	Conclusions	139
5.5	References	142
6	Chapter 6: New Methodology for Modelling of Hysteresis in WAG process	142
6.1	New hysteresis model (WAG-HW).....	143
6.1.1	Gas relative permeability during gas injection.....	144
6.1.2	Gas relative permeability during water injection	146
6.1.3	Water relative permeability during water injection.....	148
6.1.4	Water relative permeability during gas injection	149
6.1.5	Oil relative permeability during water injection	149
6.1.6	Oil relative permeability during gas injection.....	150
6.2	Verification of the WAG-HW model	152
6.3	Assessment of Larsen-Skauge model	156
6.4	Conclusions	167
6.5	References	168
7	Chapter 7: Conclusions and Recommendations	169
7.1	Conclusions	170
7.2	Recommendations	176
7.3	References	177
A.	Appendix A: Application of 3RPSim.....	178
A.1	Input data:.....	179
A.2	Running simulation:	185
A.3	Results:	186
A.4	Three phase k_r models:.....	188

Chapter 1

Introduction

1.1 Preface

Production from oil reservoirs is usually divided into three stages: primary, secondary and tertiary. The driving forces in primary recovery come from the natural energy source associated with rock and fluid in the reservoir. These mechanisms include fluid and rock expansion, natural water drive, gas-cap drive, solution gas drive and gravity drainage. The secondary recovery processes are usually implemented by water injection into the aquifer or gas injection into the gas cap to maintain the reservoir pressure which has already been depleted due to primary oil production. Tertiary recovery or enhanced oil recovery (*EOR*) methods refer to injection of one or more fluids into oil reservoir to displace the remaining oil left behind after the primary and secondary methods. The injected fluids provide additional energy in the reservoir to displace the oil towards producing wells. In addition, the injected fluids may interact with the reservoir rock/oil system to create favourable conditions for additional oil recovery. *EOR* process can be

classified into five categories: mobility-control, chemical, miscible, thermal and other processes, such as microbial EOR (Green and Willhite, 1998).

Water-Alternating-Gas (WAG) injection is one of the well established *EOR* techniques to improve oil recovery by combining effects of two traditional *EOR* methods- water injection and gas injection. This approach was originally proposed by Parrish (1966). WAG injection has been successfully applied in many oil reservoirs with the majority of them located in Canada and the U.S (Cone, 1970; Holm, 1972; Poolen, 1980; Stalkup Jr., 1983; MacLean, 1989) but there are also some other fields in North Sea region (Dalen et al., 1993; Hermansen et al., 1997). Both miscible and immiscible injections have been applied in the WAG process, and many different types of gas have been used.

1.2 Mechanism of Oil Recovery by WAG

The overall displacement efficiency of any oil recovery displacement process can be considered simply as the product of microscopic and macroscopic displacement efficiency:

$$E = E_{Micro} \cdot E_{Macro} \quad 0.1$$

Where E is total displacement efficiency (the volume of oil recovery by *EOR* divided by the amount of oil in place at start of *EOR*), E_{Micro} is microscopic displacement efficiency which refers to the displacement of the oil at pore level. In other words, E_{Micro} represents the effectiveness of the displacing fluid in mobilizing the oil at those pores of the formation where the displacing fluid contacts the oil. The E_{Macro} is macroscopic (volumetric) displacement efficiency which relates to the success of the displacing fluids in contacting the reservoir in a volumetric scale. The E_{Macro} is a quantity of how effectively the displacing fluid sweeps out the volume of a reservoir; both in areal and vertical scale, as well as how efficiently the displacing fluid moves the displaced oil toward production wells.

WAG injection improves oil recovery by modifying both microscopic and macroscopic sweep efficiencies. As the gas/oil system has lower interfacial tension (IFT) than the oil/water system, hence microscopic displacement of the oil by gas at the pore level is normally better than by water. However, high gas mobility, due its low viscosity, causes gas fingering and early gas breakthrough which reduces the macroscopic (areal

and vertical) sweep efficiency. One of the most predominant features of WAG injection is controlling the gas/oil mobility ratio defined by the following equation:

$$M = \frac{k_{rg} / \mu_g}{k_{ro} / \mu_o} \quad 0.2$$

Where M is mobility ratio, k_{rg} and k_{ro} are the relative permeabilities and μ_g and μ_o are the viscosities for gas and oil, respectively. A more efficient displacement of the oil will be achieved while having favourable mobility ratio (less than one). An unfavourable mobility ratio will be obtained once the gas has a higher mobility than the oil which causes gas fingering and decrease sweep efficiency. This problem has been reported in several gas injection field cases (Holm, 1972; Watts et al., 1982; Moffitt and Zornes, 1992). Reservoir heterogeneities like high permeable layers and fractures (Cuesta and G, 1982; Birarda et al., 1990) may assist gas fingering and result in premature breakthrough of gas. Decreasing gas permeability or increasing gas viscosity result in reducing mobility ratio and thereby improves sweep efficiency. Water injection in an alternative manner with the gas injection is an effective way of reducing gas permeability.

Another important mechanism of improving oil recovery by WAG injection is gravity segregation (Figure 0-1) which affects the vertical sweep efficiency. This mechanism displaces the oil from unswept parts of the reservoir, especially attic oil, by rising of gas towards the top and deposition of the water towards the lower parts of the formation. The vertical sweep efficiency is influenced by the relation between viscous and gravitational forces. The viscous/gravity ratio can be expressed by:

$$R_{v/g} = \left(\frac{v\mu_o}{k\Delta\rho g} \right) \left(\frac{L}{h} \right) \quad 0.3$$

Where v = Darcy velocity, μ_o = oil viscosity, L = distance between the wells, k = permeability to oil, g = gravity force, $\Delta\rho$ = density difference between fluids, and h = height of the displacement zone. The reservoir properties affecting the vertical sweep mostly include reservoir dip angle and variation in permeability and porosity. Normally, porosity and permeability increasing downward will be advantageous for the

WAG injection because this combination increases the stability of the front (Christensen et al., 1998).

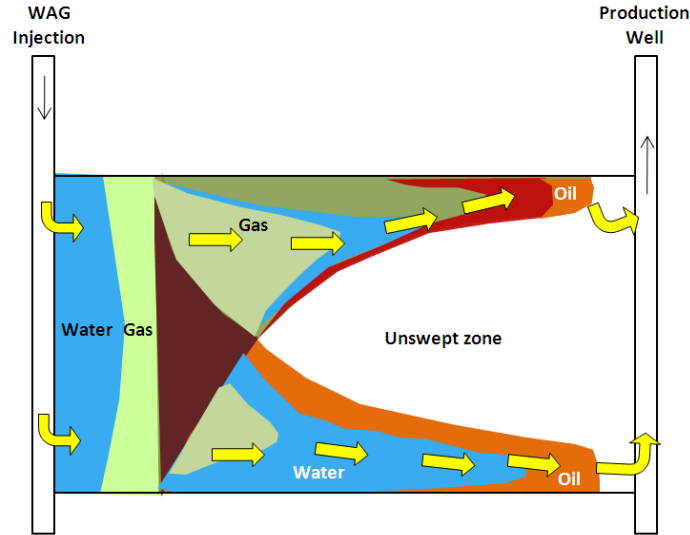


Figure 0-1: Schematic of fluid distribution and displacement front in WAG injection process.

To optimize the WAG efficiency and improve recovery, it is important to adjust the amount of injected gas and water into the oil reservoir. Large amounts of gas injection results in front instability and poor macroscopic sweep efficiency and too much water injection will reduce microscopic efficiency.

There are some other advantages for WAG injection including compositional exchanges (may give some additional oil recovery and may also influence the fluid densities and viscosities), reinjection of associated gas instead of flaring it, which is favourable due to environmental concerns.

1.3 WAG classification

The WAG processes can be classified into several types based on injection pressure and method of injection. The most common of WAG processes have been carried out so far in oil reservoirs, are miscible WAG (MWAG), immiscible WAG (IWAG), simultaneous water and gas injection (SWAG), hybrid WAG (HWAG).

1.3.1 Miscible WAG Injection (MWAG)

When injection pressure in the gas cycles of a WAG process is close or above the MMP (minimum miscibility pressure) of the reservoir fluid, the process is referred to the miscible WAG (Rogers and Grigg, 2000; Panda et al., 2011). The miscible front in MWAG process has poor volumetric sweep efficiency because of its low viscosity whereas the residual oil saturation behind miscible front is very low. So the main objective of water slug in MWAG process is to increase the macroscopic sweep efficiency. Miscible projects are mostly found onshore, and most of them have been performed on a close well spacing, but recently miscible processes have also been attempted even at offshore type well spacing (Stenmark and Andfossen, 1995; Skauge and Berg, 1997 ; Mogensen et al., 2010).

1.3.2 Immiscible WAG Injection (IWAG)

If the gas slugs in WAG process cannot develop miscibility with the reservoir oil, it's called immiscible WAG (IWAG). The main purpose of performing IWAG is to improve frontal stability or contacting unswept zones. Applications have been in reservoirs where gravity-stable gas injection cannot be applied because of limited gas resources or reservoir properties like low dip or strong heterogeneity (Christensen et al., 2001). The first gas cycle might occasionally dissolve to some extent into the oil which causes desirable changes in fluid viscosity and density at the displacement front. Therefore, the process can take place under near miscible condition (Surguchev, 1985; Dalen et al., 1993; Ramachandran et al., 2010).

1.3.3 Simultaneous water and gas injection (SWAG)

Simultaneous water and gas injection was found as an option that has better mobility control than WAG and improve gas displacement efficiency and oil recovery (Ma et al., 1995). However, the SWAG process would eliminate the need for separate water and gas injection lines which reduces operational costs. From environmental point of view, in cases where export of gas is not economical, re-injection of the produced gas in a SWAG scheme can significantly reduce or in certain cases eliminate the need for flaring. In SWAG projects, both water and gas are injected at the same time into a portion or the entire thickness of the formation. It is subdivided into two techniques. In one technique, water and gas are mixed at the surface and injected together through a

single well bore. The process is referred to as SWAG injection. In the second case the two phases are pumped separately using a dual completion injector and are selectively injected into the formation. This latter technique is known as SSWAG, and usually gas is injected at the bottom of the formation and water injected into the upper part of reservoir (Quijada, 2005).

1.3.4 Hybrid WAG Injection

WAG project in some oil field have been implemented by a large slugs of gas injection, followed by a small number of slugs of water and gas. This process is referred to as hybrid WAG injection (Jackson et al., 1985; Magruder et al., 1990; Hustad et al., 2002).

In this study, the author has investigated the three-phase flow issues applicable to immiscible with the main focus on near miscible WAG injection at the core scale.

1.4 Effective parameters in WAG performance

The major design parameters for conducting a WAG injection scheme in an oil reservoir are formation heterogeneity, composition of injection gas, injection pattern, and three-phase relative permeability (k_r).

1.4.1 Formation Heterogeneity

Reservoir stratification and heterogeneities strongly influence sweep efficiency during WAG injection. Reservoir simulation studies (Jackson et al., 1985) for various k_v/k_h (vertical to horizontal permeability) ratios suggest that higher ratios increases vertical displacement efficiency whereas it adversely affects oil recovery in the WAG process. The ratio of viscous to gravity forces (equation 0.3) is the key variable for controlling vertical conformance of the displacement and also for determining the efficiency of WAG injection.

1.4.2 Injection Gas Characteristics

The type of injection gas in WAG process is more related to the location of reservoir and availability of gas than the design criteria of it. The injection gas used in WAG can be divided into three groups: CO₂, hydrocarbons and non-hydrocarbons (CO₂ excluded). CO₂ is generally utilized for miscible WAG injection and design criteria of CO₂ suggest a minimum depth limitation as well as dictating the specific gravity and

viscosity criteria of the oil to be produced from the concerned reservoir (Goodrich, 1980; Hadlow, 1992; Grigg and Schechter, 1997). In offshore fields, the availability of hydrocarbon gas directly from production makes hydrocarbon gas injection feasible. A few fields are reported using nitrogen (Christian et al., 1981; Langston and Shirer, 1985) or flue gas/exhaust gas (Kirkpatrick et al., 1985), mainly because special supplies were available nearby.

1.4.3 Injection Pattern

The five-spot injection pattern seems to be the most popular onshore with a fairly close well spacing (Christensen et al., 2001). Because many of the field applications (especially in Texas) are miscible operations, many wells will give a good control of the field pressure and thus of the WAG-injection performance. Inverted 9-spot patterns are also reported in the Hybrid WAG projects of Shell and Unocal (Tanner et al., 1992).

1.4.4 Tapering

Tapering occurs when the water/gas ratio in the WAG process is increasing or decreasing throughout the flood. The injection volume of water relative to gas can be increased at a later stage of the WAG injection in order to control channelling and breakthrough of gas. This step is important especially when the injected gas is expensive and needs recycling (Masoner et al., 1996; Christensen et al., 2001).

1.4.5 Three-phase relative permeability

Darcy (1856) determined that the rate of flow of water through a homogenous porous media could be described by the equation:

$$q = KA \frac{h_1 - h_2}{L} \quad 0.4$$

Where q represents the rate at which water flows downward through a vertical sand pack with cross-sectional area A and length L ; the terms h_1 , and h_2 , represent hydrostatic heads at the inlet and outlet, respectively, of the sand filter, and K is a constant. Darcy's experiments were confined to the flow of water through sand packs which were 100% saturated with water.

Later investigators determined that Darcy's law could be modified to describe the flow of fluids other than water, and that the proportionality constant K could be replaced by k/μ , where k is a property of the porous material (permeability) and μ is a property of the fluid (viscosity). With this modification, Darcy's law may be written in a more general form as

$$v_s = \frac{k}{\mu} \left[\rho g \frac{dZ}{dS} - \frac{dP}{dS} \right] \quad 0.5$$

Where

S = Distance in direction of flow, which is taken as positive.

v_s = Volume of flux across a unit area of the porous medium in unit time along flow path S .

Z = Vertical coordinate, which is taken as positive downward

ρ = Density of the fluid

g = Gravitational acceleration

$\frac{dP}{dS}$ = Pressure gradient along S at the point to which v_s refers.

The volumetric flux v_s may be further defined as q/A , where q is the volumetric flow rate and A is the average cross-sectional area perpendicular to the lines of flow.

A more useful form of Darcy's law can be obtained if it's assumed that a rock which contains more than one fluid has an effective permeability to each fluid phase and that the effective permeability to each fluid is a function of its percentage saturation. The effective permeability of a rock to a fluid with which it is 100% saturation is equal to the absolute permeability of the rock. If we define relative permeability as the ratio of effective permeability to absolute permeability, Darcy's law may be restated for a system which contains three fluid phases as follow:

$$v_{os} = \frac{kk_{ro}}{\mu_o} \left[\rho_o g \frac{dZ}{dS} - \frac{dP_o}{dS} \right] \quad 0.6$$

$$v_{ws} = \frac{kk_{rw}}{\mu_w} \left[\rho_w g \frac{dZ}{dS} - \frac{dP_w}{dS} \right] \quad 0.7$$

$$v_{gs} = \frac{kk_{rg}}{\mu_g} \left[\rho_g g \frac{dZ}{dS} - \frac{dP_g}{dS} \right] \quad 0.8$$

Where the subscripts o , g , and w represent oil, gas and water, respectively. Note that k_{ro} , k_{rw} , k_{rg} are the relative permeabilities to the three fluid phases at the respective saturations of the phases within the rock (Honarpour et al., 1986). In fact, relative permeability values describe the comparative ease by which different fluids flow in a porous medium.

Three-phase flow occurs when the water saturation is higher than the irreducible level, while oil and gas are also present in the reservoir as mobile phases. As shown in Figure 0-1, the three-phase flow considerably occurs in WAG process. However, in order to precisely forecast the performance of the WAG injections using mathematical modelling knowledge of three-phase relative permeabilities values are needed.

As the main objective of this study is modelling of three-phase relative permeability during WAG coreflood experiments performed under near miscible condition. A literature survey is carried out on three subjects relevant to this study, namely, three-phase relative permeability, numerical simulation of WAG experiments and near miscible flow, which are shortly demonstrated in the following section.

1.5 Review of three-phase relative permeability

Estimation of three-phase relative permeability is needed for a variety of oil recovery mechanisms and methods, such as water drive of reservoirs at pressure below the bubble point, water alternating gas injection, hot gas/oil/water systems in thermal recovery, and low pressure gas recycling in condensate fields with aquifers. Considerable efforts have been directed towards gaining a better understanding of three phase flow in porous media and in particular determination of three-phase relative permeability values. However, an accurate estimation of three-phase relative permeabilities still remains a challenging task for the petroleum industry. While for two-phase relative permeability (oil/water, gas/oil, and gas/water) there are only two

principal displacement paths, i.e. the saturation of one phase may either increase or decrease, in contrast, in the case of three-phase relative permeability there are an infinite number of different displacement paths. This is because any three-phase displacement involves the variation of two independent saturations. It is therefore impractical to measure relative permeability (k_r) for all possible three-phase displacements that may occur in a reservoir including, for instance immiscible WAG injection.

Two approaches have traditionally been followed for determination of three-phase relative permeability based on (i) direct measurement of three-phase relative permeability by coreflood experiments (ii) prediction of three-phase relative permeability from two-phase data. In the first approach, three-phase relative permeability values are determined either through steady-state or unsteady-state experiments. The first measurement of three-phase relative permeabilities for a water-oil-gas system was reported by (Leverett and Lewis, 1941), who used a steady-state single-core dynamic method in unconsolidated sands. Oak (1990) conducted a large number of tests to measure three-phase relative permeability on water-wet, oil-wet and intermediate-wet Berea sandstone cores with a fully automated steady-state method. Water, oil and gas phase saturations were measured by an X-ray absorption method. Two saturation histories, primary DDI and IID, were studied. The experimental results showed different relative permeability versus saturation relationships, depending on the saturation history. More details on determination of three-phase relative permeability from coreflood experiments are presented and discussed in chapter four.

In the second approach, three-phase relative permeabilities are calculated from empirical correlations e.g. Stone, Baker, which are based on the corresponding two-phase relative permeability data. Stone (1970) presented a probability method which uses two sets of two-phase data to predict the relative permeability of the intermediate wet phase in a three-phase system. This model is such that it will yield the correct two-phase data when only two phases are flowing, and will provide interpolated data for three-phase flow that are consistent and continuous functions of the phase saturations. He modified his models (1973) by incorporating gas and water relative permeability in calculation of three-phase k_r of the oil in order to get better agreement with experimental data, especially in the region of low oil saturations.

One of the crucial factors that strongly influences the oil production in three-phase system, especially at low oil saturations is residual oil saturation at which oil relative permeability becomes zero. Fayers and Matthews (1984), proposed a linear equation for estimating minimum oil saturation (S_{om}) in three-phase region applicable to Stone first method. In this approach, impact of mobile water and gas phases on the amount of residual oil has been accounted for. Hustad and Holt (1992) carried out a hydrocarbon gas injection test into a water-flooded vertical core under near miscible conditions. He modified Stone's first model by imposing an exponent parameter on the saturation term of the oil relative permeability to match the production and pressure data.

Both Stone models were originally proposed for preferentially water wet systems in which water and gas relative permeabilities only depend on the water and gas saturations, respectively. Baker (1988) proposed a simple three-phase relative permeability for oil, water and gas based on saturation-weighted interpolation between two-phase relative permeability data in which three-phase k_r of each phase is assumed to be function of two saturations. He showed that interpolation model provide a better fit to the experimental data than the other models that were available at the time. Hustad and Hansen (1995), proposed an empirical correlation for three-phase relative permeabilities and phase pressure for reservoir simulators. The formulation is based on three sets of two-phase data and properly accounts for six, two-phase, residual or critical saturations. The model uses only two-phase data and an interpolation technique to obtain three-phase properties by a systematic weighting procedure based on the saturations and end point values. Detailed mathematical formulations of the aforementioned three-phase k_r models available in the commercial reservoir simulators are described in chapter three.

Characteristic parameters describing multiphase flow in porous media are process dependent. In particular, relative permeabilities are considered to be dependent on saturation and saturation history. This latter dependency is described in the literature as relative permeability hysteresis. Hysteresis on relative permeability has been experimentally observed in two-phase (Osoba et al., 1951; Land, 1971; Braun and Holland, 1995) and in three-phase flow (Skauge and Aarra, 1993; Eleri et al., 1995b) in porous media.

A few three-phase relative permeability models have been developed incorporating both hysteresis and interfacial tension effects. Jerauld (1997) developed a three-phase relative permeability correlation based on Prudhoe Bay field data. The model incorporates hysteresis in gas, oil, and water relative permeability as well as the dependence of relative permeability on composition and gas/oil interfacial tension (IFT). The functional forms chosen to correlate the relative permeability data were based on interpretation of the pore-level mechanisms that determine fluid flow. Blunt (2000) presented an empirical model for three-phase relative permeability which allows for changes in hydrocarbon composition, hysteresis, and the trapping of oil, water, and gas. The model is based on saturation-weighted interpolation between the two-phase relative permeabilities. Layer drainage of oil flow is also accounted for in the oil relative permeability for low oil saturations. Hustad and Browning (2010) proposed a coupled formulation for three-phase relative permeability for implicit compositional reservoir simulation. The formulation incorporates primary, secondary, and tertiary saturation functions. Hysteresis and miscibility were applied simultaneously to both capillary pressure and relative permeability function.

Various models have been developed to predict three-phase k_r in terms of saturation rather than two-phase relative permeability. These models are based on the concept of approximating the flow paths through a rock by the equivalent hydraulic radius of a bundle of capillary tubes. Then a tortuosity correction was incorporated to account for the differences in path length of tubes of different sizes (Corey et al., 1956; Naar and Wygal, 1961; Land, 1968). Further complexity of porous media was added to these models based on a description of the porous medium considered as a set of fractal pores. The fluids are allowed to flow together in a same pore, gas in the centre, and, for water-wet conditions, water in the vicinity of the walls and oil as an intermediate phase (Moulu et al., 1999).

A number of measurements have been performed to investigate the impact of wettability and IFT on three-phase k_r . Delshad et al. (1987) carried out a series of coreflood experiments to measure two-phase and three-phase relative permeabilities for low interfacial tension brine/oil/surfactant/alcohol mixture in Berea sandstone cores. The results showed that relative permeability of each phase is a function of only its own saturation during three-phase flow. Cinar et al. (2007) reported the experimental results that demonstrate the combined effects of variations in interfacial tension (IFT) between

one pair of three phases and wettability of a porous medium on three-phase relative permeabilities. They measured three-phase relative permeabilities for systems with IFTs between two of the three phases varying from 0.005 to 2 mN/m. Their results indicated that as IFT between the analog gas/oil pair of phases decreases, relative permeabilities for those phases increase at a given saturation. The relative permeability for the analog water phase remains nearly unchanged for water-wet porous systems, but it decreases especially at low phase saturations for oil-wet porous systems.

DiCarlo et al. (1998) studied three-phase flow in water-wet, oil-wet, and fractionally-wet sand packs. They used CT scanning to measure directly the oil and water relative permeabilities for three-phase gravity drainage. The measurement showed that the gas relative permeability is approximately twice as high in a water-wet system than in an oil-wet system at the same gas saturation. The water relative permeability in the water-wet pack and the oil relative permeability in the oil-wet pack are similar. It has been proved that the existence of wetting and spreading oil films-caused by wettability and spreading-greatly affects the flow mechanisms and consequently the recovery kinetics and the process efficiency. Accordingly, in water-wet and in fractionally-wet porous media k_{ro} is higher for spreading system than for non-spreading system (Vizika and Lombard, 1996).

Some studies have been conducted to address the accuracy of the existing three-phase k_r models against measured data (Delshad et al., 1987; Delshad and Pope, 1989; Pejic and Maini, 2003). The main result of these reviews is that no single model can fit data from different sources. This is no surprise as the experimental data involved both steady state and unsteady state methods and includes variations in fluid properties, rock properties and maybe most important wettability. Petersen et al. (2008) presented an extensive experimental study of relative permeability functions of two- and three-phase displacement processes relevant to the depressurisation of the Statfjord Field. The measured capillary pressure functions were used to properly account for capillary pressure effects in the experiments. The results showed that commonly used empirical models that predict three-phase relative permeabilities from two-phase data (e.g. Stone and saturation weighted interpolation) are not able to accurately describe the three-phase experiments.

These studies confirmed that the rock wettability, interfacial tension between fluids and the direction of saturation alteration extremely influence three-phase relative permeability, therefore existing models should only be used for those conditions where they originally have been developed. Experimental data are required to verify the applicability of these models for using beyond those particular criteria.

1.6 Experimental and simulation review of WAG

Oil recovery by immiscible WAG is dependent on the saturation cycles that occur in a core-flood or in the reservoir. In order to predict WAG behaviour in the reservoir from experimental results, numerical models with an effective cycle-dependent hysteresis description of the three-phase oil, water and gas relative permeabilities should be considered. Skauge and Larsen (1994) conducted some WAG coreflood experiments under different wettability condition and then three-phase relative permeability was obtained from different cycle of gas and water. The results indicated that the residual oil saturation can be significant lower by three-phase flow compared to two-phase waterflood or gas injection. Every phase relative permeability depicted irreversible hysteresis effect during various water and gas injection. A new relative permeability model was developed based on cycle-dependent hysteresis effects occurring during WAG injection (Larsen and Skauge, 1998). This model accounted for reduced mobility and irreversible hysteresis loops during three-phase flow. The new three-phase models use experimental wetting and non-wetting relative permeabilities as input data as well as the knowledge of relations between maximum non-wetting saturation and trapped non-wetting saturation.

Egermann et al. (2000) designed successive drainage and imbibition experiments (WAG) under various conditions of initial saturations. Then a new model was proposed to take into account drainage/imbibition hysteresis and cycle hysteresis which is characteristic of WAG injection. They also confirmed that at large scales k_v/k_h is an important factor on the extent of the three-phase zone, which in turn influences the WAG scheme overall efficiency. Element et al. (2003) performed a laboratory study to investigate secondary and tertiary immiscible WAG floods in both water-wet and intermediate-wet Berea cores. They fulfilled an assessment of the most popular hysteresis model in simulating WAG experiments. Cycle-dependent hysteresis of relative permeability, potential for the reduction in the residual oil saturation with

trapping of gas by water, reduction in both water and gas permeability, variation in Land trapping factor between hysteresis cycles were found the main important features of WAG injection. Although the published models may include some of the observed hysteresis effects, no model includes all of them. Spiteri (2005) studied the impact of using history-dependent saturation functions in reservoir simulations. First, they investigated the degree of accuracy with which different hysteretic models reproduce Oak's three-phase relative permeability data. Then the validity of existing models was assessed, and the model parameters subject to most uncertainty was identified as well. Second, they illustrated how the use of a hysteretic relative permeability model affects reservoir simulations. They found that there is striking disparity in the simulation results depending on whether a hysteretic or a non-hysteretic model is employed, and concluded that it is essential to incorporate hysteresis in the relative permeabilities in order to obtain accurate predictions of realistic WAG processes. Righi et al. (2004) carried out an experimental immiscible WAG study on the water flooded Troncoso sandstone reservoir located in Chihuido de la Sierra Negra Field in Argentina. It was found that the near-miscible conditions can be developed between a gas with 90 % CO₂ and the reservoir fluid at reasonable pressure levels. The results depicted that the compositional effects are not the main oil recovery mechanism, giving support to an immiscible WAG model based on three-phase and hysteretic effects that lead to an effective reduction of the residual oil saturation.

The important question for modelling and optimising the WAG process is, the relation between hydrocarbon trapped saturation and core/fluid characterization (Dale and Skauge, 2005).

In addition to coreflood experiments, several micromodel experiments and pore network modelling studies of the WAG injection have been carried out so far to identify the pore-scale displacement mechanisms. Sohrabi et al. (2000) used a high pressure glass micromodels of different wettability to conduct a series of WAG experiments. WAG recovery was higher for strongly oil- wet and mixed-wet micromodels than for strongly water-wet. The successive WAG cycles redistributed the residual oil resulting in improved oil recovery. Svirsky et al. (2004) developed a pore-scale network simulator for capillary-dominated three-phase flow in media where wettability varies from pore to pore. He used 2D network simulations to model the WAG floods in a water-wet micromodel that had previously been presented by Sohrabi et al. (2000). Features such

as multiple displacements, snap-off events to allow invasion of all three phases, correlations between wettability and pore sizes including wetting films and spreading layers, and gravity were included in the model. Simulations of WAG flood cycles for different wettability conditions and the related presence or absence of wetting films determined the prevailing displacement mechanisms in three-phase flow. Suicmez et al. (2006), used a physically-based three-phase network model to predict three-phase relative permeabilities for WAG flooding for different wettability conditions. The double displacement mechanisms, double imbibition (water-oil-gas) and imbibition-drainage (water-gasoil) were incorporated in pore network simulator. Cycle-dependent hysteresis and hydrocarbon trapped saturation for different wettability condition were investigated.

1.7 Near-miscible flow

Near-miscible implies very low gas/oil interfacial tension near the transition from immiscible to miscible conditions. Miscible flooding is considered unsuitable for some reservoirs because of high minimum miscibility pressure or operating pressure constraints. Hence, near-miscible gas drives appear attractive from both economic and operational standpoints. It is generally believed that miscibility may repeatedly develop and break down in a reservoir due to dispersion arising from viscous fingering and reservoir heterogeneity. Thus, many miscible processes are in fact a mixture of miscible and low IFT, near-miscible processes (Shyeh-Yung, 1991).

Bardon and Longeron (1980) determined the effect of reduced gas-oil IFT on the corresponding relative permeabilities for core flood gas injection experiments with a binary hydrocarbon mixture of liquid and vapour. They reported that both gas and oil relative permeabilities tended to be straight line functions of the respective phase saturations for gas-oil IFTs less than 0.04 mN/m. The relative importance of viscous and capillary forces, characterised by the capillary number, was also emphasised for oil-water systems with varying IFT, achieved by adding chemicals (Amaefule and Handy, 1982).

Experimental studies revealed the importance of film flow of the wetting phase at near-miscible conditions (Danesh et al., 1988; Williams and R.A. Dawe, 1988). Near-miscible gas injection is an efficient oil recovery method both as a secondary and

tertiary (post-water flood) process. The mechanisms involved in the flow and displacement of low IFT gas/oil systems at near miscibility are different from both miscible and immiscible systems (Thomas et al., 1994). In near-miscible gas injection, at the pore-scale, significant cross-flow of oil into the main flow stream takes place behind the gas front. This can lead to total recovery of the contacted oil (Sohrabi et al., 2008c). Micromodel WAG experiments under near-miscible conditions showed clear differences from the immiscible flooding cycles. In particular, there was significant oil production through “thick” films after the breakthrough of the gas finger and, in repeated gas floods, the gas finger tends to re-establish rather than to redistribute the phases as in the immiscible floods (sohrabi et al., 2005; Sorbie and Dijke, 2010).

1.8 Scope of work

1.8.1 What is the problem?

As mentioned earlier the numerical modelling of WAG injection as an EOR technique for improving oil recovery requires that we have knowledge of three-phase relative permeability. There are two traditional ways for determining three-phase relative permeability as an input data for reservoir simulators. First, direct measurement of the relative permeability by conducting coreflood experiments under reservoir conditions and the second, calculating three-phase relative permeability using two-phase relative permeability data (two phase approach). In the latter method, which is much easier and cheaper than the first approach, the measured values of two-phase k_r data are employed into the existing three-phase correlations to obtain relative permeability at three-phase flow conditions. The majority of the most practiced three-phase models available in the literature have been developed based on the limited range of coreflood data obtained under the specific core and fluid circumstances such as wettability, interfacial tension, and direction of flooding e.g. imbibitions, drainage. The decisive question when simulating a petroleum reservoir which involves three-phase flow is what model may produce the trustworthy values for the relative permeability reflecting the prevailing mechanisms happening at the reservoir conditions? In order to address this question, a series of three-phase coreflood experiments were conducted on cores with different wettability conditions using a near-miscible oil/gas system. Then these experiments

were simulated by the commercial reservoir simulator (Eclipse) employing a variety of three-phase models. The performance of each k_r model was assessed by calculating the error value between the measured data and the corresponding prediction deduced from the simulation.

As stated earlier, the first methodology in determining three-phase relative permeability is direct measurement of the relative permeability by conducting coreflood experiments under reservoir conditions. Two main methods for measuring k_r values in the laboratory are the steady-state and unsteady state displacements. In the steady state method all fluids are injected simultaneously, at given proportions, until steady-state conditions are attained, i.e., the same proportions of fluids that were injected into the core are produced at the outlet. It usually takes a very long time of fluid injection to establish steady state flow. In this approach the relative permeability of each phase can be simply calculated from Darcy equation. But in the unsteady state method, one of the fluids is injected in the core displacing the resident fluid phases which avoids losing considerable amount of time and expenses involved in steady state method. However, calculating the phase relative permeabilities using the unsteady state test data is much more complicated. In the unsteady state experiments, relative permeability can be obtained by either explicit or implicit methods. The explicit (analytical) method (Johnson et al., 1959) derives relative permeability from the laboratory measured recovery and pressure drop curves which has some difficulties with its application. In implicit (Kerig and Watson, 1986) relative permeability values are estimated in an optimization manner so that the difference between the measured and simulated values is minimized. This approach is easily applicable to two-phase relative permeability calculations and can converge to solution relatively quickly whereas in the case of three-phase flow, as more tuning parameters are involved, the process would be more complicated.

As part of this project, a computer program has been developed as an optimization tool to obtain three-phase relative permeability from unsteady-state displacement tests by matching the measured data, using Genetic Algorithm. The program gives best estimates of three-phase relative permeability based on appropriate mathematical functions defined to describe their dependency on phase saturations.

This computer program was utilized to obtain three-phase relative permeability of various cycles of the WAG experiments performed at different wettability conditions.

As another outcome of this study, the comprehensive k_r data set produced throughout the course of this project, has been interpreted in order to reveal the behaviour and the impact of some of the parameters pertinent to the WAG process including; hysteresis, trap saturation and wettability. In this part, we have attempted to address some specific questions regarding three-phase k_r which are considered “grey areas” in reservoir simulation:

- 1- How is three-phase k_r affected by sequential water and gas injection (impact of hysteresis)?
- 2- Which fluid does exhibit more hysteresis effects in relative permeability due to the reversing of the direction of displacement?
- 3- What is the role of wettability on the mobility of different fluids?
- 4- What is the relationship between the two-phase and three-phase relative permeability?
- 5- What are the deficiencies of the most widely used models in predicting the relative permeability of the near-miscible WAG process?

This knowledge may be used as benchmark for simulation of the reservoirs under three-phase flow.

Another objective of this study was to develop a new methodology for modelling of three-phase relative permeability during WAG injection. This approach addresses the hysteresis effect in relative permeability of the WAG process and attempts to overcome the inadequacies observed in the existing models.

1.8.2 Thesis content

A description of the coreflood experimental set-up and the procedure followed to conduct the coreflood experiments is given in chapter two. The work performed in order to prepare the core for displacement experiments; such as connate water establishment and wettability alteration are shortly elaborated, as well. A list of displacement tests utilized in this thesis for simulation purposes is provided at the end of this chapter.

Numerical simulation of the WAG coreflood experiments using black oil simulators (Eclipse100) and existing three-phase relative permeability models is discussed in chapter three. This exercise was aimed at evaluating the capability of many widely used three-phase models in predicting the WAG performance under different wettability conditions. The mathematical description of the existing three-phase relative permeability and hysteresis models available in the commercial reservoir simulators are given at the beginning chapter three. Then, two-phase relative permeability data measured from displacement tests are employed with the existing three-phase models to estimate the values of three-phase relative permeabilities in WAG displacement test. The estimated values of three-phase relative permeability are utilized for simulation of the WAG experiments. The accuracy of each of the existing three-phase models is assessed by comparing the production and pressure data resulted from WAG simulation with the corresponding data measured from the WAG experiments. Chapter three concludes with a summary of the conclusions of the materials presented in this chapter.

Chapter four focuses on the direct measurement of three-phase relative permeability from coreflood experiments. A brief description of the most common methods for measurement of three-phase relative permeability is presented, first. Then, the history matching algorithm devised in order to obtain the relative permeability from unsteady state displacement tests by employing genetic algorithm is described. This algorithm consists of three main modules including functional representative of three-phase relative permeability, coreflood simulator and optimization (Genetic Algorithm) which are explained in this chapter. A computer program code was also developed to implement this procedure in an iterative process. The algorithm is successfully verified against the results of the two synthetic coreflood experiment built in the black oil simulator (Eclipse) using Oak (1990) data presented in literature.

The in-house software presented in chapter four is used in chapter five to determine three-phase relative permeability of a large number of three-phase coreflood experiments performed by alternating injection of water and gas. This chapter is aimed to investigate the impact of cycle-dependent hysteresis associated with three-phase relative permeability during WAG injection. The relative permeabilities resulted from different injection scenarios are compared to each other in order to address the questions of whether, in what direction, and which phase is the hysteresis more pronounced. These results are qualitatively compared against the prediction of the WAG hysteresis

model (Larsen and Skauge, 1998) in order to demonstrate the shortcomings associated with this model. Moreover, the three-phase relative permeability of the water-wet rock is compared with the results of mixed-wet rock to highlight the impact of wettability on the mobility of the different fluids. The two-phase results are compared against three-phase relative permeability to identify the degree of closeness of the two-phase flow to the three-phase flow. In addition, because the non-wetting trapped saturation plays a significant role in the hysteresis effect, at the end of chapter five the most practiced trap model in literature (Land, 1968) is evaluated against the values measured from the WAG experiments. Finally, this chapter ends with a summary of main conclusions obtained in this chapter.

In chapter six, based on the comprehensive set of three-phase relative permeability data obtained from the WAG experiments and the shortcoming observed in the existing models, a new approach is proposed for modelling of three-phase relative permeability incorporating cyclic hysteresis effect. In this chapter, first the mathematical formula behind this model is explained, then, the relative permeability data of three sets of coreflood experiments are employed to validate this model. At the end of this chapter, the existing WAG hysteresis model (Larsen and Skauge, 1998) is assessed using our three-phase relative permeability data in order to compare the performance of the new approach against the prediction of the Larsen-Skaug model.

Finally in chapter seven, the highlights of results and points concluded in this study are given as well as some recommendation for future studies.

1.9 References

- Amaefule, J.O., and Handy, L.L., 1982, The Effect of Interfacial Tensions on Relative Oil/Water Permeabilities of Consolidated Porous Media, paper SPE 9783, (06).
- Baker, L.E., 1988, Three-Phase Relative Permeability Correlations, paper SPE 17369, presented at the SPE Enhanced Oil Recovery Symposium, Tulsa, Oklahoma.
- Birarda, G.S., Dilger, C.W., and McIntosh, I., 1990, Re-Evaluation of the Miscible WAG Flood in the Caroline Field, Alberta: SPE Reservoir Engineering, paper SPE 18066, (11).
- Blunt, M.J., 2000, An Empirical Model for Three-Phase Relative Permeability: SPE Journal, paper SPE 67950, (12).
- Braun, E.M., and Holland, R.F., 1995, Relative Permeability Hysteresis: Laboratory Measurements and a Conceptual Model: SPE Reservoir Engineering, paper SPE 28615, (08).
- Christensen, J.R., Stenby, E.H., and Skauge, A., 1998, Review of WAG Field Experience, paper SPE 39883, presented at the International Petroleum Conference and Exhibition of Mexico, Villahermosa, Mexico.
- Christensen, J.R., Stenby, E.H., and Skauge, A., 2001, Review of WAG Field Experience, paper SPE 39883, presented at the International Petroleum Conference and Exhibition of Mexico, Villahermosa, Mexico.
- Christian, L.D., Shirer, J.A., Kimbel, E.L., and Blackwell, R.J., 1981, Planning a Tertiary Oil-Recovery Project for Jay/LEC Fields Unit: SPE Journal of Petroleum Technology, paper SPE 9805, (08).
- Cinar, Y., Marquez, S., and Franklin M. Orr, J., 2007, Effect of IFT Variation and Wettability on Three-Phase Relative Permeability: SPE Reservoir Evaluation & Engineering, paper SPE 90572-PA, (06).
- Cone, C., 1970, Case History of the University Block 9 (Wolfcamp) Field A Gas-Water Injection Secondary Recovery Project: SPE Journal of Petroleum Technology, paper SPE 2837, (12).
- Corey, A.T., Rathjens, C.H., Henderson, J.H., and Wyllie, M.R.J., 1956, Three-Phase Relative Permeability: SPE Journal of Petroleum Technology, paper SPE 737-G, (11).
- Cuesta, J.F., and G, C., Merrit, 1982, Caroline W.A.G. Project Injectivity and Interference Test, A Field Example, presented at the Annual Meeting of the Petroleum Society of CIM, Calgary.
- DALE, E.I., and SKAUGE, A., 2005, FLUID FLOW PROPERTIES OF WAG INJECTION PROCESSES, presented at the 3th European Symposium on Improved Oil Recovery,

- Dalen, V., Instefjord, R., and R. Cristensen, 1993, AWAG formation Pilot in the Lower Brent Formation at the Gullfaks Field, presented at the European IOR Symposium, Moscow.
- Danesh, A., Henderson, G.D., Krinis, D., and Peden, J.M., 1988, Experimental Investigation of Retrograde Condensation in Porous Media at Reservoir Conditions, paper SPE 18316, presented at the SPE Annual Technical Conference and Exhibition, Houston, Texas.
- Darcy, H., 1856, Les Fontaines Publiques de la ville de Dyon: Victor Dalmont.
- Delshad, M., Delshad, M., Pope, G.A., and Lake, L.W., 1987, Two- and Three-Phase Relative Permeabilities of Micellar Fluids: SPE Formation Evaluation, paper SPE 13581, (09).
- Delshad, M., and Pope, G.A., 1989, Comparison of the three-phase oil relative permeability models: Transport in Porous Media, **4**(1), p. 59-83.
- DiCarlo, D.A., Sahni, A., and Blunt, M.J., 1998, The Effect of Wettability on Three-Phase Relative Permeability, paper SPE 49317, presented at the SPE Annual Technical Conference and Exhibition, New Orleans, Louisiana.
- Egermann, P., Vizika, O., Dallet, L., Requin, C., and Sonier, F., 2000, Hysteresis in Three-Phase Flow: Experiments, Modeling and Reservoir Simulations, paper SPE 65127, presented at the SPE European Petroleum Conference, Paris, France.
- Element, D.J., Masters, J.H.K., Sargent, N.C., OBE, A.J.J., and Goodyear, S.G., 2003, Assessment of Three-Phase Relative Permeability Models Using Laboratory Hysteresis Data, paper SPE 84903, presented at the SPE International Improved Oil Recovery Conference in Asia Pacific, Kuala Lumpur, Malaysia.
- Eleri, O.O., Graue, A., and Skauge, A., 1995, Steady-State and Unsteady-State Two-Phase Relative Permeability Hysteresis and Measurements of Three-Phase Relative Permeabilities Using Imaging Techniques, paper SPE 30764, presented at the SPE Annual Technical Conference and Exhibition, Dallas, Texas.
- Fayers, F.J., and Matthews, J.D., 1984, Evaluation of Normalized Stone's Methods for Estimating Three-Phase Relative Permeabilities, paper SPE 11277, (04).
- Goodrich, J.H., 1980, REVIEW AND ANALYSIS OF PAST AND ONGOING CARBON DIOXIDE INJECTION FIELD TESTS, paper SPE 8832, presented at the SPE/DOE Enhanced Oil Recovery Symposium, Tulsa, Oklahoma.
- Green, D.W., and Willhite, G.P., 1998, Enhanced Oil Recovery, **6**.
- Grigg, R.B., and Schechter, D.S., 1997, State of the Industry in CO₂ Floods, paper SPE 38849, presented at the SPE Annual Technical Conference and Exhibition, San Antonio, Texas.
- Hadlow, R.E., 1992, Update of Industry Experience With CO₂ Injection, paper SPE 24928, presented at the SPE Annual Technical Conference and Exhibition, Washington, D.C.
- Hermansen, H., Thomas, L.K., Sylte, J.E., and Aasboe, B.T., 1997, Twenty Five Years of Ekofisk Reservoir Management, paper SPE 38927, presented at the SPE Annual Technical Conference and Exhibition, San Antonio, Texas.

- Holm, L.W., 1972, Propane-Gas-Water Miscible Floods In Watered-Out Areas of the Adena Field, Colorado: SPE Journal of Petroleum Technology, paper SPE 3774, (10).
- Honarpour, M., Koederitz, L.F., and Harvey, A.H., 1986, *Relative Permeability Of Petroleum Reservoirs*, CRC Press.
- Hustad, O.S., and Browning, D.J., 2010, A Fully Coupled Three-Phase Model for Capillary Pressure and Relative Permeability for Implicit Compositional Reservoir Simulation: SPE Journal, paper SPE 125429-PA, (12).
- Hustad, O.S., and Hansen, A.G., 1995, A Consistent Correlation For Three-Phase Relative Permeabilities and Phase Pressure Based on Three Sets of Two Phase Data, presented at the 8th European IOR symposium, Vienna, Austria.
- Hustad, O.S., and Holt, T., 1992, Gravity Stable Displacement of Oil by Hydrocarbon Gas After Waterflooding, paper SPE 24116, presented at the SPE/DOE Enhanced Oil Recovery Symposium, Tulsa, Oklahoma.
- Hustad, O.S., Klav, T., Lerdahl, T.R., Berge, L.I., Stensen, J.Å.g., and Åren, P.I.-E., 2002, Gas Segregation During WAG Injection and the Importance of Parameter Scaling in Three-Phase Models, paper SPE 75138, presented at the SPE/DOE Improved Oil Recovery Symposium, Tulsa, Oklahoma.
- Jackson, D.D., Andrews, G.L., and Claridge, E.L., 1985, Optimum WAG Ratio vs. Rock Wettability in CO₂ Flooding, paper SPE 14303, presented at the SPE Annual Technical Conference and Exhibition, Las Vegas, Nevada.
- Jerauld, G.R., 1997, General Three-Phase Relative Permeability Model for Prudhoe Bay: SPE Reservoir Engineering, paper SPE 36178, (11).
- Johnson, E.F., Bossler, D.P., and Naumann, V.O., 1959, Calculation of Relative Permeability from Displacement Experiments, paper SPE 001023-G,
- Kerig, P.D., and Watson, A.T., 1986, Relative-Permeability Estimation From Displacement Experiments: An Error Analysis: SPE Reservoir Engineering, paper SPE 12589, (03).
- Kirkpatrick, R.K., Flanders, W.A., and DePauw, R.M., 1985, Performance of the Twofreds CO₂ Injection Project, paper SPE 14439, presented at the SPE Annual Technical Conference and Exhibition, Las Vegas, Nevada.
- Land, C.S., 1968, Calculation of Imbibition Relative Permeability for Two- and Three-Phase Flow From Rock Properties, paper SPE 1942, (06).
- Land, C.S., 1971, Comparison of Calculated with Experimental Imbibition Relative Permeability, paper SPE 3360, (12).
- Langston, E.P., and Shirer, J.A., 1985, Performance of Jay/LEC Fields Unit Under Mature Waterflood and Early Tertiary Operations: SPE Journal of Petroleum Technology, paper SPE 11986, (02).
- Larsen, J.A., and Skauge, A., 1998, Methodology for Numerical Simulation With Cycle-Dependent Relative Permeabilities: SPE Journal, paper SPE 38456, (06).
- Leverett, M.C., and Lewis, W.B., 1941, Steady Flow of Gas-oil-water Mixtures through Unconsolidated Sands, paper SPE 941107-G,

- Longeron, D.G., 1980, Influence of Very Low Interfacial Tensions on Relative Permeability, paper SPE 7609, (10).
- Ma, T.D., Rugen, J.A., Stoitsits, R.F., and Voungren, G.K., 1995, Simultaneous Water and Gas Injection Pilot at the Kuparuk River Field, Reservoir Impact, paper SPE 30726, presented at the SPE Annual Technical Conference and Exhibition, Dallas, Texas.
- MacLean, D.A., 1989, Design Of A Field-Wide Hydrocarbon Miscible Flood For The Kaybob Beaverhill Lake" A" Pool, paper SPE 89-03-01, (05-06).
- Magruder, J.B., Stiles, L.H., and Yelverton, T.D., 1990, Review of the Means San Andres Unit CO₂ Tertiary Project: SPE Journal of Petroleum Technology, paper SPE 17349, (05).
- Masoner, L.O., Abidi, H.R., and Hild, G.P., 1996, Diagnosing CO₂ Flood Performance Using Actual Performance Data, paper SPE 35363, presented at the SPE/DOE Improved Oil Recovery Symposium, Tulsa, Oklahoma.
- Moffitt, P.D., and Zornes, D.R., 1992, Postmortem Analysis: Lick Creek Meakin Sand Unit Immiscible CO₂ Waterflood Project, paper SPE 24933, presented at the SPE Annual Technical Conference and Exhibition, Washington, D.C.
- Mogensen, K., Hood, P., Jones, R.A., and Noman, R., 2010, Gas Injection Project in the KharaiB B Reservoir of the Giant Al Shaheen Field, paper SPE 129565, presented at the SPE EOR Conference at Oil & Gas West Asia, Muscat, Oman.
- Moulu, J.-C., Vizika, O., Egermann, P., and Kalaydjian, F., 1999, A New Three-Phase Relative Permeability Model For Various Wettability Conditions, paper SPE 56477, presented at the SPE Annual Technical Conference and Exhibition, Houston, Texas.
- Naar, J., and Wygal, R.J., 1961, Three-Phase Imbibition Relative Permeability, paper SPE 90, (12).
- Oak, M.J., 1990, Three-Phase Relative Permeability of Water-Wet Berea, paper SPE 20183, presented at the SPE/DOE Enhanced Oil Recovery Symposium, Tulsa, Oklahoma.
- Osoba, J.S., Richardson, J.G., Kerver, J.K., Hafford, J.A., and Blair, P.M., 1951, Laboratory Measurements of Relative Permeability, paper SPE 951047-G,
- Panda, M., Nottingham, D., and Lenig, D., 2011, Systematic Surveillance Techniques for a Large Miscible WAG Flood: SPE Reservoir Evaluation & Engineering, paper SPE 127563-PA, (06).
- Parrish, D.R., 1966: US, Patent Number :3,244,228.
- Pejic, D., and Maini, B.B., 2003, Three-Phase Relative Permeability of Petroleum Reservoirs, paper SPE 81021, presented at the SPE Latin American and Caribbean Petroleum Engineering Conference, Port-of-Spain, Trinidad and Tobago.
- Petersen, E.B., Lohne, A., Vatne, K.O., Helland, J.O., G.Virnovsky, and P.Eric Øren 2008, Relative Permeabilities For Two- And Three Phase Flow Processes Relevant To The Depressurization Of The Staffjord Field, presented at the International Symposium of the Society of Core Analysts, Abu Dhabi, UAE.

- Poolen, H.V., 1980, Fundamentals of Enhanced Oil Recovery: Tulsa, Pennwell Corp.
- Quijada, M.G., 2005, Optimization of A CO₂ Flood Design Wasson Field - West Texas: Master of Science thesis Texas, Texas A&M.
- Ramachandran, K.P., Gyani, O.N., and Sur, S., 2010, Immiscible Hydrocarbon WAG: Laboratory to Field, paper SPE 128848, presented at the SPE Oil and Gas India Conference and Exhibition, Mumbai, India.
- Righi, E.F., Royo, J., Gentil, P., Castelo, R., Monte, A.D., and Bosco, S., 2004, Experimental Study of Tertiary Immiscible WAG Injection, paper SPE 89360, presented at the SPE/DOE Symposium on Improved Oil Recovery, Tulsa, Oklahoma.
- Rogers, J.D., and Grigg, R.B., 2000, A Literature Analysis of the WAG Injectivity Abnormalities in the CO₂ Process, paper SPE 59329-MS, presented at the SPE/DOE Improved Oil Recovery Symposium, Tulsa, Oklahoma.
- Shyeh-Yung, J.-G.J., 1991, Mechanisms of Miscible Oil Recovery: Effects of Pressure on Miscible and Near-Miscible Displacements of Oil by Carbon Dioxide, paper SPE 22651, presented at the SPE Annual Technical Conference and Exhibition, Dallas, Texas.
- Skauge, A., and Aarra, M., 1993, Effect of wettability on the oil recovery by WAG, presented at the 7th IOR symp, Moscow.
- Skauge, A., and Berg, E., 1997 Immiscible WAG Injection in the Fensfjord Formation of the Brage Oil Field, presented at the European Symposium on Improved Oil Recovery, Hague.
- Skauge, A., and Larsen, J.A., 1994, Three-phase relative permeabilities and trapped gas measurements related to WAG processes, presented at the SCA, Stavanger.
- Sohrabi, M., Danesh, A., Tehrani, D., and Jamiolahmady, M., 2008, Microscopic mechanisms of oil recovery by near-miscible gas injection: *Transp. Porous Media*, **72**, p. 351-367.
- sohrabi, m., Danesh, A., and Tehrani, D.H., 2005, Oil Recovery by Near-Miscible SWAG Injection, paper SPE 94073, presented at the SPE Europec/EAGE Annual Conference, Madrid, Spain.
- Sohrabi, M., Henderson, G.D., Tehrani, D.H., and Danesh, A., 2000, Visualisation of Oil Recovery by Water Alternating Gas (WAG) Injection Using High Pressure Micromodels - Water-Wet System, paper SPE 63000, presented at the SPE Annual Technical Conference and Exhibition, Dallas, Texas.
- Sorbie, K.S., and Dijke, M.I.J.v., 2010, The Mechanism of Oil Recovery by Water-Alternating-Gas Injection at Near-Miscible Conditions in Mixed Wet Systems, paper SPE 129837, presented at the SPE Improved Oil Recovery Symposium, Tulsa, Oklahoma, USA.
- Spiteri, E.J., 2005, relative permeability hysteresis: a new model and impact on reservoir simulation: the degree of master of science thesis, STANFORD.
- Stalkup Jr., F.I., 1983, Status of Miscible Displacement: *SPE Journal of Petroleum Technology*, paper SPE 9992, (04).

- Stenmark, H., and Andfossen, P.O., 1995, Snorre WAG Pilot—A Case Study, presented at the European IOR Symposium, Vienna, Austria.
- Stone, H.L., 1970, Probability Model for Estimating Three-Phase Relative Permeability: SPE Journal of Petroleum Technology, paper SPE 2116, (02).
- Stone, H.L., 1973, Estimation of Three-Phase Relative Permeability And Residual Oil Data, paper SPE 73-04-06, (10-12).
- Suicmez, V.S., Piri, M., and Blunt, M.J., 2006, Pore-Scale Modeling of Three-Phase WAG Injection: Prediction of Relative Permeabilities and Trapping for Different Displacement Cycles, paper SPE 95594, presented at the SPE/DOE Symposium on Improved Oil Recovery, Tulsa, Oklahoma, USA.
- Surguchev, M., 1985, Methods of Secondary and Tertiary Oil Recovery, presented at the European IOR Symposium, Nedra, Moscow.
- Svirsky, D.S., Dijke, M.I.J.v., and Sorbie, K.S., 2004, Prediction of Three-Phase Relative Permeabilities Using a Pore-Scale Network Model Anchored to Two-Phase Data, paper SPE 89992, presented at the SPE Annual Technical Conference and Exhibition, Houston, Texas.
- Tanner, C.S., Baxley, P.T., Crump III, J.G., and Miller, W.C., 1992, Production Performance of the Wasson Denver Unit CO₂ Flood, paper SPE 24156, presented at the SPE/DOE Enhanced Oil Recovery Symposium, Tulsa, Oklahoma.
- Thomas, F.B., Holowach, N., Zhou, X., Bennion, D.B., and Bennion, D.W., 1994, Miscible or Near-Miscible Gas Injection, Which Is Better?, paper SPE 27811, presented at the SPE/DOE Improved Oil Recovery Symposium, Tulsa, Oklahoma.
- Vizika, O., and Lombard, J.-M., 1996, Wettability and Spreading: Two Key Parameters in Oil Recovery With Three-Phase Gravity Drainage: SPE Reservoir Engineering, paper SPE 28613, (02).
- Watts, R.J., Conner, W.D., Wasson, J.A., and Yost II, A.B., 1982, CO₂ Injection for Tertiary Oil Recovery, Granny's Creek Field, Clay County, West Virginia, paper SPE 10693, presented at the SPE Enhanced Oil Recovery Symposium, Tulsa, Oklahoma.
- Williams, J.K., and R.A. Dawe, R.A., 1988, Gravity effects in near-critical fluids in porous media: *J. Colloid Interface Sci.*, 124, p. 81-86.

Chapter 2

Coreflood Experiments

In order to generate a reliable source of data for a simulation study, a comprehensive set of coreflood experiments were performed at Heriot-Watt University using different cores with different wettability conditions. The experiments utilized in this research have been conducted by another PhD student (Fatemi et al., 2011) and the present author was not been involved in the laboratory work.

In this chapter descriptions of the experimental facilities and procedures followed to perform unsteady state coreflood experiments are presented together with descriptions of the core and fluids employed in the experimental work.

2.1 Coreflood Facility

A high-pressure coreflood facility was used to perform core experiments, including two-phase and three-phase experiments. The rig can take large cores of 2-inch diameter and up to around 3 feet (one meter) long. The core-flooding rig is equipped with an X-ray scanner which is used to investigate and monitor the core heterogeneity, distribution of irreducible water saturation and front propagation. The X-ray results are also used to check for experimental artefacts, such as capillary end effects, which in our experiments were not an issue due to the use of long cores.

All the displacement tests in this study were conducted into the horizontal core while the core was rotating along the horizontal axis hence the gravity force is negligible compare to viscous forces.

Figure 2-1 shows a schematic diagram of this coreflood rig. The rig has been designed to work at pressures as high as 6000 psia, with all components and their content being kept at a controlled temperature of 38 °C. The rig is equipped with six independent pumps that allow both unsteady state displacement and steady state circulation of fluids through the core.

The test fluids are present in stainless steel piston cells, with brine being injected into or withdrawn from the base of the cells by the displacement pumps to circulate the fluids around the flow system. To allow circulation of fluids through the core, two cells are allocated for each fluid, one initially full and the other initially empty. Using one of the pump barrels, gas is displaced from the piston cell initially full of gas, through the core to the large 100 cc sight glass at the core outlet. Gas is then recovered from the top of the sight glass to fill the initially empty gas cell by withdrawing water, using the second barrel of the pump. A similar procedure is followed to circulate liquid (e.g. water), using the second pump, with the liquid (oil or water) being recovered from the base of the sight glass. Differential pressure is measured using two high accuracy transducers located at the inlet and outlet of the core. The transducers provide stable differential pressure data with an accuracy of 0.01 psi during the course of the tests.

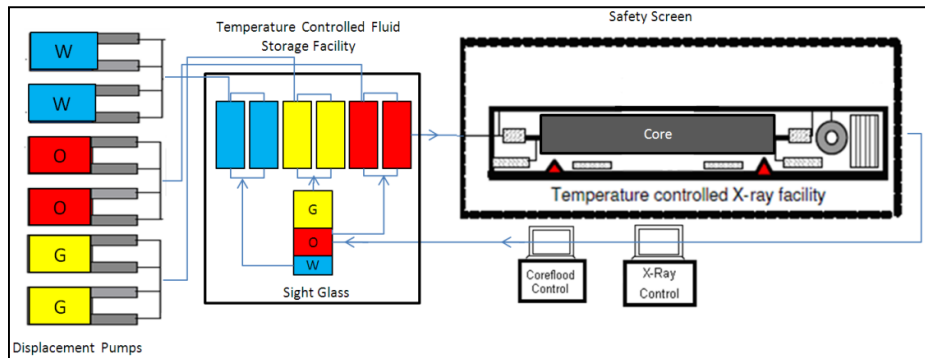


Figure 2-1: High pressure coreflood facility used for flooding tests.

2.2 Experimental Procedures

2.2.1 Core Preparation and Tracer Analysis

Prior to performing coreflood experiments, a preparation procedure was followed to determine properties of the core and also check the degree of its homogeneity.

Initially, the core was weighed and the length/area measurements taken to estimate the bulk volume. Then the core was loaded into a core holder and an X-ray scan was run to examine homogeneity of the core prior to performing the coreflood tests. This allowed us to obtain the profile of porosity along the core. Figure 2-2 depicts the profile of the porosity along the length of the 65mD core. As can be seen, apart from some normal fluctuations, the porosity value is relatively the same along the core, which indicates that there are no major heterogeneities (no fracture or shale, etc) in the core and indicates relatively homogeneous distribution for the pore volume within the core.

The helium porosity and nitrogen permeability of the core were then measured, followed by evacuation of the core, after which it was saturated with a 1% brine solution. The amount of brine imbibed into the core was measured and gave a second measurement of pore volume. A 1% sodium chloride/calcium chloride brine solution was used in order to desensitize any clay minerals and prevent them from swelling and restricting flow. The water permeability was measured, prior to core characterization.

Tracer analysis of the core was then conducted to ensure that there are no major heterogeneities, such as fractures or permeability layers, in the core, which, if not detected, might influence the results of multiphase flow experiments. This procedure also provides an accurate measurement of the pore volume of the core.

Two cores with the different permeability were used for performing unsteady-state coreflood experiments. The physical properties of these cores are given in Table 2-1. Both cores were chosen to be long enough to minimize the capillary end effect while performing flooding tests.

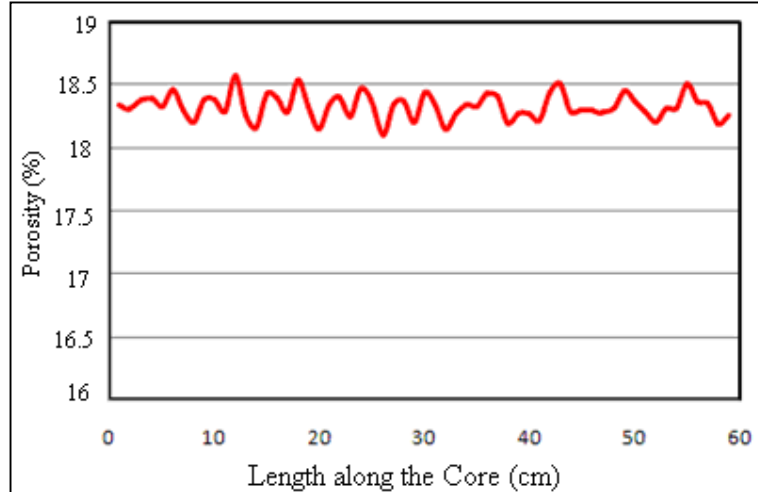


Figure 2-2: Porosity profile along the 65mD core, obtained by X-ray scan.

Table 2-1: Core properties

Core	Length cm	Diameter cm	Porosity frac.	Absolute Permeability mD
Clashach Sandstone	66.5	4.86	0.176	1000
Clashach Sandstone	60.5	5.08	0.1818	65

2.2.2 Establishing Connate Water Saturation

To establish connate water saturation, a heavy (viscous) mineral oil was initially injected into the brine-saturated core. The injection of this oil was continued until water production was greatly reduced. The viscous oil was then displaced by injecting a light (less viscous) mineral oil and subsequently by injecting Decane ($n\text{-C}_{10}$) over a period of days, to ensure that all of the mineral oil had been removed. Decane was then displaced by the injection of methane at high pressure (more than 5000 psi), to ensure miscible displacement, with the effluent from the core being monitored using gas chromatography, until there was no trace of Decane. To ensure no vaporization of the water in the core occurred during the tests, all the hydrocarbon fluids were maintained in equilibrium with water before entering the core.

The connate water establishment process resulted in 8% and 18% water saturation for 1000mD and 65mD rock, respectively.

The profile of the established immobile water saturation along the core was also obtained using X-ray analysis, which is shown in Figure 2-3 for 65mD core. This figure shows that water saturation distribution along the core is almost homogenous and the value (18%) is comparable with that obtained from the material balance (18.2%). Such x-ray scans were initially performed in both water-wet and mixed-wet conditions. Figure 2-3 shows both scans, which are very close, and indicates that the established immobile water saturations for the two wettability conditions are the same.

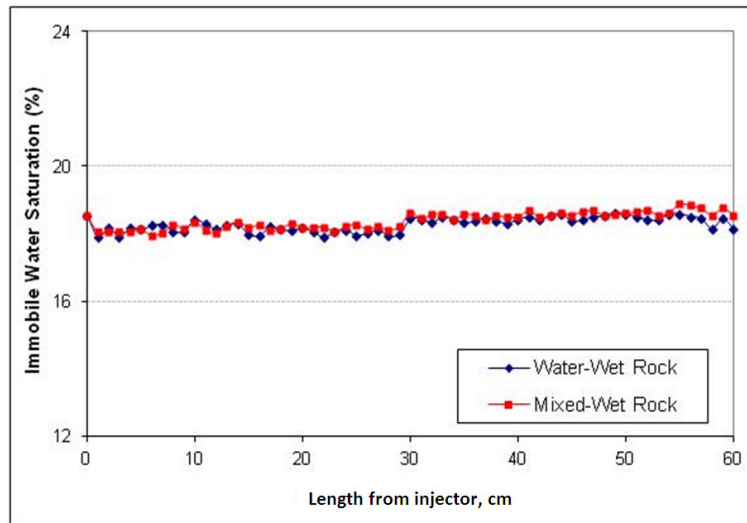


Figure 2-3: Established immobile water saturation along the core, obtained from X-ray for 65mD water-wet and mixed-wet cores.

2.2.3 Test Fluids

The brine used in the experiments was synthesized using Sodium Chloride (NaCl) and Calcium Chloride (CaCl₂) in distilled water and was degassed before use. The brine does not represent a particular reservoir's brine and is used with the main objective of desensitising any existing clay minerals in the core and preventing possible adverse reactions between water and clay (e.g. clay swelling). The hydrocarbon fluid system used in the tests is prepared from a binary mixture of methane (C₁) and n-butane (n-C₄). The mixture has a composition of 73.6 mol% methane and 26.4 mol% n-butane. To

eliminate mass transfer during the displacement experiments, all the fluids (oil, gas and brine) were pre-equilibrated at the test pressure and temperature of 1840 psia and 37.8°C and were kept under these conditions in high-pressure transfer vessels kept in a temperature-controlled oven. Table 2-2 shows the physical properties of the hydrocarbon vapour (gas) and that of hydrocarbon liquid (oil), at the prevailing conditions of the experiments. The hydrocarbon density and viscosity were measured in laboratory. The IFT values were measured in our laboratories by pendant drop method and represent equilibrium values within the equilibrium 3-phase system (Jamiolahmady et al., 2007). The PVT model of the hydrocarbon fluid is built using a PVTi package and tuned using experimental data. Figure 2-4 depicts the phase envelope (P-T diagram) of C_1 and nC_4 obtained by the PVTi software. The composition of the hydrocarbon components in the vapour and liquid phases at the equilibrium condition (1840 psia and 37.8 °C) are calculated using the package provided in Table 2-3. To ensure that the mass transfer and compositional effect between oil and gas during displacement experiments is negligible, a synthetic gas injection test into the core established with residual oil ($S_{orw} = 21\%$) and water saturation ($S_w = 79\%$) was simulated by compositional software (Eclipse300). The variation of fluid properties (viscosity and interfacial tension) alongside the core throughout the gas injection test is plotted in Figure 2-5, demonstrating insignificant change in both viscosity and IFT of the hydrocarbon system along the core.

As shown in Table 2-2, the interfacial tension between oil and gas is very low and fluids are at near miscible condition. The mechanisms involved in the flow and displacement of low IFT gas/oil systems at near miscibility are different from those for both miscible and immiscible systems (Shyeh-Yung, 1991; Thomas et al., 1994; Sohrabi et al., 2005; Sorbie and Dijke, 2010). Near-miscible gas injection happens in a wider range of gas injection processes in oil reservoirs, including high pressure hydrocarbon gas injection, CO₂ injection, multiple contact miscibility, etc. (Harbert, 1983; Christensen et al., 2001; Dong et al., 2001; Bui et al., 2010).

Table 2-2: Properties of hydrocarbon mixture and brine at 1840psia and 37.8 °C

Fluid	ρ_g (kg/m ³)	ρ_L (kg/m ³)	μ_g (mPa.s)	μ_L (mPa.s)	IFT mN/m
Hydrocarbon	211.4	317.4	0.0249	0.0405	σ (o/g) = 0.047
Brine	-	992.96	-	0.68	σ (o/w) = 55 σ (g/w) = 60

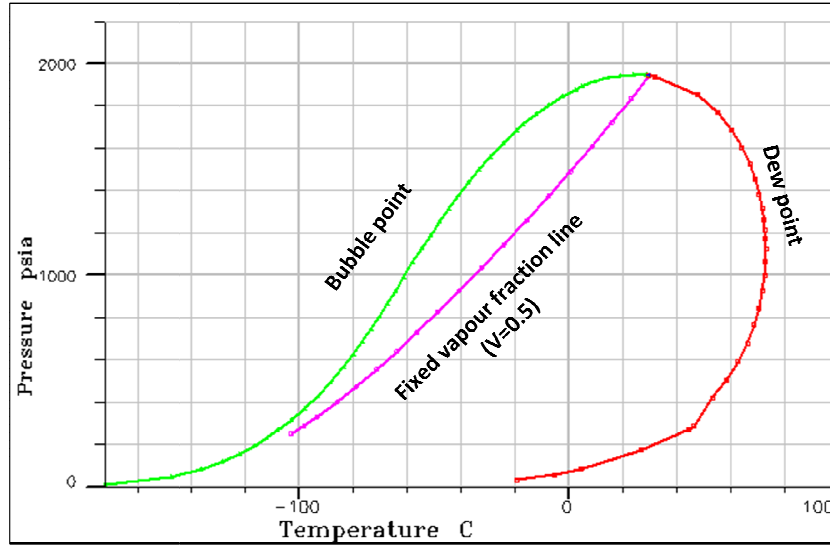


Figure 2-4: Phase envelope of mixture of C₁ and n-C₄, obtained by PVTi package.

Table 2-3: Composition (mole %) of hydrocarbon vapour and liquid at equilibrium condition (1840psia and 37.8 C).

	Mole% in Vapour Phase	Mole% in Liquid Phase
Methane (C1)	78.37	36.99
n-Butane (n-C4)	21.63	63.01

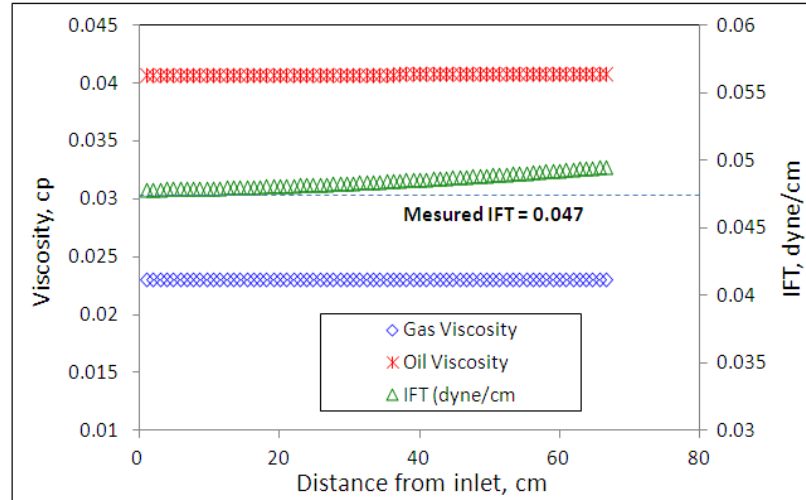


Figure 2-5: Variation of hydrocarbon viscosity and interfacial tension between oil/gas alongside the core, obtained from compositional simulation of a gas injection test into the 1000mD core, established with residual oil ($S_{orw}=21\%$) and water ($S_w = 79\%$).

2.2.4 Development of Mixed-Wettability

The actual wettability of many oil reservoir rocks is at mixed-wet condition and several studies have been directed so far to investigate the impact of wettability on the fluid flow parameters (Ayirala, 2002; Graue et al., 2002; Hwang et al., 2006). The wettability alteration processes in the coreflood laboratories is a very challenging and time consuming procedure. Also, the validity of using water-wet data for mixed-wet conditions is always questionable. To address this question, we performed the coreflood tests under different wettability conditions, to demonstrate the importance of wettability on three-phase relative permeability.

Core wettability can be altered by either suitable chemicals or by ageing in suitable crude oils. Although using chemicals is less time consuming and involves a relatively simpler procedure, the stability of the modified wettability is generally poor and open to question. Ageing in crude oils involves a more difficult procedure and requires careful planning and is much more time consuming. However, once a modified wettability condition has been achieved, it can be very stable and long lasting.

The core wettability was altered by ageing in suitable crude oils. Areas of rock surface not overlain by bulk water are subject to wettability alteration by adsorption of polar compounds from crude oil, while areas containing bulk water will retain their original

wettability. Before attempting to alter the wettability of the main rock, we tested our procedure on small core plugs and thin slides taken from the same rock. The resultant modified wettability was analysed and evaluated by both Environmental Scanning Electron Microscope (ESEM) and by wettability index (Amott and USBM) determination (Sohrabi, 2007).

Wettability of the treated thin sections was evaluated by direct visualization, using ESEM, where their surface was exposed to water condensation in an enclosed chamber. Figure 2-6 shows a magnified picture of rock grains in an untreated (water-wet) Clashach thin section. Because the rock was strongly water-wet, it was not possible for the condensing water to form droplets on the surface; the water would instead cover the grain surface with an evenly spread layer. The same thin section was pre-wet with the brine and soaked in the crude oil which was being used for making the core plugs mixed-wet. After four days of being exposed to the crude oil, the thin section was taken out and placed under the microscope again to evaluate its wettability by gradually exposing its surface to water condensation. This time, the water was observed to form droplets of varying size and contact angle on the surface. This was a direct consequence of the surface being exposed to the crude oil and wettability alteration, as a result of adsorption of organic material to the grains surface. Figure 2-7 shows magnified picture taken from this thin section (Fatemi et al., 2011).

In this research thesis “MW” and “WW” are referred to the mixed-wet and water-wet rock condition, respectively.

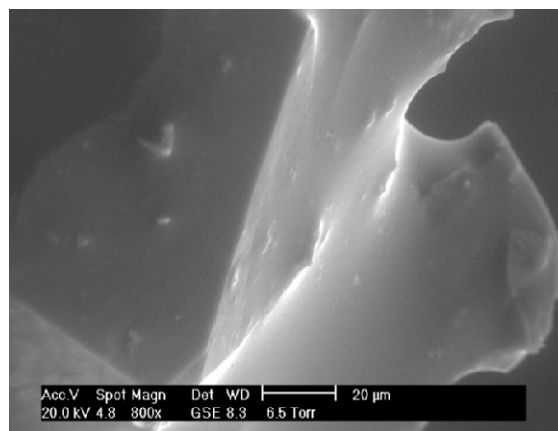


Figure 2-6: ESEM picture for a thin section of water-wet rock: water droplets were not formed on the grains of the untreated Clashach thin section, indicating that the sand grains were strongly water-wet.

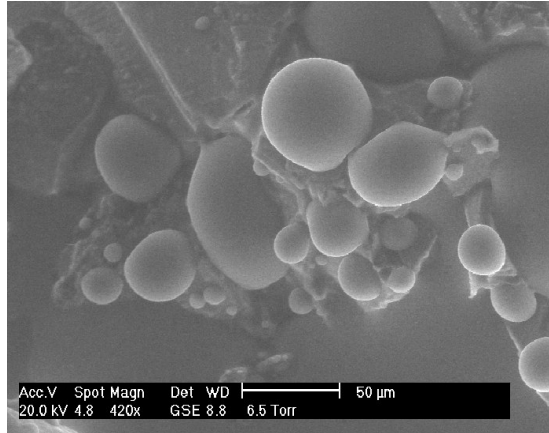


Figure 2-7: ESEM picture for a thin section of mixed-wet rock :grains in a thin section which had been exposed to the crude oil for four days showed signs of wettability alteration from water-wet towards oil-wet. Water formed droplets on the grain surfaces rather than films.

2.3 Coreflood experiments

In order to generate a reliable source of data for simulation purpose, a high-quality set of coreflood experiments were conducted in 1000mD mixed-wet, 65mD water-wet and 65mD mixed-wet core. All the coreflood tests were carried out using the unsteady-state method, in which one fluid is injected through the core to displace the resident fluids inside the core.

2.3.1 Two-phase experiment

One of the most common approaches in modelling of three-phase relative permeability is to employ two-phase relative permeability data in some of the existing models e.g. Stone, Baker to calculate the three-phase relative permeability values. Prior to performing three-phase experiments, a comprehensive set of unsteady-state two-phase experiments were conducted in order to obtain accurate two-phase relative permeability data on the cores for which three-phase relative permeability values would be calculated and measured. The two-phase experiments were carried out using all two-phase fluid combinations, i.e., oil/water, oil/gas and gas/water in different sequences. All two-phase experiments were performed in the presence of irreducible (connate) water saturation. Also, to investigate the hysteresis phenomenon in WAG simulation, the two-phase experiments were conducted in different flow directions, i.e. imbibition and drainage. Table 2-4 shows list of unsteady-state two-phase displacement tests carried

out on 65mD and 1000mD cores with some details of experiments including total injected fluid, injection rate and initial fluid saturations.

The Sendra software (2005) was employed to obtain two-phase relative permeabilities of the unsteady-state experiments (Table 2-4) by matching the production and differential pressure data of the simulation with those resulting from the experiments. There are several types of two-phase correlations (Burdine, 1953; Corey, 1954; Sigmund and McCaffery, 1979; Chierici, 1984; Lomeland., 2005) available in the Sendra package. Indeed, the variables of one selected model are automatically changed in an iterative process, such that the production and pressure results of the simulation have the least discrepancy with the corresponding measured data from the experiment. Figure 2-8 to Figure 2-10 show the two-phase relative permeability of oil/water, oil/gas and gas/water systems of 65mD core for both drainage and imbibition processes, obtained from unsteady-state displacement tests. The solid lines in these figures represent the trusted relative permeability points for the saturation range met by the experiment, while the dashed line depicts the extrapolated relative permeability beyond that saturation interval, by two-phase correlation in Sendra.

Two-phase oil/water capillary pressure (P_{cow}) of 1000mD and 65mD cores for both drainage and imbibition processes, measured by the centrifuge method, are shown in Figure 2-11 and Figure 2-12, respectively.

Table 2-4: List of unsteady-stated two-phase experiments performed at 1840 pisa and 37.8 C.

No.	Permeability mD	Wettability	Direction	Involved Fluids	Total Injected Fluid (Pore Volume)	Injection rate,cc/hr	Initial Saturation: Soi, Swi, Sgi
1	1000	Mixed-Wet	Water Injection	Oil/Water	0.917	200	0.92, 0.08, 0
2	1000	Mixed-Wet	Gas Injection	Oil/Gas	7.5	200	0.92, 0.08, 0
3	1000	Mixed-Wet	Oil Injection	Oil/Gas	2.15	200	0, 0.08, 0.92
4	1000	Mixed-Wet	Water Injection	Gas/Water	0.917	200	0, 0.49, 0.51
5	65	Water-Wet	Water Injection	Oil/Water	0.973	25	0.82, 0.18, 0
6	65	Water-Wet	Oil Injection	Oil/Water	3.43	50, 100, 200	0, 1, 0
7	65	Water-Wet	Gas Injection	Oil/Gas	6.5	50, 100	0.82, 0.18, 0
8	65	Water-Wet	Oil Injection	Oil/Gas	2.242	50, 100	0, 0.18, 0.82
9	65	Mixed-Wet	Water Injection	Oil/Water	0.973	25	0.82, 0.18, 0
10	65	Mixed-Wet	Oil Injection	Oil/Water	2.9	50, 100	0, 1, 0
11	65	Mixed-Wet	Gas Injection	Oil/Gas	9.46	50, 100	0.82, 0.18, 0
12	65	Mixed-Wet	Oil Injection	Oil/Gas	1.6	50	0, 0.18, 0.82
13	65	Mixed-Wet	Water Injection	Gas/Water	1.2	50	0, 0.18, 0.82
14	65	Mixed-Wet	Gas Injection	Gas/Water	7	50, 100	0, 1, 0

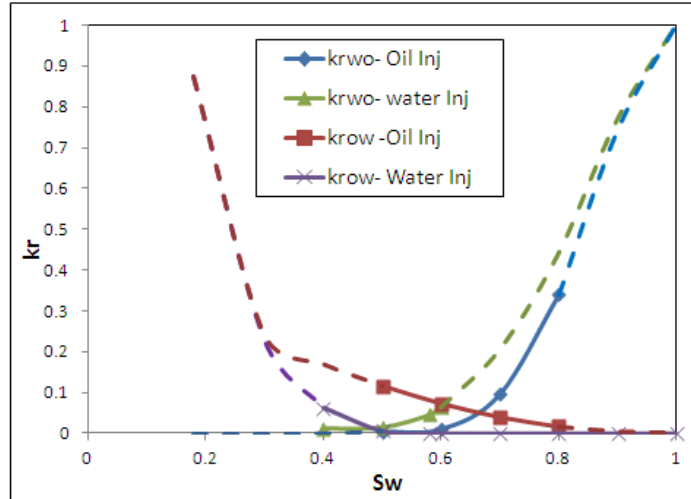


Figure 2-8: Two-phase relative permeability of 65mD-WW core for oil/water system (k_{row} and k_{rwo}) versus water saturation, obtained from water injection and oil injection (Experiments#5 & 6).

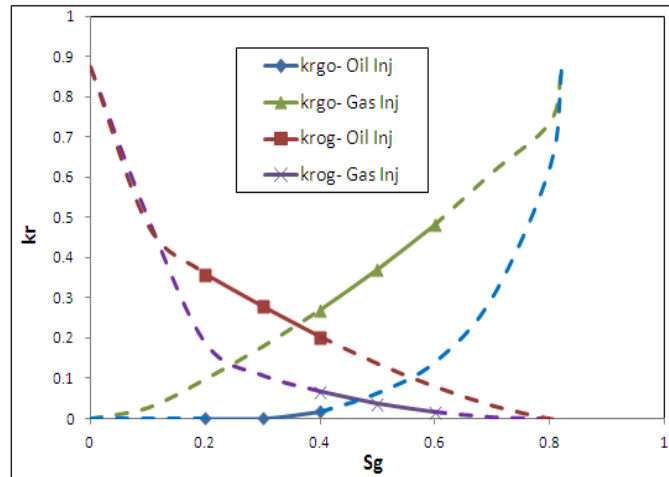


Figure 2-9: Two-phase relative permeability of 65mD-WW core for oil/gas system (k_{rog} and k_{rgo}) versus gas saturation, obtained from gas injection and oil injection (Experiments#7 & 8).

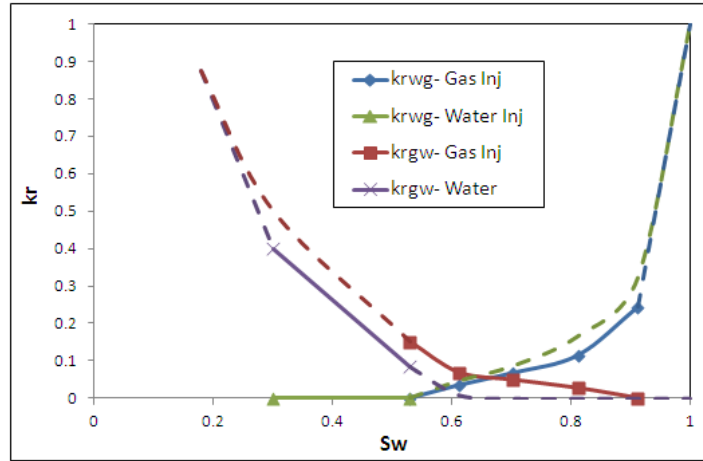


Figure 2-10: Two-phase relative permeability of 65mD-MW core for gas/water system (k_{rgw} and k_{rwg}) versus water saturation, obtained from water injection and gas injection (Experiment#13 & 14).

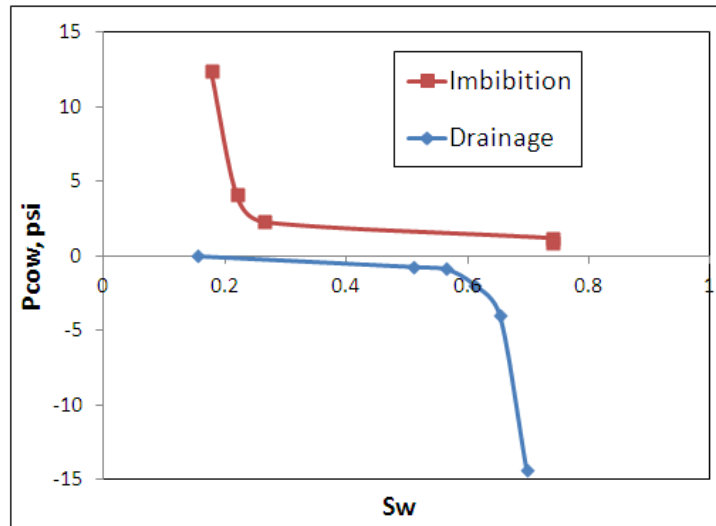


Figure 2-11: Two-phase oil/water capillary pressure of 1000mD rock versus water saturation for imbibition and drainage processes, measured by centrifuge method.

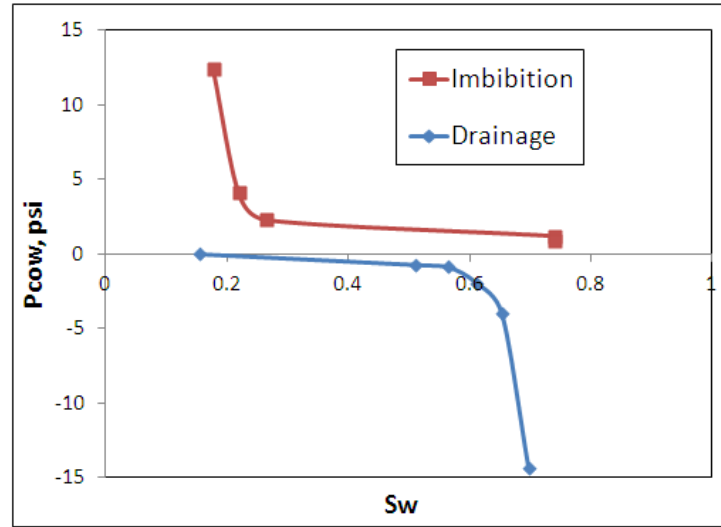


Figure 2-12: Two-phase oil/water capillary pressure of 65mD rock versus water saturation for imbibitions and drainage process, s calculated by J-function from P_{cow} of 1000mD core (Figure 2-11).

2.3.2 Three-phase experiments

Having performed a series of two-phase flow experiments, the WAG injection was carried out, starting with water injection, followed by two consecutive cycles of gas and water injection into the 1000mD mixed-wet core, which was initially saturated with 92% oil and 8% irreducible water. Also, three-cycle WAG experiments, starting with water injection at 50cc/hr were conducted in 65 mD water-wet and mixed-wet cores, where both had been initially saturated with 82% oil and 18% immobile water. The average calculated capillary numbers for our coreflood experiment is around 8×10^{-7} .

A list of different cycles of the WAG injection tests and injection rate, as well as the total injected fluid of each individual WAG cycle, is provided in Table 2-5. Hereafter, 1000mD-MW, 65mD-WW and 65mD-MW are referred to as the WAG experiments performed on 1000 mD mixed-wet, 65 mD water-wet and 65 mD-MW cores, respectively.

The saturation path in the experiment is determined by volumetric material balance calculation, knowing the amount of injected and produced fluid and initial saturation of the core. Figure 2-13, Figure 2-14 and Figure 2-15 demonstrate the saturation path for WAG experiments through 1000mD-MW, 65mD-WW and 65mD-MW cores as ternary

diagrams. The notation G_i and W_i ($i=1, 2, \dots$) in these ternary diagrams refers to the saturation paths of i^{th} gas injection and water injection, respectively.

Table 2-5: List of WAG injection experiments performed at 1840 pisa and 37.8 C.

No.	Permeability (mD)	Wettability	Direction	Total Injected Fluid (Pore Volume)	Injection rate, cc/hr
1	1000	Mixed-Wet	1st Water Injection	0.917	200
2	1000	Mixed-Wet	1st Gas Injection	1.445	200
3	1000	Mixed-Wet	2nd Water Injection	0.917	200
4	1000	Mixed-Wet	2nd Gas Injection	1.65	200
6	65	Water-Wet	1st Water Injection	0.973	25
7	65	Water-Wet	1st Gas Injection	6.21	25, 50, 100
8	65	Water-Wet	2nd Water Injection	1.31	25, 12.5
9	65	Water-Wet	2nd Gas Injection	1.28	25, 50
10	65	Water-Wet	3rd Water Injection	1.107	25, 12.5
11	65	Water-Wet	3rd Gas Injection	2.488	25
12	65	Mixed-Wet	1st Water Injection	0.973	25
13	65	Mixed-Wet	1st Gas Injection	1.748	25, 50, 100
14	65	Mixed-Wet	2nd Water Injection	0.941	25
15	65	Mixed-Wet	2nd Gas Injection	1.3	25, 50, 100
16	65	Mixed-Wet	3rd Water Injection	0.708	25
17	65	Mixed-Wet	3rd Gas Injection	2.77	25, 50, 100

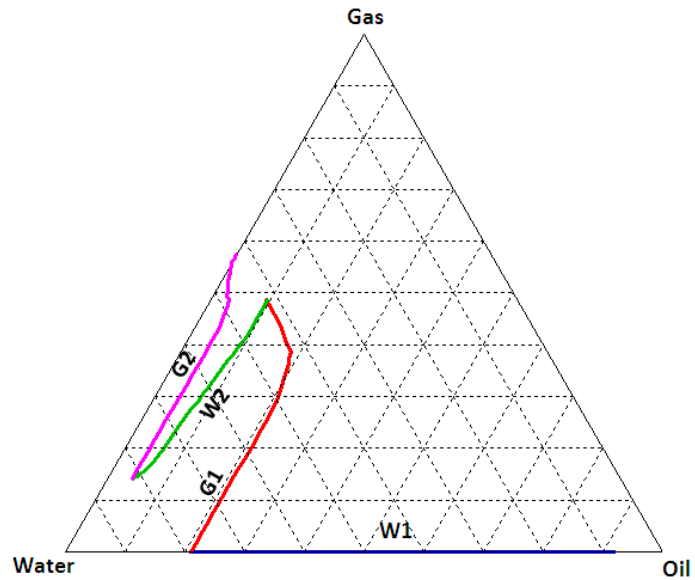


Figure 2-13: Saturation path of WAG experiment into 1000mD-MW core.

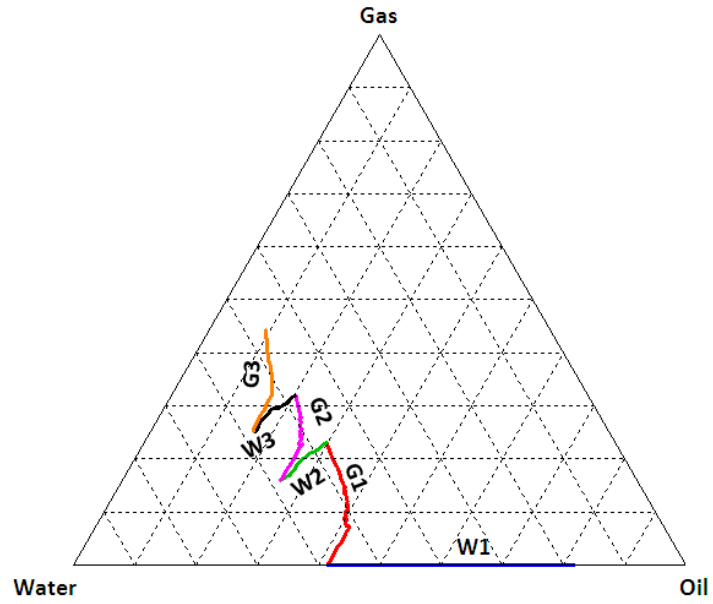


Figure 2-14: Saturation path of WAG experiment into 65mD-WW core.

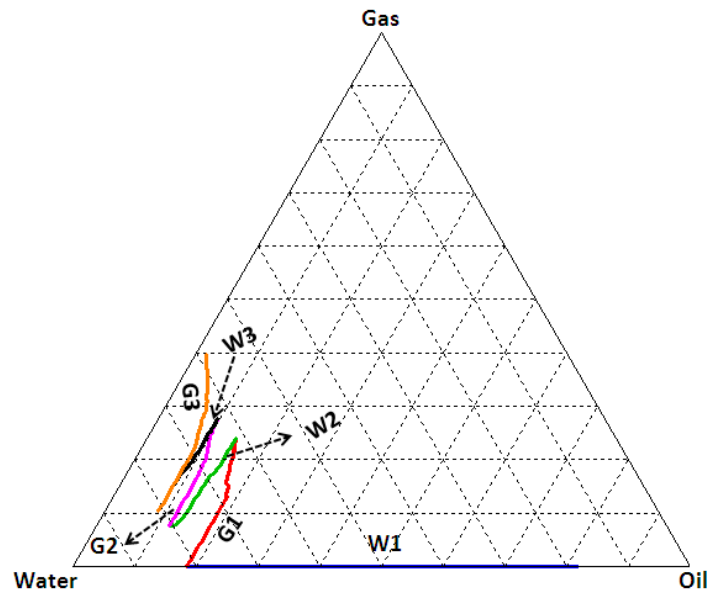


Figure 2-15: Saturation path of WAG experiment into 65mD-MW core.

2.4 References

- Ayirala, S.T., 2002, Surfactant-Induced Relative Permeability Modifications for Oil Recovery Enhancement: Msc thesis, Louisiana
- Bui, L.H., Tsau, J.-S., and Willhite, G.P., 2010, Laboratory Investigations of CO₂ Near Miscible Application in Arbuckle Reservoir, paper SPE 129710, presented at the SPE Improved Oil Recovery Symposium, Tulsa, Oklahoma, USA.
- Burdine, N.T., 1953, Relative Permeability Calculations From Pore Size Distribution Data, paper SPE 225-G.
- Chierici, G.L., 1984, Novel Relations for Drainage and Imbibition Relative Permeabilities.
- Corey, A.T., 1954, The Interrelation Between Gas and Oil Relative Permeabilities: *Prod. Monthly*, **19**, p. 38-41.
- Christensen, J.R., Stenby, E.H., and Skauge, A., 2001, Review of WAG Field Experience, paper SPE 39883, presented at the International Petroleum Conference and Exhibition of Mexico, Villahermosa, Mexico.
- Dong, M., Huang, S.S., and Srivastava, R., 2001, A Laboratory Study on Near-Miscible CO₂ Injection in Steelman Reservoir, paper SPE 01-02-05, (02).
- Graue, A., Aspenes, E., Bognø, T., Moe, R.W., and Ramsdal, J., 2002, Alteration of wettability and wettability heterogeneity: *Journal of Petroleum Science and Engineering*, **33** p. 3 – 17.
- Harbert, L.W., 1983, Low Interfacial Tension Relative Permeability, paper SPE 12171, presented at the SPE Annual Technical Conference and Exhibition, San Francisco, California.
- Hwang, S., Lee, K.P., Lee, D.S., and Powers, S., 2006, Effects of fractional wettability on capillary pressure–saturation–relative permeability relations of two-fluid systems: *Advances in Water Resources Journal*, **29** p. 212–226.
- Shyeh-Yung, J.-G.J., 1991, Mechanisms of Miscible Oil Recovery: Effects of Pressure on Miscible and Near-Miscible Displacements of Oil by Carbon Dioxide, paper SPE 22651, presented at the SPE Annual Technical Conference and Exhibition, Dallas, Texas.
- sohrabi, m., Danesh, A., and Tehrani, D.H., 2005, Oil Recovery by Near-Miscible SWAG Injection, paper SPE 94073, presented at the SPE Europec/EAGE Annual Conference, Madrid, Spain.
- Sorbie, K.S., and Dijke, M.I.J.v., 2010, The Mechanism of Oil Recovery by Water-Alternating-Gas Injection at Near-Miscible Conditions in Mixed Wet Systems, paper SPE 129837, presented at the SPE Improved Oil Recovery Symposium, Tulsa, Oklahoma, USA.
- Thomas, F.B., Holowach, N., Zhou, X., Bennion, D.B., and Bennion, D.W., 1994, Miscible or Near-Miscible Gas Injection, Which Is Better?, paper SPE 27811, presented at the SPE/DOE Improved Oil Recovery Symposium, Tulsa, Oklahoma.

- Fatemi, S.M., Sohrabi, M., Jamiolahmady, M., Ireland, S., and Robertson, G., 2011, Experimental Investigation of Near-Miscible Water-Alternating-Gas (WAG) Injection Performance in Water-wet and Mixed-wet Systems, paper SPE 145191, presented at the Offshore Europe, Aberdeen, UK.
- Jamiolahmady, M., Danesh, A., Sohrabi, M., and Ataei, R., 2007, Gas-Condensate Flow in Perforated Regions: SPE Journal, paper SPE 94072-PA, (03).
- Lomeland F., E.E., Thomas W.H., 2005, A New Versatile Relative Permeability Correlation, *International Symposium of the SCA*, Toronto, Canada.
- M. Sohrabi, D.H.T.a.M.A.-A., 2007, Performance of Near-Miscible Gas and Swag Injection in a Mixed-Wet Core, presented at the International Symposium of the Society of Core Analysts, Calgary, Canada.
- Sendra, 2005, Sendra, Weatherford Petroleum Consultants AS p. Sendra is a two-phase core flow simulator based on the black oil model, specially designed to replicate and verify SCAL experiments. Sendra determines relative permeability and capillary pressure for a well or field through an automated history matching approach, referred to as estimation.
- Sigmund, P.M., and McCaffery, F.G., 1979, An Improved Unsteady-State Procedure for Determining the Relative-Permeability Characteristics of Heterogeneous Porous Media (includes associated papers 8028 and 8777), paper SPE 6720, (02).

Chapter 3

Evaluation of Three-Phase Relative Permeability models

In this chapter, the most common three-phase relative permeability and hysteresis models available in a commercial reservoir simulator are introduced. Then, the simulation results of our coreflood experiments utilizing the above-mentioned relative permeability models are discussed.

3.1 Three-Phase Relative Permeability Models

As mentioned in the first chapter, three-phase relative permeabilities can be calculated from empirical correlations which use two-phase relative permeability data. A number of these models were basically developed for water-wet porous systems, assuming channel flow theory during three-phase flow (Stone, 1970; Hustad and Holt, 1992). The channel flow theory states that, in any flow channel, there is, at most, only one mobile fluid. A corollary of this theory for a water-wet system is that the wetting phase is located primarily in the small pore spaces and the non-wetting phase in the large pore spaces, and the intermediate phase spatially separates them. It follows that, at equal water saturations, the microscopic fluid distribution at the water-oil interface will be

identical in a water/oil system and in a water/oil/gas system, so long as the direction of change of water saturation is the same in both. This implies that water relative permeability in the three-phase system is a function of water saturation alone, irrespective of the relative saturations of oil and gas. Further, this is the same function in the three-phase system as in the two-phase water-oil system. Similarly, the gas phase relative permeability is the same function of gas saturation in the three-phase system as in the two-phase gas-oil system.

Other categories of three-phase k_r correlations were developed on the premise that all fluids' relative permeabilities (k_{ro} , k_{rw} , k_{rg}) are a function of two-independent saturation rather than their own saturation. This assumption is more suitable for mixed-wet formations (Baker, 1988). Figure 3-1 illustrates the possible pore occupancy of three-phase fluid for the mixed-wet and water-wet porous media. This figure demonstrates that at the water-wet condition the intermediate wet fluid (oil) is in contact with both wetting (water) and non-wetting fluid (gas,) whereas the wetting and non-wetting fluids are only in contact with intermediate phase. The three-phase fluid configuration at the mixed-wet rock (picture 2 in Figure 3-1) is such that the flow of each fluid would be affected by two other phases as opposed to the case of the water-wet rock, where only the flow of intermediate phase (oil) is influenced by two other fluids.

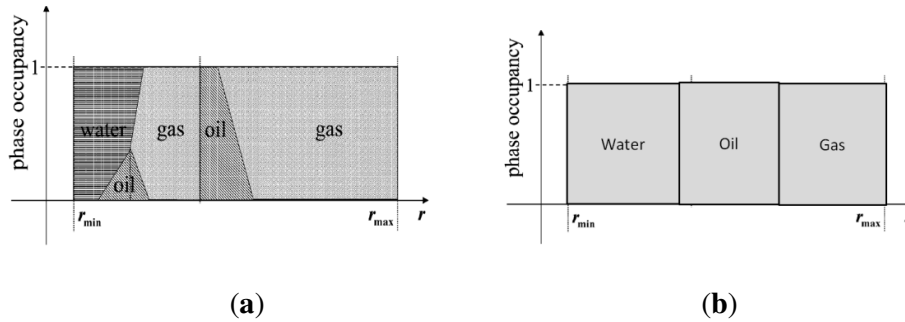


Figure 3-1: Possible pore occupancy of a mixed-wet (Figure a) and water-wet system (Figure b) (van Dijke and Sorbie, 2002)

The following section is accompanied the mathematical description of the most widely used three-phase relative permeability model available in commercial reservoir simulator (Eclipse).

3.1.1 Saturation-Weighted interpolation model

Baker (1988) used saturation-weighted interpolation between oil/water and oil/gas data to obtain three-phase oil relative permeability. In this model, the oil relative permeability is given by:

$$k_{ro} = \frac{S_g k_{rog} + (S_w - S_{wc}) k_{row}}{S_g + S_w - S_{wc}} \quad 3.1$$

where k_{rog} is the oil relative permeability for a system with oil, gas and connate water (S_{wc}) and k_{row} is the oil relative permeability for a system with oil and water only. Baker (1988) also proposed similar equations for estimating three-phase gas and water relative permeabilities using two-phase data:

$$k_{rw} = \frac{S_o k_{rwo} + S_g k_{rwg}}{S_g + S_w} \quad 3.2$$

$$k_{rg} = \frac{S_o k_{rgo} + (S_w - S_{wc}) k_{rgw}}{S_o + S_w - S_{wc}} \quad 3.3$$

where k_{rwo} and k_{rwg} are water relative permeability for the water/oil and water/gas systems, respectively. k_{rgo} is gas relative permeability for a system with gas, oil and connate water and k_{rgw} is gas relative permeability for gas/water system. In this study we refer to *SWI-1* while only using oil relative-permeability model (equation 3.1) and assuming that gas and water relative permeability are the same function in the three-phase system as in the two-phase system (channel flow theory). It is referred to as *SWI-2* when using water and gas relative permeability models (equations 3.2 and 3.3) as well as oil model.

3.1.2 Stone's first model:

This model was originally proposed by Stone (Stone, 1970) for water-wet system and then slightly modified for end point relative permeability by Aziz and Settari (1979) as below:

$$k_{ro} = k_{rocw} S_o^* F_w F_g \quad 3.4$$

Where k_{rocw} is relative permeability to oil at connate water (S_{wc}) and S_o^* , S_w^* , S_g^* , F_w and F_g are given as:

$$S_o^* = \frac{S_o - S_{om}}{1 - S_{wc} - S_{om}} \quad \text{when } S_o > S_{om} \quad 3.5$$

$$S_w^* = \frac{S_w - S_{wc}}{1 - S_{wc} - S_{om}} \quad \text{when } S_w > S_{wc} \quad 3.6$$

$$S_g^* = \frac{S_g}{1 - S_{wc} - S_{om}} \quad 3.7$$

$$F_w = \frac{k_{row}}{k_{rocw} (1 - S_w^*)} \quad 3.8$$

$$F_g = \frac{k_{rog}}{k_{rocw} (1 - S_g^*)} \quad 3.9$$

S_{om} is the minimum residual oil saturation retained during three-phase flow.

3.1.3 Stone's Second Model:

It is a modified form of the first model suggested by Stone (1973), for the mixed-wet rocks and it is given by the following formula:

$$k_{ro} = k_{rocw} \left[\left(\frac{k_{row}}{k_{rocw}} + k_{rw} \right) \left(\frac{k_{rog}}{k_{rocw}} + k_{rg} \right) - k_{rw} - k_{rg} \right] \quad 3.10$$

Where k_{rw} and k_{rg} denote the two-phase water and gas relative permeabilities for systems with oil-water and oil-gas respectively.

3.1.4 Stone's first model exponent

The formula for Stone's first model may be rearranged such that an exponent may be applied to the combination of saturation terms:

$$k_{ro} = \beta (k_{row}k_{rog})/k_{rocw} \quad 3.11$$

$$\beta = \left(\frac{S_o^*}{(1-S_w^*)(1-S_g^*)} \right)^\eta \quad 3.12$$

The β expression was proposed by Hustad and Holt (1992). The term may be interpreted as a variable that varies between zero and one for low and high oil saturations respectively. If the exponent, η , is equal to 1.0, the formula corresponds to Stone's first model. Values above 1.0 cause the oil isoperms to spread within the saturation space, whereas values below 1.0 have the opposite effect. The value of the exponent may be used, therefore, to match the predicted oil recovery to the observed data. This mode is denoted by *Stone-Exp* in this study.

3.1.5 IKU method

The idea behind the IKU method is to estimate three-phase relative permeabilities by using two-phase relative permeability values in a weighting scheme dependent on the saturations of the system Hustad and Hansen (1995). This method applied to all three phases symmetrically but here we only use the formulation for the oil relative permeability. Equivalent formulation may be derived for the other phases as well.

A typical ternary diagram is illustrated in Figure 3-2 where the relevant oil two-phase end point values are indicated, S_{org} , S_{gro} , S_{orw} and S_{wro} . Straight lines may be drawn to connect two end point saturations. These lines connect the two-phase end points representing the minimum and maximum oil saturations for oil flow. Given the three-phase saturation, labelled (S_g , S_w) in Figure 3-2, draw a straight line running through this point and the oil apex. This defines two intersection points with the line connecting

the end point values. The associated oil coordinates to the intersection points are represented by S_{omn} and S_{omx} . These values represent the minimum and maximum oil saturations for the three-phase flow, and are given by:

$$S_{omn} = \frac{S_w S_{orw} + S_g S_{org} + S_{org} S_{orw} (S_o - 1)}{S_g (1 - S_{orw}) + S_w (1 - S_{org})} \quad 3.13$$

$$S_{omx} = \frac{S_w S_{gro} + S_g S_{wro} + S_{gro} S_{wro} (S_o - 1)}{S_g S_{wro} + S_w S_{gro}} \quad 3.14$$

The corresponding normalized three-phase oil saturation is then:

$$S_o^* = \frac{S_o - S_{omn}}{S_{omx} - S_{omn}} \quad 3.15$$

The normalized oil saturation may then be used to obtain representative two-phase oil relative permeabilities from normalized two-phase relative permeabilities:

$$\hat{k}_{rog} = k_{rog}^n (S_o^*) \quad \text{and} \quad \hat{k}_{row} = k_{row}^n (S_o^*) \quad 3.16$$

The superscript n indicates that the relative permeabilities are normalized to saturation values between zero and one. Lastly, these representative two-phase oil relative permeability may be weighted by the saturations in the three-phase region to obtain the three-phase oil relative permeability:

$$k_{ro} = \frac{S_w}{S_w + S_g} \hat{k}_{row} + \frac{S_g}{S_w + S_g} \hat{k}_{rog} \quad 3.17$$

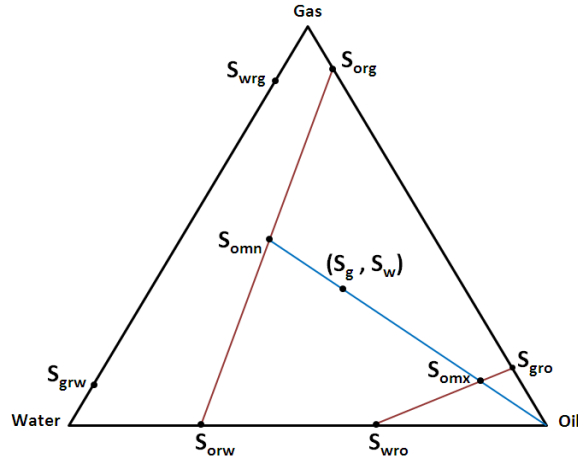


Figure 3-2: Ternary diagram showing typical end point values for oil relative permeability.

3.1.6 ODD3P Method

Hustad (2010) also developed the ODD3P model which is the extended version of IKU method for three-phase relative permeability. This model incorporates both hysteresis and miscibility simultaneously.

Given the grid block's three saturation values and three interfacial tension values at the start of a time step, the phase relative permeability is determined via following procedure:

- 1- Set the IFT scaling factor,

$$f_{ij} = \left(\frac{\sigma_{ij}}{\sigma_{ij}^r} \right)^{n_{ij}} \quad 3.18$$

σ_{ij} represents the interfacial tension between the phases i and j , superscript r refers to a reference state, and the power n_{ij} is a user-specified constant.

- 2- Set the six grid block endpoint saturations $(\bar{S}_{gro}^r, \bar{S}_{grw}^r, \bar{S}_{orw}^r, \bar{S}_{org}^r, \bar{S}_{wrg}^r, \bar{S}_{wro}^r)$ and multiply by IFT scaling factor, to obtain the IFT-adjusted saturation for phase i in presence of phase j :

$$\bar{S}_{ij} = \bar{S}_{ij}^r \cdot f_{ij} \quad 3.19$$

3- Calculate the normalized saturations :

$$\bar{S}_{imn} = \frac{\bar{S}_j \bar{S}_{irj} + \bar{S}_k \bar{S}_{irk} + \bar{S}_{irj} \bar{S}_{irk} (\bar{S}_i - 1)}{\bar{S}_j (1 - \bar{S}_{irk}) + \bar{S}_k (1 - \bar{S}_{irj})} \quad 3.20$$

$$\bar{S}_{imx} = \frac{\bar{S}_j \bar{S}_{kri} + \bar{S}_k \bar{S}_{jri} + \bar{S}_{jri} \bar{S}_{kri} (\bar{S}_i - 1)}{\bar{S}_j \bar{S}_{kri} + \bar{S}_k \bar{S}_{jri}} \quad 3.21$$

Where subscripts $i, j,$ and k represent either the gas, oil, or water phases.

The grid block saturations are then normalized by:

$$S_i = \frac{\bar{S}_i - \bar{S}_{imn}}{\bar{S}_{imx} - \bar{S}_{imn}} \quad i = o, g, w \quad 3.22$$

4- Determine the normalized hysteresis saturation:

$$S_i^h = S_i^e + (S_i - S_i^t) \left(\frac{1 - S_i^e}{1 - S_i^t} \right), \quad S_i \geq S_i^t \quad 3.23$$

$$S_i^h = S_i \left(\frac{S_i^e}{S_i^t} \right), \quad S_i \leq S_i^t \quad 3.24$$

Which equation 3.23 is used for increasing saturation and equation 3.24 is applicable for decreasing saturation. The turning-point saturation (S_i^t) represents the saturation at which the process direction changes on the mirrored two-phase system. The equivalent saturation (S_i^e) represents the saturation value for which the two-phase relative permeability on the increasing curve equals that on the decreasing curve on the mirrored two-phase system.

5- Set the appropriate normalized saturation using equations 3.25 through 3.27 and then look up representative relative permeability values, by equation 3.28.

$$\text{For the gas-water system: } \hat{S}_w^h = 1 - S_g^h \quad 3.25$$

$$\text{For the oil-water system: } \hat{S}_w^h = 1 - S_o^h \quad 3.26$$

$$\text{For the gas-oil system: } \hat{S}_g^h = 1 - S_o^h \quad 3.27$$

$$\tilde{k}_{rgo}(S_g^h), \tilde{k}_{rgw}(\hat{S}_w^h), \tilde{k}_{rog}(\hat{S}_g^h), \tilde{k}_{row}(\hat{S}_w^h), \tilde{k}_{rwg}(S_w^h), \tilde{k}_{rwo}(S_w^h) \quad 3.28$$

6- Scale relative permeability values with IFT scaling factor:

$$\hat{k}_{rij} = f_{ij} \cdot \tilde{k}_{rij} + (1 - f_{ij}) \cdot S_i, \quad f_{ij} \leq 1 \quad 3.29$$

$$\hat{k}_{rij} = \tilde{k}_{rij}, \quad f_{ij} > 1 \quad 3.30$$

7- Calculate grid block three-phase phase relative permeability values :

$$k_{ri} = \frac{\bar{S}_j}{\bar{S}_j + \bar{S}_k} \hat{k}_{rij} + \frac{\bar{S}_k}{\bar{S}_j + \bar{S}_k} \hat{k}_{rik} \quad 3.31$$

3.2 Hysteresis

Dynamic parameters that govern multiphase flow in porous media are often process dependent. In particular, relative permeabilities are considered to be influenced by direction of saturation alteration e.g. imbibitions or drainage. This dependency is described in the literature as relative permeability hysteresis. The number of mobile phases present in porous media is extremely important when discussing hysteresis. The problem of hysteresis increases significantly when moving from two-phase to three-phase flow systems, as the number of flow paths increases. This is mainly because the complex displacement sequences that can occur in three-phase systems are not observed in two-phase flow systems. These include double-displacement mechanisms and the spreading behaviour of the intermediate wetting phase (Larsen and Skauge, 1998). Hysteresis on relative permeability has been experimentally observed in two-phase flow (Osoba et al., 1951; Land, 1971; Braun and Holland, 1995) and more rarely in three-phase flow (Skauge and Aarra, 1993; Eleri et al., 1995b).

Physically, there are two kinds of hysteresis in relative permeability. The first is referred to as directional hysteresis, which occurs while switching from imbibitions to drainage or vice versa. The second is referred to as cyclic hysteresis, happening between different cycles of one injection process, for instance, 1st gas injection and 2nd

gas injection in a WAG process. Both types of hysteresis play a significant role in the WAG performance and need to be taken into account for modelling.

Two approaches have traditionally been used for accounting for hysteresis in numerical simulation of three-phase flow and WAG injection in particular. The first method is to apply two-phase hysteresis models e.g. Killough's, or Carlson's methods, with the existing three-phase k_r models like Stone, Baker, etc., but excluding those k_r models which contain their own hysteresis model, such as ODD3P. It is essential that the two-phase flow experiments reproduce a similar saturation history to that of the three-phase scenario to be estimated. For example, if the reservoir undergoes primary production by gas cap or aquifer drive followed by water flooding, the appropriate two-phase experiments are probably: (1) a gas-oil flow experiment at immobile water saturation, with increasing gas saturation and (2) a water-oil flow experiment, with increasing water saturation. The second technique is to directly utilize a three-phase hysteresis model specifically developed for WAG simulation (Larsen and Skauge, 1998). This method considers cycle-dependent hysteresis in relative permeability for both wetting and non-wetting phases during cyclic injection of water and gas into an oil reservoir.

The first step in predicting relative permeability hysteresis including two-phase and three-phase is to estimate the trapping of non-wetting phase saturation left behind by the wetting phase advancing into the porous media.

Mathematical formulations of the most popular trapping and hysteresis models are given in the following section.

3.2.1 Trapping Models

A trapping model is a mathematical model expressing the relationship between the initial non-wetting-phase saturation and the trapped non-wetting-phase saturation during an imbibitions process. Generally, gas is assumed to be non-wetting phase, in presence of water and oil, in porous media.

Land Trapping Model

The first trapping model was proposed by Land (1968), and is the most widely used empirical trapping model. His model was originally developed for trapped gas saturation as a function of the initial saturation based on published experimental data from water-wet sandstone cores.

$$S_{gt} = \frac{S_{gi}}{1 + CS_{gi}} \quad 3.32$$

Where S_{gi} is the initial gas saturation or the saturation at the flow reversal, and C is the Land trapping parameter. The Land coefficient is computed from the bounding drainage and imbibition curves as follows:

$$C = \frac{1}{S_{gt,max}} - \frac{1}{S_{gi,max}} \quad 3.33$$

Where $S_{gi,max}$ and $S_{gt,max}$ are the maximum initial and trapped gas saturation values, associated with the bounding drainage and imbibition curves, respectively.

Carlson Trapping Model

A simplified hysteresis and trapping model was developed by Carlson (1981) that requires the bounding drainage and imbibition curves. The mathematical formula of this model is:

$$(S_{gt,max} - S_{gt}) = (S_{gi,max} - S_{gi}) \Rightarrow S_{gt} = S_{gt,max} - \Delta S_{gi} \quad 3.34$$

Where ΔS_{gi} is difference between initial gas saturation where the flow reversed and the initial gas saturation of bounding imbibition curve, Figure 3-4.

3.2.2 Two-phase hysteresis models

Experimental data strongly suggest that the non-wetting phase experiences much more pronounced hysteresis than the wetting phase. Therefore, in water-wet systems, the gas phase shows the largest hysteretic effects, and in water-oil systems oil displays strong hysteresis. Indeed, hysteresis model gives a prediction for the relative permeability scanning curve due to flow reversal by using bounding imbibition and drainage curves.

Killough's Hysteresis Model

A typical krg hysteresis of the Killough model (1976) and pertinent saturation values are shown in Figure 3-3. In Killough model when flow reversal from imbibition to

drainage occurs, k_{rg} is assumed to follow the imbibition curve until S_g reaches the historical maximum gas saturation, $S_{g,Hyst}$. For gas saturations greater than this maximum, k_{rg} follows the drainage curve.

The trapped gas saturation S_{gt} , is calculated using the equation developed by Land (1968) using $S_{g,Hyst}$ as the initial non-wetting saturation.

Following is mathematical equation for calculating imbibitions scanning curve:

$$k_{rg}^{imb}(S_g) = \frac{k_{rg}^{imb}(S_{g,norm}) \times k_{rg}^{Dr}(S_{g,Hyst})}{k_{rg}^{Dr}(S_{gi,max})}, \quad 3.35$$

Where $S_{g,norm}$ is the normalized gas saturation computed as follow:

$$S_{n,norm} = \left(\frac{(S_g - S_{gt}) \cdot (S_{gi,max} - S_{gt,max})}{(S_{g,Hyst} - S_{gt})} \right) + S_{gt,max} \quad 3.36$$

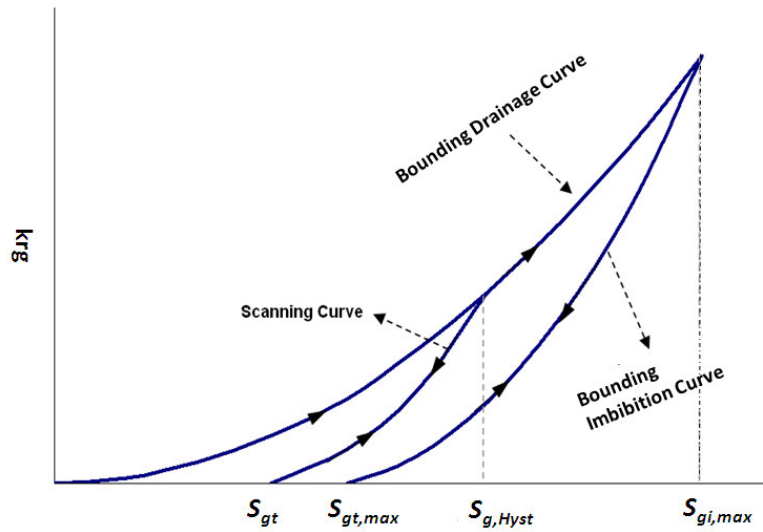


Figure 3-3: Gas relative permeability curve in drainage-imbibition cycles, calculated by the Killough hysteresis model.

Carlson Hysteresis model

Carlson’s method (1981) produces a scanning curve that is parallel to the imbibition curve. It can be visualized by shifting the imbibition curve horizontally until it intersects the drainage curve at S_{gi} , Figure 3-4. A common feature of Killough and Carlson's models is that the scanning imbibition curve is assumed to also represent of any subsequent drainage process.

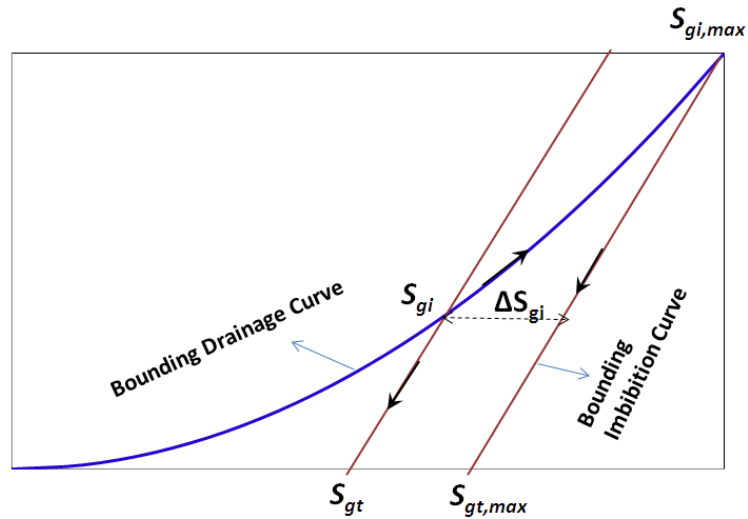


Figure 3-4: Geometric interpretation of the gas relative permeability and trapped saturation during an imbibition process utilizing Carlson trapping model.

3.2.3 Three-phase (WAG) hysteresis model

When saturation oscillations occur during three-phase flow such as water alternating gas (WAG), the two-phase hysteresis models will generally not be able to describe relative permeabilities obtained from corefloods. Larsen and Skauge (1998) proposed a WAG hysteresis model for both wetting and nonwetting phase permeabilities. This model is hereafter referred to as *WAG-Hyst* in this study.

Hysteresis model for nonwetting (gas) phase

Here is the Larsen & Skauge’s mathematical formulation for predicting scanning curve of the gas relative permeability while gas saturation is increasing:

$$\left[k_{rg}^{Dr} (S_g, S_w^I, S_w^{start}) \right]_n = \left\{ \left[k_{rg}^{input} (S_g) - k_{rg}^{input} (S_g^{start}) \right] * \left(\frac{S_{wc}}{S_w^I} \right)^\alpha \right\} + \left[k_{rg}^{imb} (S_g^{start}) \right]_{n-1} \quad 3.37$$

Where n is number of hysteresis loop, α is tuning parameter selected by user, k_{rg}^{input} is primary gas k_r (input relative permeability), $k_{rg}^{input}(S_g^{start})$ is the input relative permeability at the gas saturation at the start of the secondary drainage, S_w^I is the water saturation at the start of the secondary drainage and $k_{rg}^{imb}(S_g^{start})$ is the relative permeability at the start of the secondary drainage process (that is the k_{rg} at the end of the imbibition). As can be seen, the gas relative permeability is coupled to both the historical water saturation and gas saturations, but is not a function of the present water saturation.

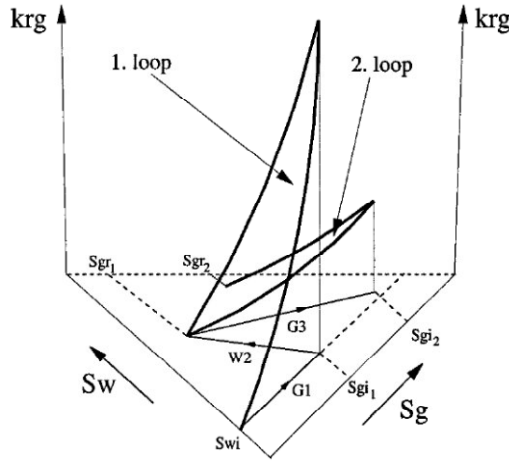


Figure 3-5: Gas relative permeability scanning curves calculated with the Larson-Skauge's three-phase hysteresis model.

The k_{rg} model, while gas saturation decreases in the system, is based on the theory developed by Land (1968). Consider a typical drainage process followed by an imbibition process. The flowing gas (S_{gf}) saturation is calculated by:

$$S_{gf} = \frac{1}{2} \left\{ (S_g - S_{gt}) + \sqrt{(S_g - S_{gt})^2 + \frac{4}{C} (S_g - S_{gt})} \right\} \quad 3.38$$

Where S_{gt} is calculated by the Land trapping model and C is the Land coefficient. Then the imbibitions k_{rg} is predicted by:

$$k_{rg}^{imb}(S_g) = k_{rg}^{Dr}(S_{gf}) \quad 3.39$$

Figure 3-5 demonstrates the schematic curves of hysteresis loops including imbibition and drainage cycles considered in the *WAG-Hyst* (Larsen & Skauge's) model.

Hysteresis model for wetting (water) phase

Inputs to the numerical model are primary water-relative-permeability curve, W1, and a secondary water-relative-permeability curve, W2, after gas injection. The initial saturation state for the primary process is immobile water and oil and the W1 process is, accordingly, a two-phase flow process. Gas saturation at the start of the three-phase W2 process must be known, and it is denoted as maximum gas saturation $S_{g,max}$. The Land constant must also be known such that $S_{gt,max}$ can be calculated. The scanning curves for increasing water saturation are interpolated between k_{rw}^{W1} and k_{rw}^{W2} :

$$k_{rw}^{imb}(S_w, S_g^I) = k_{rw}^{W1} \left[1 - \frac{S_g^I}{S_{g,max}} \right] + k_{rw}^{W2} \left[\frac{S_g^I}{S_{g,max}} \right] \quad 3.40$$

Here, S_g^I = the gas saturation at the start of the increasing water saturation process. If the porous medium is in a two-phase oil/water situation, the W1 curve will be followed. For initial gas saturation of zero or the maximum gas saturation, the bounding curves W1 and W2, respectively, will be used.

There are three displacement cycles for decreasing water saturation that have been considered; increasing gas saturation, decreasing gas saturation (oil flood), and constant gas saturation. The gas saturation at the start of the drainage process, S_g^I , determines the water relative-permeability-hysteresis behaviour:

For $(S_g - S_g^I) > 0$ or gas flood the scanning curve for k_{rw} is:

$$k_{rw}^{Dr} = (k_{rw}^{imb})_f \left(1 - \frac{S_g - S_g^I}{S_{g,max} - S_g^I} \right) + k_{rw}^{W2} \left(\frac{S_g - S_g^I}{S_{g,max} - S_g^I} \right) \quad 3.41$$

For $(S_g - S_g^{start}) < 0$ or oil flood the scanning curve for k_{rw} is as:

$$k_{rw}^{Dr} = (k_{rw}^{imb})_f \left(1 - \frac{S_g^I - S_g}{S_g^I} \right) + k_{rw}^{W1} \left(\frac{S_g^I - S_g}{S_g^I} \right) \quad 3.42$$

For constant gas saturation flood the scanning curve for k_{rw} is as:

$$k_{rw}^{Dr} = (k_{rw}^{imb})_f \quad 3.43$$

Note that $(k_{rw}^{imb})_f$ is the relative permeability curve from the last (former) increasing water saturation process.

Intermediate wetting phase (oil) hysteresis

The change in residual oil saturation with trapped gas observed in several experimental studies is included in the oil relative permeability description (Skauge and Larsen, 1994; Munkerud et al., 1996). *Stone-I* model has been used in *WAG-Hyst* method to calculate three-phase oil-relative-permeability. A linear equation was proposed by Larsen-Skauge (1998) to predict the minimum oil saturation (S_{om}) of *Stone-I* model using trapped gas saturation. Three-phase oil relative permeability is calculated by finding the corresponding trapped gas saturation from which the residual (minimum, S_{om}) oil saturation is derived:

$$S_{om} = (S_{or})_{S_{gt}=0} - aS_{gt} \quad 3.44$$

Where $(S_{or})_{S_{gt}=0}$ is maximum residual oil saturation attained during water flooding in absence of gas, S_{gt} is dynamic trapped gas saturation during three-phase flow and a is user defined parameter used for history matching. Based on this equation the oil relative permeability will increase when the trapped gas saturation is increased and the residual oil is correspondingly reduced.

3.3 Coreflood Simulation

Using a wide range of three-phase k_r and hysteresis models available in the commercial reservoir simulator (Eclipse), three-phase coreflood experiments listed in Table 2-3 were simulated to evaluate the capability of the most common k_r models in simulation of three-phase flow experiments under different rock conditions.

3.3.1 Input data

As mentioned earlier, to minimize mass transfer and compositional effects during coreflood tests, all the fluids (oil, gas and brine) were pre-equilibrated at the test pressure and temperature. Furthermore, the average core pressure was monitored and kept at the constant test pressure of 1840 psia, to ensure that fluids are at immiscible conditions during displacement tests. The black oil reservoir simulator (Eclipse100) was used for simulating the coreflood experiments in this study.

The required data for mathematical simulation of a coreflood experiment are core properties including dimensions, porosity and permeability, fluid properties, relative permeabilities, capillary pressure and injection and production constraints.

Since the displacement tests in this study were conducted into the horizontal core while the core was rotating along the horizontal axis, the gravity force is negligible compared to viscous forces. Furthermore, the calculated Bond number (around $5E-9$) was quite low for our experiments, representing minimal impact of gravity force. Therefore, for the simulation purposes, the core was horizontally divided into 70 grids in the X-direction (Figure 3-6).

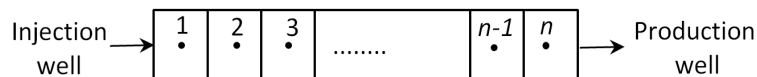


Figure 3-6: One dimensional core gridding.

Two-phase relative permeability data of different systems, including oil/water, oil/gas and gas/water, and different flow directions, i.e. imbibition and drainage, are needed for simulation of three-phase flow experiments using existing three-phase relative

permeability models discussed in previous section. These data were obtained by performing unsteady-state displacement through 1000mD-MW, 65mD-WW and 65mD-MW cores (Table 2-4 and Figure 2-8 to Figure 2-10).

In our experiments the interfacial tension between oil and gas is very small, which causes negligible capillary pressure for the oil/gas system, hence the behaviour of the capillary pressure between oil and water (P_{cow}) at three-phase flow condition approaches to that of the two-phase P_{cow} . Therefore, for simulation of three-phase coreflood experiments, the two-phase oil/water capillary pressure (Figure 2-11 and Figure 2-12) has been employed as an approximation for three-phase capillary pressure.

Three-phase coreflood experiments listed in table 2-3 were simulated using the reservoir simulator (Eclipse100) with the existing three-phase k_r models i.e. *Stone-I*, *Stone-II*, *Stone-Exponent*, *SWI-I*, *SWI-II*, *IKU*, *ODD3P* and *WAG-Hyst*. In order to incorporate hysteresis effects occurring throughout WAG injection, the Killough hysteresis model was also employed alongside the k_r models, excluding those which have their own hysteresis option, such as *ODD3P* and *WAG-Hyst*. Having accomplished the simulation process by Eclipse, the simulation results relevant to each k_r model (fluid production and pressure drop across the core) were compared with the measured data in the laboratory. Then the error values between experimental and simulation results were calculated to assess the capability of the corresponding relative permeability models in predicting WAG performance.

3.3.2 Error analysis

The error value between simulation and experimental results is obtained by applying standard error of estimate as below:

$$SEE\% = \sqrt{\frac{\sum_{i=1}^n \left(\frac{Q_{Exp} - Q_{Sim}}{Q_{Exp}} \right)^2}{n-1}} \times 100 \quad 3.45$$

Where “*SEE%*” is the percentage of standard error of estimate, n is number of data points and Q_{Exp} and Q_{Sim} are experimental observation and simulation results, including production and pressure drop data. The *SEE%* was separately calculated for oil

production ($SEE_{oil}\%$), water production ($SEE_{water}\%$), gas production ($SEE_{gas}\%$) and pressure drop across the core ($SEE_{DP}\%$). $SEE_{Rec}\%$ denotes the error value of production data obtained by arithmetic averaging between $SEE_{oil}\%$, $SEE_{water}\%$ and $SEE_{gas}\%$ and the total error, represented by $SEE_{total}\%$, is then calculated by arithmetic averaging of production error ($SEE_{Rec}\%$) and pressure drop error ($SEE_{DP}\%$).

For those points where the Q_{Exp} is zero and Q_{Sim} is non-zero value, to overcome the infinity problem, $SEE\%$ is assumed to be 100%.

3.3.3 Simulation results and discussion

Simulation vs. experimental results on 1000mD-MW core

Figure 3-7 presents the error chart of the different fluid production data obtained by comparing experimental and simulation results of the WAG injection conducted in 1000mD-MW rock, using various ranges of three-phase k_r models. The $SEE\%$ of oil recovery has the largest error value amongst the production data for all k_r models. This indicates that oil production is highly sensitive to the relative permeability model and has much greater influence than either water or gas production. Water production shows the smallest error value compared to the oil and gas recoveries, which implies least sensitivity of water to the three-phase relative permeability modelling. The lowest error value of the oil production resulted from using the *SWI-I* method, whilst the *Stone-II* model produced the highest error for oil recovery. The $SEE_{Rec}\%$ (i.e. the average of all fluid production errors) and pressure drop errors resulting from the use of different k_r models for the same 1000mD-MW rock are presented in Figure 3-8. A comparison between production and pressure drop errors of the 1000mD-MW core reveals that the error value of the pressure drop is greater than that of the production amongst k_r models except for the *IKU* technique. This graph highlights the impact of the relative permeability model on the pressure drop calculation. As shown in Figure 3-8, in general, the *WAG-Hyst* model results in the least error for predicting production and pressure data of the WAG experiment in 1000mD-MW core, although the errors are still rather large at 30%!.

Since the first water injection in the WAG injection has been carried out at the two-phase flow oil/water condition, only the two-phase relative permeability of the oil/water

system would influence the simulation results. Therefore, simulation of 1st water injection using different k_r models would lead to the oil recovery profiles matching the experimental oil production. Thus, to make the cumulative production data comparable, all the production values of the WAG injections in this study have been plotted after primary water flooding, which are calculated as fractions of S_{orw} (saturation of the remaining oil after the first water injection), rather than in cm^3 . Figure 3-9 shows the cumulative oil production as a fraction of S_{orw} versus injected pore volume, obtained from experiments and simulation of WAG injection through 1000mD-MW core using various three-phase k_r models. The notations G1, W2 and G2, separated by dashed lines in Figure 3-9, represent the production profile resulting from first gas injection, second water injection and second gas injection, respectively.

It is clear that, although some of the k_r models estimate the WAG performance better than others, none of the models can predict the oil production profile satisfactorily. The ultimate oil recovery values resulting from the *SWI-I* and *SWI-II* models are very close to the experimental value but the calculated values of both models in the intermediate cycles of the WAG injection are very poor. Despite the fact that *SWI-I* in Figure 3-9 give the closest prediction to the experimental data amongst all models, the pressure drop prediction given by this model has a significant deviation (around 60%) the measured pressure. As the accurate prediction of all observation data (i.e. production and pressure) of WAG injection is the desired aim, the total error of production and pressure data ($SEE_{total}\%$) should be considered as a key criterion decision point in selecting the best relative permeability model.

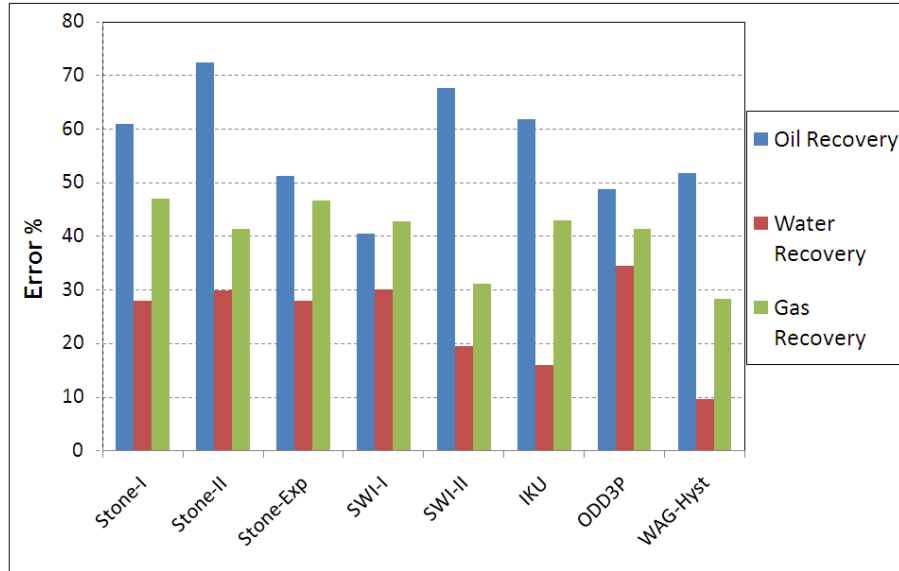


Figure 3-7: SEE% of oil, water and gas production, obtained by comparing experimental and simulation results of WAG injection through 1000mD-MW core using different k_r models available in Eclipse100 simulator.

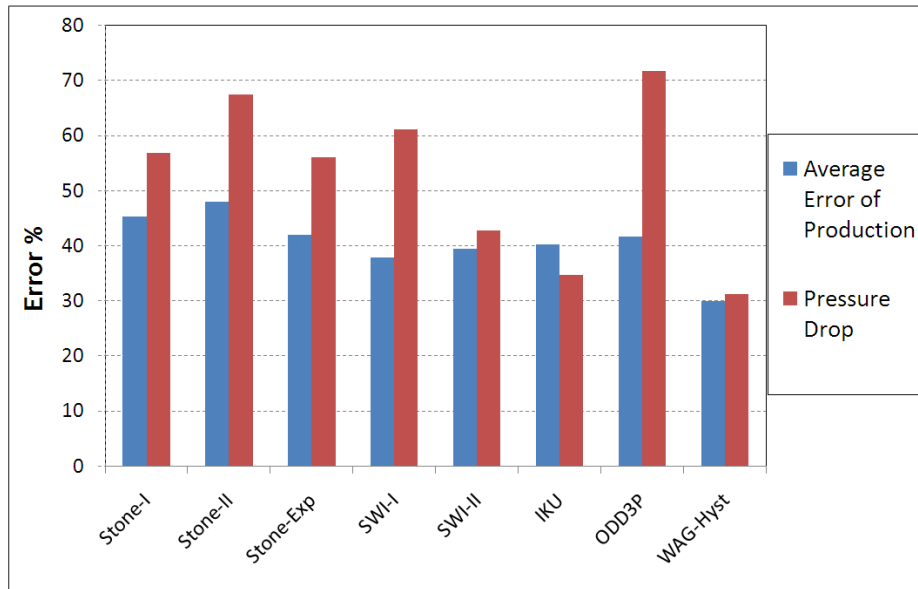


Figure 3-8: Average errors of all fluid production ($SEE_{Rec}\%$) and errors of pressure drop ($SEE_{DP}\%$), obtained by comparing experimental and simulation results of WAG injection through 1000mD-MW core for different k_r models in Eclipse100.

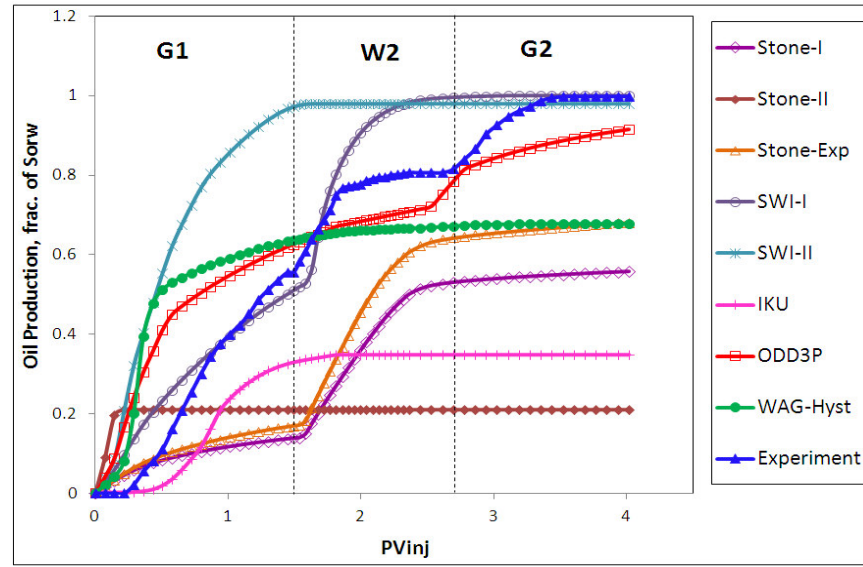


Figure 3-9: Cumulative oil production as a fraction of S_{orw} (saturation of the remaining oil after first water injection) versus injected pore volume, obtained from experiment and simulation of 1000mD-MW core using various three-phase k_r models of the Eclipse100.

Simulation vs. Experimental Results on 65mD-WW core

Figure 3-10 presents calculated errors of oil, water and gas production ($SEE_{oil}\%$, $SEE_{water}\%$ and $SEE_{gas}\%$) using various three-phase relative permeability models in Eclipse 100, corresponding to the WAG injection through 65mD-WW core. Similarly to the 1000mD-MW, the largest error belongs to the oil production, for all k_r models, which again emphasizes the strong impact of the relative permeability model in simulation of WAG performance. This graph shows that using an inappropriate k_r model (e.g., *SWI-II* and *ODD3P* methods) for WAG simulation can substantially (up to 325%) miscalculate the oil production. The lowest error values for oil production resulted from using the *Stone-I* and *Stone-Exp* models and the highest error values came from the use of the *SWI-II* and *ODD3P* models. Figure 3-11 shows the average errors of all fluid production values ($SEE_{Rec}\%$) and errors of pressure drop values ($SEE_{DP}\%$) when using different k_r models to simulate WAG experiments through 65mD-WW core. As shown in this figure, the error values of pressure drop is significantly high for all the models, which highlights the effect of using three-phase relative permeability models on pressure calculations. Considering recovery and pressure drop errors together, the *Stone-I* model as well as the *Stone-Exp* model give the best match, relatively speaking, with the experiment data.

Figure 3-12 represents cumulative oil production as a fraction of S_{orw} versus injected pore volume, obtained from experiment and simulation of the 65mD-WW core using various three-phase k_r models. This graph shows the oil production profile after primary water flooding for various cycles of WAG injection, for which notation of W and G represent water injection and gas injection periods, respectively. The ultimate oil recovery is significantly underestimated by up to 20% by *Stone-I* and *Stone-Exp*, despite both models giving the closest match with the experimental oil recovery profile.

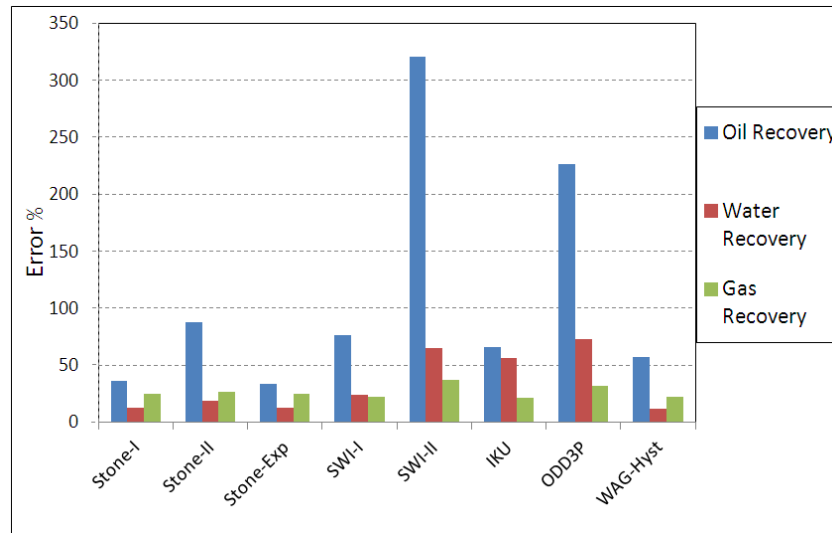


Figure 3-10: SEE% of oil, water and gas production, obtained by comparing experimental and simulation results of WAG injection through 65mD-WW core using the different k_r models of the Eclipse100 simulator.

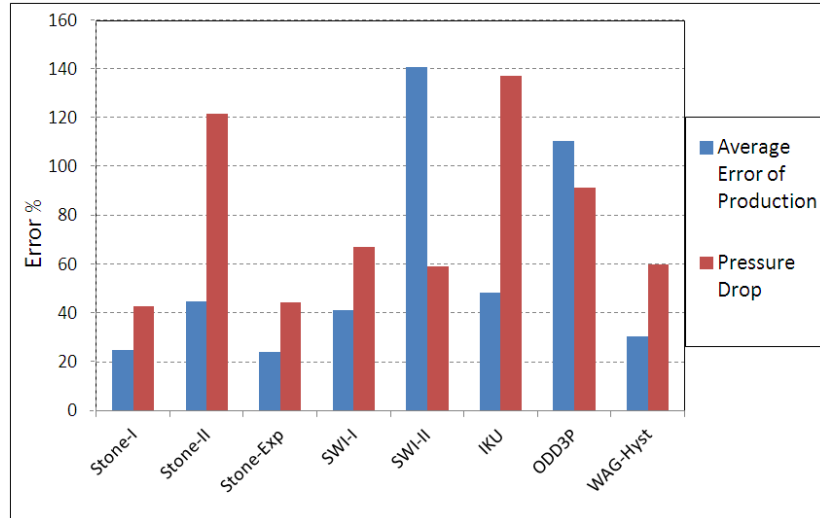


Figure 3-11: Average errors of all fluid production ($SEE_{Rec}\%$) and errors of pressure drop ($SEE_{DP}\%$), obtained by comparing experimental and simulation results of WAG injection through 65mD-WW core for different k_r models available in Eclipse100.

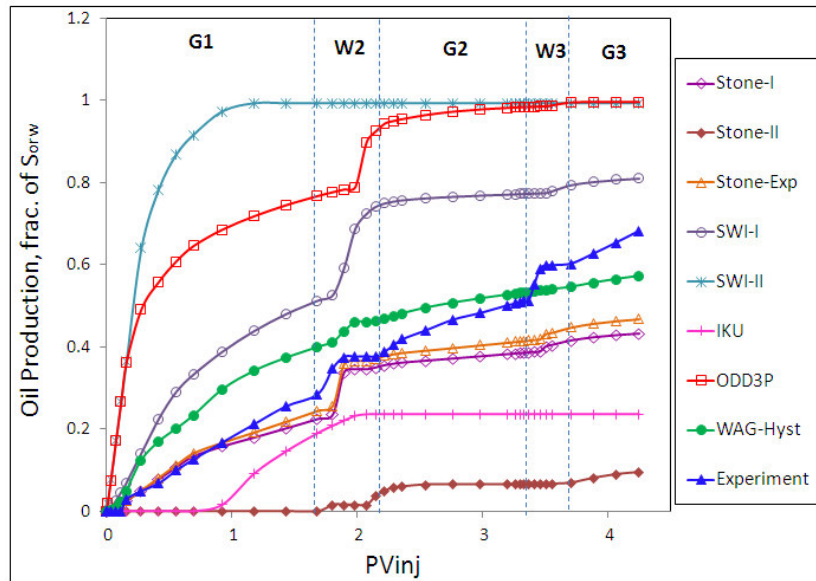


Figure 3-12: Cumulative oil production as fraction of S_{orw} (saturation of the remaining oil after first water injection) versus injected pore volume, obtained from experiment and simulation results of 65mD-WW core using different three-phase k_r models available in Eclipse100.

Simulation vs. experimental results on 65mD-MW core

Figure 3-13 shows the error values of the oil, water and gas production obtained by comparing the experimental and simulation results of WAG injection through 65mD-MW core for different k_r models available in the Eclipse100 simulator. The error in oil production (SEE_{oil}) is a lot larger than the error of water (SEE_{water}) and gas production (SEE_{gas}), highlighting the impact of three-phase k_r models in calculating WAG performance. Figure 3-14 presents the average errors of all fluid production values ($SEE_{Rec}\%$) and errors of pressure drop values ($SEE_{DP}\%$), obtained by comparing experimental and simulation results of the WAG injection through 65mD-MW core for various k_r models. Applying the *SWI-I* method results in the lowest mismatch for production data, whilst using *WAG-Hyst* leads to the lowest error in pressure drop calculation for this mixed-wet core. However, this emphasizes that no unique model exists to precisely predict all observational data (i.e. production and pressure) from WAG injection. In other words, a particular k_r model may satisfactorily simulate the production data but its calculation for pressure data would be very poor, or vice versa.

Figure 3-15 shows cumulative oil production as a fraction of S_{orw} versus injected pore volume, obtained from experimental observation and simulation of 65mD-MW core, using various three-phase k_r models. The closest match between simulation and experimental oil recovery is given by the *SWI-I* model. The oil recovery prediction by the *SWI-I* model in the middle cycles is largely overestimated. Although this technique perfectly matches the ultimate oil recovery and the oil production profile during the first gas injection period, it gives a very poor match for the other WAG cycles. As illustrated in Figure 3-15, none of the k_r models can accurately predict the complete oil production profile, as obtained from the core flood test. Furthermore, the predictions made by the existing models can be very variable and various models can predict vastly different 3-phase k_r values from the same 2-phase data. While some models perform better than others, all of the 3-phase k_r models examined in this study fail to predict the continued production of oil after the breakthrough of the gas, which is one of the features of gas and WAG injection experiments at low gas-oil interfacial tension (Sohrabi et al., 2005; Sohrabi et al., 2008c).

One imperative issue to be noted here is that all the three-phase models examined in this study have originally been developed and verified based on the three-phase data

obtained from the fully immiscible system (high interfacial tension) which behaves in a way that completely different from near-miscible flow. In other words, the existing empirical models may not be accurately applicable for the low interfacial tension hydrocarbon. Reservoir engineers therefore need to be careful about choosing appropriate correlations for simulation of reservoirs with three-phase systems undergoing near-miscible flow.

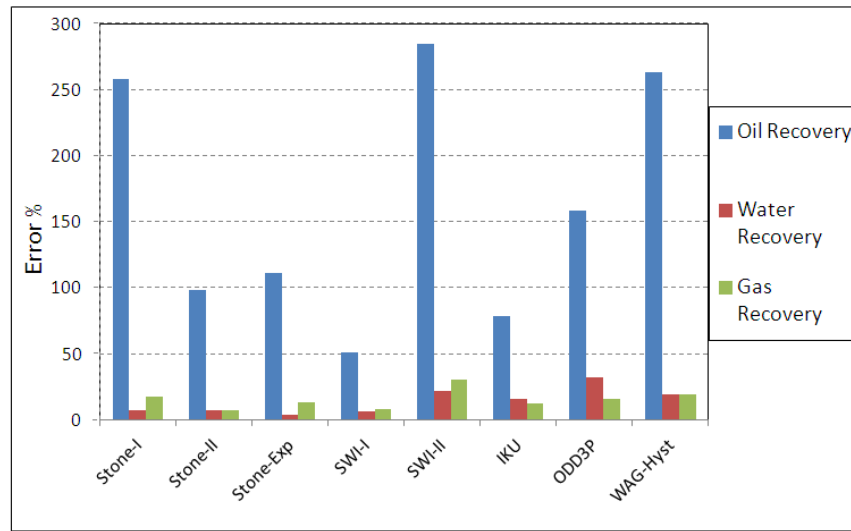


Figure 3-13: SEE% of oil, water and gas production, obtained by comparing experimental and simulation results of WAG injection through 65mD-MW core using the different k_r models of the Eclipse100 simulator.

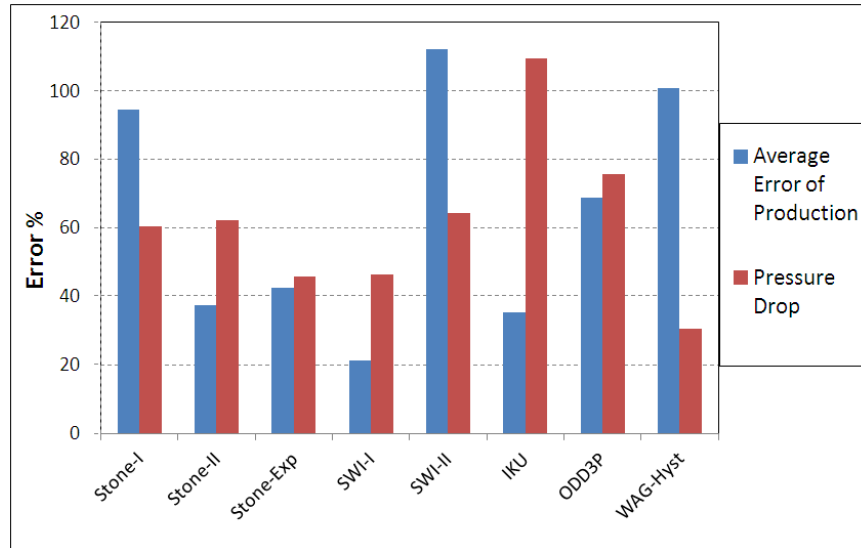


Figure 3-14: Average errors of all fluid production ($SEE_{Rec}\%$) and errors of pressure drop ($SEE_{DP}\%$), obtained by comparing experimental and simulation results of WAG injection through 65mD-MW core for different k_r models available in Eclipse100.

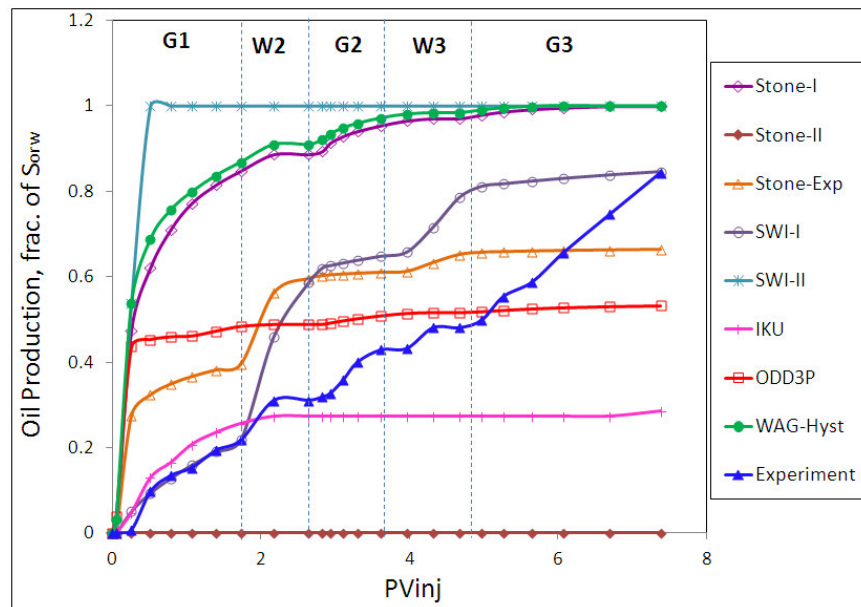


Figure 3-15: Cumulative oil production as a fraction of S_{orw} (saturation of the remaining oil after first water injection) versus injected pore volume, obtained from experiment and simulation results of 65mD-MW core using different three-phase k_r models available in Eclipse100.

Mixed-wet versus water-wet comparison of 65 mD coreflood tests:

The total error ($SEE_{total}\%$) of the WAG injection of 65mD water-wet and mixed-wet core, as obtained by different k_r models, is plotted in Figure 3-16. This graph exhibits the effect of wettability, as reflected by the use of different k_r models for WAG simulation. It can be seen that the behaviour of the various models in the simulation of the water-wet core is quite different from that observed in the mixed-wet core. In some k_r models, the error values of the water-wet core are less than that of the mixed-wet core, whereas in the other models the trend is in opposite direction. Employing *Stone-exp* model leads to lowest error value for predicting the WAG performance in the water-wet rock, whilst the *SWI-I* gives the least mismatch for the mixed-wet core. Using *ODD3P* produces the highest errors for the water-wet case and *SWI-II* produces the highest errors for the mixed-wet case. Although both cores have the same pore size distribution and same permeability, the performance of WAG injection in water-wet rock is absolutely different from that in mixed-wet rock. However, this highlights the impact of wettability on relative permeability during WAG injection and the importance of performing these experiments under representative wettability of the reservoir.

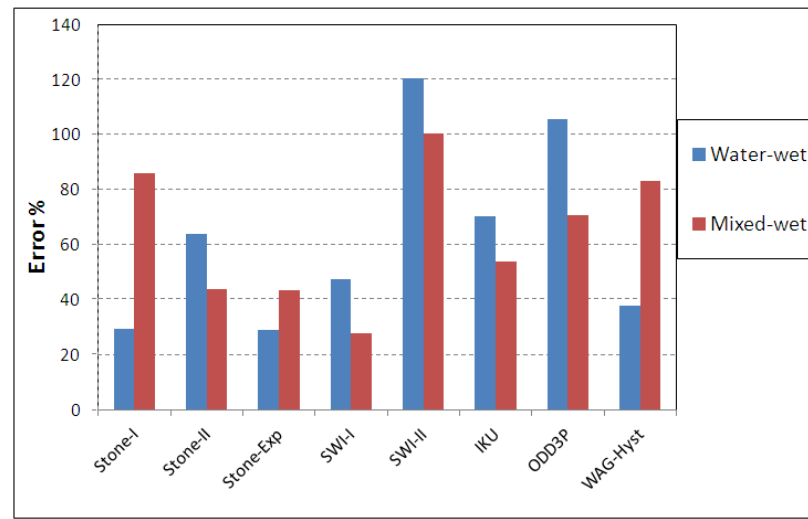


Figure 3-16: Effect of wettability in WAG simulation, based on $SEE_{total}\%$ of the WAG injection in 65mD water-wet and mixed-wet cores for different k_r models.

High permeability (1000 mD) versus low permeability (65 mD)

Figure 3-17 shows the total errors produced using various k_r models, when comparing simulation and experimental results of the WAG injection through the 65mD and 1000mD cores, both under mixed-wet conditions. In this case there is no consistent behaviour: while some of the models predict lower errors for the high permeability core other models show the reverse. This graph, therefore, demonstrates the effect of absolute permeability in three-phase relative permeability calculations. In general, the lower the absolute permeability, the higher will be the errors in relative permeability calculation.

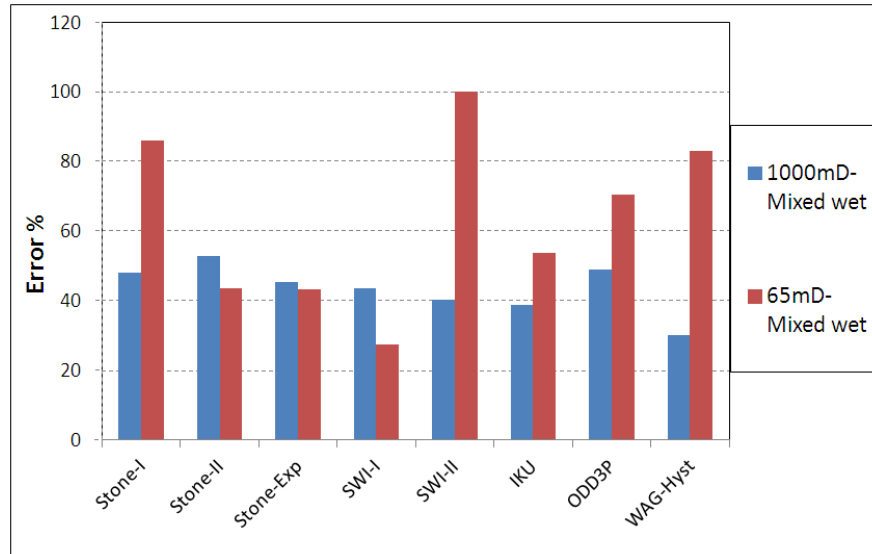


Figure 3-17: Effect of absolute rock permeability on calculated $SEE_{total}\%$ of the WAG injection through 65mD-MW and 1000mD-MW cores, using different k_r models.

Some similar studies in literature directed toward the assessment of existing three-phase relative permeability models confirms that, in most cases, the existing models cannot adequately provide satisfactory matches with the experimental data (Delshad and Pope, 1989; Pejic and Maini, 2003; Cao and S, 2010).

3.4 Conclusions

The following conclusions can be drawn from the simulation study of the WAG experiments through different cores using a wide range of three-phase relative permeability models:

- 1- One imperative issue which should be noted here is that all the three-phase models examined in this study were originally been developed and verified based on the three-phase data of the fully immiscible (high interfacial tension) system, which behaves thoroughly different from near-miscible flow. In other words the existing empirical models may not be accurately applicable for the low interfacial hydrocarbon flow. Reservoir engineers are thus advised to be careful about choosing appropriate correlations for simulation of reservoirs with three-phase systems undergoing near-miscible flow.
- 2- The results show that choosing an inappropriate three-phase k_r model in simulation of the WAG experiments can lead to large errors in prediction of fluid production and pressure. The predictions made by the existing models are very variable i.e., various models can predict vastly different 3-phase k_r values from the same set of 2-phase data. While some models perform better than others, all of the 3-phase k_r models examined in this study fail to predict the continued production of oil after the breakthrough of the gas which is one of the features of gas and WAG injection experiments at low gas-oil IFT (interfacial tension).
- 3- The methodology of using two-phase relative permeability to estimate three-phase relative permeability which is the basic technique of all the existing three-phase models may be questionable because the WAG performance obtained by all the models depicted substantial errors when compared with the observed data using rocks of different wettability and permeability.
- 4- The WAG simulation of all core experiments revealed that the error value of the oil production is much larger than that of water and gas production. This highlights the strong impact of the three-phase relative permeability on flow of oil.
- 5- Comparison between simulation results of the experiments on the water-wet and mixed-wet core revealed that the wettability has a significant effect on three-phase flow and WAG performance. In other words, each three-phase relative

permeability model may give totally different predictions for water-wet and mixed-wet cores. This highlights the impact of wettability on relative permeability during WAG injection and the importance of performing these experiments under wettability conditions representative of those of the reservoir rock.

3.5 Reference

- Aziz, K., and Settari, A., 1979, *Petroleum Reservoir Simulation*: London, Applied Science.
- Baker, L.E., 1988, Three-Phase Relative Permeability Correlations, paper SPE 17369, presented at the SPE Enhanced Oil Recovery Symposium, Tulsa, Oklahoma.
- Braun, E.M., and Holland, R.F., 1995, Relative Permeability Hysteresis: Laboratory Measurements and a Conceptual Model: SPE Reservoir Engineering, paper SPE 28615, (08).
- Cao, P., and S, S., 2010, Three-Phase Unsteady State Relative Permeability Measurement In Consolidated Cores Using Three Immiscible Liquids, presented at the International Symposium of the Society of Core Analysis, Halifax, Canada.
- Carlson, F.M., 1981, Simulation of Relative Permeability Hysteresis to the Nonwetting Phase, paper SPE 10157, presented at the SPE Annual Technical Conference and Exhibition, San Antonio, Texas.
- Delshad, M., and Pope, G.A., 1989, Comparison of the three-phase oil relative permeability models: *Transport in Porous Media*, 4(1), p. 59-83.
- Eleri, O.O., Graue, A., and Skauge, A., 1995, Steady-State and Unsteady-State Two-Phase Relative Permeability Hysteresis and Measurements of Three-Phase Relative Permeabilities Using Imaging Techniques, paper SPE 30764, presented at the SPE Annual Technical Conference and Exhibition, Dallas, Texas.
- Hustad, O.S., and Browning, D.J., 2010, A Fully Coupled Three-Phase Model for Capillary Pressure and Relative Permeability for Implicit Compositional Reservoir Simulation: *SPE Journal*, paper SPE 125429-PA, (12).
- Hustad, O.S., and Hansen, A.G., 1995, A Consistent Correlation For Three-Phase Relative Permeabilities and Phase Pressure Based on Three Sets of Two Phase Data, presented at the 8th European IOR symposium, Vienna, Austria.
- Hustad, O.S., and Holt, T., 1992, Gravity Stable Displacement of Oil by Hydrocarbon Gas After Waterflooding, paper SPE 24116, presented at the SPE/DOE Enhanced Oil Recovery Symposium, Tulsa, Oklahoma.
- Killough, J.E., 1976, Reservoir Simulation With History-Dependent Saturation Functions, paper SPE 5106, (02).
- Land, C.S., 1968, Calculation of Imbibition Relative Permeability for Two- and Three-Phase Flow From Rock Properties, paper SPE 1942, (06).
- Land, C.S., 1971, Comparison of Calculated with Experimental Imbibition Relative Permeability, paper SPE 3360, (12).
- Larsen, J.A., and Skauge, A., 1998, Methodology for Numerical Simulation With Cycle-Dependent Relative Permeabilities: *SPE Journal*, paper SPE 38456, (06).
- Munkerud, P.K., Duqueroix, J.P., and Virnovski, G., 1996, Gas Mobility During Three-Phase Flow in Combined Gas/Water Injection Processes, presented at the RUTH Norwegian Research Program on Improved Oil Recovery,
- Osoba, J.S., Richardson, J.G., Kerver, J.K., Hafford, J.A., and Blair, P.M., 1951, Laboratory Measurements of Relative Permeability, paper SPE 951047-G,

- Pejic, D., and Maini, B.B., 2003, Three-Phase Relative Permeability of Petroleum Reservoirs, paper SPE 81021, presented at the SPE Latin American and Caribbean Petroleum Engineering Conference, Port-of-Spain, Trinidad and Tobago.
- Skauge, A., and Aarra, M., 1993, Effect of wettability on the oil recovery by WAG, presented at the 7th IOR symp, Moscow.
- Skauge, A., and Larsen, J.A., 1994, Three-phase relative permeabilities and trapped gas measurements related to WAG processes, presented at the SCA, Stavanger.
- Sohrabi, M., Danesh, A., Tehrani, D., and Jamiolahmady, M., 2008, Microscopic mechanisms of oil recovery by near-miscible gas injection: *Transp. Porous Media*, 72, p. 351-367.
- sohrabi, m., Danesh, A., and Tehrani, D.H., 2005, Oil Recovery by Near-Miscible SWAG Injection, paper SPE 94073, presented at the SPE Europec/EAGE Annual Conference, Madrid, Spain.
- Stone, H.L., 1970, Probability Model for Estimating Three-Phase Relative Permeability: *SPE Journal of Petroleum Technology*, paper SPE 2116, (02).
- Stone, H.L., 1973, Estimation of Three-Phase Relative Permeability And Residual Oil Data, paper SPE 73-04-06, (10-12).
- van Dijke, M.I.J., and Sorbie, K.S., 2002, The relation between interfacial tensions and wettability in three-phase systems: consequences for pore occupancy and relative permeability: *Journal of Petroleum Science and Engineering*, 33(1-3), p. 39-48.

Chapter 4:

Determination of Three-Phase Relative Permeability from Unsteady-State Coreflood Experiment

As, demonstrated in the previous chapter, none of the existing relative permeability models could adequately predict the observed production and pressure performance of our coreflood WAG experiments. The important question will therefore be, how should we determine three-phase relative permeabilities using the data obtained from two and three-phase displacement experiments. This chapter addresses this question and illustrates the methodology devised for estimating k_r values directly from unsteady state coreflood test data.

4.1 Introduction

Three-phase flow may occur quite frequently in many oil recovery processes of interest to the oil and gas industry, such as gas injection and water-alternating-gas (WAG) injection. Considerable efforts have been directed towards gaining a better

understanding of three phase flow in porous media and in particular determination of three-phase relative permeability values. However, an accurate estimation of three-phase relative permeability is still a challenging task for reservoir engineers. For two-phase relative permeability (oil/water, gas/oil, and gas/water), there are only two principal displacement paths (i.e. when saturation of one phase increases, saturation of the other phase decreases or vice versa). In contrast, in the case of three-phase relative permeability there are an infinite number of different displacement paths. This is because any three-phase displacement involves variation of two independent saturations. It is therefore impossible to measure relative permeability (k_r) for all possible three-phase displacements that may occur in a reservoir.

The most common approach currently used in modelling of three-phase flow in porous media is to calculate the three-phase k_r values from laboratory-measured two-phase relative permeability data by correlations available in the literature. Core flood experiments and micromodel tests have recently demonstrated that three-phase and two-phase flow processes in porous media are completely different (Sohrabi, 2001; Cao and S, 2010). In other words, calculating three-phase relative permeabilities by simply combining two-phase relative permeability data may lead to highly erroneous results. Hence three-phase k_r values are required to be measured directly from displacement experiments.

Two main methods for measuring k_r values in the laboratory are the steady-state and unsteady state displacements. In the steady state method (Figure 4-1), all fluids are injected simultaneously, at given proportions, until steady-state conditions are attained, i.e. the same proportions of fluids that were injected into the core are produced at the outlet. It usually takes a very long period of fluid injection to establish steady state flow. But in the unsteady state (Figure 4-2) method, one of the fluids is injected into the core, displacing the resident fluid phases.

In the steady-state approach, the relative permeability of each phase can be directly calculated from the Darcy law as follows:

$$k_{ri} = \frac{q_i \mu_i L}{k A \Delta p} \quad 4.1$$

where k_{ri} , μ_i and q_i are relative permeability, viscosity and flow rate of the phase i , respectively; Δp is pressure drop across the core and A and L are cross-sectional area and length of the core.



Figure 4-1: Steady-state coreflood experiment for determining relative permeability. The fluid proportions produced at the outlet are equal to the proportions injected at the inlet.

Unsteady state methods are used to avoid losing the considerable amount of time and expense involved in the steady state method. However, calculating the phase relative permeabilities using the unsteady state test data is much more complicated. In the unsteady state experiments, relative permeability can be obtained by either explicit or implicit methods. The most common explicit method to calculate relative permeability from the laboratory measured recovery and pressure drop curves, the JBN method (Johnson et al., 1959), has some difficulties with its application. One disadvantage of the explicit method is that capillary pressure effects cannot easily be taken into account in the interpretive procedure. In addition, in the JBN method the derivative of the production and pressure data have to be calculated which tend to be highly varied and difficult to measure accurately, and adding to the uncertainty of the k_r values so obtained.

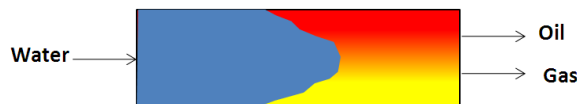


Figure 4-2: Unsteady-state coreflood experiment.

In implicit or parameter estimation computations (Bard, 1974), relative permeability values are estimated in an optimization manner so that the difference between the measured and simulated values is minimized. To use this approach, a functional form

containing tuning parameters is selected to represent each phase k_r . Matching the experimental data is then attempted repeatedly by changing these coefficients until the closest match is obtained.

This method was originally proposed for estimating two-phase k_r curves by Kerig and Watson (1986) and then extended to three-phase flow by Mejia et al. (1996). They used gradient methods, such as that of Levenberg-Marquardt (1963), to find appropriate values of the coefficients for relative permeability functions. This approach is easily applicable to two-phase relative permeability calculations and can converge to solution relatively quickly, whereas in the case of three-phase flow, where more tuning parameters are involved, the process would be more complicated. For those complex problems which involve many unknown coefficients, the minimization of an objective error function is more complex and can encounter a number of local minima, resulting in spurious answers. Utilizing a gradient method for finding lowest value of such objective functions can encounter divergence problems. However, by implementing the stochastic approach used in this study, e.g. by application of a Genetic Algorithm (GA) (Holland, 1975), the minimum value of the objective error function can easily be captured by repeated random selection of unknown coefficients.

A computer program was developed as an optimization tool to obtain three-phase relative permeability from unsteady-state displacement test results by trying to match the measured data using a Genetic Algorithm. The program gives best estimates of three-phase relative permeability based on suitable mathematical functions defined to describe their dependency on phase saturations. In this approach, no assumptions are made regarding the dependency of the multiphase flow functions on a specific saturation. Figure 4-3 shows the schematic flow chart of our k_r determination approach, which consists of three segments: k_r functions, core flood simulator and GA optimization Algorithm. The calculation starts with an initial guess for the k_r functions as input to the core simulator. The difference between experimental and modelling results, referred to as misfit (objective error function), is minimized iteratively by adjusting the parameters of k_r functions until an error tolerance is achieved. In this simulator the genetic algorithm has been used as an optimisation procedure to minimise the objective function and find the global minimum for the misfit.

Unlike the JBN method, this method takes into account the capillary forces between fluids. Another important feature of this approach is that the three-phase k_r of each of the three fluids, oil, water and gas, is assumed to depend on two saturation values. This is in contrast to the intrinsic assumption made in most of the existing three-phase k_r models (e.g. Stone), that only the intermediate wetting phase (oil) k_r is a function of two independent saturations [i.e. $k_{ro} = k_{ro}(S_w, S_g)$], while wetting and non-wetting phase k_r values are functions of their own saturations [i.e. $k_{rw} = k_{rw}(S_w)$, $k_{rg} = k_{rg}(S_g)$]. This point is particularly important for simulation of three-phase flow in mixed-wet or weakly-wet systems, which are believed to be more realistic wetting conditions, representing most oil reservoirs, than the assumption of strongly water-wet or oil-wet systems.

Successful GA solutions have been presented by other authors to determine two-phase relative permeability from coreflood experiments (Tokuda and Takahashi, 2004; Sun and Mohanty, 2005; Wang and Buckley, 2006). Since the two-phase flow involves only one independent saturation path, i.e., the k_r function in optimization processes is represented in terms of one saturation, finding the solution is relatively easy. However, in this study we have used the modified B-Spline equation, representing any of the three-phase relative permeabilities as a function of two independent saturation values. Hence the number of unknown coefficients involved in three-phase flow is more than that in two-phase flow calculations. That makes the optimization process more complicated and difficult to converge to solution. An efficient mutation and crossover method was applied to the relative permeability function in order to successfully match the measured data obtained from the three-phase flow core experiments. As far as we know, currently, there is no optimization or history matching software published in the oil industry for calculating three-phase relative permeabilities directly from unsteady-state coreflood data.

Detailed explanations of each parts of this approach are given below.

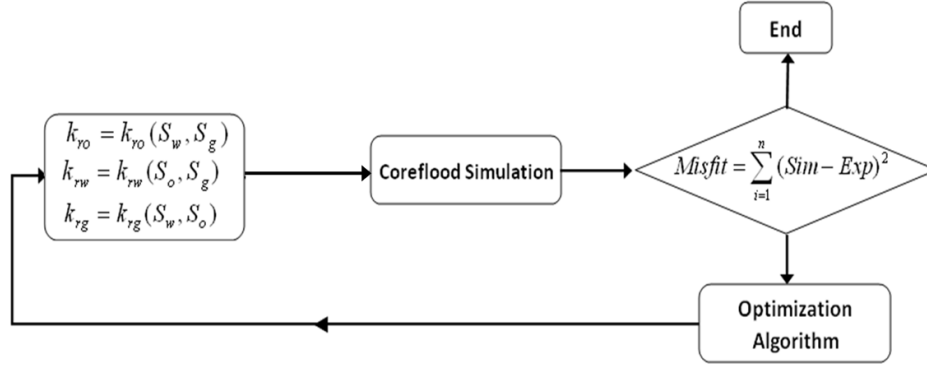


Figure 4-3: Work flow for determination of three phase k_r values from unsteady state coreflood experiment.

4.2 Theory

The methodology presented here for estimating three-phase relative permeability function has been developed by extending regression-based method originally proposed by Kerig and Watson (1986) for two phase flow. The methodology consists of three principal components. First, a mathematical model (coreflood simulator in Figure 4-3) is chosen to represent the fluid flow through the porous medium under consideration. The model is adequately comprehensive to represent all the important physical effects within the range covered by the displacement experiments. The second element in implementation of this approach is a functional representation for relative permeability curves that need to be estimated and the third element is an optimization tool which is utilized to minimize the objective function.

4.2.1 Mathematical model (Coreflood Simulator)

Using the continuity equation for immiscible flow of each phase through porous media combined with the Darcy flow equation as momentum term, and the capillary pressure functions we will have the following equations:

$$\nabla \cdot \left[\frac{k k_{ri}}{\mu_i} \nabla P_i \right] = \frac{\partial(\phi S_i)}{\partial t} + q_i \quad i = \text{oil, gas, water} \quad 4.2$$

$$P_{cgo} = P_g - P_o, \quad P_{cow} = P_o - P_w, \quad S_o + S_w + S_g = 1 \quad 4.3$$

Where k_{ri} , μ_i , P_i , q_i , S_i , are relative permeability, viscosity, pressure, injection or production rate and saturation of phase i , respectively. k , t and ϕ are permeability, time and porosity, respectively.

Since pressure and temperature variations within the core under the coreflood conditions are relatively small, all compressibility effects of rock and fluids or compositional variations of the fluids or changes in the IFT, within the core have been neglected and the flows of three-phase are fully immiscible. Single point upstream weighting was used to approximate the mobility terms (i.e., terms involving k_r) to avoid numerical problems. The constant rate at the inlet and outlet of the core are two essential boundary conditions utilized in solving the fluid flow equation.

Because in our experiments the core is placed horizontally and the diameter of the core is small against the length, the fluid flow in Y and Z direction is negligible (Figure 4-4). For simulation of three-phase flow in horizontal coreflood experiment, equation 4.3 should be written for oil, water and gas in X direction (horizontal direction) under immiscible condition. The finite difference method is implemented to implicitly solve these sets of coupled, nonlinear partial differential equations (Aziz and Settari, 1979). By solving equation 4.2 the saturation and pressure profile of the different fluids versus time for various grid blocks are obtained. However, the saturation profile data resulted from equation 4.2 is employed to estimate the cumulative fluid production out of the core using volumetric material balance calculation. Also, the pressure drop across the core is easily calculated utilizing the pressure profile data along the core.

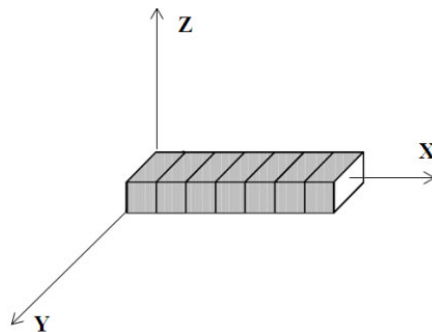


Figure 4-4: Cartesian core gridding in X direction

4.2.2 Relative permeability function

In general, for the case of three-phase flow, there are three relative permeability functions (k_{ro} , k_{rg} & k_{rw}) to be estimated. These are each a function of two independent saturations, hence each function represents a three dimension surface in terms of two saturations. To apply the optimisation method the unknown functions must be represented with a finite number of parameters. The larger the number of such parameters the more exponentially difficult will the achievement of the solution be. Since in two-phase flow there is only one independent variable (saturation) for each phase, the problem can relatively easily be solved by application of B-spline method with accurate results. This approach has been extended to the three-phase case representing the flow functions using two-dimensional B-spline (Shumaker, 1981; Mejia et al., 1996) relative permeability function, which is given by:

$$k_{ri}(S_I, S_{II}) = \sum_{k=1}^{m+n} \sum_{l=1}^{m+n} a_{k,l}^i B_{k,l}(S_I, S_{II}, y^I, y^{II}) \quad 4.4$$

Where m and n are Spline orders and number of knots, respectively and $a_{k,l}^i$ are unknown coefficients which should be estimated. The function $B_{k,l}(S_I, S_{II}, y^I, y^{II})$ is the B-spline basic function determined by the spline orders (m and n) and extended partition vectors, y^i . Directions I and II can be along any two saturation axes. Saturation coordinates S_I and S_{II} are selected in such a way that the produced relative permeabilities are monotonic functions of their respective saturations. For example, oil relative permeability needs to be represented by water and gas saturation planes, because by keeping one of these two saturations constant and increasing the other one, the oil saturation would definitely decrease and thus oil relative permeability would also decrease, and vice versa.

A key advantage of Spline function is the degree of control. In other words many different shapes of relative permeability curves can be easily provided by these functions using a few knots. We used a quadratic B-Spline function ($n=3$) with one interior knot ($m=1$) in each coordinate, so the oil, water and gas k_r functions can be introduced as follows:

$$k_{ro}(S_w, S_g) = \sum_{k=1}^4 \sum_{l=1}^4 a_{k,l}^{oil} B_{k,l}(S_w, S_g, y^{Sw}, y^{Sg}) \quad 4.5$$

$$k_{rw}(S_o, S_g) = \sum_{k=1}^4 \sum_{l=1}^4 a_{k,l}^{water} B_{k,l}(S_o, S_g, y^{So}, y^{Sg}) \quad 4.6$$

$$k_{rg}(S_w, S_o) = \sum_{k=1}^4 \sum_{l=1}^4 a_{k,l}^{gas} B_{k,l}(S_w, S_o, y^{Sw}, y^{So}) \quad 4.7$$

The optimization process can be made more efficient by imposing constrains on the estimated values of the coefficients ($a_{k,l}^i$). For example, relative permeability of each phase is taken to be monotonic with respect to saturation and limited between zero and one. The mathematical expressions of these constraints are as follows:

$$0 \leq k_{r,i} \leq 1 \quad \text{for} \quad 0 \leq S_i \leq 1 \quad 4.8$$

$$\left(\frac{\partial k_{r,i}}{\partial S_k} \right)_{S_j=Const} \leq 0 \quad \text{for} \quad 0 \leq S_k \leq 1 \quad 4.9$$

The unknown parameters in the Spline functions are selected in such a way that the above criteria are met. Based on the order of the Spline function, the number of knots and the above constraints, an unknown vector for each function is given by the following matrix:

$$\vec{\beta} = \begin{bmatrix} a_{11}, & a_{12}, & a_{13}, & a_{14} \\ a_{21}, & a_{22}, & a_{23}, & 0 \\ a_{31}, & a_{32}, & 0, & 0 \\ a_{41}, & 0, & 0, & 0 \end{bmatrix} \quad 4.10$$

The extended version of equation 4.4 for a two-phase oil relative permeability are given in equation 4.11 to 4.14.

$$k_{ro}(S_o) = a_1 B_{1,2}(S_o) + a_2 B_{2,2}(S_o) + a_3 B_{3,2}(S_o) + a_4 B_{4,2}(S_o) \quad 4.11$$

$$\begin{cases} B_{i,0}(S_o) = 1 & \text{if } t_i \leq t < t_{i+1} \\ B_{i,0}(S_o) = 0 & \text{otherwise} \end{cases} \quad 4.12$$

$$B_{i,n}(S_o) = \frac{S_o - t_i}{t_{i+n} - t_i} B_{i,n-1}(S_o) + \frac{t_{i+n+1} - S_o}{t_{i+n+1} - t_{i+1}} B_{i+1,n-1}(S_o) \quad 4.13$$

$$t_0 = 0, t_1 = 0, t_2 = 0, t_3 = 0.5, t_4 = 0, t_5 = 0, t_6 = 0, \quad 4.14$$

where a_1, a_2, a_3 and a_4 are unknown variables that should be tuned in the optimization process.

Table 4-1 demonstrates an example of three-phase oil relative permeability as a function of water and gas saturation, generated by equation 4.5. Also, the surface plot of three-phase oil relative permeability data provided in Table 4-1 is presented in Figure 4-5.

Table 4-1: An example of three-phase oil relative permeability as function of water and gas saturation generated by equation 4.5.

		Sw										
		0	0.1	0.2	0.3	0.4	0.5	0.6	0.7	0.8	0.9	1
Sg												
0		0.6736	0.4543	0.2808	0.1533	0.0717	0.0362	0.0238	0.0130	0.0054	0.0012	0.0000
0.1		0.4325	0.2919	0.1806	0.0987	0.0463	0.0234	0.0150	0.0075	0.0024	0.0000	
0.2		0.2448	0.1654	0.1025	0.0562	0.0265	0.0134	0.0081	0.0031	0.0000		
0.3		0.1105	0.0749	0.0466	0.0257	0.0122	0.0061	0.0031	0.0000			
0.4		0.0295	0.0203	0.0128	0.0072	0.0035	0.0017	0.0000				
0.5		0.0020	0.0016	0.0012	0.0007	0.0003	0.0000					
0.6		0.0013	0.0010	0.0007	0.0003	0.0000						
0.7		0.0007	0.0006	0.0003	0.0000							
0.8		0.0003	0.0002	0.0000								
0.9		0.0001	0.0000									
1		0.0000										

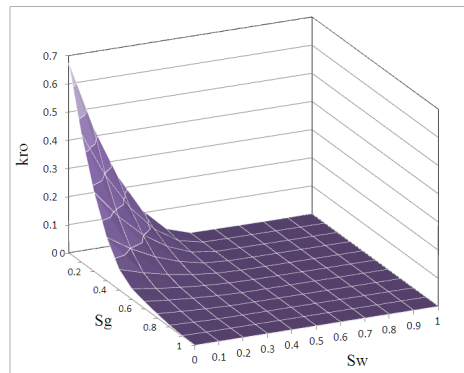


Figure 4-5: 3-D plot of three-phase oil relative permeability data (Table 4-1) as a function of water and gas saturation.

4.2.3 Estimation procedure

The determination of the coefficient within the B-Spline representations are carried out by solving a minimization problem using Genetic algorithm. An objective function is formulated as a weighted sum of squared difference between the measured data and corresponding values calculated from mathematical model of the experiment:

$$J(\vec{\beta}) = [\vec{Y} - F(\vec{\beta})]^T W [\vec{Y} - F(\vec{\beta})] \quad 4.15$$

Where $\vec{\beta}$ is the matrix of unknowns given in equation 4.10, Y is a vector of data measured in the experiment and $F(\vec{\beta})$ are the corresponding value calculated with the mathematical model of the experiment. The weighting factor matrix W is selected according to statistical criteria so that, with an appropriate choice of a mathematical model and unknown coefficients ($a_{k,l}^i$), maximum-likelihood estimates are obtained. Generally, it can be taken to be a diagonal matrix with entries equal to the inverse of the estimated variances of data measured errors.

Before giving an overview of the GA implementation, a glossary of the GA terms used in our methodology is provided here:

Individual (chromosomes): refer to a possible solution of the problem. In our case, a set of oil, water and gas relative permeability are considered as a chromosome.

Genes: Refer to a single element of an individual. Each coefficient in the B-Spline function is considered as a gene.

Population or generation: is a group of individuals at any time step of the evolution. The population size refers to the number of individuals in a population.

The executive procedure of the GA used in our work is illustrated in Figure 4-9 and can be explained as follows:

1. Generate a random population of n chromosomes (suitable solutions for the problem). By using equations 4.5 to 4.7, choosing random values for a_{jk}^i and considering

constrains presented by equation 4.8 and 4.9, n individual of relative permeabilities will be created.

2. Core flood simulation is run for each set of chromosomes and the misfit value between experimental and simulated data of each Individual is calculated.
3. Select two parent chromosomes from a population according to their fitness (the better the fitness, the bigger the chance of being selected).
4. Crossover is one of the reproduction operations. Two selected individuals exchange their genes to generate a new individual (Chromosome). One crossover point is then selected from the beginning of the chromosome to the crossover point and is copied from one parent and the rest is copied from the second parent. For instance, the chromosomes A and B as given in Figure 4-6 are two selected chromosome from the population.

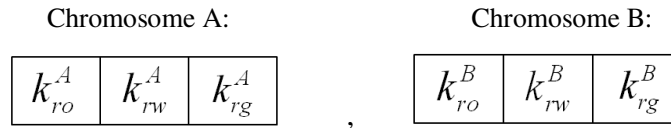


Figure 4-6: Two selected chromosome A and B from population.

Then new offspring can be obtained using following equation:

$$\text{New offspring} = \lambda \times (\text{Chrom A}) + (1 - \lambda) \times (\text{Chrom B}) \quad 4.16$$

Where λ is crossover probability which can be chosen as a random value between 0 and 1. Based on Figure 4-6 and equation 4.16 the new offspring for the given crossover point is shown in Figure 4-7.

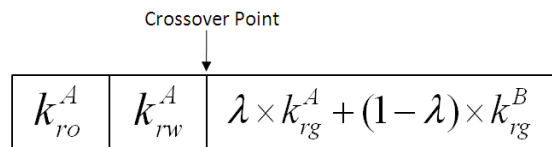


Figure 4-7: New offspring for the given crossover point.

5. Having performed crossover, the mutation must be done. This is to prevent all solutions of the population falling into a local optimum of the solved problem. Mutation randomly changes the new offspring. For example, one of the parameters in the new offspring can be changed slightly by altering a few of its B-Spline coefficients (Figure 4-8).

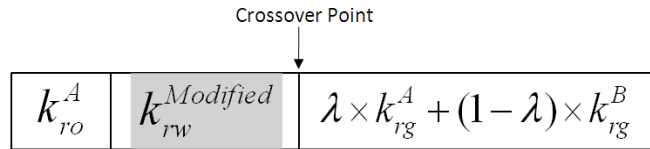


Figure 4-8: Mutation operation on new offspring.

6. Accepting: The new misfit value obtained by running the simulator with the new mutated offspring should be compared with other misfits in the population. If the new misfit value is less than the maximum misfit in the population, then the new offspring would be placed in the population and the one with the highest misfit value will be withdrawn from the population list.

This loop (Step3 to 6) will be repeated until a satisfactory misfit is achieved.

Software named *3RPSim* was developed based on the aforementioned methodology in order to determine three-phase relative permeability from unsteady-state coreflood experiment. A quick demonstration of this software is given in appendix A.

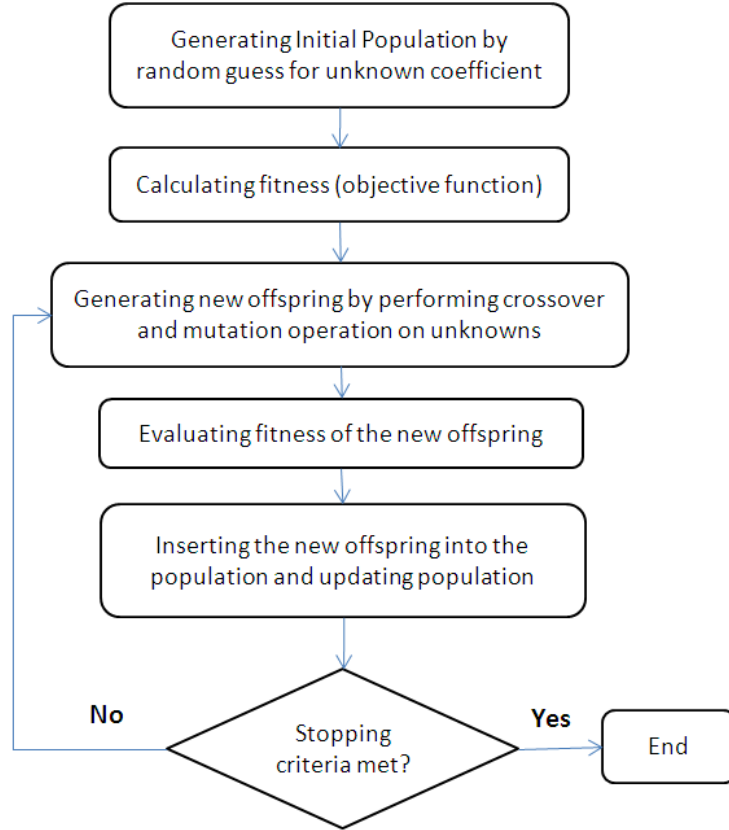


Figure 4-9: Flowchart of implementation of the Genetic Algorithm

4.3 Verification of the algorithm

To validate the integrity of our Algorithm and the program, two sets of three-phase k_r values (Oak, 1991) were used in simulation of the unsteady state coreflood experiment. Oak (1991) used a Berea sandstone core with the permeability of 1010 mD and 310 mD with intermediate wettability for measuring relative permeabilities.

Two gas injection coreflood displacement experiments using Oak data were synthetically designed by the black oil reservoir simulator, Elipse100, to generate fluid production and pressure data. In the first experiment, gas was injected at 200 cm³/h into the 1010 mD core, with an initial saturation of 50% oil and 50% water. A total of 68 PV (pore volume) of gas was injected into the core. The second gas injection was performed on the 310mD core with the same length, which was initially saturated with 45% water, 10% gas and 45% oil. The rate of injection was selected at 200 cm³/h and a

total of around 100 pore volume of gas was injected into the core. The core and fluid properties are provided in Table 4-2.

Table 4-2: Core and fluid properties for synthetic experiment

----- Core-----			
Length cm	Diameter cm	Porosity frac.	Absolute Permeability mD
19	5.1	0.21	1010 & 310

----- Fluid-----		
Oil Viscosity, cp	Gas Viscosity, cp	Water Viscosity, cp
1.4	0.0187	1

The data obtained from Eclipse100 by simulating the experiments including, fluid recovery data and the pressure drop across the core, were used as the input data for my history matching software to back-calculate the oil, water and gas relative permeability values by matching with the data obtained from Genetic Algorithm (GA). The GA started with 20 populations, then crossover and mutation took place via 800 iterations to reach a global minimum value of the misfit. Both experiments were successfully matched with the observed data. The comparison between relative permeability resulting from the history matching process and real relative permeability entered into Eclipse are given below.

4.3.1 Results of first gas injection

The production of each fluid and its corresponding pressure drop across the core for both the measured (simulated) and the history matched results of the first gas injection test are shown in Figure 4-10 and Figure 4-11, respectively. As can be seen, there are good agreements between the simulated and the history matched data (i.e. fluid recoveries, pressure drop). The k_r values estimated from history matching of the displacement experiment are relevant in the vicinity of the saturation trajectory in which the experiment occurred. In other words, those saturation ranges where the flow and

displacements occurred have more reliable k_r values compared to k_r values obtained for saturations outside that range.

A comparison of the experimentally derived and estimated k_{r0} versus oil saturation for the experimental saturation path (Figure 4-12) is shown in Figure 4-13. Similarly, Figure 4-14 depicts three-phase water relative permeability versus water saturation. Comparison of the three-phase k_{rg} versus gas saturation is presented in Figure 4-15. As can be seen, in all cases there is a satisfactory match between the laboratory-derived k_r value (Oak, 1991) and the estimated values resulted from our history matching.

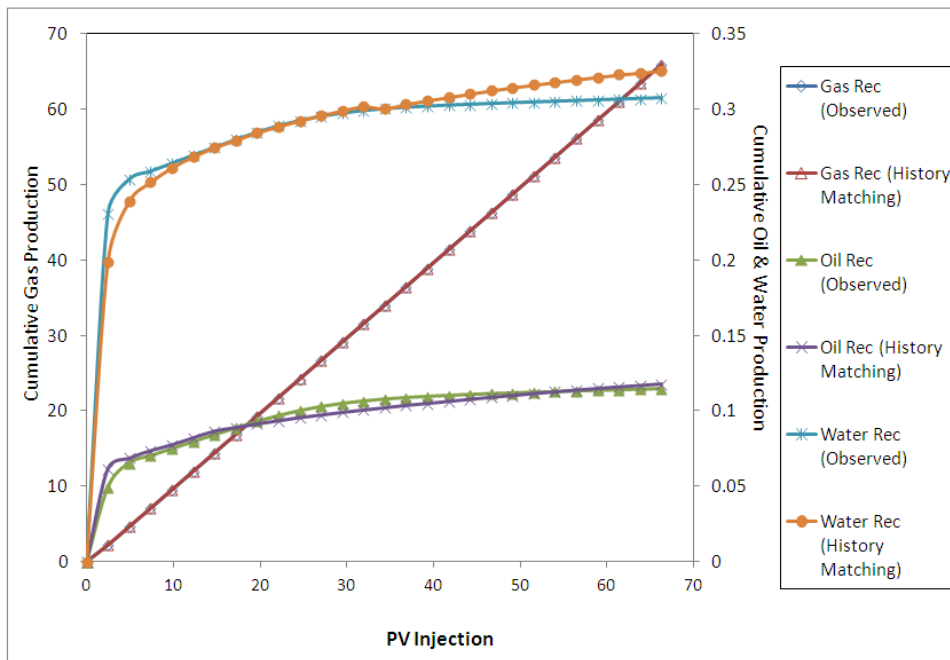


Figure 4-10: History matched (GA) and ‘observed’ (ECLIPSE100) production vs., injected gas pore volume, obtained from the first gas injection test.

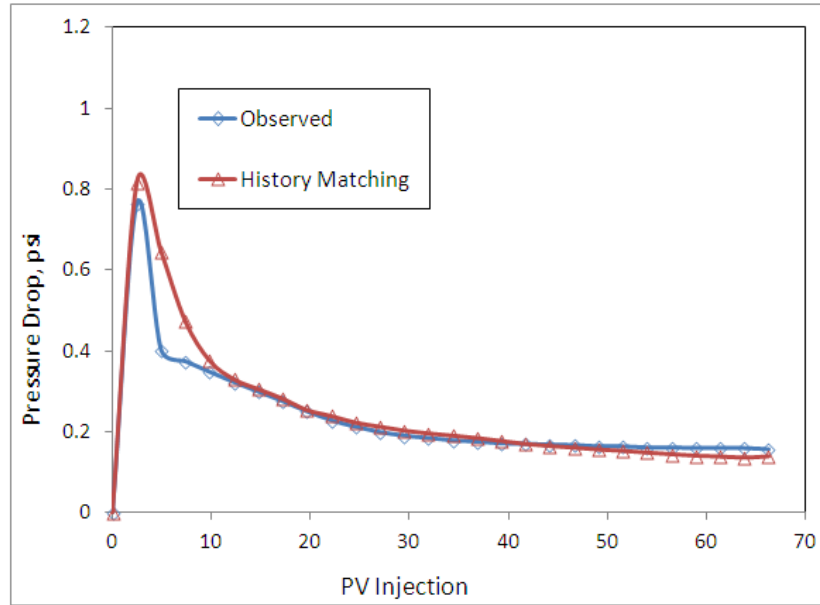


Figure 4-11: History matched (GA) and 'observed' (ECLIPSE100) pressure drop vs., injected gas pore volume across the core, obtained from the first gas injection test.

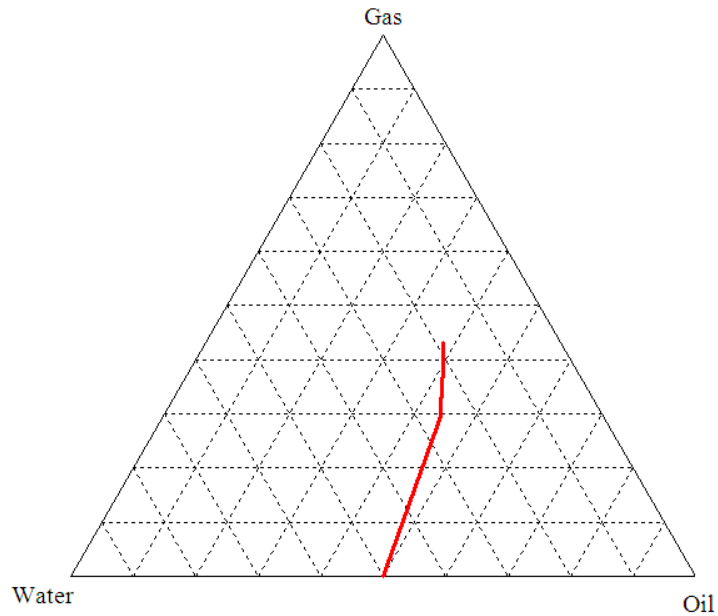


Figure 4-12: Saturation path of the first gas injection.

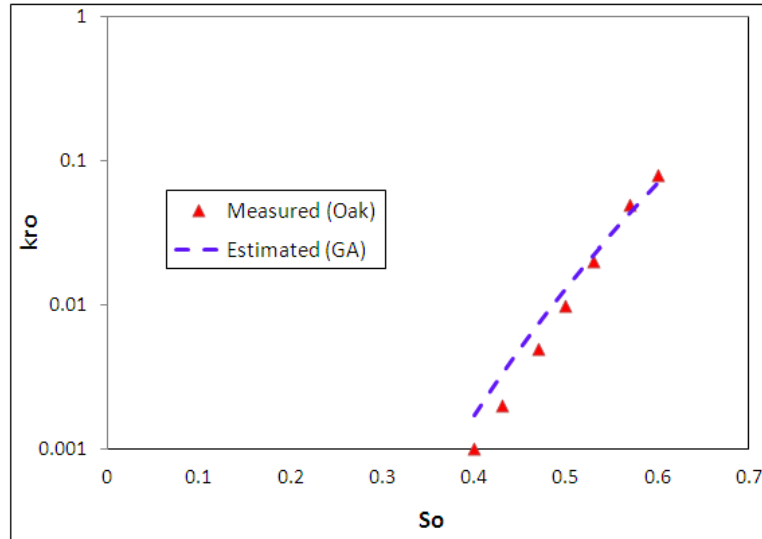


Figure 4-13: Semi-log plot of the oil relative permeability versus oil saturation of the Oak data and history matching results from the first gas injection.

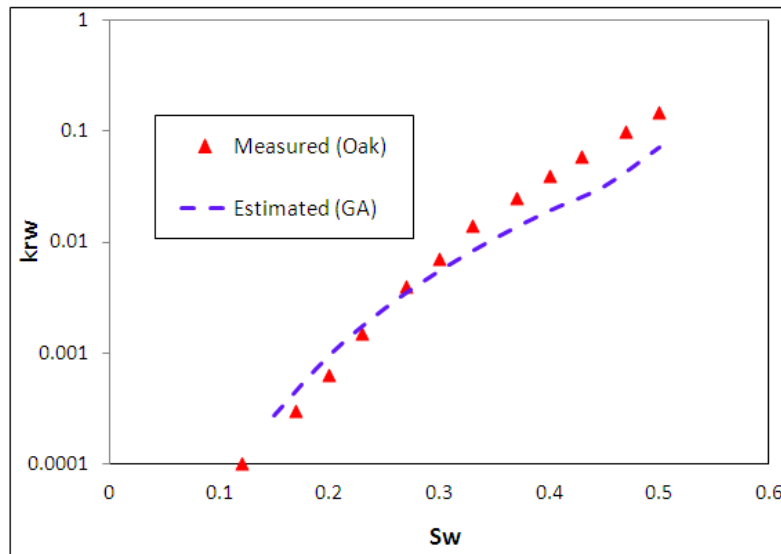


Figure 4-14: Semi-log plot of the water relative permeability versus water saturation of the Oak data and history matching results from the first gas injection.

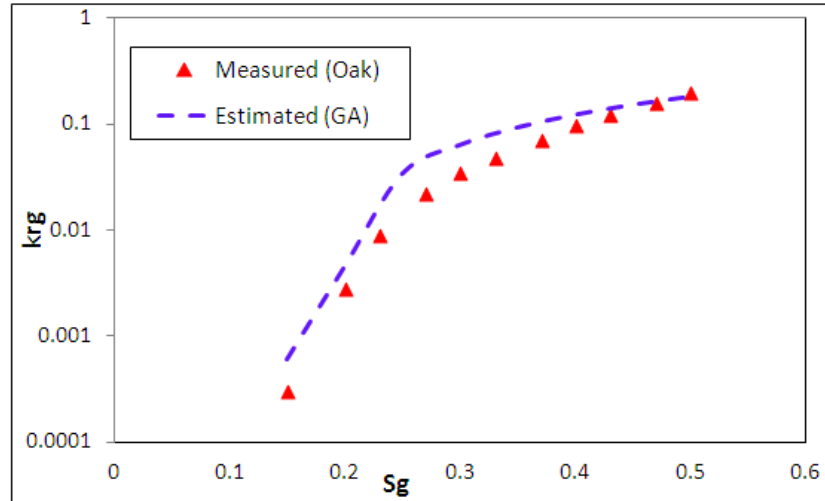


Figure 4-15: Semi-log plot of the gas relative permeability versus gas saturation of the Oak data and history matching results from the first gas injection.

4.3.2 Results of second gas injection

The second gas injection test was designed and history matched incorporating oil-water and oil-gas capillary pressure, given in Figure 4-16. The results of cumulative oil, water and gas production versus injected pore volume, obtained from Eclipse100 and history matching is provided in Figure 4-17. The corresponding pressure drop across the core obtained from Eclipse100 and history matching is shown in Figure 4-18. Both figures demonstrate a reasonable match between observation (Eclipse100) and history matching results.

Three-phase relative permeability of each phase, estimated from history matching, is plotted versus its own phase saturation for the range of saturation paths occurring in the the experiment (Figure 4-19). In order to assess the precision of the calculated relative permeability data, these were compared with the real relative permeability at the same saturation range. Figure 4-20 presents calculated and measured oil relative permeability versus oil saturation. The water relative permeability versus water saturation estimated by history matching and the real data is shown in Figure 4-21. Figure 4-22 illustrates gas relative permeability versus gas saturation for both calculated and observed data. The close match between measured and estimated relative permeability in Figure 4-20

to Figure 4-22 indicates a great degree of accuracy for the matching algorithm presented above.

In order to evaluate the efficiency of the algorithm in reducing misfit value (difference between observation and simulation), we have plotted the best misfit value obtained in each population versus generation number for both gas injection tests, in Figure 4-23. As each population has 20 members and the total number of simulation runs is 1000, the total generation (population) number becomes 50. However, the decreasing trend of misfit curves in Figure 4-23 highlights that the optimization process (genetic algorithm) is converging fast enough. Furthermore, the slope of misfit curves is becoming almost zero toward the end, which demonstrates that performing further simulations after generation 50 wouldn't more reduce the misfit value.

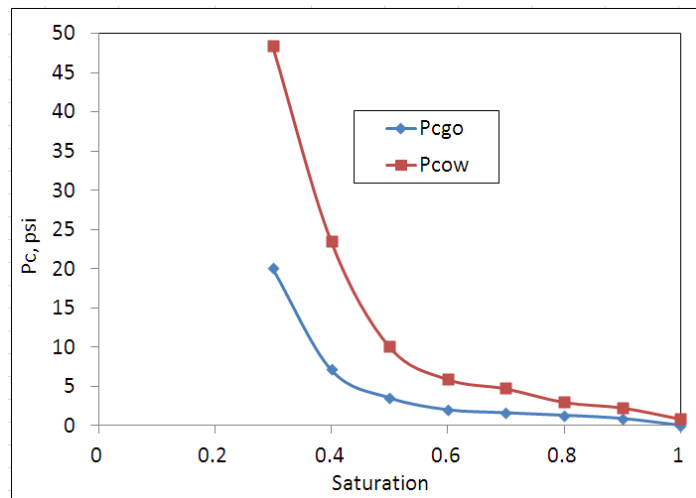


Figure 4-16: Oil-water and oil-gas capillary pressure versus wetting phase saturation used in simulation (Eclipse100) and history matching.

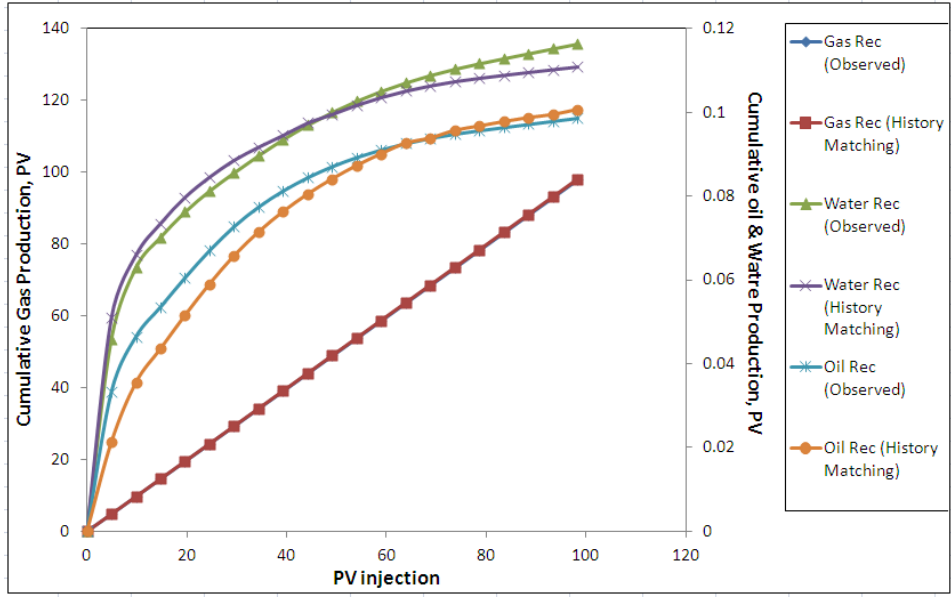


Figure 4-17: History matched (GA) and ‘observed’ (ECLIPSE100) production vs., injected gas pore volume , from the second gas injection test.

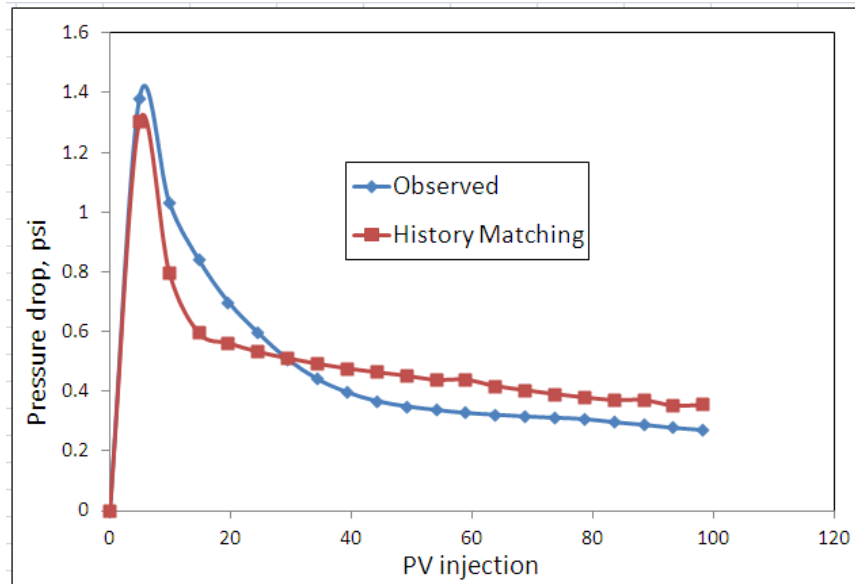


Figure 4-18: History matched (GA) and ‘observed’ (ECLIPSE100) pressure drop vs., injected gas pore volume across the core, obtained from the second gas injection test.

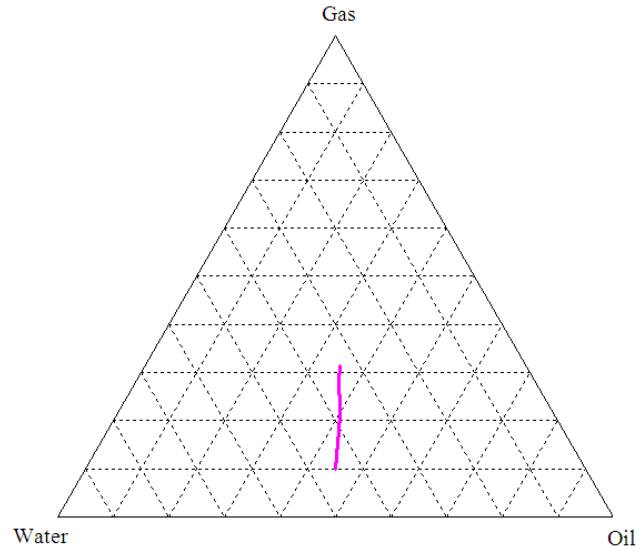


Figure 4-19: Saturation path of the second gas injection.

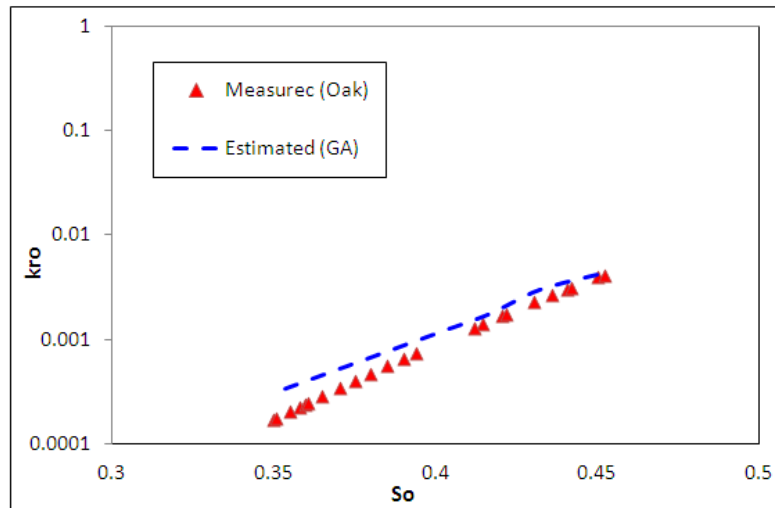


Figure 4-20: Semi-log plot of the oil relative permeability versus oil saturation of the Oak data and history matching results from the second gas injection.

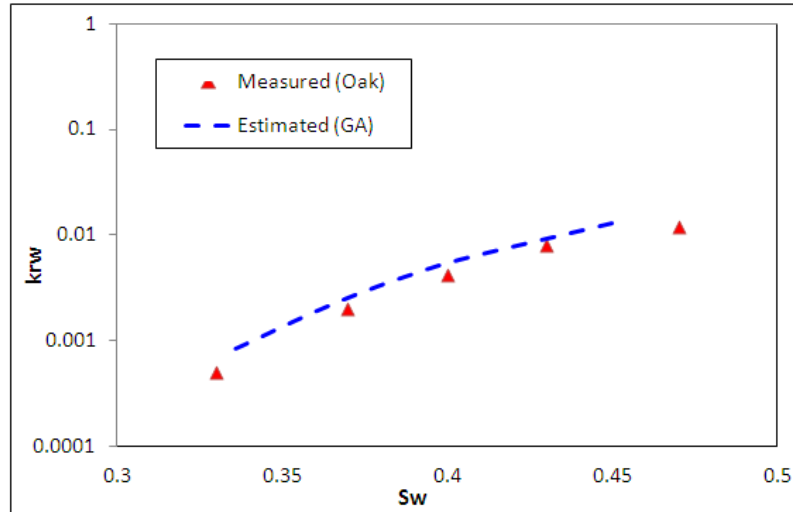


Figure 4-21: Semi-log plot of the water relative permeability versus water saturation of the Oak data and history matching results from the second gas injection.

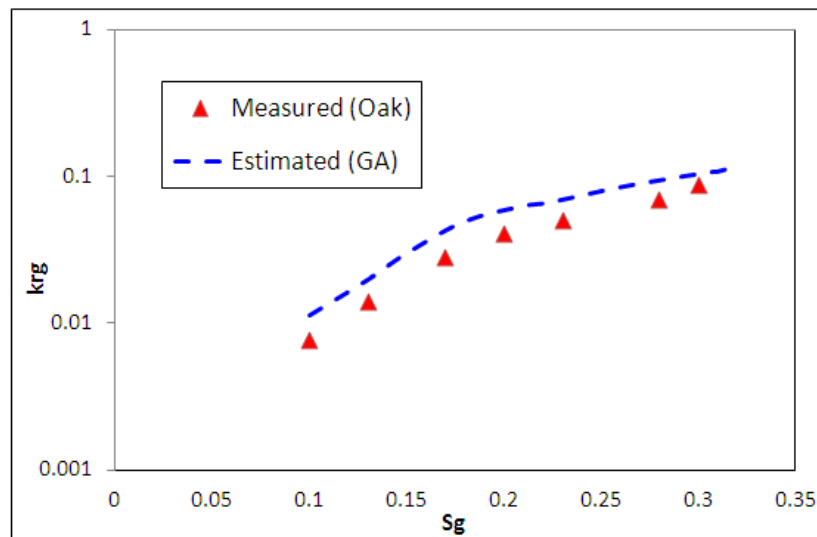


Figure 4-22: Semi-log plot of the gas relative permeability versus gas saturation of the Oak data and history matching results from the second gas injection.

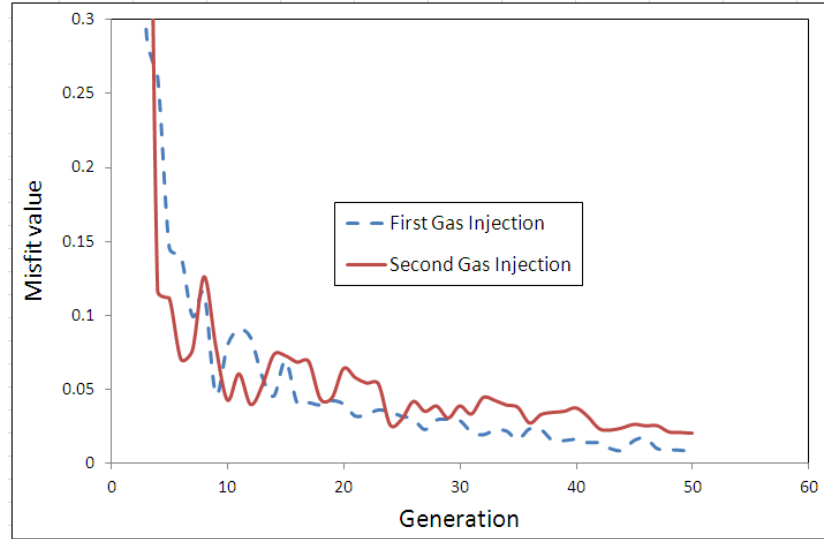


Figure 4-23: Best misfit value obtained in each population versus generation number for first and second gas injection

4.4 Conclusions

The major conclusions of this chapter are summarized as follows:

1. A powerful tool has been developed to accurately estimate three-phase k_r from experimentally measured production and pressure drop of unsteady-state coreflood displacement tests. An appropriate and flexible function was chosen for three-phase relative permeability, to generate maximum set of relative permeability curves in an optimization process to obtain results corresponding to the minimum error values.
2. To overcome the limitations of most of the existing three-phase k_r models, regarding the dependency of k_{rw} and k_{rg} on only their own saturation [$k_{rw} = k_{rw}(S_w)$, $k_{rg} = k_{rg}(S_g)$], the author concentrated our efforts on three-phase k_{rw} , k_{rg} and k_{ro} as a function of two saturations [$k_{rw} = k_{rw}(S_o, S_g)$, $k_{rg} = k_{rg}(S_o, S_w)$, $k_{ro} = k_{ro}(S_g, S_w)$].
3. By applying this approach, we can overcome some of the restrictions present in the explicit methods (such as the JBN) which neglect capillary forces.
4. The integrity of the presented history matching approach was successfully verified by employing synthetic data built by the Eclipse reservoir simulator. The method was also successfully used to generate three-phase k_r curves by

history matching three-phase coreflood experiments carried out in the laboratory.

4.5 Reference

- Aziz, K., and Settari, A., 1979, *Petroleum Reservoir Simulation*: London, Applied Science.
- Bard, Y., 1974, *Nonlinear Parameter Estimation*: Washington, DC, Academic Press Inc.
- Cao, P., and S, S., 2010, Three-Phase Unsteady State Relative Permeability Measurement In Consolidated Cores Using Three Immiscible Liquids, presented at the International Symposium of the Society of Core Analysis, Halifax, Canada.
- Holland, j., 1975, *Adaptation in Natural and Artificial Systems* University of Michigan Press.
- Johnson, E.F., Bossler, D.P., and Naumann, V.O., 1959, Calculation of Relative Permeability from Displacement Experiments, paper SPE 001023-G,
- Kerig, P.D., and Watson, A.T., 1986, Relative-Permeability Estimation From Displacement Experiments: An Error Analysis: SPE Reservoir Engineering, paper SPE 12589, (03).
- Marquardt, D.W., 1963, An Algorithm For Least-Square Estimation of Nonlinear Parameters: Soc. Industrial Applied Math Journal, 11, p. 431-441.
- Mejia, G.M., Watson, A.T., and Nordtvedt, J.E., 1996, Estimation of Three-phase Functions In Porous Media: AIChE Journal, 42(7).
- Oak, M.J., 1991, Three-Phase Relative Permeability of Intermediate-Wet Berea Sandstone, paper SPE 22599, presented at the SPE Annual Technical Conference and Exhibition, Dallas, Texas.
- Shumaker, L.L., 1981, *Spline Functions: Basic Theory*: New York, Wiley.
- Sohrabi, M., 2001, *Water Alternating Gas (WAG) Injection Studies: Degree of Doctoral of Philosophy thesis* Edinburgh, Heriot-Watt University.
- Sun, X., and Mohanty, K.K., 2005, Estimation of Flow Functions During Drainage Using Genetic Algorithm: SPE Journal, paper SPE 84548-PA, (12).
- Tokuda, N., and Takahashi, S., 2004, Development of Automatic History Matching Program Base on Genetic Algorithm For X-Ray CT Core Flooding Experiment, presented at the International Symposium of the society of Core Analysis, Abu Dhabi, UAE.
- Wang, J., and Buckley, S., 2006, Automatic History Matching Using Differential Evolution Algorithm, presented at the International Symposium of the society of Core Analysis, Trondheim, Norway.

Chapter 5

Characterization of Three-Phase k_r and Hysteresis effect in the WAG Process

In this section, the results of history matching of fluid production and pressures obtained from various displacement experiments using our in-house software described in the previous section are first reported. Then, the trend of relative permeability curves and hysteresis effect between various cycles under different wettability conditions, are discussed. Since the non-wetting trapped saturation plays a significant role in hysteresis, the most practised trap model in literature (Land, 1968) is evaluated against the values measured from the WAG experiments at the end of this chapter.

5.1 History matching results

As reported in the previous chapter, an in-house coreflood simulator was developed in order to obtain relative permeability values from unsteady-state experiments by history matching the measured recovery and differential pressure profiles. All cycles of WAG experiments given in table 2-3 have been successfully history matched using the in-house coreflood simulator to estimate three-phase k_r values corresponding to each cycle of these WAG experiments.

The interfacial tension between oil and gas is very small, which causes negligible capillary pressure for an oil/gas system, and hence the behaviour of capillary forces between oil and water (P_{cow}) at three-phase flow condition approaches the P_{cow} under two-phase flow circumstances. Therefore, for history matching of WAG experiments, the two-phase oil/water capillary pressure (Figure 2-11 and Figure 2-12) has been employed as an approximation for three-phase capillary pressure.

The results of the history matching of coreflood tests are given below.

5.1.1 1000mD-MW

Figure 5-1 demonstrates the comparison between experimental and history matched cumulative oil production as a fraction of residual oil saturation, S_{orw} (remaining oil after 1st water flooding) versus cumulative injected pore volume obtained from WAG injection into the 1000mD-WW core. It should be noted that the first water flooding of all WAG experiments has been conducted under two-phase flow (oil-water) conditions. The corresponding cumulative pore volumes (PV) of water and gas production and pressure drop across the core versus cumulative injected PV for all cycles are presented in Figure 5-2 to Figure 5-4. The notation G1, W2 and G2, distinguished by the dashed lines in Figure 5-1 to Figure 5-4 refer to results obtained from first gas injection, second water injection and second gas injection, respectively. The production and pressure drop results obtained from history matching show good agreement with the equivalent measured data. The optimization process for history matching of this WAG experiment took place in around 200 iterations, using the values of 1 and 0.1 as weight factors for production and pressure drop, respectively, in the objective function.

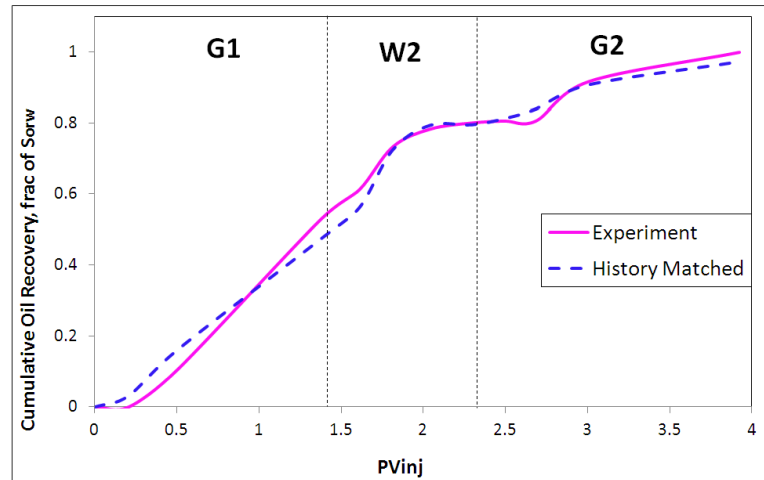


Figure 5-1: Cumulative oil production as a fraction of S_{orw} (saturation of the remaining oil after first water injection) versus cumulative pore volume injected into the 1000mD-MW core, experimental and history matched data.

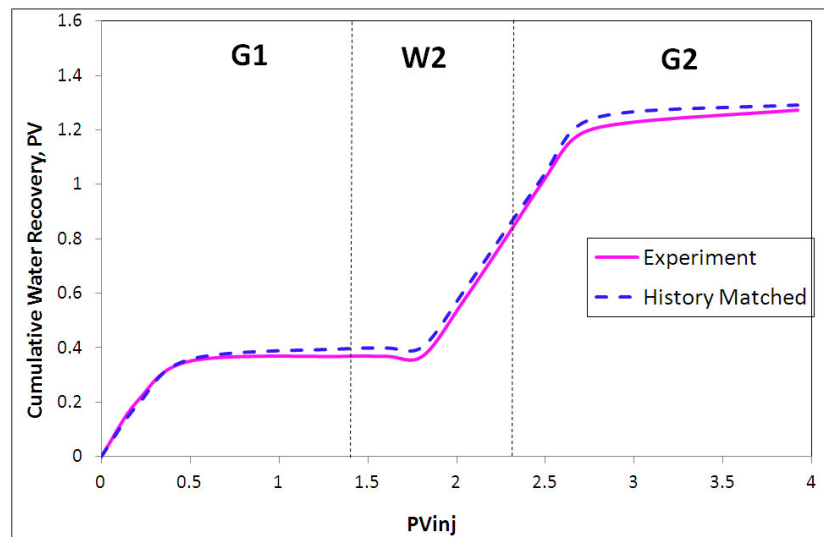


Figure 5-2: Cumulative water production versus cumulative pore volume injected into the 1000mD-MW core, experimental and history matched data..

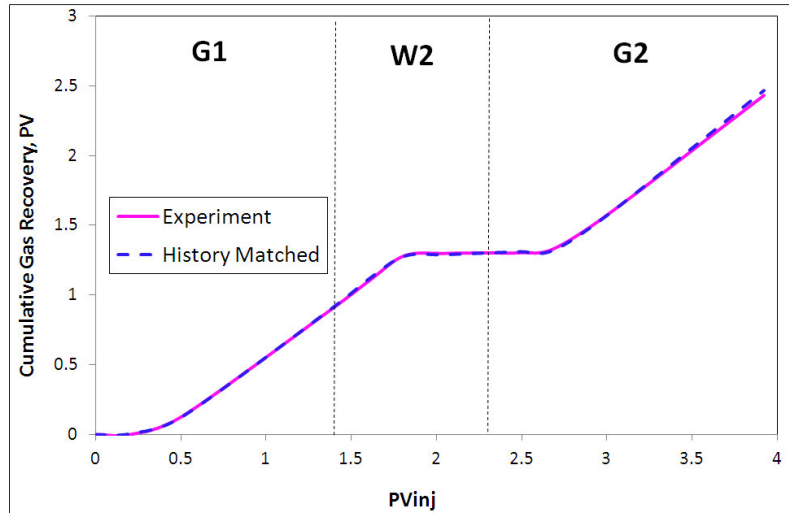


Figure 5-3: Cumulative gas versus cumulative pore volume injected into the 1000mD-MW core, experimental and history matched data.

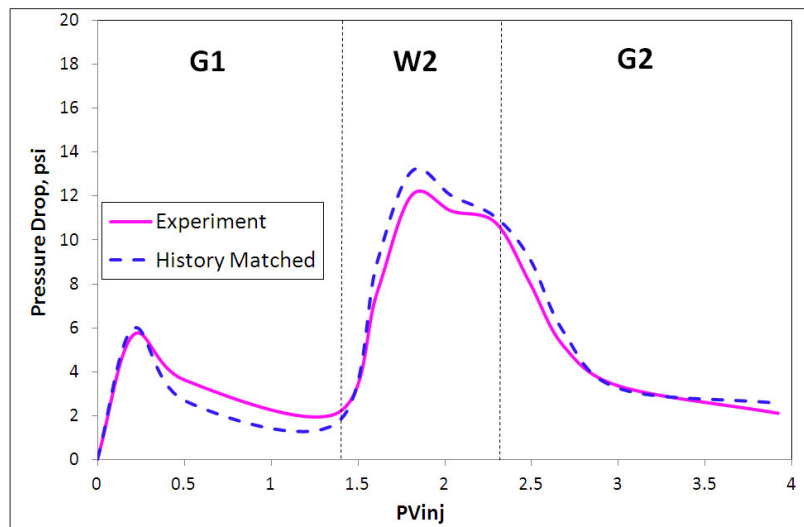


Figure 5-4: Pressure drop across the core versus cumulative pore volume injected into the 1000mD-MW core, experimental and history matched data.

5.1.2 65mD-WW

History matching of the WAG experiment through the 65mD water-wet core was successfully implemented in about 700 iterations, utilizing the values of 1 and 0.01 as the weighting factors for production and pressure, respectively, in the objective functions. The cumulative oil production as a fraction of S_{orw} versus cumulative injected pore volume resulted from history matching and experiment is shown in Figure

5-5. The corresponding cumulative water and gas production and pressure drop across the core are shown in Figure 5-6 to Figure 5-8. In Figure 5-5 to Figure 5-8, G1 stands for the first gas injection, G2 denotes the second gas injection, and so forth. The close match between the simulation and observed data obtained via the optimization process demonstrates that the estimated relative permeabilities are very well represented by the fluid flow functions in the 65mD water-wet core.

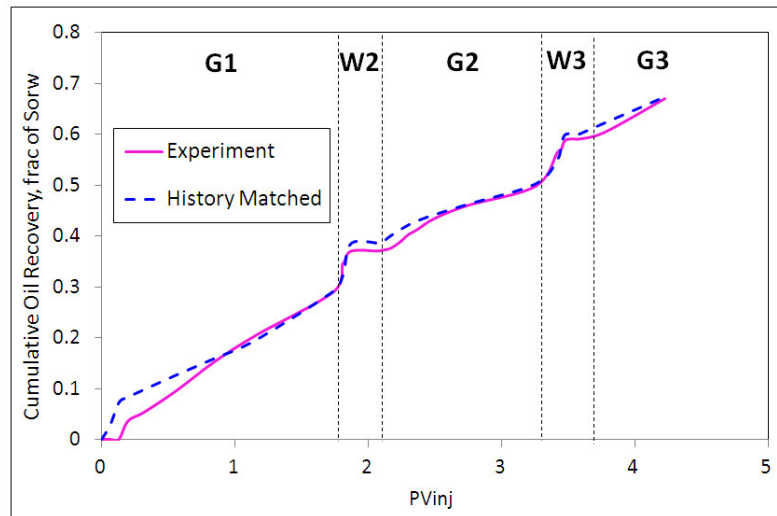


Figure 5-5: Cumulative oil production as a fraction of S_{orw} (saturation of the remaining oil after first water injection) versus cumulative pore volume injected into the 65mD-WW core, experimental and history matched data.

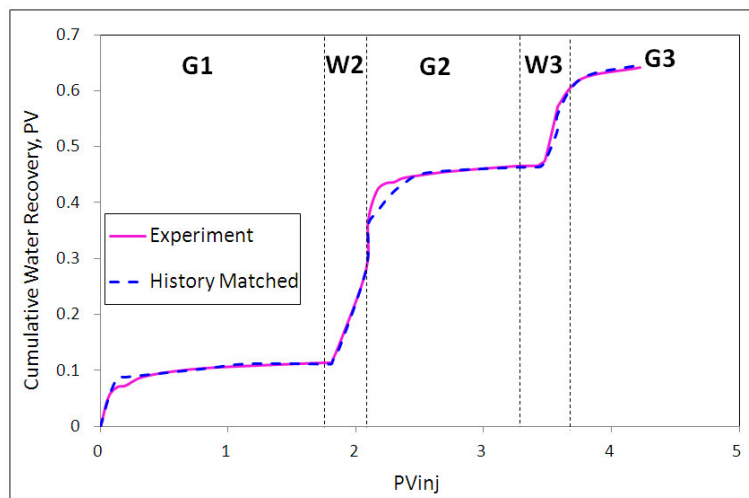


Figure 5-6: Cumulative water production versus cumulative pore volume injected into the 65mD-WW core, experimental and history matched data.

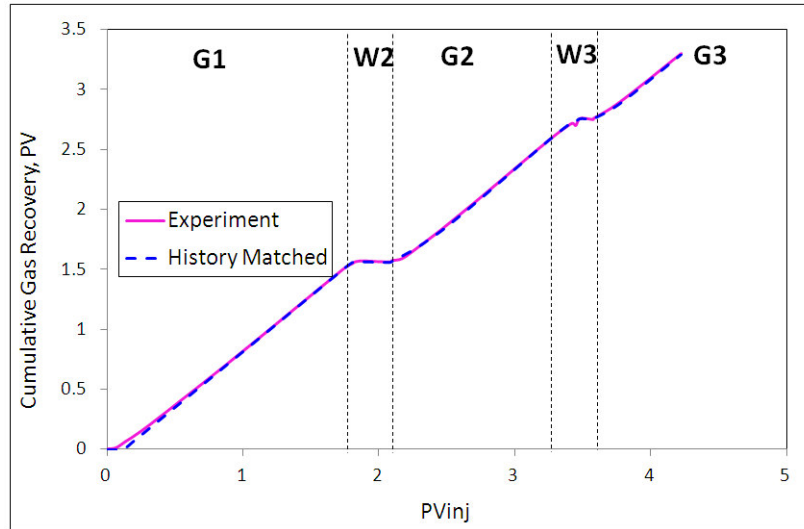


Figure 5-7: Cumulative gas production versus cumulative pore volume injected into the 65mD-WW core, experimental and history matched data.

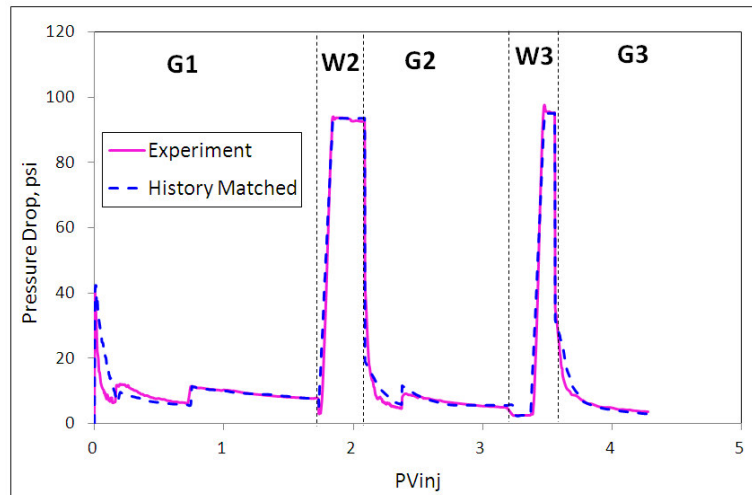


Figure 5-8: Pressure drop across the core versus cumulative pore volume injected into the 65mD-WW core, experimental and history matched data.

5.1.3 65mD-MW

The history matching of the WAG experiment of the 65mD mixed-wet core was implemented in approximate 1000 iterations while using the values of 0.1 and 0.01 as the weight factors of production and pressure data in the objective functions. The

comparisons between history matching and experimental observations for oil, water and gas recoveries and pressure drop profile are shown in Figure 5-9 to Figure 5-12.

A comparison between the number of iterations for the optimization processes of the WAG experiments in 1000mD-MW and 65mD-MW reveals that the history matching of lower permeability core-test is much more difficult than that of the rock of higher permeability. Moreover, the number of iterations in history matching of a WAG test in the 65mD mixed-wet-core is greater than that in the 65 mD water-wet-core, which highlights the fact that the fluid flow in mixed-wet porous media would be more complex than that in a water-wet system.

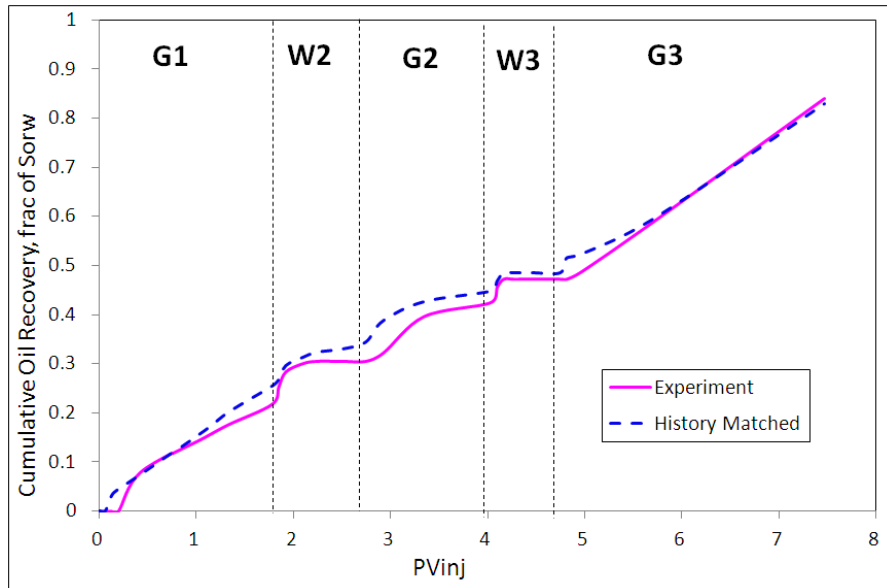


Figure 5-9: Cumulative oil production as fraction of S_{orw} (saturation of the remaining oil after first water injection) versus cumulative pore volume injected into the 65mD-MW core, experimental and history matched data.

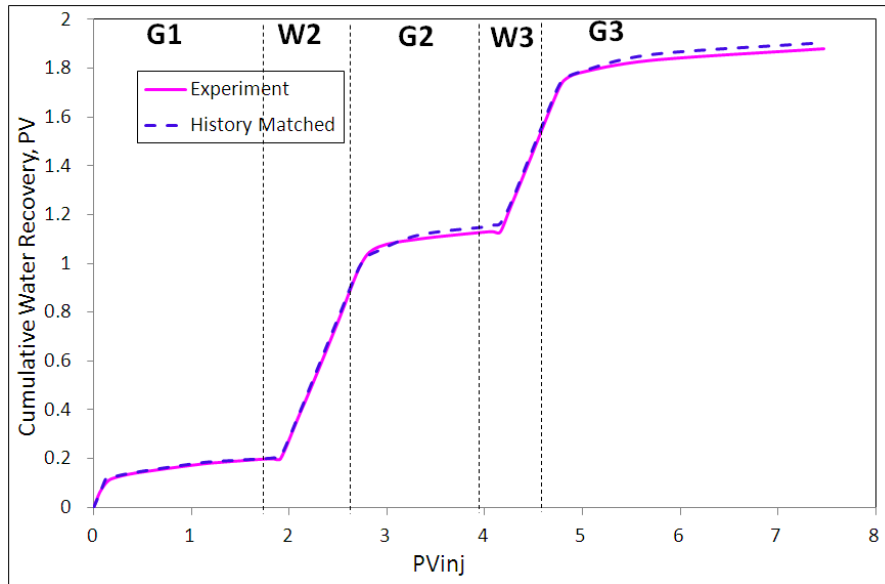


Figure 5-10: Cumulative water production versus cumulative pore volume injected into the 65mD-MW core, experimental and history matched data.

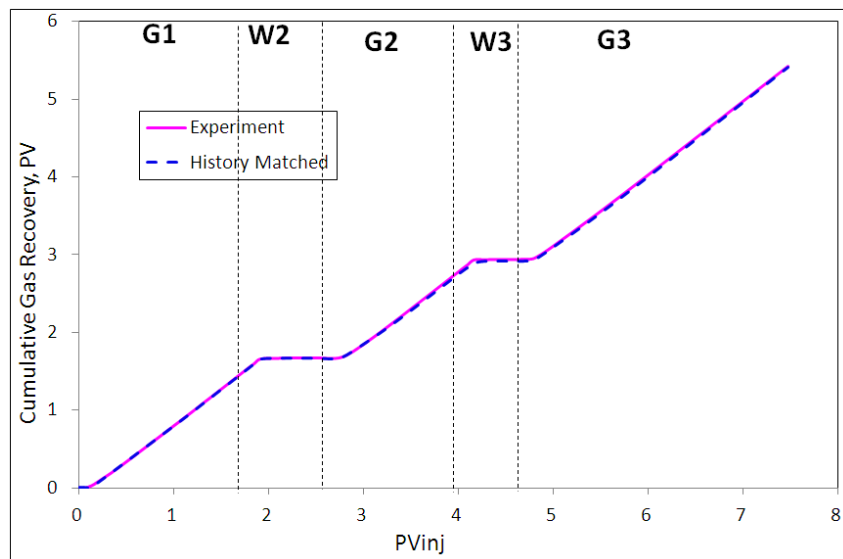


Figure 5-11: Cumulative gas production versus cumulative pore volume injected into the 65mD-MW core, experimental and history matched data.

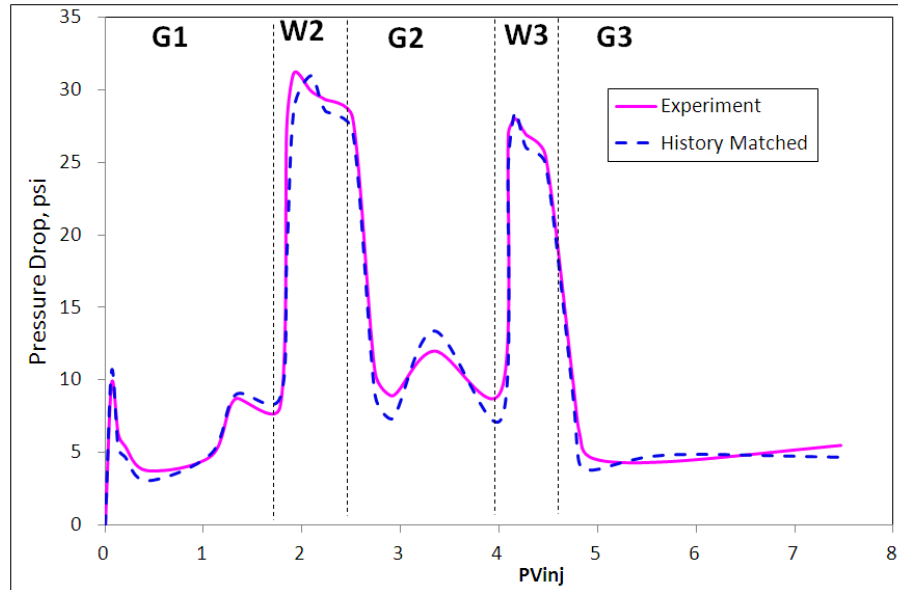


Figure 5-12: Pressure drop across the core versus cumulative pore volume injected into the 65mD-MW core, experimental and history matched data.

5.2 Three-phase relative permeabilities

The corresponding three-phase relative permeability values estimated from the history matching of the various WAG experiments are reported in this section. The relative permeabilities are plotted against the saturation path in Figures 2-2 to 2-4. The impact of hysteresis and wettability, and the comparison between two-phase and three-phase relative permeability are discussed here.

5.2.1 Hysteresis

Hysteresis refers to irreversibility or path dependence. The previous studies have reported two kinds of hysteresis effects taking place in the relative permeability data. The first is the traditional hysteresis effect attributed to the reversing of the saturation changes from increasing to decreasing or vice versa (i.e. imbibition to drainage or drainage to imbibition). This hysteresis effect has been investigated and modelled widely in two-phase and rarely in three-phase relative permeability (Land, 1968; Killough, 1976; Baker, 1988; Eleri et al., 1995a; Larsen and Skauge, 1998; Egermann et al., 2000; Element et al., 2003). The second kind of hysteresis effect in relative

permeability occurs between two consecutive injections in the scenario when they are carried out in the same direction (Eleri et al., 1995a; Larsen and Skauge, 1998; Spiteri and Juanes, 2004). For instance, the significant discrepancy between k_{rg} of the different gas injections performed in alternation with the water injection arises from this kind of hysteresis. In this work, the first hysteresis effect refers to the conventional hysteresis and the second refers to the cyclic hysteresis. Here, we investigate both cyclic and conventional hysteresis in relative permeability occurring during WAG processes.

Cyclic hysteresis in gas relative permeability

Figure 5-13 to Figure 5-15 show gas relative permeability versus gas saturation obtained from gas injection into the three different cores of 1000mD-MW, 65mD-WW and 65mD-MW. Advancing gas within the core increases the gas mobility. However, as shown in these figures, when gas injection follows a water injection cycle, its relative permeability curve does not follow the trend of the previous gas cycle. In other words, comparing k_{rg} of the 1st gas with 2nd gas reveals that gas relative permeability of the 2nd gas has a lower value than that of the 1st gas, at the same gas saturation (S_g). This trend is also observed between 2nd and 3rd gas injections in Figure 5-14 and Figure 5-15. This behaviour is observed in the WAG injection of all the three cores. The reason is that any water injection performed prior to the gas injection traps some amount of the mobile gas, rendering it immobile in the core. Such trapped (non-wetting) gas will not contribute towards the mobility of the new total injected gas. In other words, every new gas injection cycle following a water injection cycle commences with higher amount of immobile gas, which reduces the mobility of the total in-situ gas. As illustrated in Figure 5-13 and Figure 5-15, the gap between the k_{rg} curve of the 2nd and 3rd cycles is less than that between the 1st and 2nd cycles. Thus, we notice that the difference between subsequent pairs of k_{rg} curves diminishes continually because the rate of increasing trapped gas in the system reduces. Comparison of k_{rg} of the water-wet core with that of the mixed-wet core (both 65mD) (Figure 5-14 and Figure 5-15) reveals that cyclic hysteresis of k_{rg} for the water-wet system is more pronounced than that in the mixed-wet system. One important conclusion that can be drawn from these results is that one should expect the gas injectivity to significantly reduce as the WAG injection proceeds.

Gas relative permeability versus gas saturation obtained from the second and the third water injection cycles through 65mD-WW and 65mD-MW cores is shown in Figure 5-16 and Figure 5-17, respectively. It is noted that as water advances within the porous media, it reduces the saturation of the gas and therefore its mobility. These Figures demonstrate a slight hysteresis effect of k_{rg} between the 2nd and 3rd water injections, which is much less than the hysteresis during gas injection observed in Figure 5-13 and Figure 5-15. As can be seen, in Figure 5-16 and Figure 5-17, k_{rg} of the 3rd water injection is horizontally shifted to the higher gas saturation (right hand side) against the k_{rg} of the 2nd water injection, such that both curves are the almost parallel. The reason is that during the water flooding process the amount of instant gas saturation inside the core is composed of two elements, flowing gas (S_{gf}) and trapped gas (S_{gt}) as follows:

$$S_g = S_{gf} + S_{gt} \quad 5.1$$

in which only the flowing gas saturation contributes to the gas mobility. Hence, the same value for k_{rg} can occur at different gas saturations for the 2nd and 3rd water injections because their flowing gas saturation is the same.

Larsen (1998) and Spiter (2004) have also reported a hysteresis effect in gas relative permeability during successive gas injections which follow water injection cycles. Larsen and Skauge (1998) proposed a numerical model to reproduce qualitatively hysteresis behaviour in the gas phase. This model uses different scanning curves for increasing and decreasing gas saturation. A scanning curve for decreasing gas saturation is calculated from the scanning curve for increasing gas saturation in the same hysteresis loop. The main feature of this model is reduction of gas mobility during the hysteresis loop, in presence of increasing water saturation.

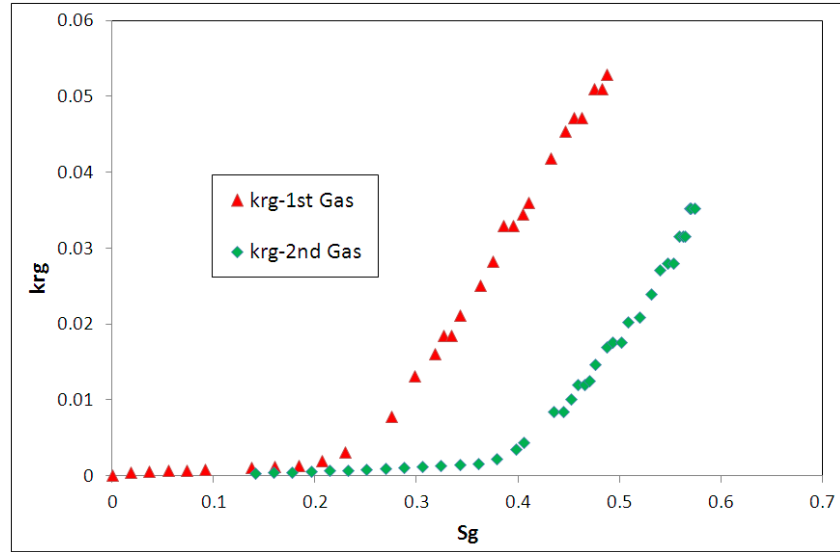


Figure 5-13: Gas relative permeability versus gas saturation, obtained from two gas injection cycles, with intermediate water injection, 1000mD-MW core.

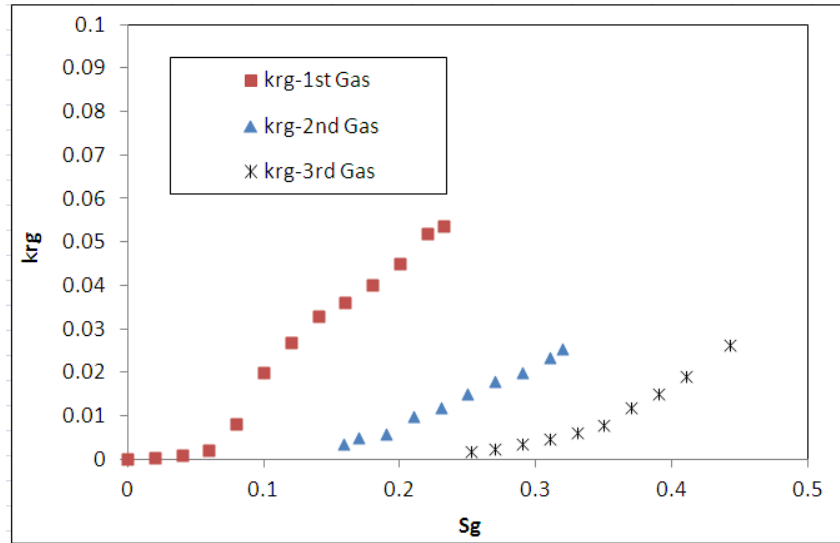


Figure 5-14: Gas relative permeability versus gas saturation, obtained from three gas injection cycles, with intermediate water injections, 65mD-WW core.

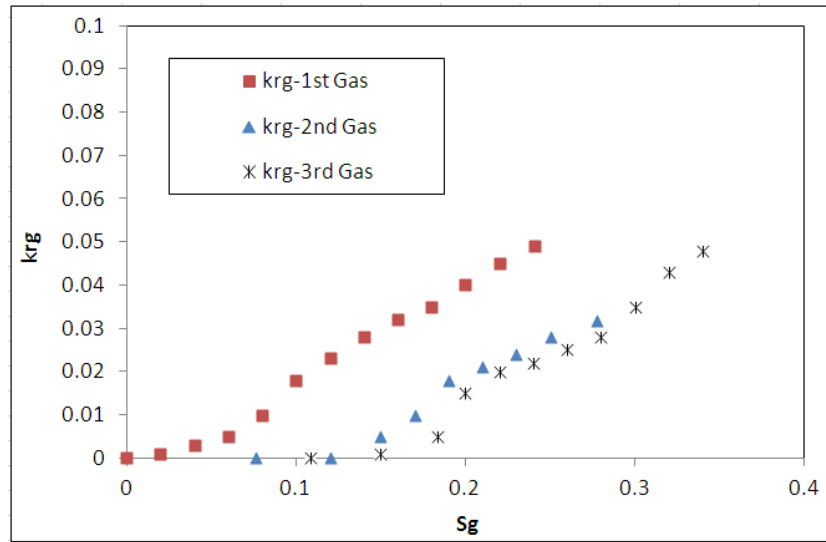


Figure 5-15: Gas relative permeability versus gas saturation, obtained from three gas injection cycles, with intermediate water injections, 65mD-MW core.

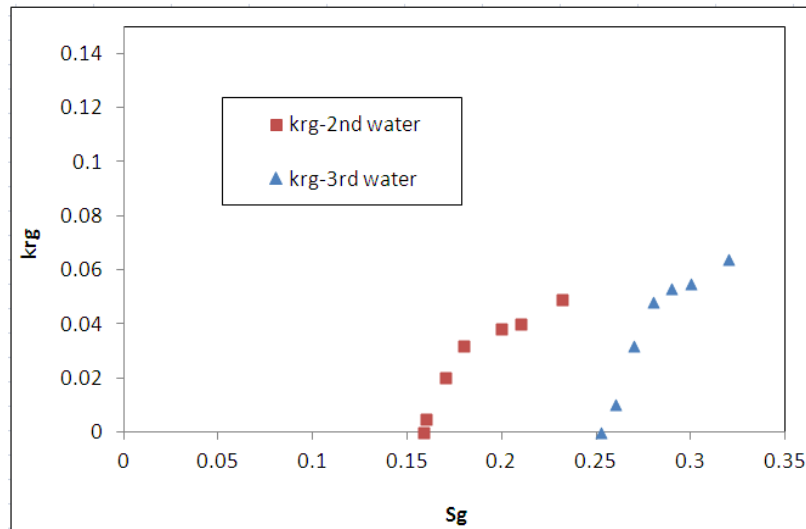


Figure 5-16: Gas relative permeability versus gas saturation, obtained from 2nd and 3rd water injections, with intermediate gas injection, 65mD-WW core.

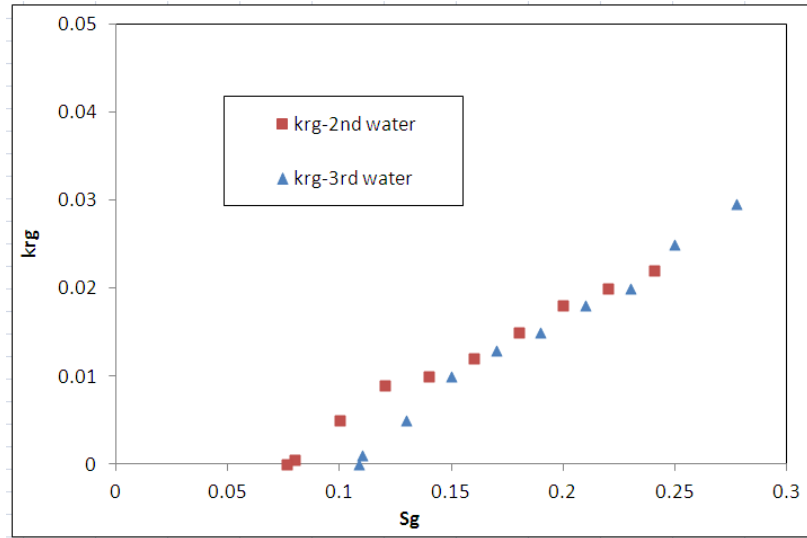


Figure 5-17: Gas relative permeability versus gas saturation, obtained from 2nd and 3rd water injections, with intermediate gas injection, 65mD-MW core.

Conventional hysteresis in gas relative permeability

Semi-log plots of gas relative permeability versus gas saturation, obtained from different water and gas injection cycles through 1000mD-MW, 65mD-WW, and 65mD-MW cores are shown in Figure 5-18 to Figure 5-20. In all the figures, k_{rg} of the second water injection is less than that of the first gas injection, but this trend is not seen in comparing k_{rg} of the second gas and third water injection in Figure 5-19 and Figure 5-20. In other words, no chronological relationship is observed between k_{rg} of the gas injection and k_{rg} of the following water injection. However, this finding somewhat contradicts the hysteresis models previously proposed for two-phase (Killough, 1976; Carlson, 1981) and three-phase relative permeability (Larsen and Skauge, 1998), which assumed that the k_{rg} of imbibitions process (water injection) is less than that of the former drainage process (gas injection).

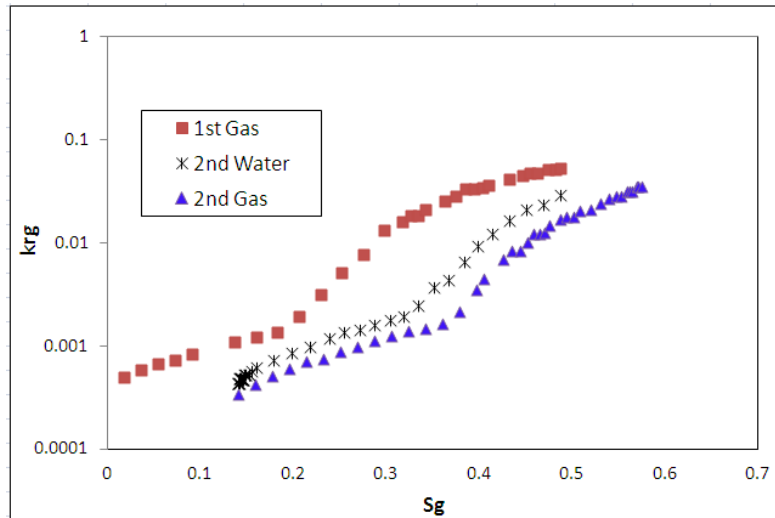


Figure 5-18: Semi-log plot of gas relative permeability versus gas saturation, obtained from successive water and gas injection 1000mD-MW core.

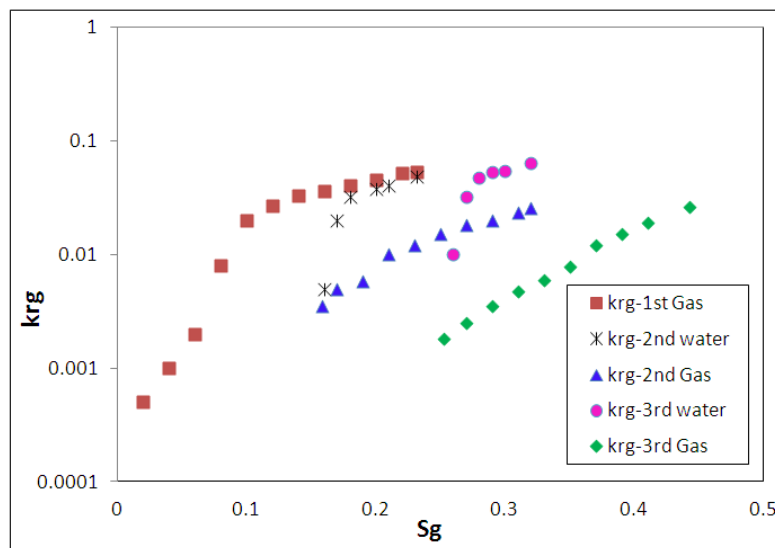


Figure 5-19: Semi-log plot of gas relative permeability versus gas saturation, obtained from successive water and gas injection, 65mD-WW core.

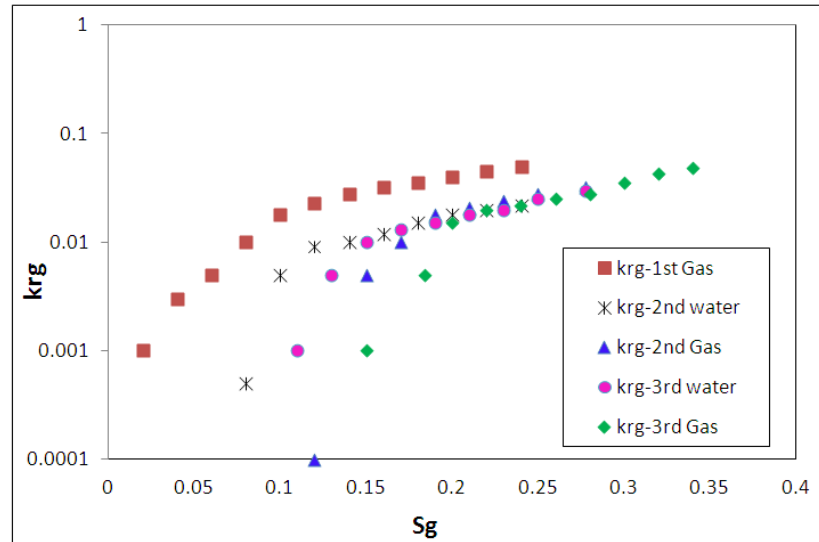


Figure 5-20: Semi-log plot of gas relative permeability versus gas saturation, obtained from successive water and gas injection, 65mD-MW core.

Cyclic hysteresis in water relative permeability

Water relative permeability for the various gas injection cycles in 1000mD-MW, 65mD-WW and 65mD-MW rocks is shown in Figure 5-22, Figure 5-23 and Figure 5-24, respectively. As the gas advances forward in the gas injection process, it displaces the water phase in porous media which consequently reduces the water mobility. The negligible difference between k_{rw} of the various gas injections in the mixed wet systems (Figure 5-22 and Figure 5-24) demonstrates insignificant cyclic hysteresis in water relative permeability during gas injections. This underlines the fact that in the mixed wet rocks, three-phase water relative permeability obtained from the first gas injection can be employed for simulation of the successive gas injection that follows a water injection cycle. However the results of the water-wet core (Figure 5-23) indicate that k_{rw} is reduced by performing successive gas injections, which is attributable to the increase of trapped gas saturation. Figure 5-21 presents a gas injection into a schematic pore throat occupied by the mobile water and trapped gas obtained from former water injection. As can be seen, the higher amount of trapped gas can further restrict the flow of water inside the pore and accordingly decreases the relative permeability of the water.

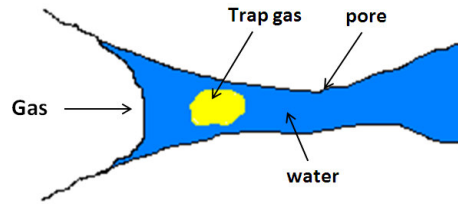


Figure 5-21: Schematic picture of a pore filled by water and trapped gas which is displaced by gas flooding.

Eleri et al. (1995a) performed some unsteady state coreflood experiments in a water wet Clashach core to calculate three-phase oil, water and gas relative permeabilities. The results showed that water relative permeability is saturation history dependent, during consecutive gas injection that follows water injection. In other words, successive gas injection reduces water relative permeability at the same water saturation, which is in line with our observation.

The water relative permeabilities obtained from the second and third water injection into 65mD-WW and 65mD-MW core are plotted versus water saturation, in Figure 5-25 and Figure 5-26, respectively. The k_{rw} of the water-wet core does not exhibit a considerable hysteresis effect, whereas the mixed-wet core shows slight hysteresis, in which the k_{rw} of the 3rd water injection is greater than that of the 2nd. This may indicate a slight increase in the water injectivity with the subsequent water injection in the WAG process under mixed-wet conditions. In the mixed-wet system the intermediate pores are oil-wet and occupied by the oil phase. The successive water injection displaces oil from oil-wet pores toward the outlet of the core; hence, at the higher injection cycles more oil-wet pores are occupied by the water. In other words, the further the water injection cycle progresses, the more oil-wet pores are invaded by the water. The flow of water in the oil-wet pores is better than that in the water-wet pores, due to less tendency of water to be attracted towards the pore surface, and hence, the mobility of water in the oil-wet pores is greater than that in the water-wet pores. Based on the above explanation and what is shown in Figure 5-26, the k_{rw} of the 3rd water is higher than that of the 2nd water because in the 3rd water injection, more oil-wet pores are contributing to the flow of water, compared to the 2nd water injection.

Skauge and Larsen (1994) conducted some unsteady-state WAG experiments into the water-wet, oil-wet and intermediate sandstone rock, to measure three-phase relative

permeability of different mobile phases. The water-wet results showed a slight tendency to hysteresis in the water relative permeability whereas k_{rw} in oil-wet and mixed-wet core showed substantial hysteresis and dependence on the saturation history, in which k_{rw} decreases with subsequent water injection. This latter finding of Skauge and Larsen (1994) for a mixed-wet system is in contradiction to the k_{rw} of the mixed wet system (Figure 5-26) obtained in this research.

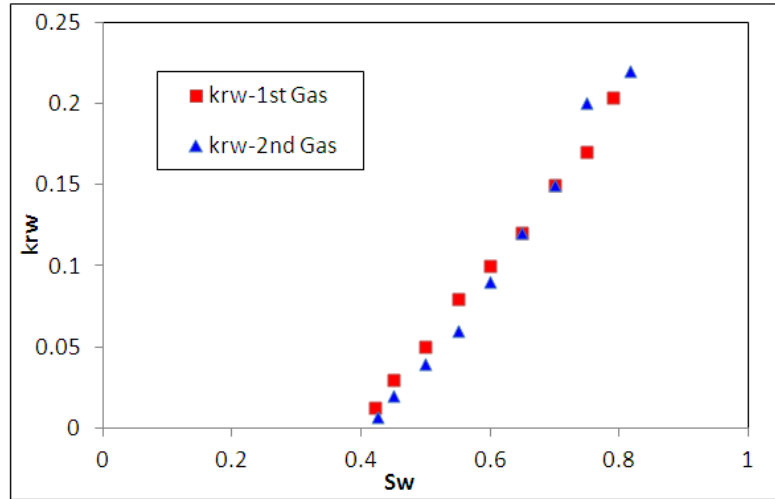


Figure 5-22: Water relative permeability versus water saturation, obtained from two gas injection cycles with an intermediate water-injection, 1000mD-MW core.

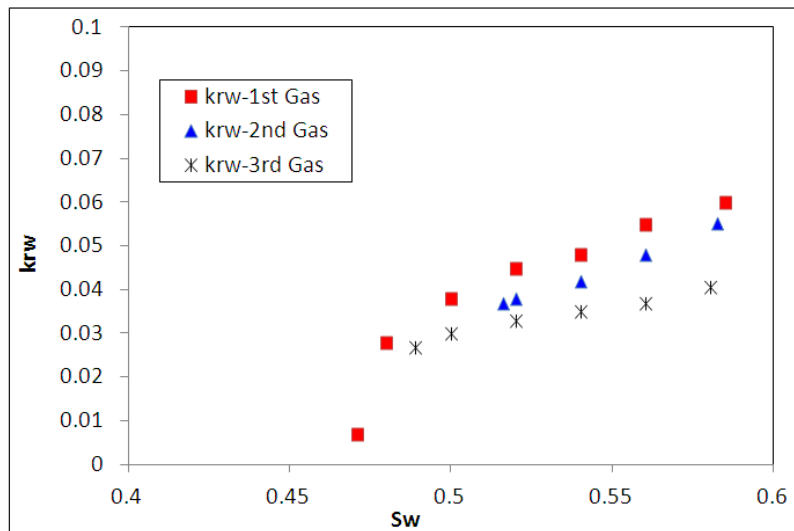


Figure 5-23: Water relative permeability versus water saturation, obtained from three gas injection cycles with intermediate water injection, 65mD-WW core.

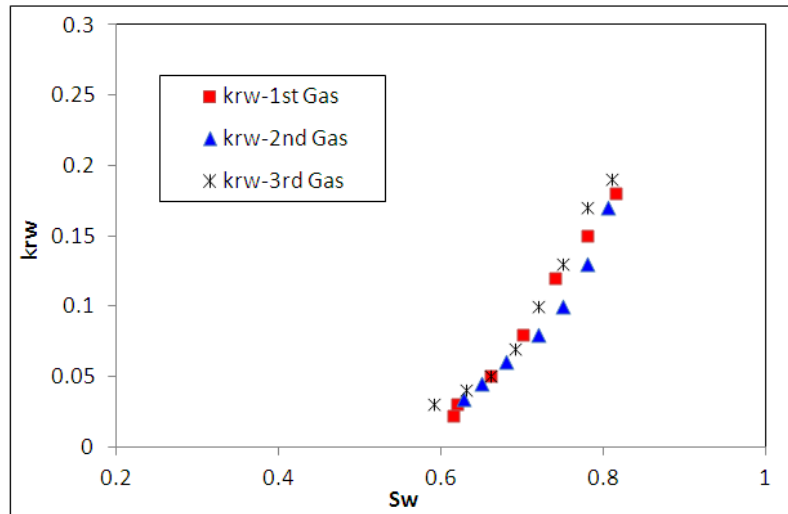


Figure 5-24: Water relative permeability versus gas saturation, obtained from three gas injection cycles with intermediate water injection, 65mD-MW core.

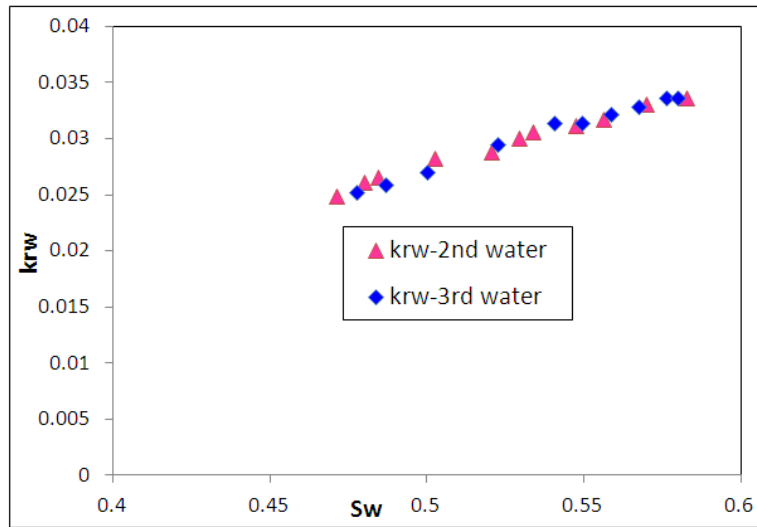


Figure 5-25: Water relative permeability versus water saturation, obtained from 2nd and 3rd water injections with an intermediate gas injection, 65mD-WW core.

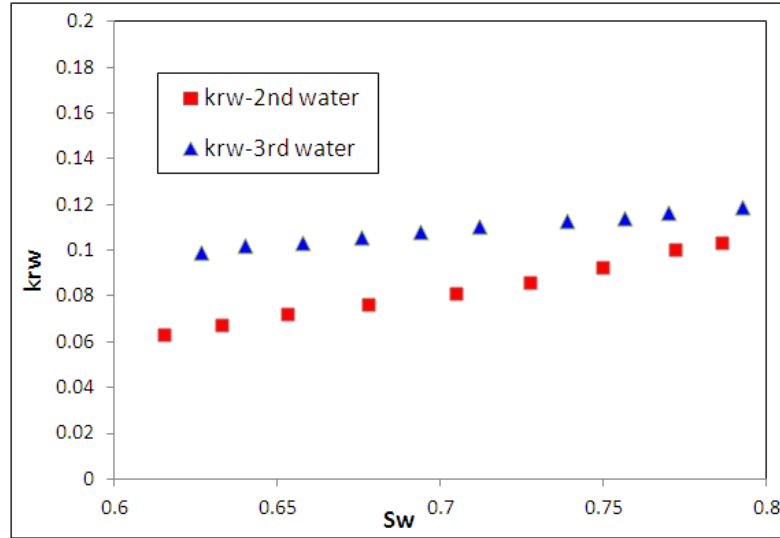


Figure 5-26: Water relative permeability versus water saturation, obtained from 2nd and 3rd water injections with an intermediate gas injection, 65mD-MW core.

Conventional hysteresis in water relative permeability

Figure 5-27, Figure 5-28 and Figure 5-29 show semi-log plot of the water relative permeability versus water saturation obtained from consecutive water and gas injection into 1000mD-MW, 65mD-WW and 65mD-MW cores. The results of both mixed wet rocks (Figure 5-27 and Figure 5-29) depict that k_{rw} of the water injection is slightly higher than that of the gas injection, which is supported by the existing hysteresis model (Killough, 1976), whereas k_{rw} of 65mD-WW core demonstrates an opposite tendency, in which water relative permeabilities of the water injection cycles are less than those of gas injection cycles.

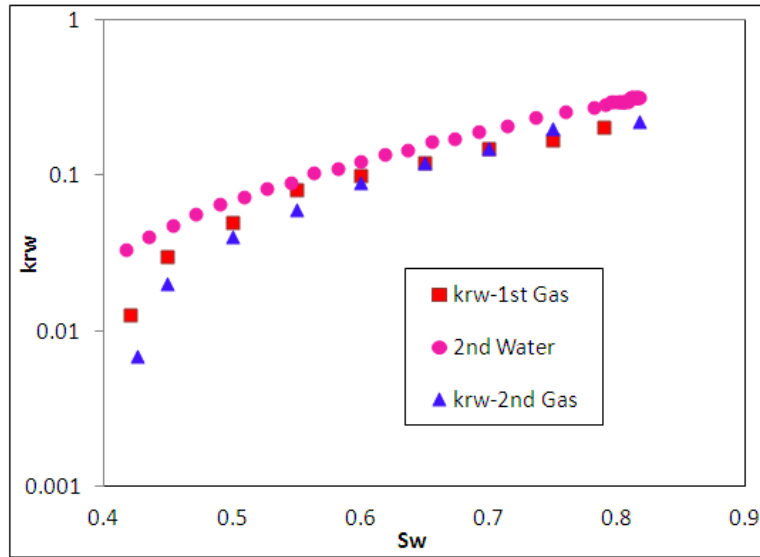


Figure 5-27: Semi-log plot of water relative permeability versus water saturation, obtained from successive water and gas injection, 1000mD-MW core.

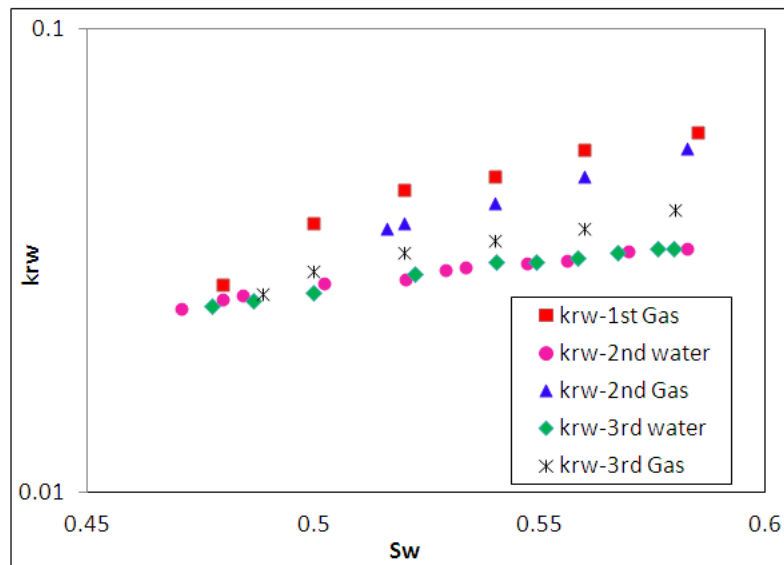


Figure 5-28: Semi-log plot of water relative permeability versus water saturation, obtained from successive water and gas injection, 65mD-WW core.

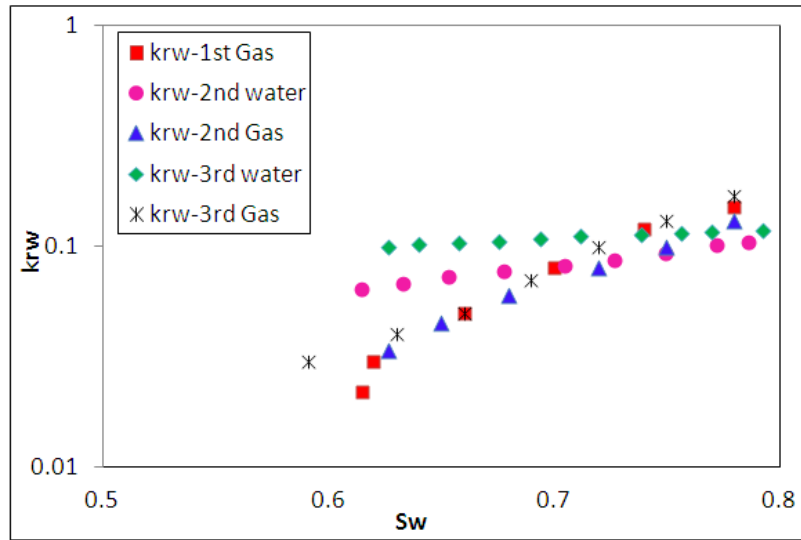


Figure 5-29: Semi-log plot of water relative permeability versus water saturation, obtained from successive water and gas injection, 65mD-MW core.

Cyclic hysteresis in oil relative permeability

Semi-log plot of the oil relative permeability versus oil saturation for various gas injection cycles through 1000mD-MW, 65mD-WW and 65mD-MW cores are given in Figure 5-30, Figure 5-31 and Figure 5-32, respectively. As the gas advances in porous media, it displaces the oil and henceforth reduces the oil relative permeability. As shown in all the three Figures, insignificant hysteresis effects are observed in the oil relative permeability during different gas injection periods.

Semi-log plot of the oil relative permeability versus oil saturation for 2nd and 3rd water injection cycles into 65mD-WW and 65mD-MW cores are exhibited in Figure 5-33 and Figure 5-34, respectively. The water-wet core depicts much more hysteresis effect than the mixed wet core. Hysteresis in the oil relative permeability during water injection is attributed to the trapped oil saturation attained by increasing water in the porous medium. The fluid saturation values of both the water-wet and the mixed-wet cores demonstrate that the trapped hydrocarbon (oil + gas) saturation remains constant during various water injection periods. Since the trapped gas saturation continually increases by cyclic water and gas injection, the immobile oil saturation reduces successively. Therefore, the residual oil reached by 3rd water injection is less than that by 2nd water which influences k_{ro} positively as shown in Figure 5-33 and Figure 5-34. This mechanism is similar to what described for gas relative permeability (equation 5.1)

stating that increasing trapped gas saturation in the subsequent water injection shifts the k_{rg} curve horizontally to the higher gas saturation for the each water cycle compare to the former one. While in the oil phase because of decreasing immobile oil (residual oil) the k_{ro} of 3rd water injection moves to the lower oil saturation (left hand side) against the 2nd water injection.

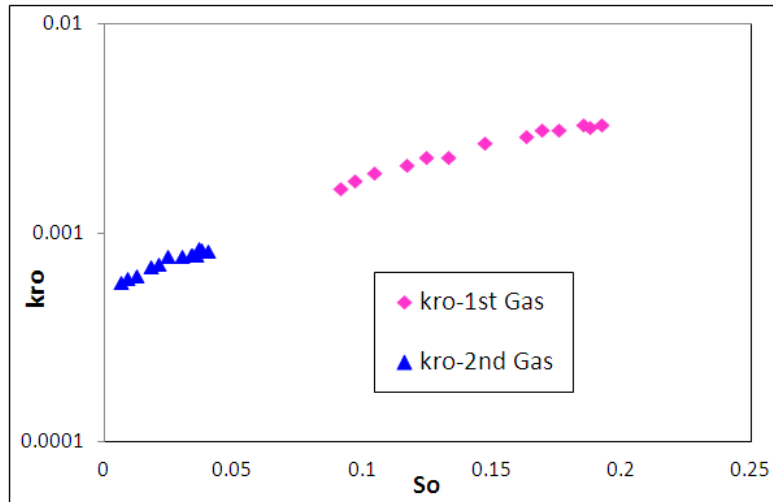


Figure 5-30: Semi-log plot of oil relative permeability versus oil saturation, obtained from two gas injection cycles, with intermediate water injection, through 1000mD-MW core.

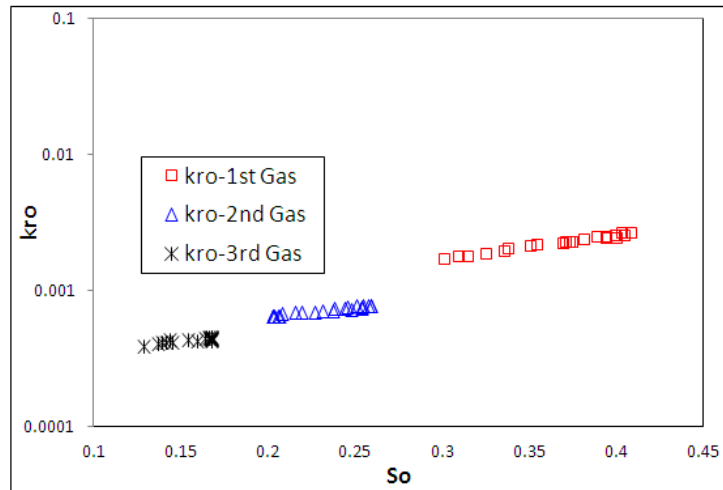


Figure 5-31: Semi-log plot of oil relative permeability versus oil saturation, obtained from three gas injection cycles, with intermediate water injection, through 65mD-WW core.

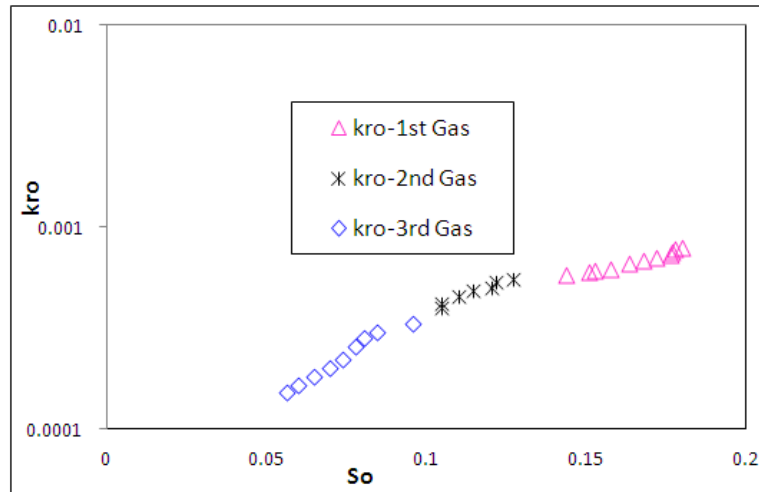


Figure 5-32: Semi-log plot of oil relative permeability versus oil saturation, obtained from three gas injection cycles, with intermediate water injection, through 65mD-MW core.

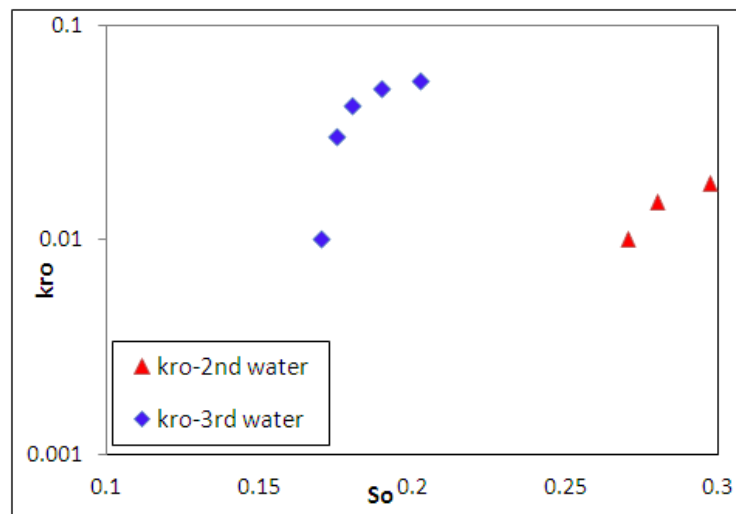


Figure 5-33: Semi-log plot of oil relative permeability versus oil saturation, obtained from 2nd and 3rd water injection cycles, with intermediate gas injection, through 65mD-WW core.

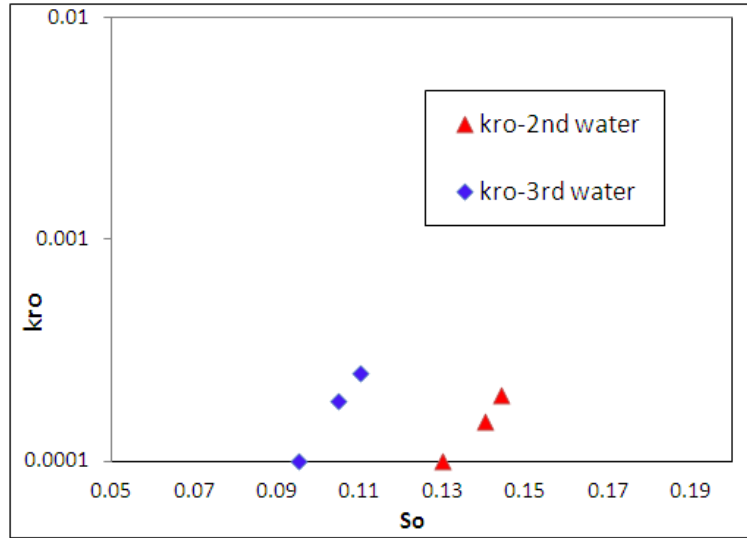


Figure 5-34: Semi-log plot of oil relative permeability versus oil saturation, obtained from 2nd and 3rd water injection cycles, with intermediate gas injection, through 65mD-MW core.

Conventional hysteresis in oil relative permeability

Oil relative permeability versus oil saturation, obtained from water alternating gas injection into 1000mD-MW, 65mD-WW and 65mD-MW are plotted in Figure 5-35 to Figure 5-37. The corollaries of the mixed-wet cores i.e. 1000mD-MW and 65mD-MW (Figure 5-35 to Figure 5-37) reveal that k_{ro} of the water injection cycles is less than that of the gas injection cycles, whilst the results for the water-wet core (Figure 5-36) indicate that the k_{ro} of water injections is significantly greater than the k_{ro} of gas cycles. In fact, this conclusion highlights the impact of wettability on the sequence of oil relative permeability curves throughout water alternating gas injection. An inappropriate incorporation of oil hysteresis in a numerical reservoir simulator may lead to a substantial error in the oil recovery forecast. However, to the author's best knowledge, no model has yet been developed to capture the hysteresis effect in oil relative permeability during WAG injection.

The relative permeability results of the WAG experiment published in the literature (Skauge and Larsen, 1994) confirm that k_{ro} in water-wet and oil-wet cores undergoes only minor change with saturation history, whilst k_{ro} in mixed-wet systems shows strong variation with process and sequence, such that the oil relative permeability of primary gas injection is higher than that of secondary water flooding. This latter

conclusion was confirmed by our k_{ro} observation obtained from WAG tests at the mixed-wet conditions (Figure 5-35 to Figure 5-37).

Comparing k_{ro} of gas injections with that of the water injection cycles in all the WAG experiments (Figure 5-35 to Figure 5-37) indicates that k_{ro} data during gas injections have a less steep compared to k_{ro} during water injections. This trend confirms the mechanism of the flow of connected oil-film at the low oil saturation by near-miscible gas injection, which has already been observed in the coreflood and micromodel experiments (Sohrabi et al., 2007; Sohrabi et al., 2008a; Sohrabi et al., 2008b; Fatemi et al., 2011).

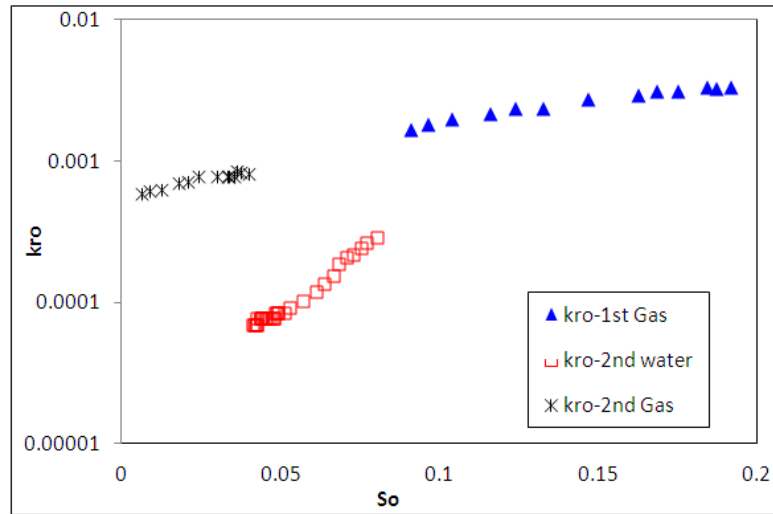


Figure 5-35: Semi-log plot of oil relative permeability versus oil saturation, obtained from successive water and gas injection, 1000mD-MW core.

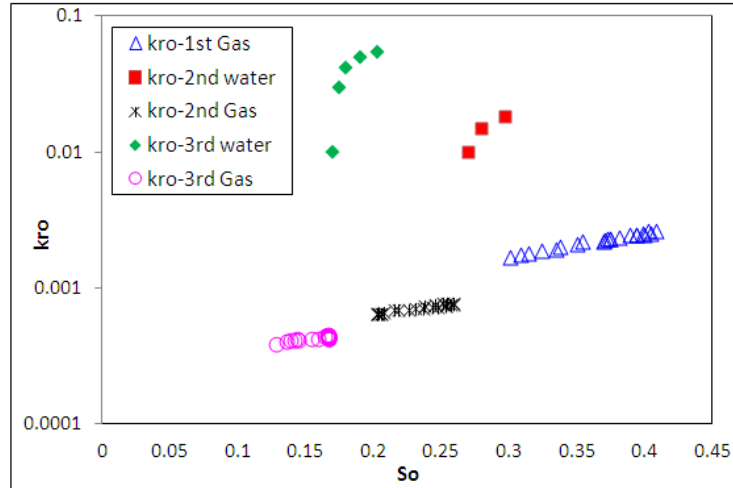


Figure 5-36: Semi-log plot of oil relative permeability versus oil saturation, obtained from successive water and gas injection, 65mD-WW core.

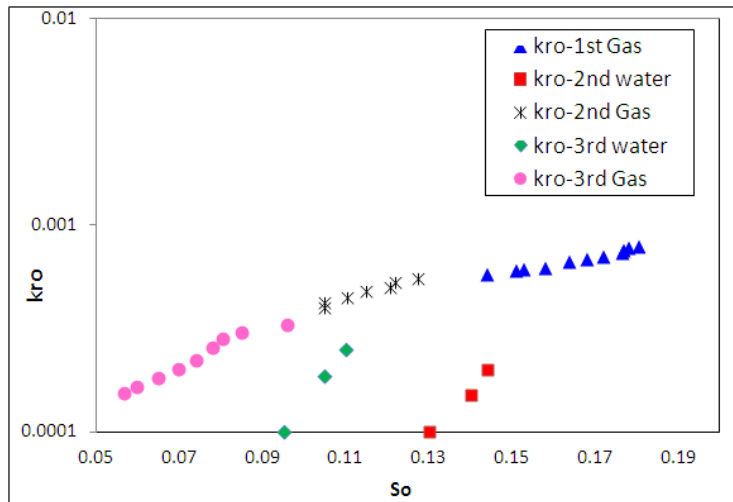


Figure 5-37: Semi-log plot of oil relative permeability versus oil saturation, obtained from successive water and gas injection, 65mD-MW core.

5.2.2 Water-wet versus mixed-wet

Rock wettability has a strong impact on the fluid distribution and mobility of the immiscible phases in the porous media. Many efforts have been directed towards finding an appropriate relationship between fluid flow functions under different wettability conditions (Skauge and Aarra, 1993; Vizika and Lombard, 1996; DiCarlo et al., 1998; Hwang et al., 2006; Cinar et al., 2007). However, it is crucial to perform coreflood experiments under conditions close to the actual reservoir wettability.

Here, a comparison is made between three-phase relative permeabilities obtained from 65mD-WW and 65mD-MW cores to demonstrate the impact of rock wettability on relative permeability. In order to make a sensible comparison between water-wet and mixed-wet system, relative permeability data of those experiments performed in the same direction (e.g. gas injection or water injection) and having a closer saturation range to each other are selected.

Figure 5-38 shows the three-phase k_{rg} versus gas saturation resulting from the 1st gas injection in 65mD water-wet and mixed-wet cores. As we would expect, the k_{rg} of water-wet and mixed-wet cores are relatively close to each other, because the gas phase in both wettability conditions acts as the non-wetting phase. That is, the impact of wettability on the gas mobility is very minimal.

Figure 5-39 presents the three-phase k_{rw} versus water saturation, obtained from the second water injection into the 65mD water-wet and mixed-wet cores. The difference between k_{rw} of the water-wet and that of the mixed-wet systems underlines the extensive role of wettability in influencing flow of water in the presence of oil and gas in porous media. Since water has a stronger affinity towards the pore surface in water-wet rock than in the mixed-wet rock, it is much harder for the water to flow in water-wet pores than that in the mixed-wet pores. This is reflected by larger values for water relative permeability in the mixed-wet core compared to that in the water-wet core, as shown in Figure 5-39.

Figure 5-40 shows a semi-log plot of the three-phase k_{ro} obtained from the 3rd water injection into the 65mD water-wet and mixed-wet cores. Although the absolute magnitude of the oil relative permeability in this example is rather low, as expected, a relatively large difference between k_{ro} of water-wet and that of the mixed-wet rocks exists. This again demonstrates the significance of rock wettability in the flow of oil in multiphase flow in porous media. Unlike the water relative permeability, which was smaller in water-wet core than in mixed-wet core (Figure 5-39) the oil relative permeability is larger in the water-wet core, as demonstrated in Figure 5-40. This is attributed to the fact that, in the mixed-wet core, some pore surfaces are oil-wet whereas in the water-wet core all the pores are water-wet. Therefore, the overall affinity of oil towards the rock in the mixed-wet core is higher than that in the water-wet core.

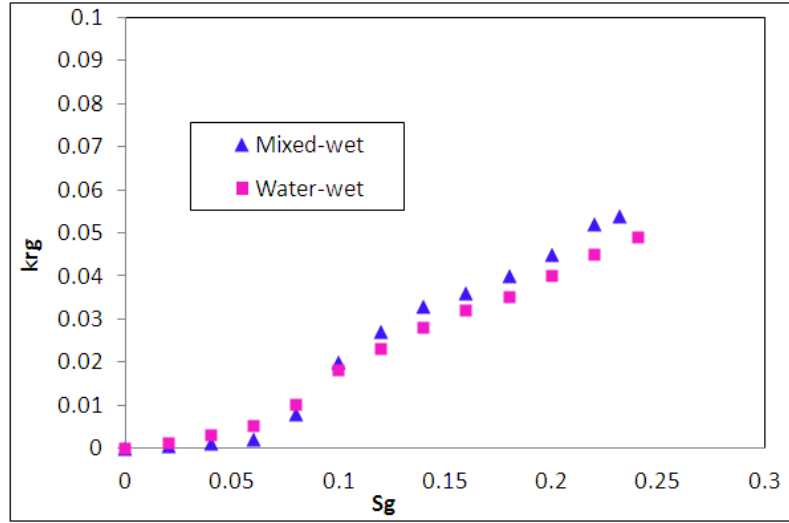


Figure 5-38: Gas relative permeability versus gas saturation, obtained from 1st gas injection into the 65mD water-wet and mixed-wet core.

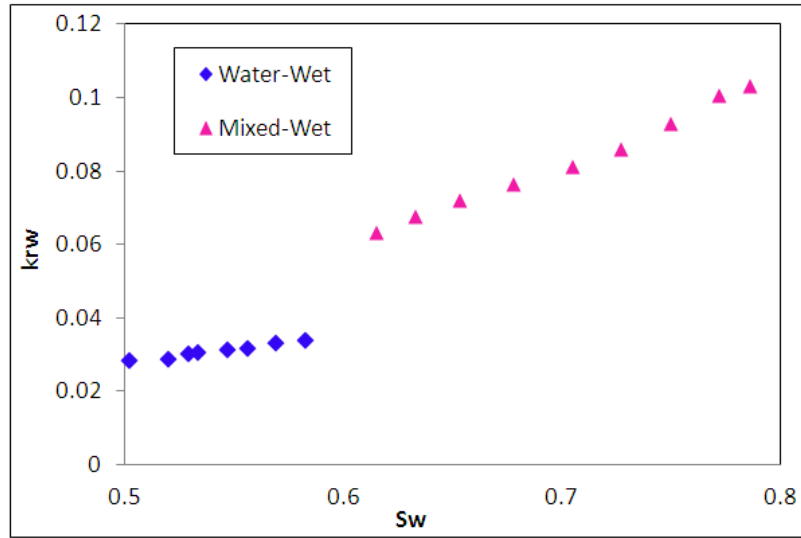


Figure 5-39: Water relative permeability versus water saturation, obtained from 2nd water injection into the 65mD water-wet and mixed-wet core.

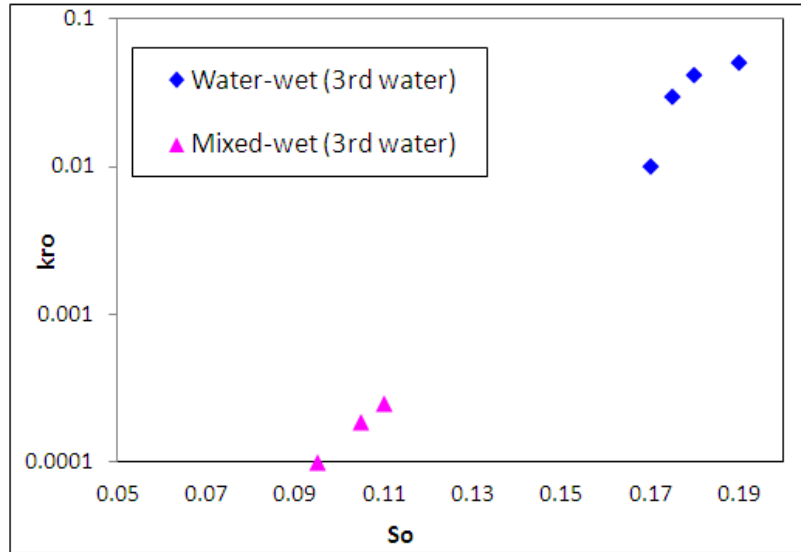


Figure 5-40: Semi-log plot of oil relative permeability versus water saturation, obtained from 3rd water injection into the 65mD water-wet and mixed-wet core.

5.2.3 Three-phase k_r versus two-phase k_r

The number of fluid phases present in the porous media significantly affects the relative permeability of each fluid. While in the two-phase system (oil/water, gas/oil, and gas/water) there are only two principal displacement paths (i.e. when saturation of one phase increases, saturation of the other phase decreases or vice versa), in the case of three-phase there are an infinite number of different displacement paths. This is because any three-phase displacement involves variation of two independent fluid saturations. In general, relative permeability of two-phase system is a function of one fluid saturation, whereas the relative permeability of a fluid in a three-phase system is affected by presence of the other two fluids, thus it is a function of two independent fluid saturations.

Many attempts have been directed toward finding a representative relationship between two-phase and three-phase k_r (Stone, 1970; Baker, 1988; Hustad and Hansen, 1995; Blunt, 2000). Some of these models make the simplistic assumption that relative permeability of wetting phase (water) and non-wetting phase (gas) acts in the same way in a three-phase system as in a two-phase system. In other words, k_{rw} and k_{rg} in three-phase flow are assumed to be functions of their own respective saturation values. This can be partly attributed to the fact that there have not been many directly measured

three-phase relative permeability data available, because of the associated time and expense needed for acquiring such data. The comparative results of the two-phase against three-phase relative permeability are discussed here to assess the validity, or otherwise, of this assumption.

Comparison of k_{rgo} (in two-phase system) with three-phase k_{rg} :

Figure 5-41, Figure 5-42 and Figure 5-43 present three-phase and two-phase relative permeability of gas versus gas saturation for the 1000mD-MW, 65mD-WW and 65mD-MW cores. Both the two-phase and the three-phase k_r values were obtained from experiments performed under similar conditions. Two-phase k_{rgo} obtained from gas injection conducted into the core saturated with the oil and connate water (zero S_g) and three-phase k_{rg} determined from the 1st gas injection carried out into the core that was initially saturated with mobile water and oil left from the 1st water injection (S_{orw}). The results of all cores (1000mD-MW, 65mD-WW, 65mD-MW) reveal relatively large discrepancies between the two-phase and the three-phase gas relative permeabilities, showing that the mobility of gas is much higher in the two-phase system than that in the three-phase system (for the same gas saturation). It may be concluded that presence of the mobile water adversely affects three-phase gas relative permeability. The explanation for this behaviour is that the gas/water interfacial tension is much higher than the IFT of a gas/oil system; hence, the resistance of water against the flow of gas is higher than the resistance of oil. In the two-phase gas injection process, the gas fully targets the oil phase whereas, in the three-phase gas flooding, the gas displaces both oil and water phase: therefore, the presence of water reduces the gas relative permeability. Moreover, the disagreement between the two-phase and three-phase k_{rg} grows at the higher values of S_g , because gas initially invades the larger pores occupied by the oil, then goes to the smaller pores filled by the water, as the gas flooding proceeds. In other words, the capillary contacts between water and gas phases at the higher gas saturation are; more pronounced than that in the lower S_g therefore, by raising the gas saturation, the contribution of water in the gas mobility increases.

The observed difference between the two-phase and the three-phase k_{rg} is more pronounced for the high permeability core (1000mD-MW) than that in the low permeability core (65mD-MW). Also, such discrepancies are larger for water-wet core (65mD-WW) than those in the mixed-wet (65mD-MW) rock. Contrary to the

assumption made in most existing models (Naar and Wygal, 1961; Stone, 1970; Stone, 1973; Dietrich and Bondor, 1976) , these results demonstrate that three-phase k_{rg} values for all cases, including water-wet, mixed-wet, high permeability and low permeability rocks, are a strong function of two saturation values (oil and water) and are significantly different from the two-phase k_{rgo} values

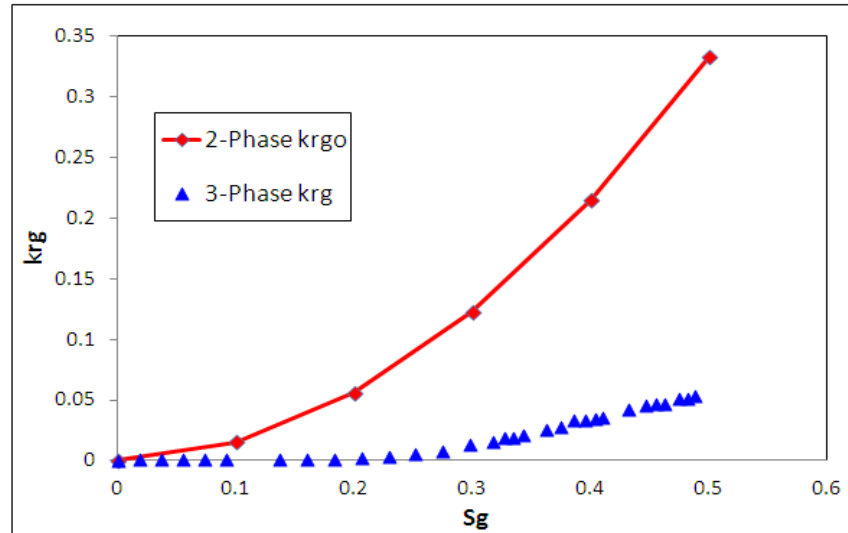


Figure 5-41: Three-phase and two-phase gas relative permeability, obtained from gas injection into the 1000mD-MW core.

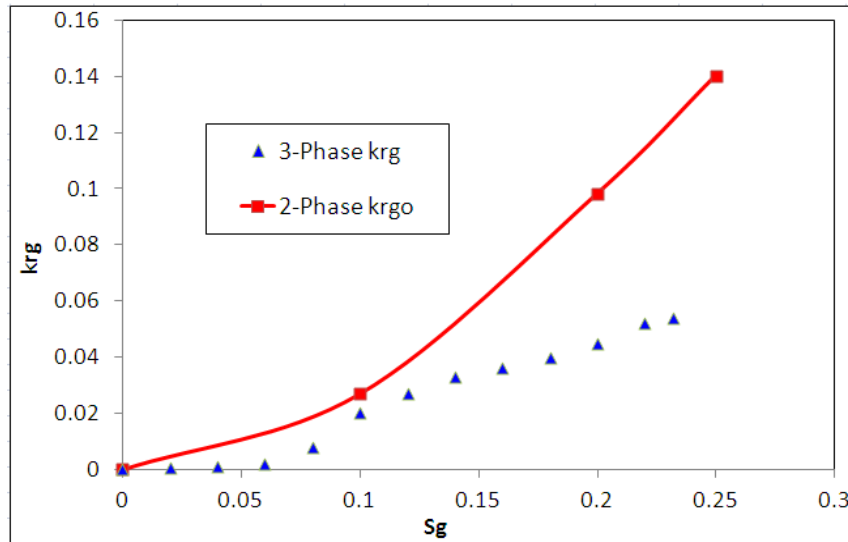


Figure 5-42: Three-phase and two-phase gas relative permeability, obtained from gas injection into the 65mD-WW core.

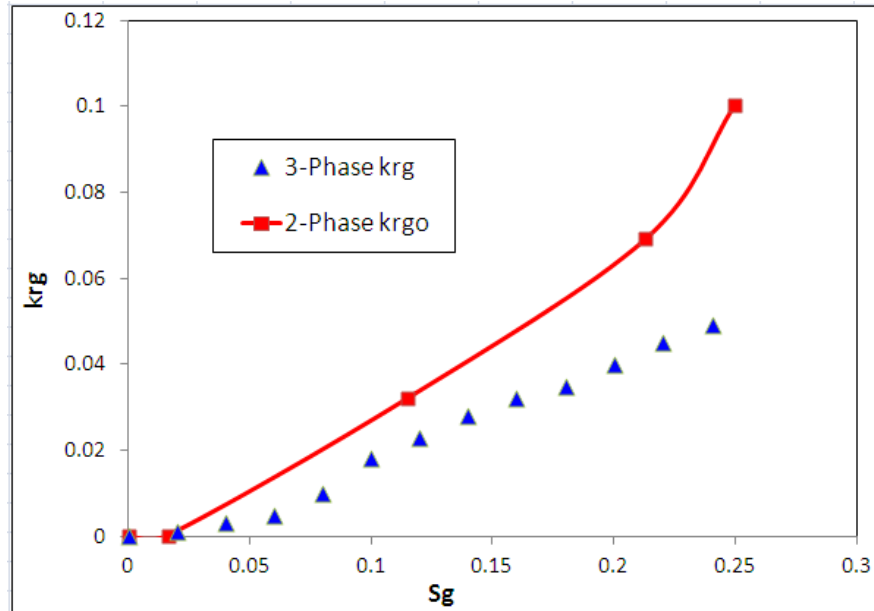


Figure 5-43: Three-phase and two-phase gas relative permeability, obtained from gas injection into the 65mD-MW core.

Comparison of k_{rwo} in two-phase systems with three-phase k_{rw} .

Water relative permeability under two-phase and three-phase conditions, obtained from water injection into the 1000mD-MW, 65mD-WW and 65mD-MW cores are shown in Figure 5-44, Figure 5-45 and Figure 5-46, respectively. The two-phase water relative permeability (k_{rwo}) was obtained from water injection into the core saturated with the oil and connate water, while the three-phase k_{rw} was obtained from the 2nd water injection into the core that contained mobile oil, water and gas. The results of all the three core tests demonstrate substantial discrepancy between the two-phase and the three-phase k_{rw} , in which the value of the two-phase k_{rwo} is always below that of the three-phase k_{rw} . Prior to the three-phase experiment, mobile water has been established inside the core, whereas in the two-phase water injection, there is no initial mobile water in the core. Therefore, water relative permeability for this particular three-phase water injection test is greater than that in the two-phase experiment. This is in the opposite direction of the behaviour observed in gas relative permeability (Figure 5-41 to Figure 5-43.). In another study (Shahverdi, 2011) we have shown a different relationship between two-phase and three-phase k_{rw} . However, depending on the type of flooding process and saturation distribution in the porous media, the behaviour between two-

phase and three-phase relative permeability may be different and a general rule therefore cannot be proposed. The main conclusion that can be drawn from these results is that the three-phase k_{rw} is a function of two saturation values (rather than its own saturation) and the assumption made in the existing models (Naar and Wygal, 1961; Stone, 1970; Stone, 1973; Dietrich and Bondor, 1976) that three-phase k_{rw} acts the same as the two-phase k_{rwo} is invalid for these results.

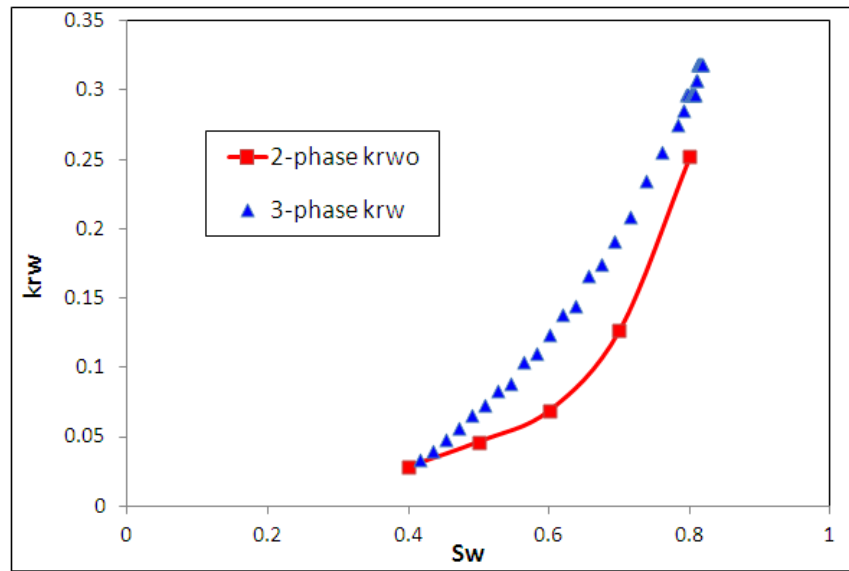


Figure 5-44: Three-phase and two-phase water relative permeability, obtained from water injection into 1000mD-WW core.

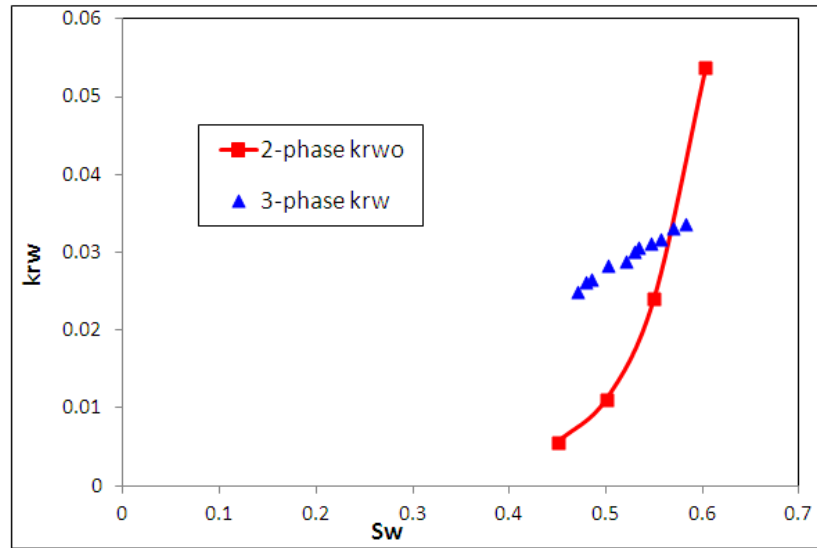


Figure 5-45: Three-phase and two-phase water relative permeability, obtained from water injection into 65mD-WW core.

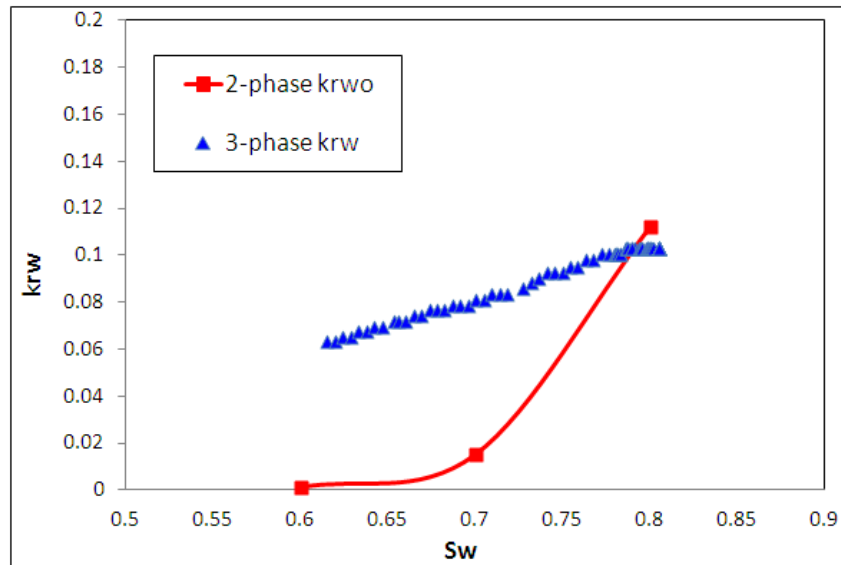


Figure 5-46: Three-phase and two-phase water relative permeability, obtained from water injection into 65mD-MW core.

Comparison of k_{rog} in a two-phase system with three-phase k_{ro} .

Figure 5-47 to Figure 5-49 show the two-phase oil relative permeability (k_{rog}) and the three-phase k_{ro} versus oil saturation, obtained from gas injection into the 1000mD-MW,

65mD-WW and 65mD-MW cores. The two-phase gas injection was carried out through the core saturated with the oil and connate water, while the three-phase gas injection (1st gas of WAG) was conducted into the core that initially contained oil and mobile water. The results from all cores exhibit significant differences between the two-phase and the three-phase k_{ro} , indicating that the three-phase oil relative permeability is a function of two saturation values rather than its own saturation. This large discrepancy is likely to be due to the difference in the displacement mechanism of oil by gas between two-phase and three-phase gas injection. In the two-phase experiment, gas invades pores occupied by mobile oil and irreducible water whereas in the three-phase test, gas displaces residual oil retained by the former water flooding. In other words, in a three-phase system, gas should displace residual oil whose mobility has been significantly reduced by the previous water flooding, whilst in the two-phase test, gas sweeps the entire amount of oil in the pores.

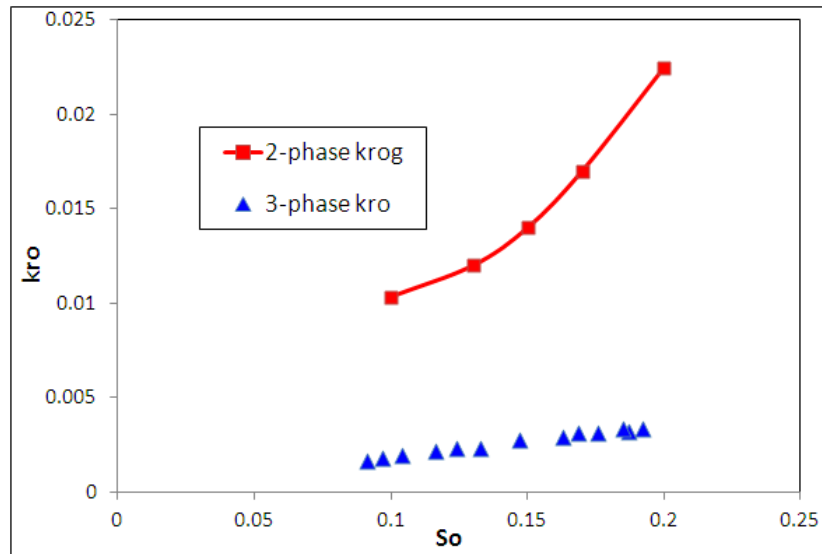


Figure 5-47: Three-phase and two-phase oil relative permeability, obtained from gas injection into the 1000mD-MW core.

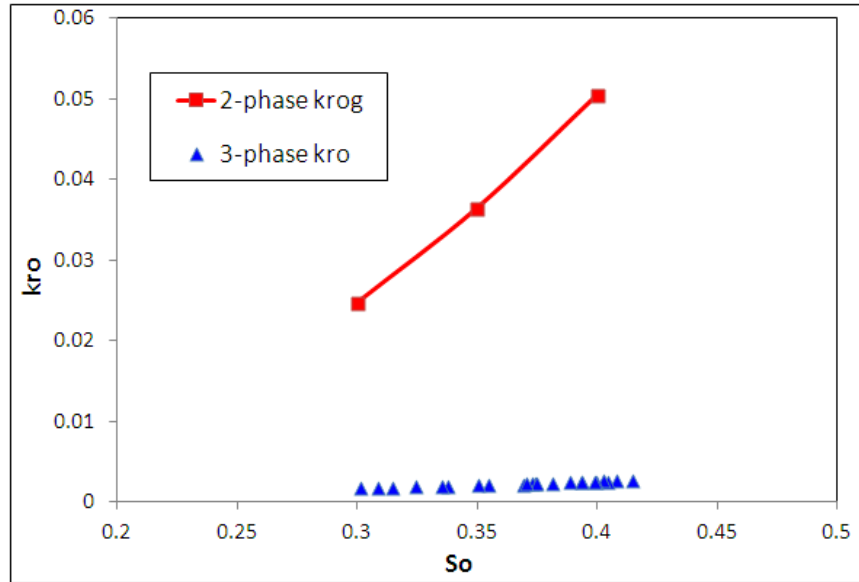


Figure 5-48: Three-phase and two-phase oil relative permeability, obtained from gas injection into the 65mD-WW core.

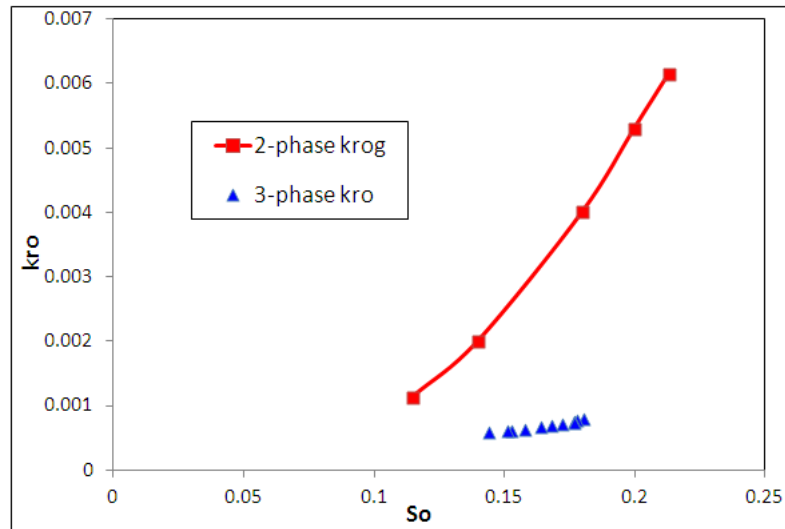


Figure 5-49: Three-phase and two-phase oil relative permeability, obtained from gas injection into the 65mD-MW core.

5.3 Trapped gas and oil saturation

The advancing wetting phase (water) into the porous media traps some amount of the non-wetting phase (oil & gas), whereby the relative permeability of the non-wetting fluid becomes zero at that saturation. The trapping of a phase can be characterised by the relationship between initial and trapped saturation, known as the capillary trapping curve (Holmgren and Morse, 1951; Dyes, 1954; Kyte et al., 1956; Land, 1968; Jerauld,

1997; Pentland, 2010). As mentioned earlier in chapter 3, the initial stage in modelling of the hysteresis in relative-permeability is to predict the amount of trapped saturation attained by the imbibition processes.

Extensive experimental and theoretical work has been directed toward the characterization of trapping of the non-wetting phase (Geffen et al., 1951; Land, 1968; Carlson, 1981; Chatzis et al., 1983; Jerauld, 1997; Skauge and Ottesen, 2002; Spiteri et al., 2008; Pentland, 2010). The most commonly used trapping model is that proposed by Land (1968), which states that the difference in the reciprocal of the initial and trapped gas saturation are approximately constant for a given sand (Equation 3-32). The constant value, named as the Land coefficient, depends on the rock wettability, pore structures and interfacial tension between the fluids. In this model, trapped gas saturation increases with an increase in initial gas saturation. When the initial gas saturation is unity, the residual (trapped) gas saturation is the maximum. The Land coefficient is traditionally determined from a water injection test into the core initially full saturated with the non-wetting phase.

Here, we assess the integrity of the Land equation in predicting trapped oil and gas saturation throughout water injection followed by gas injection. Table 5-1 shows initial and trapped oil saturation (S_{oi} , S_{ot}) obtained from the water injection test for various cores performed at two-phase oil-water conditions. Table 5-2 shows initial and trapped gas saturation (S_{gi} , S_{gt}) determined from water injection through different cores, carried out at two-phase water-gas flow conditions. The value of the Land coefficient for oil and gas are denoted by C_o and C_g , respectively, calculated using the Land equation.

Table 5-1: Initial and trapped oil saturation resulting from water injection test for different cores, performed at two-phase oil-water conditions.

No.	Core	Experiment	Soi	Sot	Co
1	1000mD-MW	2-phase (oil/water)	0.92	0.214	3.59
2	65mD-WW	2-phase (oil/water)	0.82	0.415	1.19
3	65mD-MW	2-phase (oil/water)	0.82	0.185	4.19

Table 5-2: Initial and trapped gas saturation resulting from water injection test for different cores performed at two-phase gas-water conditions.

No.	Core	Experiment	S _{gi}	S _{gt}	C _g
1	1000mD-MW	2-phase (gas/water)	0.51	0.13	5.7315
2	65mD-WW	2-phase (gas/water)	0.82	0.2745	2.4235
3	65mD-MW	2-phase (gas/water)	0.82	0.2745	2.4235

Figure 5-50 presents trapped oil saturation versus initial oil saturation for 1000mD-mW core obtained from the Land equation and the 2nd water injection test with rock initially containing three mobile fluids, i.e. oil, water and gas. As shown in this figure, the amount of trapped oil saturation for 2nd water injection is nearly 35% overestimated. The residual (trapped) oil saturation versus initial oil saturation obtained from the Land equation and water injection tests (2nd and 3rd) for 65mD water-wet and mixed-wet cores are shown in Figure 5-51 and Figure 5-52, respectively. As can be seen in Figure 5-51, the trapped oil of the 2nd water injection is perfectly matched with the Land curve whilst the result of the 3rd water injection depicts around 18% error. The results of the 65mD-MW core in Figure 5-52 show a slight difference between the trapped oil saturation of the 2nd water injection and that of the Land prediction, while this difference becomes larger for the 3rd water injection, up to 30%. The results presented in Figure 5-50 to Figure 5-52, in most cases reveal unsatisfactory degree of precision for the proportion/ fraction of trapped oil calculated by the Land model.

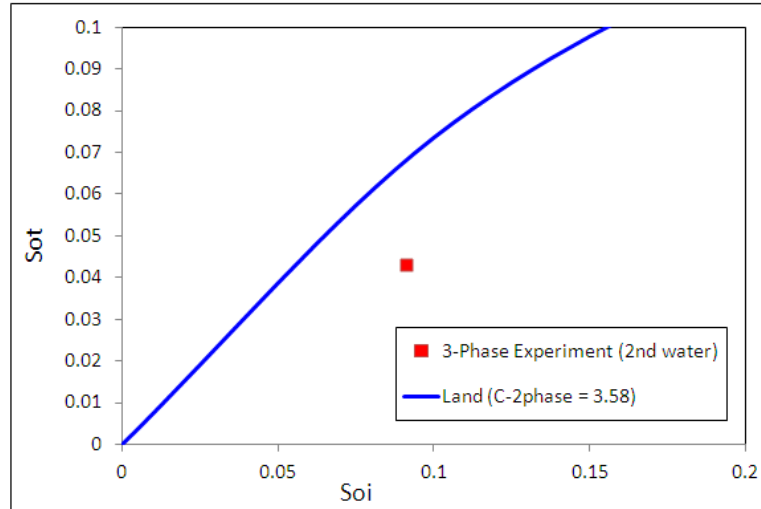


Figure 5-50: Trapped oil saturation versus initial oil saturation, obtained from the Land model and three-phase experiment (2nd water injection) performed on the 1000mD-MW core.

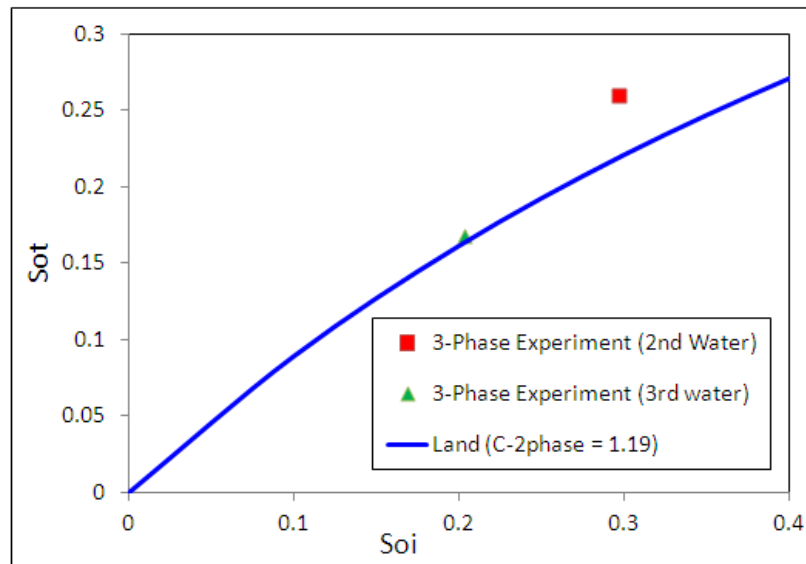


Figure 5-51: Trapped oil saturation versus initial oil saturation, obtained from the Land model and three-phase experiments (2nd and 3rd water injection) performed on the 65mD-WW core.

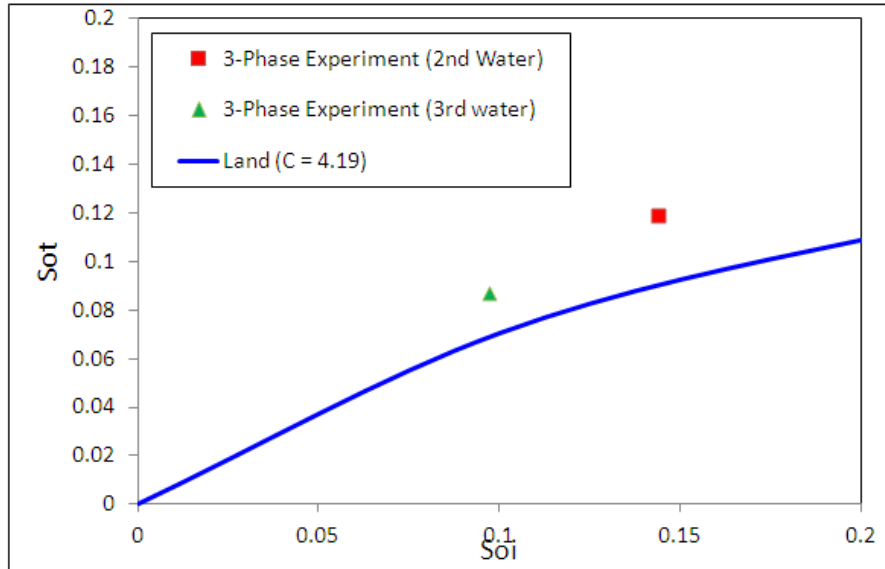


Figure 5-52: Trapped oil saturation versus initial oil saturation, obtained from the Land model and three-phase experiments (2nd and 3rd water injection) performed on the 65mD-MW core.

Figure 5-53 shows trapped gas versus initial gas saturation for the 1000mD-MW core, obtained from the 2nd water injection test and Land model. The value predicted by the Land equation is very close to the experimental point in Figure 5-53. Similar trends were observed for the 65mD water-wet and mixed-wet cores as shown in Figure 5-54 and Figure 5-55, respectively. The trapped gas saturation for the 65mD-WW core obtained from 2nd water injection shows good agreement with the Land prediction whereas the trapped gas of the 3rd water injection is largely underestimated (Figure 5-54). Results for the 65mD mixed-wet core in Figure 5-55 illustrate significant inconsistency between measured and predicted trapped-gas values. The poor performance of the Land model in estimating the trapped gas saturation might affect the end point of the gas relative-permeability curve, which could render a substantial error in the fluid production predicted by numerical simulators.

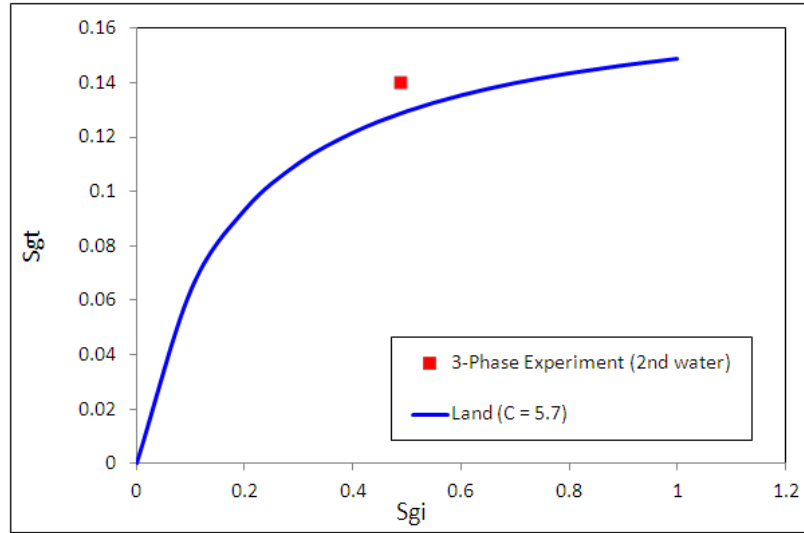


Figure 5-53: Trapped gas saturation versus initial gas saturation, obtained from the Land model and three-phase experiment (2nd water injection) performed on the 1000mD-MW core.

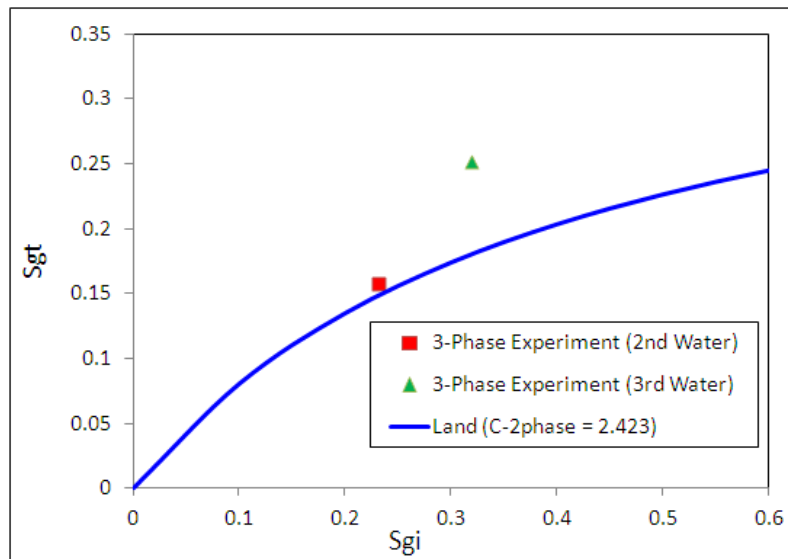


Figure 5-54: Trapped gas saturation versus initial gas saturation, obtained from the Land model and three-phase experiments (2nd and 3rd water injection) performed on the 65mD-WW core.

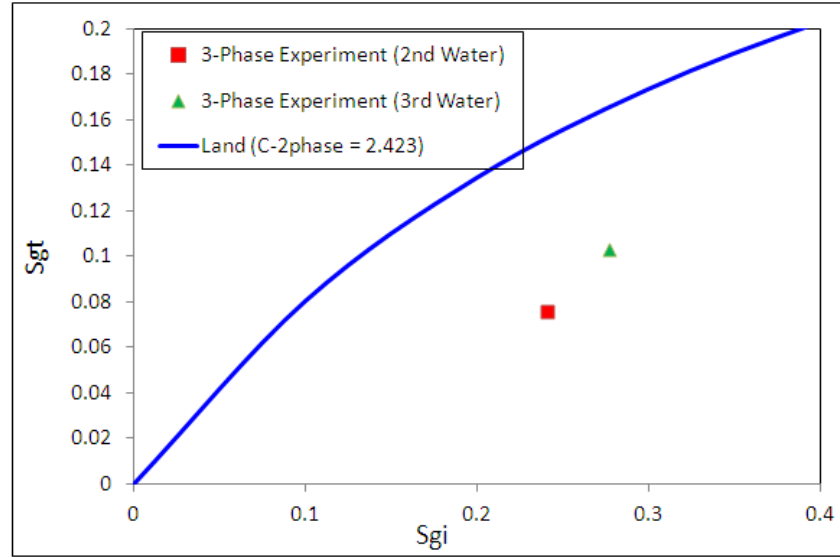


Figure 5-55: Trapped gas saturation versus initial gas saturation, obtained from the Land model and three-phase experiments (2nd and 3rd water injection) performed on the 65mD-MW core.

Eleri et al. (1995a) demonstrated that the presence of trapped gas reduces the residual (trapped) oil saturation during WAG process. Larsen and Skauge (1998) proposed a linear relationship between trapped gas and residual oil saturation obtained during imbibition cycles:

$$S_{om} = (S_{orw})_{S_{gt}=0} - aS_{gt} \quad 5.2$$

Where $(S_{orw})_{S_{gt}=0}$ is the maximum residual oil saturation obtained during water flooding in the absence of gas, S_{gt} is the dynamic trapped gas saturation during three-phase flow and a is the user defined parameter employed for history matching.

Figure 5-56, Figure 5-57 and Figure 5-58 show the residual oil saturation (S_{or}) versus trapped gas saturation (S_{gt}) obtained from different water injections into the 1000mD-MW, 65mD-WW and 65mD-MW cores, respectively. The measured data in three cores exhibit a linear relationship between trapped gas saturation and residual saturation, supporting Equation 5.2. The tuning parameter (a) in Equation 5.1 is equal to one for both the 65mD water-wet and mixed-wet cores and is 1.22 for the 1000mD-MW core.

It should be mentioned that the accurate value of the trapped gas saturation is required in Equation 5.1 to calculate the residual oil saturation of the WAG injection.

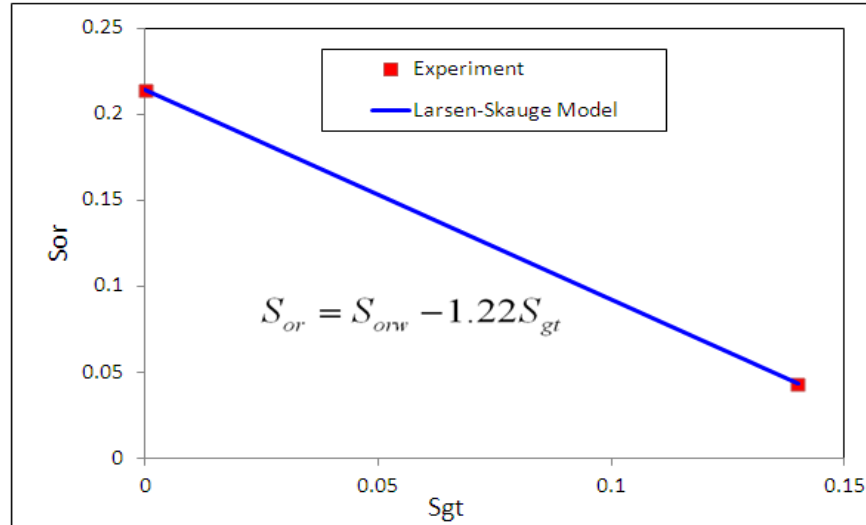


Figure 5-56: Residual oil saturation versus trapped gas saturation for the 1000mD-MW core obtained from the experiment (1st and 2nd water injection) and Larsen-Skauge model (Equation 5.1).

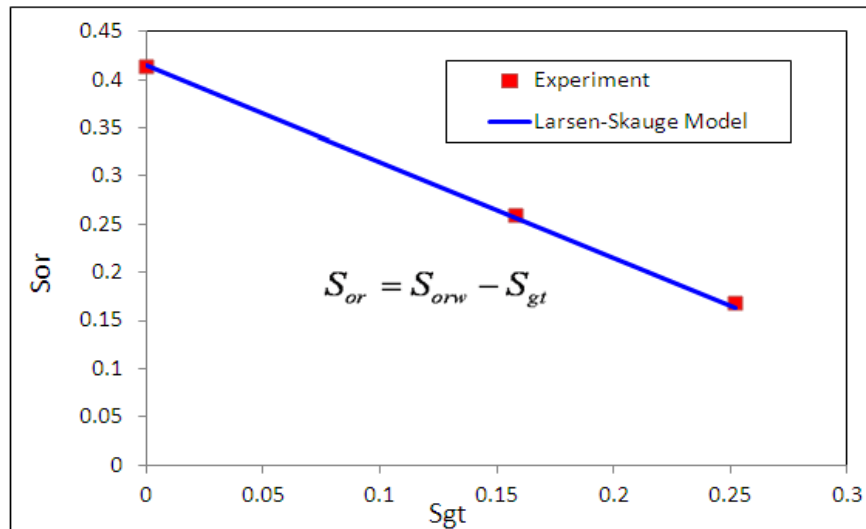


Figure 5-57: Residual oil saturation versus trapped gas saturation for the 65mD-WW core, obtained from the experiment (1st and 2nd water injection) and Larsen-Skauge model (Equation 5.1).

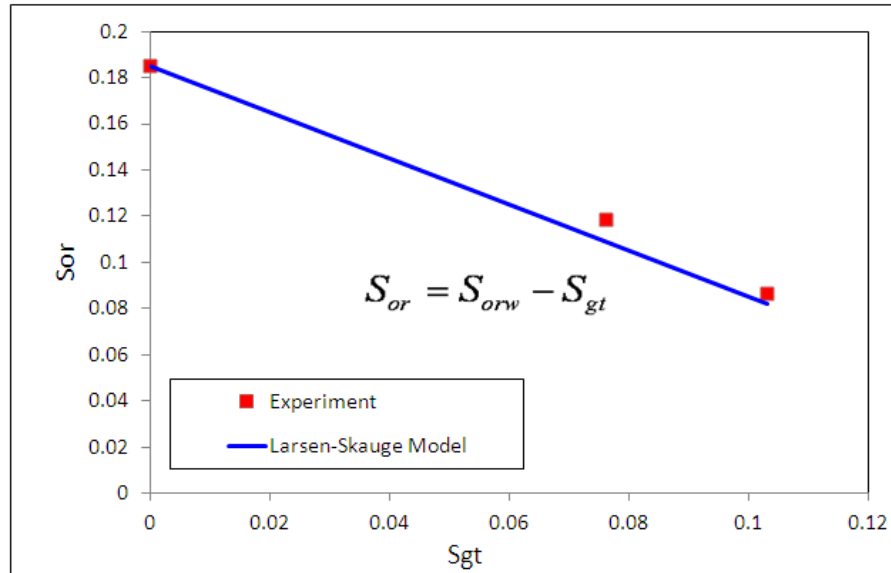


Figure 5-58: Residual oil saturation versus trapped gas saturation for the 65mD-MW core, obtained from the experiment (1st and 2nd water injection) and Larsen-Skauge model (Equation 5.1).

5.4 Conclusions

The main conclusions drawn from interpretation of three-phase relative permeability obtained from different injection scenarios are summarized as follows:

Hysteresis effect:

1. Three-phase gas relative permeability is reduced in consecutive gas injection cycles and accordingly the gas injectivity drops significantly with successive gas injections during the WAG process, under different rock conditions. The gas relative permeability of the 2nd and 3rd water injections exhibits only a slight hysteresis effect, which is less than the substantial hysteresis effect observed during the gas injection cycles. The trend of hysteresis in k_{rg} partly contradicts the existing hysteresis model available in the literature.
2. The results of the mixed-wet system demonstrate negligible cyclic hysteresis in water relative permeability during gas injections, whereas k_{rw} of the water-wet rock is reduced by the successive gas injection that follows water injection.
3. The k_{rw} of the water-wet core does not exhibit any considerable hysteresis effect during different water injections, whereas the mixed-wet core shows slight hysteresis, in which k_{rw} of the 3rd water injection is greater than that of the 2nd.

This may indicate a slight increase of the water injectivity by the subsequent water injection in the WAG process under mixed-wet conditions.

4. Insignificant hysteresis is observed in the oil relative permeability during different gas injection cycles, for both water-wet and mixed-wet rocks. However, a considerable cyclic hysteresis effect in k_{ro} is observed during various water injections, which is attributed to the reduction of the residual oil saturation during successive water injections. k_{ro} of the water-wet core exhibits a much more cyclic hysteresis effect than that of the mixed wet core. Furthermore, no model has currently been developed to capture the cyclic hysteresis effect in oil relative permeability for the WAG process.

Effect of wettability:

1. The discrepancy between k_{rg} of the water-wet and mixed-wet systems is relatively negligible because the gas phase at both wettability conditions acts as non-wetting phase in the presence of oil and water in porous media.
2. Some differences are observed between k_{rw} of the water-wet and mixed-wet systems, which underlines the important role of wettability in influencing the flow of water in presence of oil and gas. Water relative permeability of the mixed-wet core has a larger value, compared to that of the water-wet rock.
3. Unlike water relative permeability, oil relative permeability of the water-wet core is much larger than that of the mixed-wet core.

Two-phase k_r versus three-phase k_r

1. Two-phase gas relative permeability (k_{rgo}) in oil-gas systems is much higher than three-phase k_{rg} . In other words, the presence of the mobile water adversely influences three-phase k_{rg} .
2. Comparison between two-phase and three-phase k_{rw} demonstrates that the two-phase k_{rwo} is significantly less than the three-phase k_{rw} . This indicates that the presence of gas positively affects the mobility of water. Furthermore this finding contradicts the general assumption in the industry that three-phase k_{rw} is less than two-phase k_{rw} .
3. Three-phase k_{rw} and k_{rg} obtained under different rock wettability conditions reveal that both relative permeabilities are a function of two fluid saturations (rather than their own saturation): thus the simplistic assumption made in some

of the existing models, e.g. Stone (1970), that the three-phase k_{rw} and k_{rg} are similar to the two-phase k_{rwo} and k_{rgo} is not justified.

4. Investigation of oil relative permeability under different rock wettability conditions confirmed that the value of the three-phase k_{ro} is significantly less than the two-phase k_{row} at the same value of oil saturation.

Trap saturation

1. The amount of trapped oil and gas obtained from the WAG experiments are poorly predicted by the Land model.
2. The linear relationship between trapped gas and residual oil saturation proposed by Larsen-Skauge (1998) predicts reasonably well the trapped saturations obtained from our WAG experiments.

5.5 References

- Baker, L.E., 1988, Three-Phase Relative Permeability Correlations, paper SPE 17369, presented at the SPE Enhanced Oil Recovery Symposium, Tulsa, Oklahoma.
- Blunt, M.J., 2000, An Empirical Model for Three-Phase Relative Permeability: SPE Journal, paper SPE 67950, (12).
- Carlson, F.M., 1981, Simulation of Relative Permeability Hysteresis to the Nonwetting Phase, paper SPE 10157, presented at the SPE Annual Technical Conference and Exhibition, San Antonio, Texas.
- Chatzis, I., Morrow, N.R., and Lim, H.T., 1983, Magnitude and Detailed Structure of Residual Oil Saturation, paper SPE 10681, (04).
- Cinar, Y., Marquez, S., and Franklin M. Orr, J., 2007, Effect of IFT Variation and Wettability on Three-Phase Relative Permeability: SPE Reservoir Evaluation & Engineering, paper SPE 90572-PA, (06).
- DiCarlo, D.A., Sahni, A., and Blunt, M.J., 1998, The Effect of Wettability on Three-Phase Relative Permeability, paper SPE 49317, presented at the SPE Annual Technical Conference and Exhibition, New Orleans, Louisiana.
- Dietrich, J.K., and Bondor, P.L., 1976, Three-Phase Oil Relative Permeability Models, paper SPE 6044, presented at the SPE Annual Fall Technical Conference and Exhibition, New Orleans, Louisiana.
- Dyes, A.B., 1954, Production of Water-Driven Reservoirs Below Their Bubblepoint: SPE Journal of Petroleum Technology, paper SPE 417-G, (10).
- Egermann, P., Vizika, O., Dallet, L., Requin, C., and Sonier, F., 2000, Hysteresis in Three-Phase Flow: Experiments, Modeling and Reservoir Simulations, paper SPE 65127, presented at the SPE European Petroleum Conference, Paris, France.
- Element, D.J., Masters, J.H.K., Sargent, N.C., OBE, A.J.J., and Goodyear, S.G., 2003, Assessment of Three-Phase Relative Permeability Models Using Laboratory Hysteresis Data, paper SPE 84903, presented at the SPE International Improved Oil Recovery Conference in Asia Pacific, Kuala Lumpur, Malaysia.
- Eleri, O., A.Graue, A.Skaue, and J.A.Larsen, 1995, CALCULATION OF THREE-PHASE RELATIVE PERMEABILITIES FROM DISPLACEMENT EXPERIMENTS WITH MEASUREMENTS OF IN-SITU SATURATION presented at the SCA,
- Fatemi, S.M., Sohrabi, M., Jamiolahmady, M., Ireland, S., and Robertson, G., 2011, Experimental Investigation of Near-Miscible Water-Alternating-Gas (WAG) Injection Performance in Water-wet and Mixed-wet Systems, paper SPE 145191, presented at the Offshore Europe, Aberdeen, UK.
- Geffen, T.M., Owens, W.W., Parrish, D.R., and Morse, R.A., 1951, Experimental Investigation of Factors Affecting Laboratory Relative Permeability Measurements, paper SPE 951099-G,
- Holmgren, C.R., and Morse, R.A., 1951, Effect of Free Gas Saturation on Oil Recovery by Water Flooding, paper SPE 951135-G,

- Hustad, O.S., and Hansen, A.G., 1995, A Consistent Correlation For Three-Phase Relative Permeabilities and Phase Pressure Based on Three Sets of Two Phase Data, presented at the 8th European IOR symposium, Vienna, Austria.
- Hwang, S., Lee, K.P., Lee, D.S., and Powers, S., 2006, Effects of fractional wettability on capillary pressure–saturation–relative permeability relations of two-fluid systems: *Advances in Water Resources Journal*, **29** p. 212–226.
- Jerauld, G.R., 1997, General Three-Phase Relative Permeability Model for Prudhoe Bay: *SPE Reservoir Engineering*, paper SPE 36178, (11).
- Killough, J.E., 1976, Reservoir Simulation With History-Dependent Saturation Functions, paper SPE 5106, (02).
- Kyte, J.R., Jr., R.J.S., Jr., S.C.S., and Rapoport, L.A., 1956, Mechanism of Water Flooding in the Presence of Free Gas, paper SPE 536-G.
- Land, C.S., 1968, Calculation of Imbibition Relative Permeability for Two- and Three-Phase Flow From Rock Properties, paper SPE 1942, (06).
- Larsen, J.A., and Skauge, A., 1998, Methodology for Numerical Simulation With Cycle-Dependent Relative Permeabilities: *SPE Journal*, paper SPE 38456, (06).
- Naar, J., and Wygal, R.J., 1961, Three-Phase Imbibition Relative Permeability, paper SPE 90, (12).
- Pentland, C.H., 2010, *Measurements of Non-wetting Phase Trapping in Porous Media: PhD thesis* London, Imperial College London.
- Skauge, A., and Aarra, M., 1993, Effect of wettability on the oil recovery by WAG, presented at the 7th IOR symp, Moscow.
- Skauge, A., and Larsen, J.A., 1994, Three-phase relative permeabilities and trapped gas measurements related to WAG processes, presented at the SCA, Stavanger.
- Skauge, A., and Ottesen, B., 2002, A SUMMARY OF EXPERIMENTALLY DERIVED RELATIVE PERMEABILITY AND RESIDUAL SATURATION ON NORTH SEA RESERVOIR CORES, presented at the SCA,
- Sohrabi, M., Danesh, A., and Jamiolahmady, M., 2008a, Visualisation of Residual Oil Recovery by Near-miscible Gas and SWAG Injection Using High-pressure Micromodels: *Transport in Porous Media*, **74**(2), p. 239-257.
- Sohrabi, M., Danesh, A., Tehrani, D., and Jamiolahmady, M., 2008b, Microscopic Mechanisms of Oil Recovery By Near-Miscible Gas Injection: *Transport in Porous Media*, **72**(3), p. 351-367.
- Sohrabi, M., Tehrani, D., and Al-Abri, M., 2007, Performance of Near-Miscible Gas and SWAG Injection in a Mixed-Wet Core, presented at the proceedings of the International Symposium of the Society of Core Analysts, Calgary, Canada.
- Spiteri, E.J., and Juanes, R., 2004, Impact of Relative Permeability Hysteresis on the Numerical Simulation of WAG Injection, paper SPE 89921, presented at the SPE Annual Technical Conference and Exhibition, Houston, Texas.
- Spiteri, E.J., Juanes, R., Blunt, M.J., and Orr, F.M., 2008, A New Model of Trapping and Relative Permeability Hysteresis for All Wettability Characteristics: *SPE Journal*, paper SPE 96448-PA, (09).

- Stone, H.L., 1970, Probability Model for Estimating Three-Phase Relative Permeability: SPE Journal of Petroleum Technology, paper SPE 2116, (02).
- Stone, H.L., 1973, Estimation of Three-Phase Relative Permeability And Residual Oil Data, paper SPE 73-04-06, (10-12).
- Vizika, O., and Lombard, J.-M., 1996, Wettability and Spreading: Two Key Parameters in Oil Recovery With Three-Phase Gravity Drainage: SPE Reservoir Engineering, paper SPE 28613, (02).

Chapter 6

New Methodology for Modelling of Hysteresis in the WAG process

As discussed in Chapter 3, the simulation of WAG experiments using existing three-phase k_r models led to erroneous results. The main weakness of the existing published models is that they attempt to use two-phase relative permeability data and some empirical correlations which have not been verified by actual three-phase flow laboratory experiments. Moreover, as described in Chapter 5, the hysteresis phenomena in relative permeability of different WAG cycles is considerable, and ignoring this hysteresis effect may cause erroneous simulation results in production and pressure data. The other weakness of the existing relative permeability models is the lack of an appropriate hysteresis model applicable for WAG simulation. To tackle these shortcomings, a hysteresis methodology applicable for WAG simulation is proposed here, which is developed based on the three-phase relative permeability data that we have obtained from WAG experiments. This technique is a direct method which uses the measured three-phase k_r data obtained from first cycle of WAG to predict the relative permeability of the subsequent cycles. This approach is hereafter referred to the WAG-HW model. In this chapter, first the mathematical formulation of this model is

fully explained. Following this, the relative permeability data from three sets of coreflood experiments are employed to validate this model. At the end of this chapter, the most common WAG hysteresis model (Larsen and Skauge, 1998) described in Chapter 3 is assessed, using our three-phase relative permeability data, in order to compare the performance of the WAG-HW approach against Larsen-Skaug model.

6.1 New hysteresis model (WAG-HW)

The concept behind this approach is to utilize the three-phase relative permeability values measured from the first cycle of WAG injection in order to predict the k_r values of the subsequent cycles, using the following equation:

$$\{k_{ri}(S_i)\}_n = H \times \{k_{ri}(S_i)\}_{n-1} \quad 6.1$$

where k_{ri} is relative permeability of fluid i (oil, gas or water), S_i is saturation of phase i , H is the hysteresis coefficient and n refers to the cycle number. This equation is a general formula for application to the cyclic hysteresis. H is a hysteresis function which depends on the phase saturation and the injection process, i.e. water injection or gas injection. The base relative permeability data required in using Equation 6.1 are k_{ro} , k_{rw} and k_{rg} and the corresponding fluid saturation values obtained from the first gas injection (after initial waterflooding) and the subsequent water injection, under three-phase flow conditions. In fact, Equation 6.1 quantifies the cyclic hysteresis in relative permeability which occurs between either different gas injections or different water injection cycles. In other words, Equation 6.1 calculates the relative permeability of successive cycles of the same injection strategies i.e. water injection or gas injection, hence the hysteresis coefficient in the above equation is different from the water injection to the gas injection.

As mentioned in Chapter 5, a kind of hysteresis effect widely reported in the literature (Killough, 1976; Carlson, 1981) and also observed during our WAG experiments is conventional hysteresis, happening between k_r of water injection and that of gas injection. Furthermore, based on k_r data obtained from our experiments, it was revealed that the conventional hysteresis effect during WAG injection, in the most cases, is unsystematic and unpredictable. However, this concern is resolved once using Equation 6.1 because this technique predicts the relative permeability of gas injection and water injection independently. Utilizing at least one set of measured three-phase k_r data in

Equation 6.1 is another advantage of this methodology. Because employing measured three-phase data is more realistic and accurate compare to the interpolation technique used in the existing model in which three-phase k_r is determined from two-phase data (Stone, 1970; Baker, 1988; Hustad and Hansen, 1995; Hustad and Browning, 2010).

We extend Equation 6.1 for gas, water and oil relative permeability with appropriate values for the hysteresis coefficient, consistent with cyclic hysteresis observed in our WAG experiments.

6.1.1 Gas relative permeability during gas injection

Plotting gas relative permeability of the various gas injection cycles versus gas saturation revealed that k_{rg} had significantly reduced in subsequent gas injection cycles, at both water-wet and mixed-wet conditions. The gas relative permeability of gas injection cycles can be determined by

$$\{k_{rg}^{GI}(S_g)\}_n = \left(\frac{S_{g,start}^{n-1}}{S_{g,start}^n} \right) \times \{k_{rg}^{GI}(S_g^*)\}_{n-1} \quad 6.2$$

$$S_g^* = S_g - (S_{g,start}^n - S_{g,start}^{n-1}) \quad 6.3$$

where superscript *GI* refers to the gas injection, n is number of cycles and starts from 2, $S_{g,start}^n$ and $S_{g,start}^{n-1}$ are gas saturation values at the beginning of the current and previous gas injection cycles. The S_g is the instant gas saturation of the grid block in which k_{rg} should be calculated. The gas relative permeability of the first cycle (k_{rg}^{GI}) _{$n=1$} is required while using Equation 6.2. In fact, this formula is a hysteresis loop that is producing the gas relative permeability of each gas injection cycle from previous gas cycles.

The second term on the right hand side of Equation 6.2, $k_{rg}^{GI}(S_g^*)$, is gas relative permeability of the previous gas injection, which should be computed at $S_g^* = S_g - (S_{g,start}^n - S_{g,start}^{n-1})$ rather than S_g . In fact, computing k_{rg} at S_g^* shifts the k_{rg} curve of the previous cycle ($n-1$) horizontally to the right hand side, by a value of $(S_{g,start}^n - S_{g,start}^{n-1})$, as shown in Figure 6-1. The first bracket on the right hand side of Equation 6.2 represents the hysteresis coefficient (H). Since, by successive gas injections, the amount of gas in the system continually increases, the initial gas at the

beginning of each gas injection would be higher than that of the previous gas injection.

Therefore the value of the saturation ratio, $\left(\frac{S_{g,start}^{n-1}}{S_{g,start}^n}\right)$ in Equation 6.2 becomes less than

one, which causes a reduction in k_{rg} of the present gas cycles compared to that of the former gas injection. If the initial gas saturation at the beginning of a gas injection cycle is zero, the value of the saturation ratio in Equation 6.2 should be considered equal to one. However, both effects, including transformation of k_{rg} to the right hand side and hysteresis coefficient, cause a reduction in the gas relative permeability of the new cycle (n) compared to k_{rg} of the previous cycle. This reduction effect is consistent with the experimental observation described in Chapter 5. Figure 6-2 shows the flow diagram for calculating k_{rg} of consecutive gas injections throughout a WAG process.

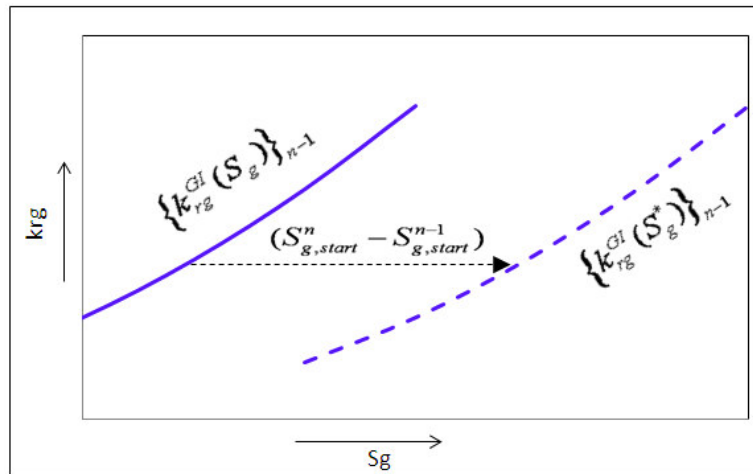


Figure 6-1: Horizontal Transformation of k_{rg} to the right hand side by a value of $(S_{g,start}^n - S_{g,start}^{n-1})$.

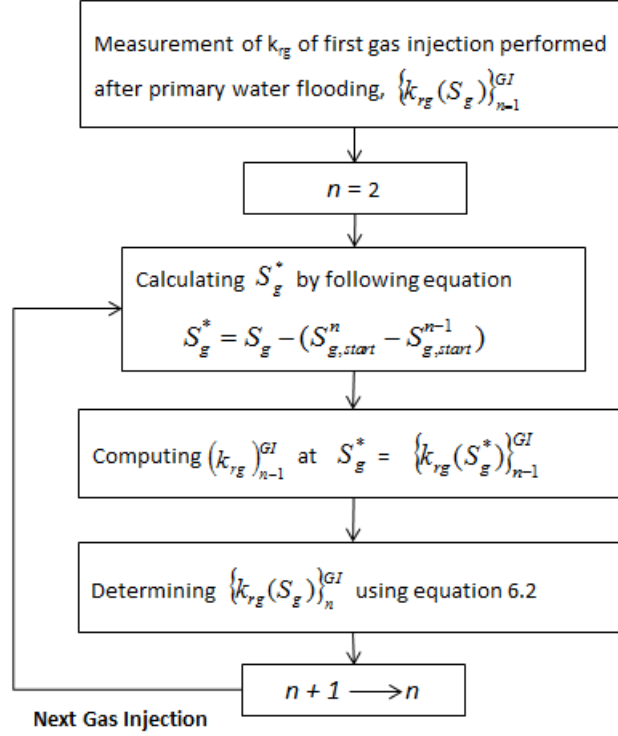


Figure 6-2: Flow diagram for calculating k_{rg} of successive gas injection.

6.1.2 Gas relative permeability during water injection

As shown in the previous chapter, the gas relative permeability of the various water injection cycles during the WAG experiments, obtained in both water-wet and mixed-wet rocks, revealed hysteresis effects. The following formula is proposed for calculating k_{rg} of the further water injections:

$$\{k_{rg}^{WI}(S_g)\}_n = \left[\frac{S_{g,start}^n}{S_{g,start}^{n-1}} \right]^{WI} \times \{k_{rg}^{WI}(S_g^*)\}_{n-1} \quad 6.4$$

$$S_g^* = S_g - (S_{gt}^n - S_{gt}^{n-1}) \quad 6.5$$

where WI denotes water injection, k_{rg} is gas relative permeability expressed in terms of gas saturation and n is the number of cycles and starts from 2. The crucial point in determining gas relative permeability during water injection is the value of the trapped gas saturation (S_{gt}) at which k_{rg} falls to zero ($k_{rg}^{WI}(S_g \leq S_{gt}) = 0$). Equation 6.4 applies to gas saturation values greater than the trapped saturation. The required input data in using Equation 6.4 are k_{rg} of the very first water injection, performed at three-phase

condition ($\{k_{rg}^{WI}(S_g^*)\}_{n=1}$), the initial gas saturation at the beginning of current (n) and previous ($n-1$) water injections ($S_{g,start}^n$ and $S_{g,start}^{n-1}$) and corresponding trapped gas saturation of the present and former water cycles (S_{gt}^n and S_{gt}^{n-1}). The second term on the right hand side of Equation 6.4, $\{k_{rg}^{WI}(S_g^*)\}_{n-1}$, is gas relative permeability of the previous water injection cycle, which should be computed at S_g^* (given in Equation 6.5) rather than S_g . In fact, calculating k_{rg} at S_g^* shifts the gas relative permeability curve horizontally to the right hand side by a value of $(S_{gt}^n - S_{gt}^{n-1})$ (similar to what is shown in Figure 6-1). Furthermore, as the amount of gas saturation in the system at the present (n) cycle is higher than that at the earlier cycle ($n-1$), physically, the value of k_{rg} of the water injection cycle n is larger than that of water cycle $n-1$. This fact is met in Equation 6.4 by incorporating saturation ratio $\frac{S_{g,start}^n}{S_{g,start}^{n-1}}$, which is always greater than one.

Investigation of the trapped gas saturation attained by several water injection tests in both water-wet and mixed-wet cores matched the predictions made by the Carlson model (Carlson, 1981). This model states that the difference between the initial and the trapped saturation of the non-wetting phase (gas) remains constant during various imbibition cycles, i.e.,:

$$\left[S_{g,start}^n - S_{gt}^n \right]^{WI} = \left[S_{g,start}^{(n-1)} - S_{gt}^{(n-1)} \right]^{WI} = \text{Constant} \quad 6.6$$

It should be noted that trapped gas saturation in Equation 6.5, for a reservoir simulation, should be obtained either from a trapping model e.g. Land, Carlson or from experimental data. The calculation procedure of Equation 6.5 is given in Figure 6-3.

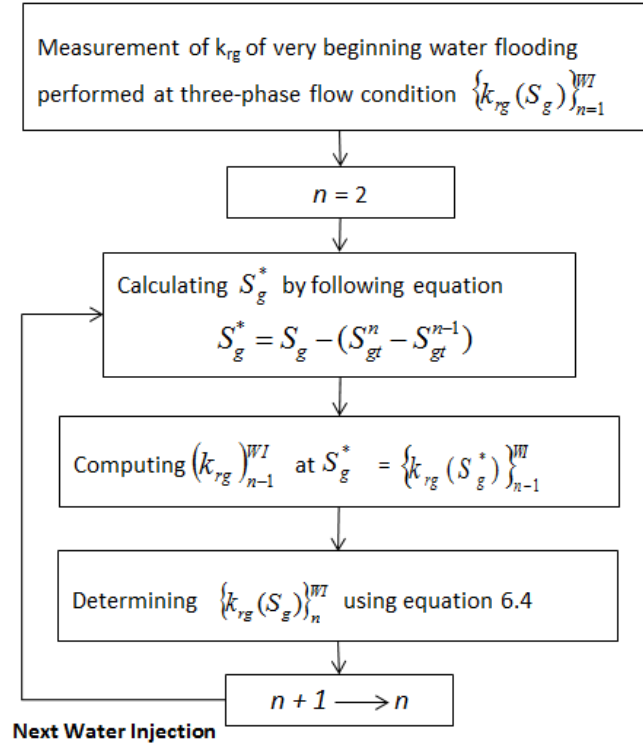


Figure 6-3: Flow diagram for calculating k_{rg} of the successive water injections.

6.1.3 Water relative permeability during water injection

Investigating water relative permeability of the consecutive water injections into a water-wet core did not reveal any hysteresis effect, whilst the results of k_{rw} of the mixed wet system showed some hysteresis effects. A mathematical formula similar to the model of gas relative permeability during water injection (Equation 6.4) is suggested for modelling of the hysteresis in k_{rw} during water injection:

$$\{k_{rw}^{WI}(S_w)\}_n = \left[\frac{S_{g,start}^n}{S_{g,start}^{n-1}} \right]^{WI} \times \{k_{rw}^{WI}(S_w)\}_{n-1} \quad 6.7$$

The gas saturation ratio $\left(\frac{S_{g,start}^n}{S_{g,start}^{n-1}}\right)$ in the first pair of brackets on the RHS of Equation 6.7

should be obtained from the water injection cycles. However, since the gas saturation in the system continually increases during WAG injection, the saturation ratio in the above equation would be greater than one in which increases the k_{rw} of the present cycle compare to that of former cycle.

6.1.4 Water relative permeability during gas injection

As presented in Chapter 5, the water relative permeability obtained from various gas injections through the water-wet media demonstrated increasing values of k_{rw} as injection cycles progressed. The following equation is proposed to capture this hysteresis effect in water relative permeability:

$$\{k_{rw}^{GI}(S_w)\}_n = \left[\frac{S_{g,start}^{n-1}}{S_{g,start}^n} \right]^{GI} \times \{k_{rw}^{GI}(S_w)\}_{n-1} \quad 6.8$$

This equation is similar to the formula proposed for the gas relative permeability during the gas injection processes (Equation 6.2). The successive gas injections lead to increase of gas saturation and, consequently, each gas injection commences with the higher initial gas saturation than its previous cycle. Thus, the ratio of the initial gas saturation $\left(\frac{S_{g,start}^n}{S_{g,start}^{n-1}} \right)$ in Equation 6.8 is greater than one and causes k_{rw} to rise as

injection progresses. When $S_{g,start}^{n-1} = 0$ the saturation ratio $\left(\frac{S_{g,start}^n}{S_{g,start}^{n-1}} \right)$ must be set equal to one.

6.1.5 Oil relative permeability during water injection

One of the factors affecting the oil relative permeability during water injection is the residual oil saturation retained by the advancing water. It is apparent that the decrease in residual oil saturation is accompanied by an increase in oil relative permeability in successive WAG injection cycles. A mathematical formula is proposed to predict the k_{ro} value at various points in the water injection cycles:

$$\{k_{ro}^{WI}(S_o)\}_n = \left[\frac{1}{S_{w,start}^n} \frac{S_{o,start}^{n-1}}{S_{o,start}^n} \right]^{WI} \times \{k_{ro}^{WI}(S_o^*)\}_{n-1} \quad 6.9$$

$$S_o^* = S_o + S_{or}^{n-1} - S_{or}^n \quad 6.10$$

The input data required in employing Equation 6.9 are oil relative permeability of the water injection performed after 1st gas injection $(\{k_{ro}^{WI}(S_o^*)\}_{n-1})$, initial oil and water saturation at the beginning of cycles and residual oil saturation for present and former water injection cycles. The residual saturation in Equation 6.9 can be determined either

from experiment or trapping models e.g. Land, Carlson. Water relative permeability of the former water injection in Equation 6.9 should be computed at S_o^* , given in Equation 6.10. Computing $(k_{ro})_{n-1}$ at S_o^* transforms it horizontally by a value of $(S_{or}^{n-1} - S_{or}^n)$ to the left hand side, as shown in Figure 6-4.

Since performing various gas injections increase the amount of gas saturation, trapped gas saturation rises during successive water injections. In addition, as mentioned earlier in the previous chapter, the total trapped hydrocarbon (oil + gas) saturation remains constant during various water injection cycles. Therefore the trapped oil saturation is continually reduced during water injection cycles, which increases the oil mobility. This point is accounted for in Equation 6.9 by including a saturation ratio term ($\frac{1}{S_{w,start}^n} \frac{S_{o,start}^{n-1}}{S_{o,start}^n}$) which is always greater than one and causes an increase in the oil relative permeability of water cycle n compare to water cycle $n-1$.

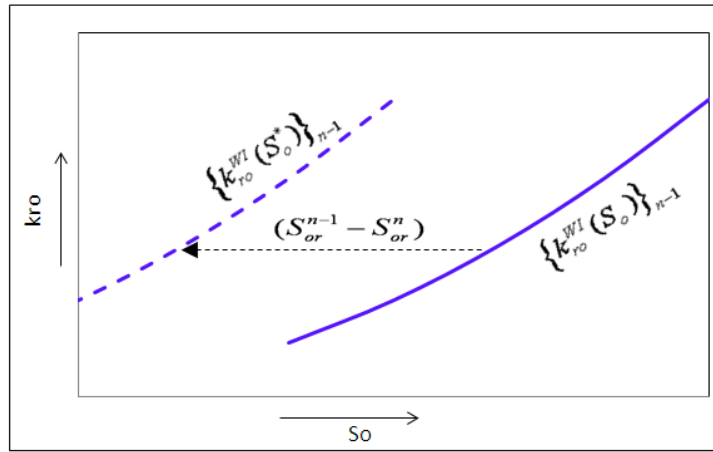


Figure 6-4: Horizontal transformation of k_{ro} to the left hand side by a value of $(S_{or}^{n-1} - S_{or}^n)$.

6.1.6 Oil relative permeability during gas injection

Three-phase oil relative permeability obtained from various gas injection cycles in water-wet and mixed-wet cores did not exhibit any significant hysteresis effect. However, investigation of oil relative permeability in 65mD water-wet core for the oil saturation values below S_{orw} (remaining oil after primary water injection) demonstrates

that the value of oil relative permeability is proportional to the quadratic of oil saturation ($k_{ro} \propto S_o^2$). This quadratic behaviour has already been reported by other lab measurements in published literature (Oak, 1990; Fenwick and Blunt, 1998; Blunt, 2000; DiCarlo et al., 2000). One theoretical explanation is that oil resides in crevices in the pore space, between water which is next to the solid surface and gas in the centre of the pores. The oil saturation is roughly proportional to the area occupied by this oil layer. The hydrodynamic conductance, and hence relative permeability, is proportional to the oil area squared, leading to $k_{ro} \propto S_o^2$. This suggests a simple way to extrapolate the oil relative permeability to saturation values lower than those achieved in an experiment (Blunt, 2000). Figure 6-5 shows three-phase oil relative permeability of the various gas injections in 65mD water-wet rock obtained from our experiments and extrapolated to the lower saturation values by the quadratic model, for comparison. Using the value of 0.015 as the coefficient in equation, $k_{ro} \propto S_o^2$ would give close match with measured k_{ro} .

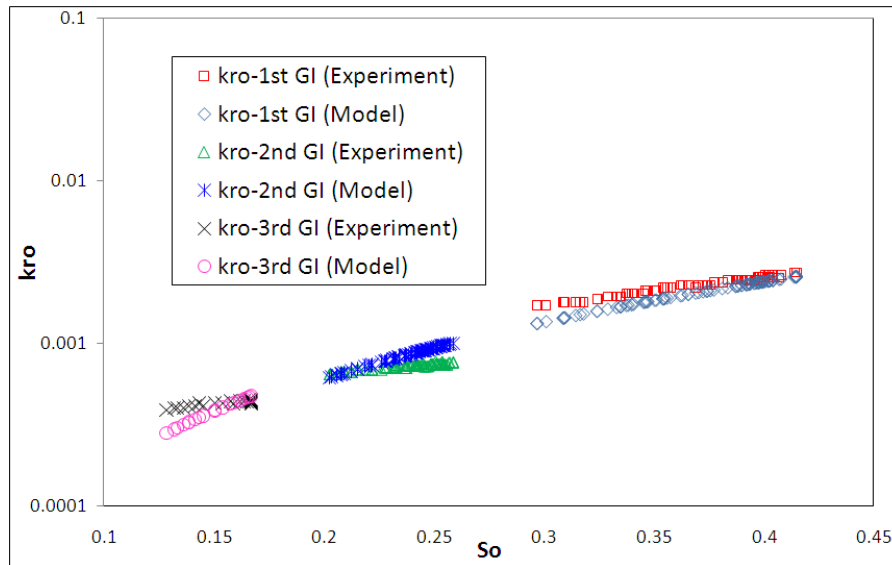


Figure 6-5: Oil relative permeability of various gas injections in 65mD-WW core, obtained from experiments and model ($k_{ro} = 0.015 S_o^2$).

6.2 Verification of the WAG-HW model

The relative permeability data obtained from different cycles of WAG experiments through 65md-WW, 65md-MW and 1000mD-MW cores are used in this section to validate the accuracy of the WAG-HW model described above.

The measured k_{rg} of the first gas injection is employed as input data in Equation 6.2 to determine gas relative permeability of the second and third gas injections. Figure 6-6 and Figure 6-7 show log-log plots of the experimental gas relative permeability against k_{rg} of the WAG-HW model for 65mD-WW and 65mD-MW cores, respectively. A straight line with a unit slope in these figures represents perfect agreement between experiment and model. In other words, if the scatter points are sufficiently close to the straight line the model performs accurately. Figure 6-8 presents the correlation between measured and predicted gas relative permeability of the second gas injection of 1000mD-MW core. The comparison between calculated and observed k_{rg} of different cores illustrated in Figure 6-6 to Figure 6-8 demonstrate satisfactory precision for the WAG-HW model (Equation 6.2).

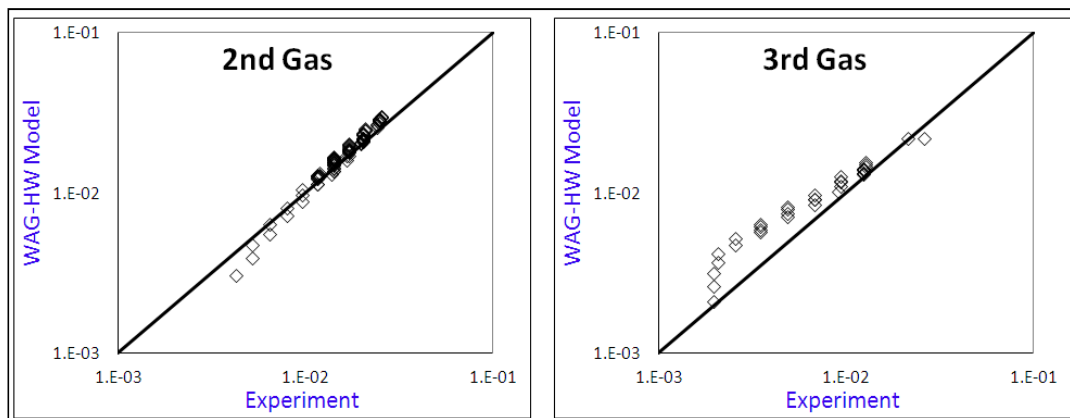


Figure 6-6: Gas relative permeability of 2nd and 3rd gas injections of 65mD-WW core obtained from the experiment versus that calculated by the WAG-HW model (Equation 6.2).

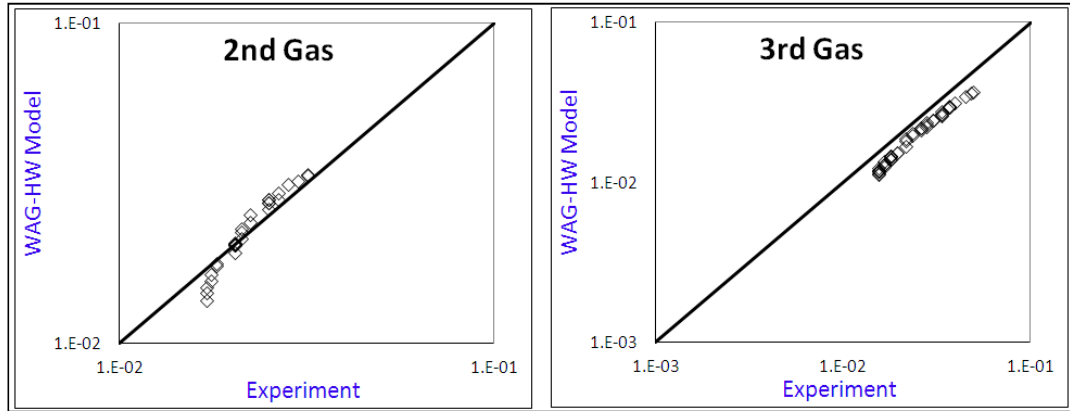


Figure 6-7: Gas relative permeability of 2nd and 3rd gas injections of 65mD-MW core obtained from experiment versus that calculated by the WAG-HW model (Equation 6.2).

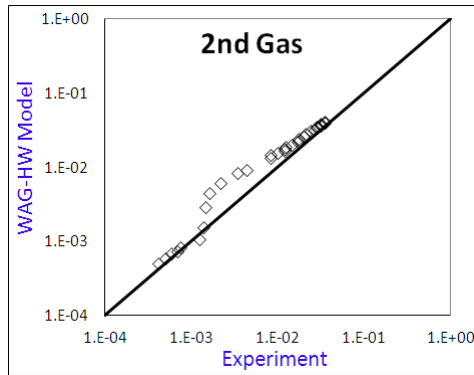


Figure 6-8: Gas relative permeability of 2nd gas injection of 1000mD-MW core obtained from experiment versus that calculated by the WAG-HW model (Equation 6.2).

The gas relative permeability of the second water injection and the trapped gas saturation attained by the second and third water injections are employed as input data in Equation 6.4 to predict k_{rg} of the third water injection. The k_{rg} of 3rd water injection of 65mD water-wet and mixed-wet rocks obtained from experiment against that estimated by the WAG-HW model are given in Figure 6-9 and Figure 6-10, respectively. As shown, in both rocks, the scatter points lie on top of the straight line, indicating that the values estimated by the model are in perfect agreement with the corresponding measured values.

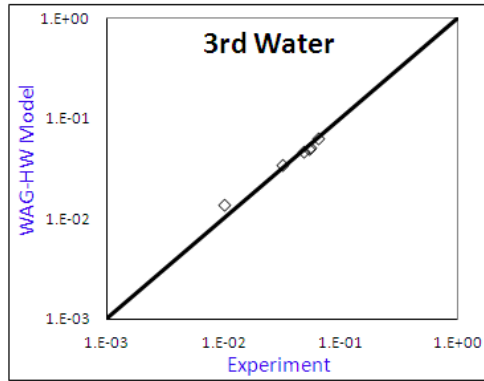


Figure 6-9: Gas relative permeability of 3rd water injection of 65mD-WW core obtained from experiment versus that calculated by the WAG-HW model (Equation 6.4).

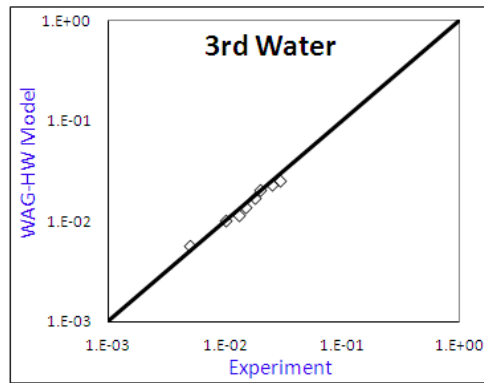


Figure 6-10: Gas relative permeability of 3rd water injection of 65mD-MW core obtained from experiment versus that calculated by the WAG-HW model (Equation 6.4).

The water relative permeability of the third water injection of 65mD-MW core is calculated from Equation 6.7 by employing k_{rw} of the second water injection. Comparison of the results for experiment and model given in Figure 6-11 shows satisfactory performance for the WAG-HW model. The water permeability of the 2nd and 3rd gas injections into 65mD-WW rock is predicted using Equation 6.8. The measured k_{rw} versus estimated k_{rw} for the 2nd and 3rd water injection, given in Figure 6-12, indicates reasonable precision for Equation 6.8.

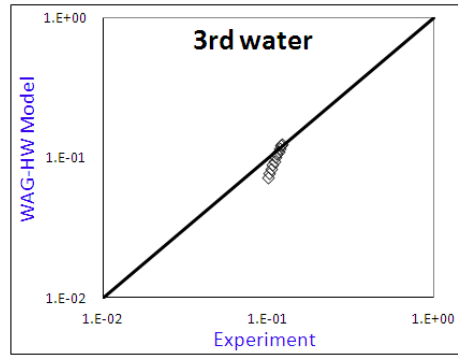


Figure 6-11: Water relative permeability of 3rd water injection of 65mD-MW core obtained from experiment versus that calculated by the WAG-HW model (Equation 6.7).

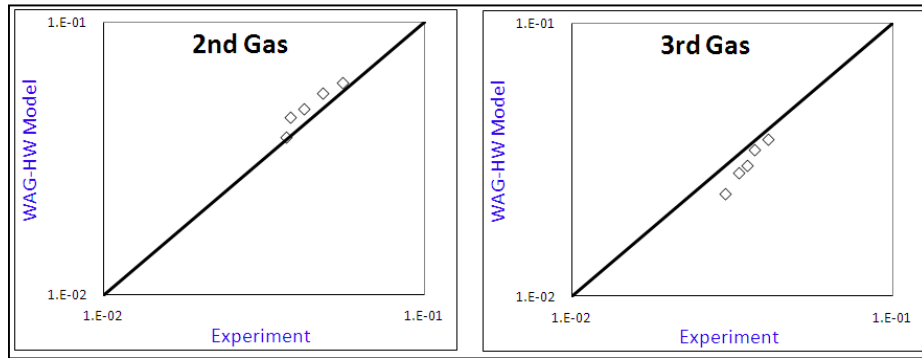


Figure 6-12: Water relative permeability of 2nd and 3rd gas injection of 65mD-WW core obtained from experiment versus that calculated by the WAG-HW model (Equation 6.8).

The oil relative permeabilities of the 3rd water injection in 65mD water-wet and mixed-wet cores against those obtained from the WAG-HW model are shown in Figure 6-13 and Figure 6-14, respectively. The k_{ro} of the second water injection and the residual oil saturation reached by the 2nd and 3rd water injections are utilized in Equation 6.9. The calculated k_{ro} of the 3rd water injection for both cores reveal reasonable agreement with the corresponding experimental data.

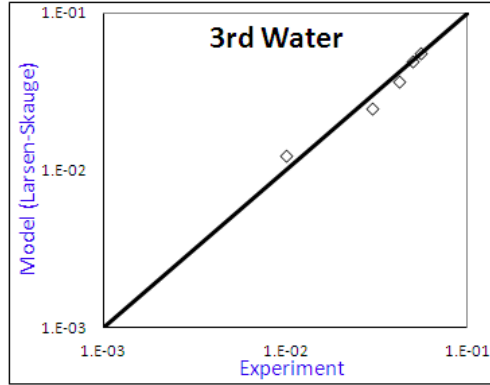


Figure 6-13: Oil relative permeability of 3rd water injection of 65mD-WW core obtained from experiment versus that calculated by the WAG-HW model (Equation 6.9).

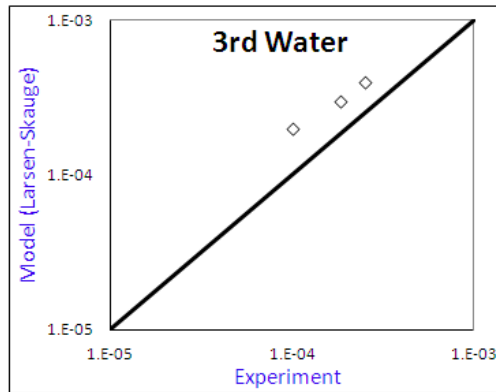


Figure 6-14: Oil relative permeability of 3rd water injection of 65mD-MW core obtained from experiment versus that calculated by the WAG-HW model (Equation 6.9).

6.3 Assessment of Larsen-Skauge model

The methodology proposed by Larsen and Skauge (1998) for capturing the cyclic hysteresis effect in relative permeability of different WAG processes, is one of the most popular models available in reservoir simulators. The mathematical formula of this technique is fully described in Chapter 3, section 3.2.3. Here, we evaluate the capability of this model in predicting relative permeability of the various cycles of our WAG experiments, in order to identify the inadequacies associated with this method.

Gas relative permeability

The input data for calculating gas relative permeability of the successive gas and water injection using Larsen-Skauge model (Equation 3.37) are:

- 1- Two-phase gas relative permeability (k_{rg0}) of the primary gas injection performed in presence of irreducible water and oil.
- 2- The end point value of k_{rg} of the former water injection, $\left[k_{rg}^{imb} (S_g^{start}) \right]_{n-1}$. The S_g^{start} here is gas saturation at the beginning of gas injection, which is same as the last gas saturation point of the former water injection.
- 3- Tuning parameter, α
- 4- Land coefficient, C

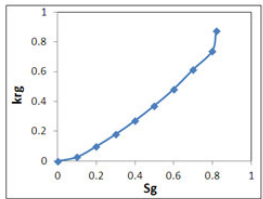
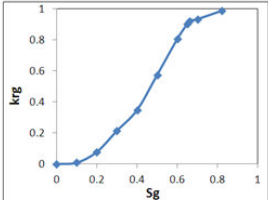
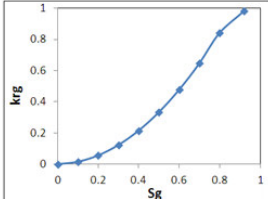
The above data for different cores are provided in Table 2-1. The Land coefficient can be determined from the Land equation (Equation 3.33), knowing the values of the initial and trapped gas from a water injection test at two-phase gas-water condition (Table 5-2). The tuning parameter, α is selected with the aim of ensuring the least mismatch between calculated and experiment data. The end point value of k_{rg} of the 1st water injection is zero because it has been carried out in absence of gas saturation. Figure 3-5 shows a schematic plot for the gas relative permeability of the different cycles of WAG injection, calculated using the Larsen-Skauge model.

The log-log plots of measured k_{rg} against predicted k_{rg} for various cycles of WAG injection through 65mD-WW, 65mD-MW and 1000mD-MW cores are presented in Figure 6-16, Figure 6-17 and Figure 6-18, respectively. The tuning parameter is kept constant ($\alpha = 0.7$) during calculation for all cycles. The results of the 1st gas injection of the 65mD-WW core in Figure 6-16 is on top of the straight line whilst the calculated k_{rg} of the other cycles are significantly overestimated. The calculated k_{rg} of the 65mD-MW and 1000mD-MW cores (Figure 6-17 and Figure 6-18) also exhibit substantial disagreement with the corresponding measured data. However, these results indicate the inaccuracy of the Larsen-Skauge model for prediction of k_{rg} of our WAG experiment performed at near miscible condition. The main shortcomings of this model can be expressed thus:

- 1- Using two-phase k_{rg0} obtained from primary gas injection (in the absence of mobile water) for calculating three-phase k_{rg} of a system containing three mobile fluids. Basically the physics of flow in a two-phase system is different from three-phase systems; therefore, determination of three-phase k_r from two-phase data may lead to erroneous results, as shown in Chapter 3 and in some papers in the literature (Petersen et al., 2008; Cao and S, 2010).

- 2- Using an inappropriate trapping model for obtaining trapped gas saturation throughout the imbibition process. As demonstrated in Chapter 5, the Land equation failed to predict the accurate values of the trapped gas saturation obtained by the water injection process under three-phase flow conditions. Moreover, the Land model was originally proposed for two-phase systems and may not be applicable in three-phase flow circumstances.
- 3- Investigation of k_{rg} of the gas injection and water injection processes resulting from the different core experiments (Figure 5-19 and Figure 5-20) does not indicates a chronological relationship between k_{rg} of water injection and that of gas injection. However, in the Larsen-Skauge model (Figure 3-5) the k_{rg} of water injection (decreasing gas saturation) is assumed to be less than the k_{rg} of the previous gas injection (increasing gas saturation).

Table 6-1: Required input data for calculating k_{rg} using Larsen-Skauge model

Core	k_{rg} -Primary gas injection	α	C
65mD-WW		0.7	2.423
65mD-MW		0.3	2.423
1000mD-MW		1	5.7

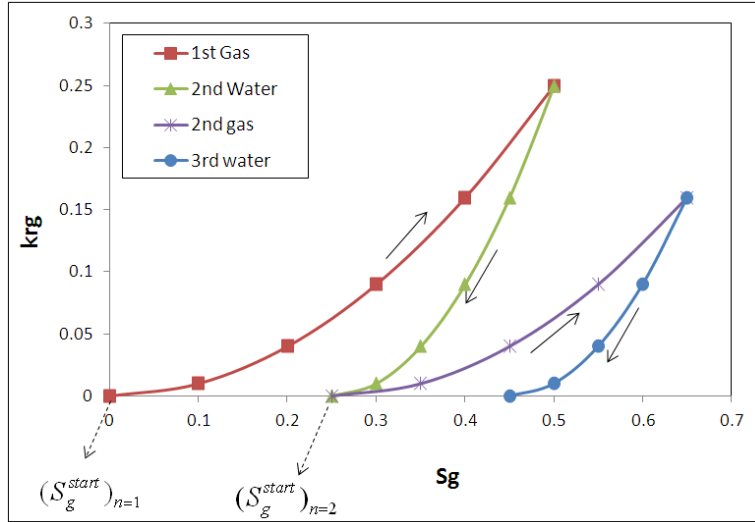


Figure 6-15: Schematic gas relative permeability scanning curves of different cycles of WAG injection, predicted with the Larson-Skauge model.

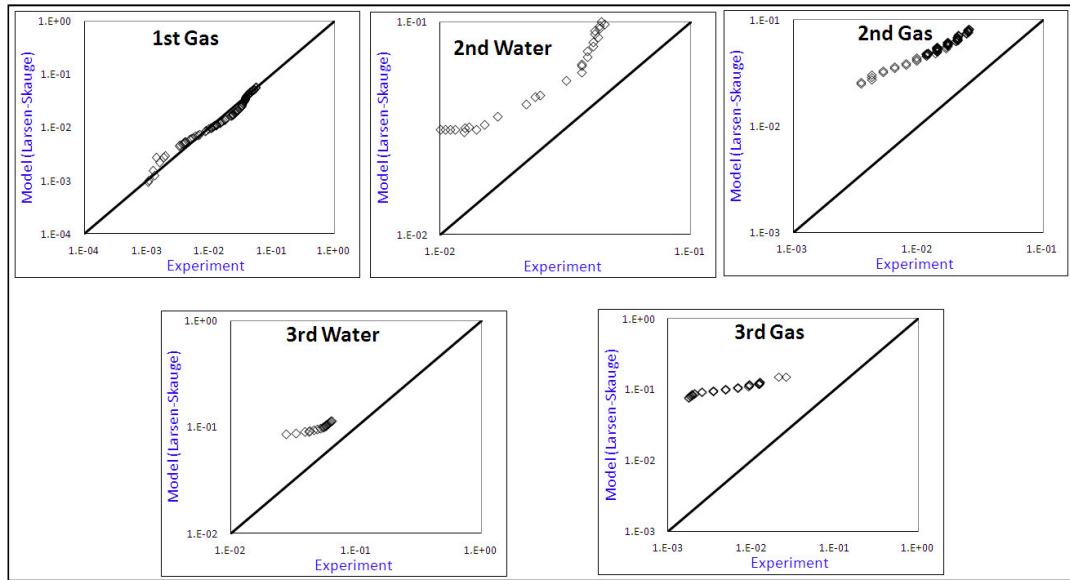


Figure 6-16: Gas relative permeability of the various water and gas injections of 65mD-WW core obtained from experiment versus that calculated by Larsen-Skauge model.

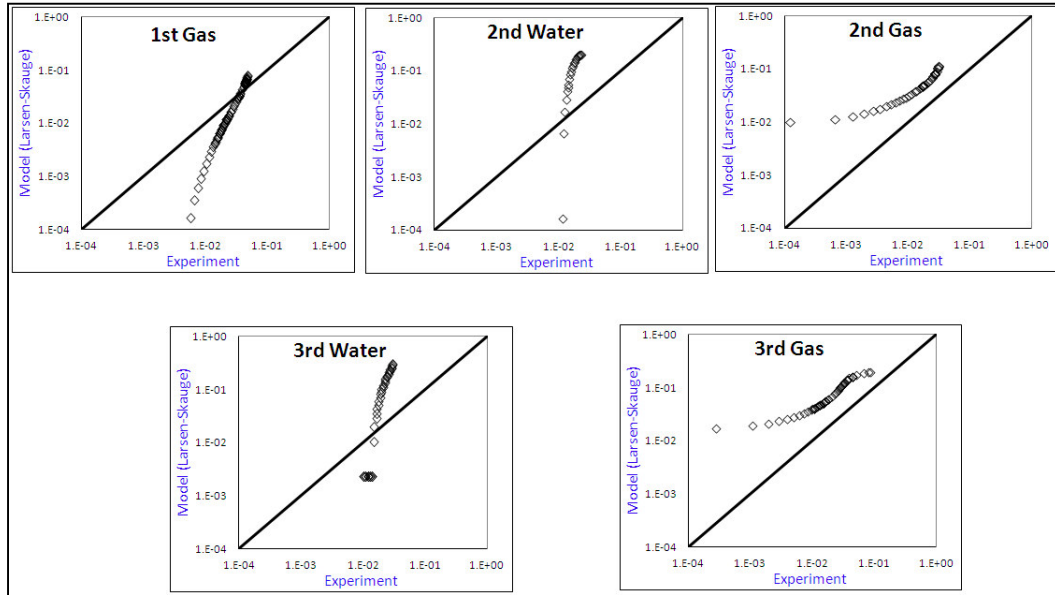


Figure 6-17: Gas relative permeability of the various water and gas injections of 65mD-MW core obtained from experiment versus that calculated by Larsen-Skauge model.

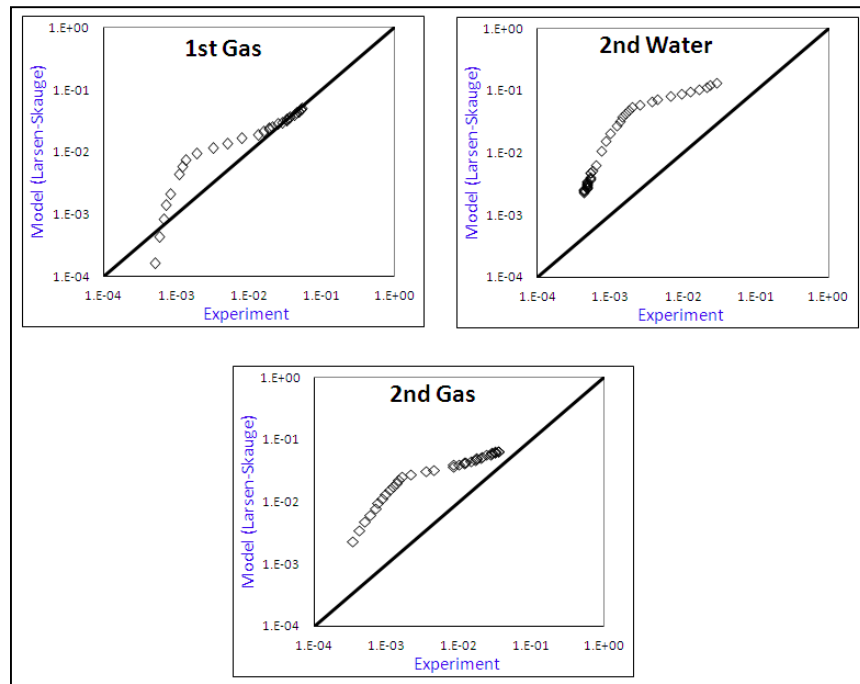


Figure 6-18: Gas relative permeability of the various water and gas injections of 1000mD-MW core obtained from experiment versus that calculated by Larsen-Skauge model.

Water relative permeability

Larsen and Skauge (1998) proposed two different equations for determining k_{rw} of the increasing gas saturation (gas injection) and decreasing gas saturation (water injection)

during a WAG process (Equations 6.11 and 6.12). In this method, the water relative permeability of the different cycles of WAG are calculated by interpolation between k_{rw} of the primary water flooding (oil-water) and k_{rw} of the second water injection performed after first gas injection (Figure 6-19). Hence, the essential input data for predicting k_{rw} by this model are k_{rw} of the primary and secondary water injections. These data are provided for different rocks, in Figure 5-43 to Figure 5-45.

The water permeability obtained from the various cycles of the WAG experiments versus the corresponding k_{rw} calculated by the Larsen-Skauge model for 65mD-WW, 65mD-MW and 1000mD-MW cores are presented in Figure 6-20, Figure 6-21 and Figure 6-22, respectively. The predicted k_{rw} of the 65mD-WW core, shown in Figure 6-19, reveals a relatively large inconsistency with the corresponding measured results, whilst the estimated k_{rw} of both mixed-wet cores (65mD & 1000mD), shown in Figure 6-21 and Figure 6-22, exhibit reasonable agreement with the respective observed data.

The key shortcomings associated with the water model are:

- 1- Based on the physics of multiphase flow, the relative permeability curve of each fluid must be monotonically increasing in terms of its own saturation. In other words, from a mathematical point of view, the derivative of relative permeability of each fluid with respect to its own saturation must be a positive value. This basic rule may be violated by the water permeability model (Larsen-Skauge), given by Equations 6.11 and 6.12. The explanation of this inconsistency is that, in a WAG process, the value of gas saturation at the start of a water injection or gas injection (S_g^I) may occasionally be higher than the $S_{g,max}$ (gas saturation at the start of the secondary water (W2) process). Thus, the value of $\frac{S_g^I}{S_{g,max}}$ in Equations 6.11 and 6.12 becomes greater than one. If that happens, then the saturation terms in Equations 6.11 and 6.12 would be either greater than one or a negative value which might produce an abnormal value for the calculated k_{rw} , not supporting the monotonically increasing rule. Moreover, the derivative of Equation 6.10 with respect to the water saturation given in Equation 6.13 appears to contain a negative term which can lead to a negative value for the derivative of k_{rw} . The negative value of the derivative of k_{rw} means that k_{rw} is monotonically decreasing with its own saturation. Hence the Equation 6.12, in some saturation ranges may generate an

unrealistic shape for water relative permeability. This contradiction occurs in the predicted k_{rw} of the 1st gas, 3rd gas and 3rd water injections of 65mD-WW core in Figure 6-20. The scatter points in these graphs at the same saturation regions represent a negative slope.

$$k_{rw}^{imb}(S_w, S_g^I) = k_{rw}^{W1} \left[1 - \frac{S_g^I}{S_{g,max}} \right] + k_{rw}^{W2} \left[\frac{S_g^I}{S_{g,max}} \right] \quad 6.11$$

$$k_{rw}^{Dr} = (k_{rw}^{imb})_f \left(1 - \frac{S_g - S_g^I}{S_{g,max} - S_g^I} \right) + k_{rw}^{W2} \left(\frac{S_g - S_g^I}{S_{g,max} - S_g^I} \right) \quad 6.12$$

$$\frac{d(k_{rw}^{Dr})}{d(S_w)} = (1 - \beta) \frac{d(k_{rw}^{imb})_f}{d(S_w)} + \left(\frac{1}{S_{g,max} - S_g^I} \right) (k_{rw}^{imb})_f + \frac{d(k_{rw}^{W2})}{d(S_w)} \beta - \left(\frac{1}{S_{g,max} - S_g^I} \right) k_{rw}^{W2} \quad 6.13$$

where $\beta = \frac{S_g - S_g^I}{S_{g,max} - S_g^I}$

- 2- The second weakness of the k_{rw} model is the use of two-phase k_{rw} of the primary water flooding for predicting three-phase k_{rw} . As explained earlier, this approach is questionable and may lead to erroneous results. Moreover, the comparison between two-phase and three-phase k_{rw} made in Chapter 5 (section 5.2.3) indicate that, unlike the Larsen-Skauge model (Figure 6-19), the two-phase k_{rwo} is less than the k_{rw} once three mobile fluids exist.

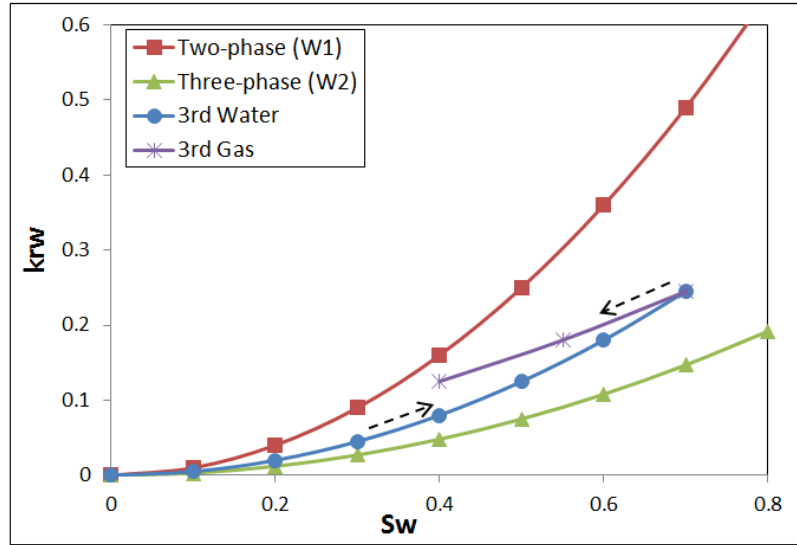


Figure 6-19: Schematic water relative permeability scanning curves of different cycles of WAG injection, calculated with the Larson-Skauge model.

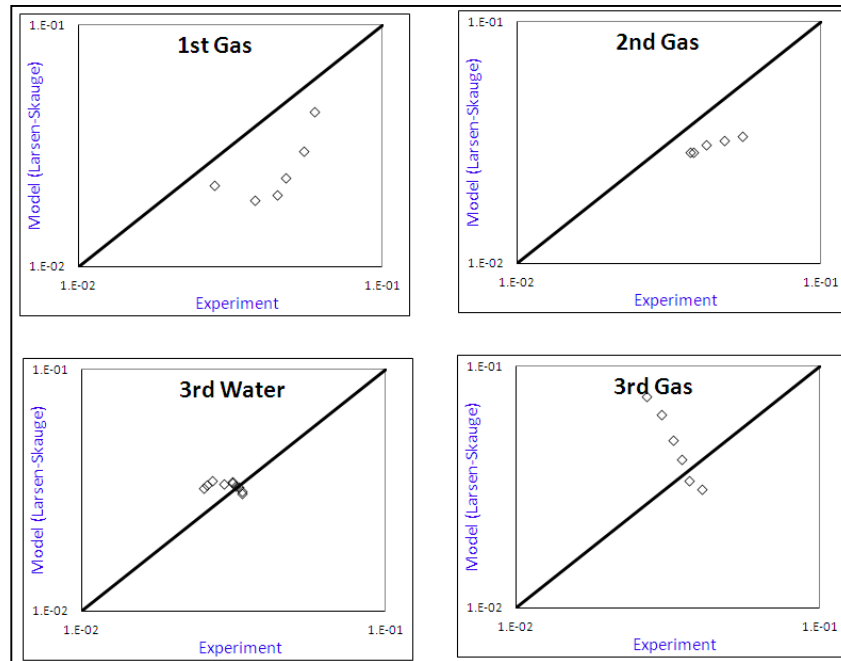


Figure 6-20: Water relative permeability of the various water and gas injections of 65mD-WW core obtained from experiment versus that calculated by Larsen-Skauge model.

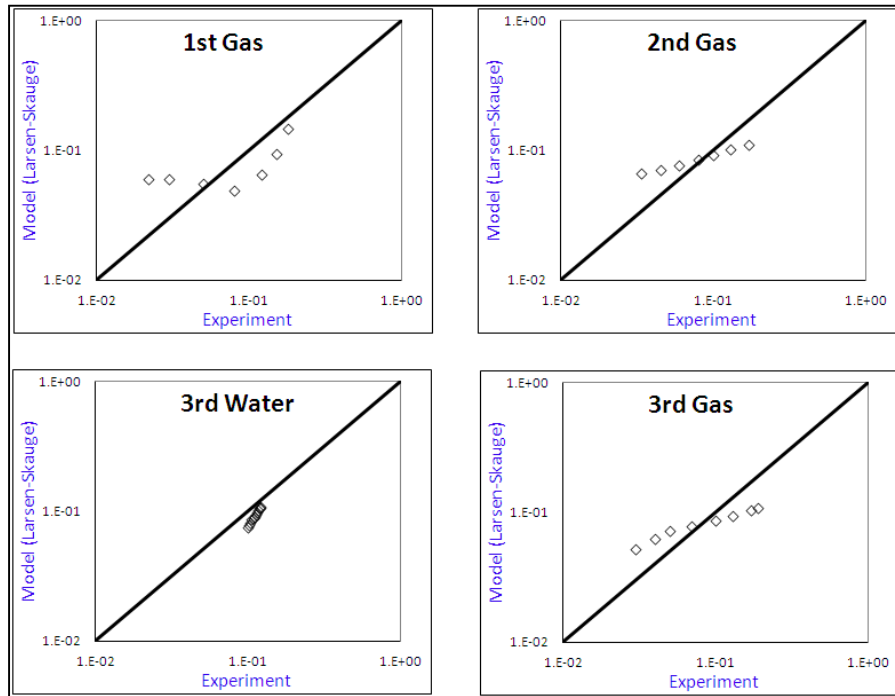


Figure 6-21: Water relative permeability of the various water and gas injections of 65mD-MW core obtained from experiment versus that calculated by Larsen-Skauge model.

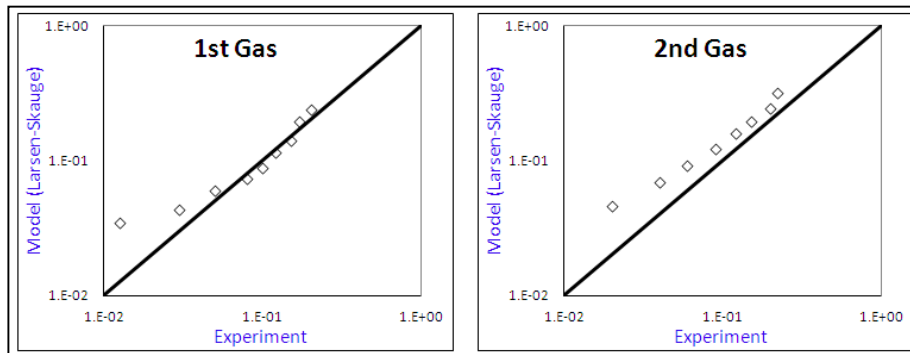


Figure 6-22: Water relative permeability of the 1st and 2nd gas injections of 1000mD-MW core obtained from experiment versus that calculated by Larsen-Skauge model.

Oil relative permeability

In the Larsen-Skauge technique, the Stone-I model (Stone, 1970) is employed for estimating oil relative permeability during the WAG process. As described in Chapter three, two-phase k_{row} and k_{rog} are used for interpolating three-phase oil relative permeability. Larsen-Skauge accounts for the residual oil saturation (computed from trapped gas saturation by Equation 5.1) as minimum oil saturation (S_{om}) in the Stone-I

model, in order to incorporate the hysteresis effect occurring in k_{ro} during the WAG process. The oil relative permeability of the experiment versus that predicted by the Stone-I model for 65mD-WW, 65mD-MW and 1000mD-MW cores are shown in Figure 6-23, Figure 6-24 and Figure 6-25, respectively. The real values of trapped oil saturation measured from different water injections (Table 5-1) were utilized as minimum oil saturation in the Stone-I model. The predicted values for 2nd and 3rd gas injections for the 65mD-WW core are relatively close to the corresponding observed data, whilst the results of 1st gas, 2nd water and 3rd water injections exhibit large discrepancy with the corresponding measured k_{ro} . The results of all the cycles of 65mD-MW core are substantially overestimated while the predicted values for 1000mD-MW core are significantly underestimated. Although the exact values of the trapped oil saturation measured from the experiment are employed in the Stone-I model, the calculated k_{ro} of the different water injections reveal large disagreement with the corresponding measured k_{ro} . This highlights the fact that, even using trapped oil saturation, the Stone-I model cannot adequately represent the oil relative permeability and cyclic hysteresis of our WAG experiments.

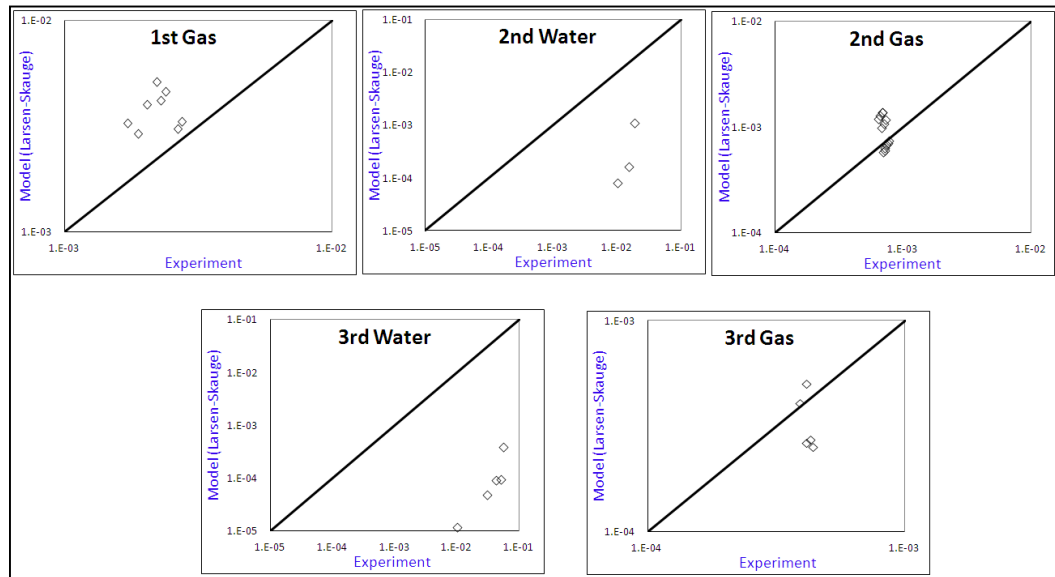


Figure 6-23: Oil relative permeability of the various water and gas injections of 65mD-WW core obtained from experiment versus that calculated by the Stone-I model, incorporating residual oil saturation.

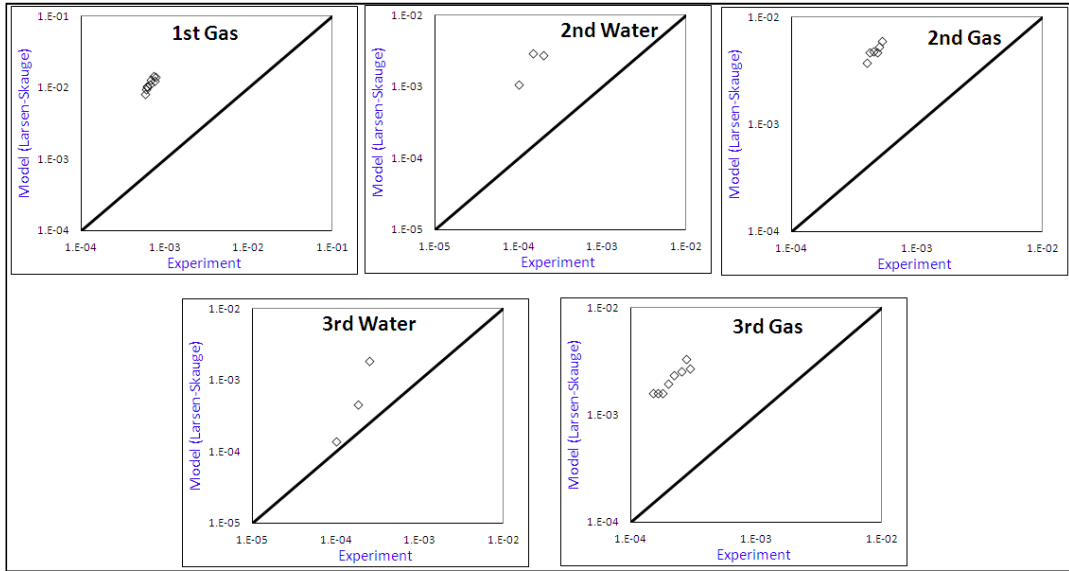


Figure 6-24: Oil relative permeability of the various water and gas injections of 65mD-MW core obtained from experiment versus that calculated by the Stone-I model, incorporating residual oil saturation.

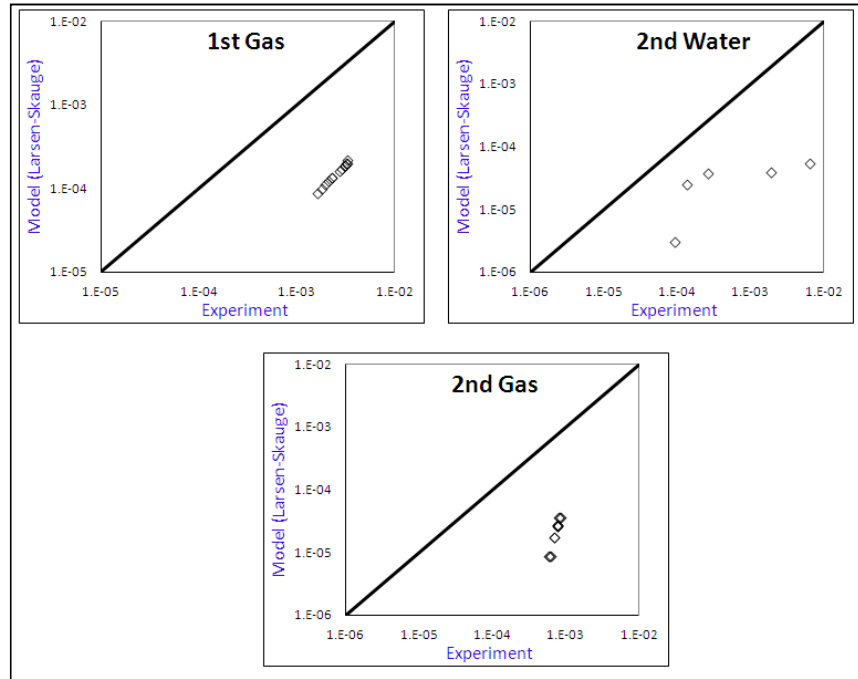


Figure 6-25: Oil relative permeability of the various water and gas injections of 1000mD-MW core obtained from experiment versus that calculated by the Stone-I model, incorporating residual oil saturation.

It should be noted that the proposed WAG hysteresis model in this study has been developed and verified based on the limited number of WAG experiments performed at

near-miscible condition and may not be adequately applicable for other systems (e.g. higher IFT, other WAG sequences). However, the general hysteresis approach (Equation 6.1) suggested in this thesis, which utilizes the measured three-phase k_r of the first WAG cycle for calculating k_r of the subsequent cycles, may be applicable for the other WAG processes performed under different circumstance. However, the hysteresis coefficient employed in this equation would need to be precisely developed for any system by conducting some WAG experiments at its own conditions.

6.4 Conclusions

The main conclusions drawn from this chapter are :

- 1- A new approach is proposed for modelling the three-phase relative permeability of the WAG process by incorporating the cyclic hysteresis effect. This technique is a direct method, which uses the measured three-phase k_r data obtained from the first cycle of WAG to predict the relative permeability of the subsequent cycles. Utilizing at least one set of measured three-phase k_r data in the WAG-HW model is one of the advantages of this methodology because employing measured three-phase data is more realistic and accurate compared to the interpolation technique used in the existing model, in which three-phase k_r is determined from two-phase data. The second advantage of this method is that there is no concern relating to the conventional hysteresis occurring between the drainage and imbibition processes because in the WAG-HW model the relative permeability of drainage is calculated independently of the imbibition process. This methodology was successfully verified against three sets of relative permeability data obtained from WAG experiments.
- 2- Assessment of the most popular WAG hysteresis model (Larsen and Skauge, 1998) revealed some serious shortcomings associated with the gas and water equation. In addition, employing the Stone-I model for calculating oil relative permeability led to erroneous results. Even incorporating the real values of residual oil saturation as the minimum oil in the Stone-I model cannot adequately captures the cyclic hysteresis of the k_{ro} occurring between various water injections.

6.5 References

- Baker, L.E., 1988, Three-Phase Relative Permeability Correlations, paper SPE 17369, presented at the SPE Enhanced Oil Recovery Symposium, Tulsa, Oklahoma.
- Blunt, M.J., 2000, An Empirical Model for Three-Phase Relative Permeability: SPE Journal, paper SPE 67950, (12).
- Cao, P., and S, S., 2010, Three-Phase Unsteady State Relative Permeability Measurement In Consolidated Cores Using Three Immiscible Liquids, presented at the International Symposium of the Society of Core Analysis, Halifax, Canada.
- Carlson, F.M., 1981, Simulation of Relative Permeability Hysteresis to the Nonwetting Phase, paper SPE 10157, presented at the SPE Annual Technical Conference and Exhibition, San Antonio, Texas.
- DiCarlo, D.A., Sahni, A., and Blunt, M.J., 2000, Three-Phase Relative Permeability of Water-Wet, Oil-Wet, and Mixed-Wet Sandpacks: SPE Journal, paper SPE 60767, (03).
- Fenwick, D.H., and Blunt, M.J., 1998, Network Modeling of Three-Phase Flow in Porous Media: SPE Journal, paper SPE 38881, (03).
- Hustad, O.S., and Browning, D.J., 2010, A Fully Coupled Three-Phase Model for Capillary Pressure and Relative Permeability for Implicit Compositional Reservoir Simulation: SPE Journal, paper SPE 125429-PA, (12).
- Hustad, O.S., and Hansen, A.G., 1995, A Consistent Correlation For Three-Phase Relative Permeabilities and Phase Pressure Based on Three Sets of Two Phase Data, presented at the 8th European IOR symposium, Vienna, Austria.
- Killough, J.E., 1976, Reservoir Simulation With History-Dependent Saturation Functions, paper SPE 5106, (02).
- Larsen, J.A., and Skauge, A., 1998, Methodology for Numerical Simulation With Cycle-Dependent Relative Permeabilities: SPE Journal, paper SPE 38456, (06).
- Oak, M.J., 1990, Three-Phase Relative Permeability of Water-Wet Berea, paper SPE 20183, presented at the SPE/DOE Enhanced Oil Recovery Symposium, Tulsa, Oklahoma.
- Petersen, E.B., Lohne, A., Vatne, K.O., Helland, J.O., G.Virnovsky, and P.Eric Øren 2008, RELATIVE PERMEABILITIES FOR TWO- AND THREE PHASE FLOW PROCESSES RELEVANT TO THE DEPRESSURIZATION OF THE STATFJORD FIELD, presented at the International Symposium of the Society of Core Analysts, Abu Dhabi, UAE.
- Stone, H.L., 1970, Probability Model for Estimating Three-Phase Relative Permeability: SPE Journal of Petroleum Technology, paper SPE 2116, (02).

Chapter 7

Conclusions and Recommendations

Three-phase flow occurs during many important processes in oil reservoirs, including tertiary gas and water-alternating-gas (WAG) injection. Accurate estimation of three-phase relative permeability (k_r) is required to describe and predict the behaviour in these multi-phase flow conditions. Furthermore, irreversible hysteresis phenomena occurring due to the reversal of the flow direction makes the modelling of the process of WAG injection a particularly challenging task. The current standard methods for determining three-phase relative permeability as input data for the reservoir simulators are; i) estimating three-phase relative permeability using two-phase relative permeability data using correlations (e.g. Stone, Baker, etc), ii) direct measurement of the relative permeabilities by conducting coreflood experiments under reservoir conditions. In this study, both methodologies have been pursued to better characterize the three-phase k_r and the hysteresis effects in the WAG process, performed under different wettability conditions using near miscible oil/gas systems.

This chapter presents the main conclusions drawn from this work followed by some recommendations for future studies.

7.1 Conclusions

A summary of the work and the main conclusions derived from each chapter are as follows:

Chapter 3: Evaluation of the three-phase relative permeability models

The various WAG experiments performed on cores were simulated by the black oil simulator (Eclipse100), employing a variety of existing three-phase relative permeability and hysteresis models. This exercise was aimed at evaluating the capability of the most widely used three-phase models in predicting the WAG performance under different wettability conditions. For this purpose, the two-phase relative permeability data measured from displacement tests were utilized with the existing three-phase models to estimate the values of three-phase relative permeabilities in the WAG tests. The estimated values of three-phase relative permeability were then used for the numerical simulation of the WAG experiments. The accuracy of each of the models was assessed by comparing the production and pressure data resulting from the WAG simulations with the corresponding data measured in the experiments.

- 1- One imperative issue which should be noted here is that all the three-phase models examined in this study were originally been developed and verified based on the three-phase data of the fully immiscible (high interfacial tension) system, which behaves thoroughly different from near-miscible flow. In other words the existing empirical models may not be accurately applicable for the low interfacial hydrocarbon flow. Reservoir engineers are thus advised to be careful about choosing appropriate correlations for simulation of reservoirs with three-phase systems undergoing near-miscible flow.
- 2- The results show that choosing an inappropriate three-phase k_r model in simulation of the WAG experiments can lead to large errors in prediction of fluid production and pressure. The predictions made by the existing models are very variable i.e., various models can predict vastly different 3-phase k_r values from the same set of 2-phase data. While some models perform better than others, all of the 3-phase k_r models examined in this study fail to predict the continued production of oil after the breakthrough of the gas which is one of the

features of gas and WAG injection experiments at low gas-oil IFT (interfacial tension).

- 3- The methodology of using two-phase relative permeability to estimate three-phase relative permeability which is the basic technique of all the existing three-phase models may be questionable because the WAG performance obtained by all the models depicted substantial errors when compared with the observed data using rocks of different wettability and permeability.
- 4- The WAG simulation of all core experiments revealed that the error value of the oil production is much larger than that of water and gas production. This highlights the strong impact of the three-phase relative permeability on flow of oil.
- 5- Comparison between simulation results of the experiments on the water-wet and mixed-wet core revealed that the wettability has a significant effect on three-phase flow and WAG performance. In other words, each three-phase relative permeability model may give totally different predictions for water-wet and mixed-wet cores. This highlights the impact of wettability on relative permeability during WAG injection and the importance of performing these experiments under wettability conditions representative of those of the reservoir rock.

Chapter 4: Determination of three-phase relative permeability from unsteady-state coreflood experiment

In Chapter 4, a new history matching technique was proposed, based on a Genetic Algorithm, to estimate three-phase k_r (relative permeability) from unsteady-state coreflood experiments. In this method, relative permeabilities (k_r) are represented by quadratic B-Spline functions. Adjustable coefficients in k_r functions are changed in an iterative process to minimize an objective function. The objective function is defined as the difference between the measures and simulated values of the pressure drop across the core and fluid recovery during the experiment. One important aspect of this algorithm is that it considers inequality constraints to ensure that physically acceptable k_r curves are maintained throughout the iterative optimization process.

A three-phase coreflood optimizer has been developed, based on this methodology, that generates best k_r values by matching experimental data. The integrity of the developed software was first successfully verified by using two sets of experimental three-phase k_r data published in the literature. To the best of our knowledge, there is no commercial software available at the present able to calculate the three-phase k_r values from unsteady state displacement tests.

1. A powerful tool has been developed to accurately estimate three-phase k_r from experimentally measured production and pressure drop of unsteady-state coreflood displacement tests. An appropriate and flexible function was chosen for three-phase relative permeability, to generate maximum set of relative permeability curves in an optimization process to obtain results corresponding to the minimum error values.
2. To overcome the limitations of most of the existing three-phase k_r models, regarding the dependency of k_{rw} and k_{rg} on only their own saturation [$k_{rw} = k_{rw}(S_w)$, $k_{rg} = k_{rg}(S_g)$], the author concentrated our efforts on three-phase k_{rw} , k_{rg} and k_{ro} as a function of two saturations [$k_{rw} = k_{rw}(S_o, S_g)$, $k_{rg} = k_{rg}(S_o, S_w)$, $k_{ro} = k_{ro}(S_g, S_w)$].
3. By applying this approach, we can overcome some of the restrictions present in the explicit methods (such as the JBN) which neglect capillary forces.
4. The integrity of the presented history matching approach was successfully verified by employing synthetic data built by the Eclipse reservoir simulator. The method was also successfully used to generate three-phase k_r curves by history matching three-phase coreflood experiments carried out in the laboratory.

Chapter 5: Characterization of Three-Phase k_r and Hysteresis effect in WAG Process

The in-house software developed in this work was used to determine three-phase relative permeability for a large number of three-phase coreflood experiments performed by alternating injection of water and gas. This section was aimed to investigate the impact of cycle-dependent hysteresis associated with three-phase relative permeability in the WAG process. The results were qualitatively compared against the prediction of the commonly used WAG hysteresis model (Larsen and Skauge, 1998) in

order to identify the limitations associated with this model. Moreover, the three-phase relative permeability of the water-wet rock is compared with the results of mixed-wet rock tests to highlight the impact of wettability on the mobility of the different fluids. The results of two-phase tests are also compared against three-phase relative permeability to discover the degree of closeness of the two-phase flow to the three-phase flow. In addition, because the non-wetting phase trapped saturation plays a significant role in the hysteresis effect, the most commonly used trapping model in the literature (Land, 1968) was assessed against the values measured from the WAG experiments.

Hysteresis effect:

1. Three-phase gas relative permeability is reduced in consecutive gas injection cycles and accordingly the gas injectivity drops significantly with successive gas injections during the WAG process, under different rock conditions. The gas relative permeability of the 2nd and 3rd water injections exhibits only a slight hysteresis effect, which is less than the substantial hysteresis effect observed during the gas injection cycles. The trend of hysteresis in k_{rg} partly contradicts the existing hysteresis model available in the literature.
2. The results of the mixed-wet system demonstrate negligible cyclic hysteresis in water relative permeability during gas injections, whereas k_{rw} of the water-wet rock is reduced by the successive gas injection that follows water injection.
3. The k_{rw} of the water-wet core does not exhibit any considerable hysteresis effect during different water injections, whereas the mixed-wet core shows slight hysteresis, in which k_{rw} of the 3rd water injection is greater than that of the 2nd. This may indicate a slight increase of the water injectivity by the subsequent water injection in the WAG process under mixed-wet conditions.
4. Insignificant hysteresis is observed in the oil relative permeability during different gas injection cycles, for both water-wet and mixed-wet rocks. However, a considerable cyclic hysteresis effect in k_{ro} is observed during various water injections, which is attributed to the reduction of the residual oil saturation during successive water injections. k_{ro} of the water-wet core exhibits a much more cyclic hysteresis effect than that of the mixed wet core. Furthermore, no

model has currently been developed to capture the cyclic hysteresis effect in oil relative permeability for the WAG process.

Effect of wettability:

1. The discrepancy between k_{rg} of the water-wet and mixed-wet systems is relatively negligible because the gas phase at both wettability conditions acts as non-wetting phase in the presence of oil and water in porous media.
2. Some differences are observed between k_{rw} of the water-wet and mixed-wet systems, which underlines the important role of wettability in influencing the flow of water in presence of oil and gas. Water relative permeability of the mixed-wet core has a larger value, compared to that of the water-wet rock.
3. Unlike water relative permeability, oil relative permeability of the water-wet core is much larger than that of the mixed-wet core.

Two-phase k_r versus three-phase k_r

1. Two-phase gas relative permeability (k_{rgo}) in oil-gas systems is much higher than three-phase k_{rg} . In other words, the presence of the mobile water adversely influences three-phase k_{rg} .
2. Comparison between two-phase and three-phase k_{rw} demonstrates that the two-phase k_{rwo} is significantly less than the three-phase k_{rw} . This indicates that the presence of gas positively affects the mobility of water. Furthermore this finding contradicts the general assumption in the industry that three-phase k_{rw} is less than two-phase k_{rw} .
3. Three-phase k_{rw} and k_{rg} obtained under different rock wettability conditions reveal that both relative permeabilities are a function of two fluid saturations (rather than their own saturation): thus the simplistic assumption made in some of the existing models, e.g. Stone (1970), that the three-phase k_{rw} and k_{rg} are similar to the two-phase k_{rwo} and k_{rgo} is not justified.
4. Investigation of oil relative permeability under different rock wettability conditions confirmed that the value of the three-phase k_{ro} is significantly less than the two-phase k_{row} at the same value of oil saturation.

Trap saturation

1. The amount of trapped oil and gas obtained from the WAG experiments are poorly predicted by the Land model.
2. The linear relationship between trapped gas and residual oil saturation proposed by Larsen-Skauge (1998) predicts reasonably well the trapped saturations obtained from our WAG experiments.

Chapter 6: New Methodology for Modelling of Hysteresis in WAG processes

Based on the comprehensive set of relative permeability data derived from the WAG experiments and the shortcomings observed in the existing models, a new approach was proposed for modelling of three-phase relative permeability, incorporating the cyclic hysteresis effect. The integrity of the model was confirmed by the k_r values obtained from our WAG experiments. Moreover, the k_r data set produced in this study was used to assess the performance of the most used WAG hysteresis model in the literature (Larsen and Skauge, 1998) against our new approach.

- 1- A new approach is proposed for modelling the three-phase relative permeability of the WAG process by incorporating the cyclic hysteresis effect. This technique is a direct method, which uses the measured three-phase k_r data obtained from the first cycle of WAG to predict the relative permeability of the subsequent cycles. Utilizing at least one set of measured three-phase k_r data in the WAG-HW model is one of the advantages of this methodology because employing measured three-phase data is more realistic and accurate compared to the interpolation technique used in the existing model, in which three-phase k_r is determined from two-phase data. The second advantage of this method is that there is no concern relating to the conventional hysteresis occurring between the drainage and imbibition processes because in the WAG-HW model the relative permeability of drainage is calculated independently of the imbibition process. This methodology was successfully verified against three sets of relative permeability data obtained from WAG experiments.
- 2- Assessment of the most popular WAG hysteresis model (Larsen and Skauge, 1998) revealed some serious shortcomings associated with the gas and water equation. In addition, employing the Stone-I model for calculating oil relative

permeability led to erroneous results. Even incorporating the real values of residual oil saturation as the minimum oil in the Stone-I model cannot adequately capture the cyclic hysteresis of the k_{ro} occurring between various water injections.

7.2 Recommendations

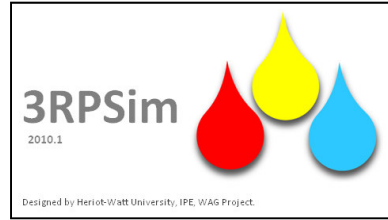
- 1- The trapped saturation of the non-wetting phase obtained by the advancing of the wetting phase (imbibition process) in displacing the non-wetting phase is a key parameter in the hysteresis effect, specifying the end point of the relative permeability curves. In this study, we noticed that the most widely used trap model (Land, 1968) is unable to predict precisely the trapped hydrocarbon saturation reached by different cycles of the WAG injection. More extensive studies are required to be directed towards measurement and modelling of the trapped oil and gas saturation at the condition where three mobile fluids are present in the porous media. The wettability of the rock effectively controls the trapping mechanisms, which consequently manipulate the trapped hydrocarbon saturation during the imbibition process. Therefore, the impact of wettability should be taken into account in modelling of trapped oil or gas saturation.
- 2- In this research, the relative permeability data of the low IFT oil/gas system was employed for modelling and simulation purpose. However, it is recommended to characterize the relative permeability and pertinent cyclic hysteresis in the WAG process by performing coreflood experiments under higher IFT of an oil/gas system. In addition, the new hysteresis model (WAG-HW) needs to be tested against the k_r data of the higher IFT system.
- 3- As the WAG injection proceeds in the oil reservoirs, an oil bank may form, which displaces the water and gas ahead. Hence, the relative permeability of the oil injection necessitates the numerical simulation of those grid blocks in which oil saturation is increasing. It is recommended to perform some oil injection tests into the core initially saturated with mobile oil, water and gas in order to obtain k_r values at increasing oil saturation stages in the process.
- 4- Capillary pressure is one of the most prevailing parameter affecting fluid distribution and recovery in oil reservoirs. Measurement of two-phase capillary

pressure using a displacement test e.g. centrifuging, is frequently carried out in the oil industry whilst measurement of the capillary pressure at three-phase flow conditions is a much more challenging task due to the infinite number of saturation paths existing in a three-phase system. Extensive experimental and theoretical work should be conducted to gain a better understanding of capillary pressure and hysteresis effects in a three-phase system.

7.3 References

- Land, C.S., 1968, Calculation of Imbibition Relative Permeability for Two- and Three-Phase Flow From Rock Properties, paper SPE 1942, (06).
- Larsen, J.A., and Skauge, A., 1998, Methodology for Numerical Simulation With Cycle-Dependent Relative Permeabilities: SPE Journal, paper SPE 38456, (06).

Appendix A



Application of 3RPSim

Here, we explain the main features and applications of the coreflood optimized (3RPSim) described in chapter 4 for modelling of three-phase relative-permeability either by utilizing coreflood data or using existing kr models available in literature.

The main page of 3RPSim comes up when you start the program, Figure A-1. This window has three sections; Menu bar, Toolbar and Project Explorer. The Menu bar consists of seven menus:

- 1- **File** (Initiating a new project, Saving the current project and Opening an existing project),
- 2- **View** (viewing Error messages, Estimation plot, Estimation status),
- 3- **Properties** (importing core and fluid properties, defining injection and production wells, experimental results, two phase kr and Pc),
- 4- **Run** (starting or stopping simulation),
- 5- **Results** (plotting and exporting simulation results),
- 6- **Tools** (defining constraints for kr and Pc, option, existing three phase kr models).
- 7- **Helps** (User guide)

Three major steps for determining kr curves by using this program are; inputting data, running simulation and viewing results as demonstrated below:

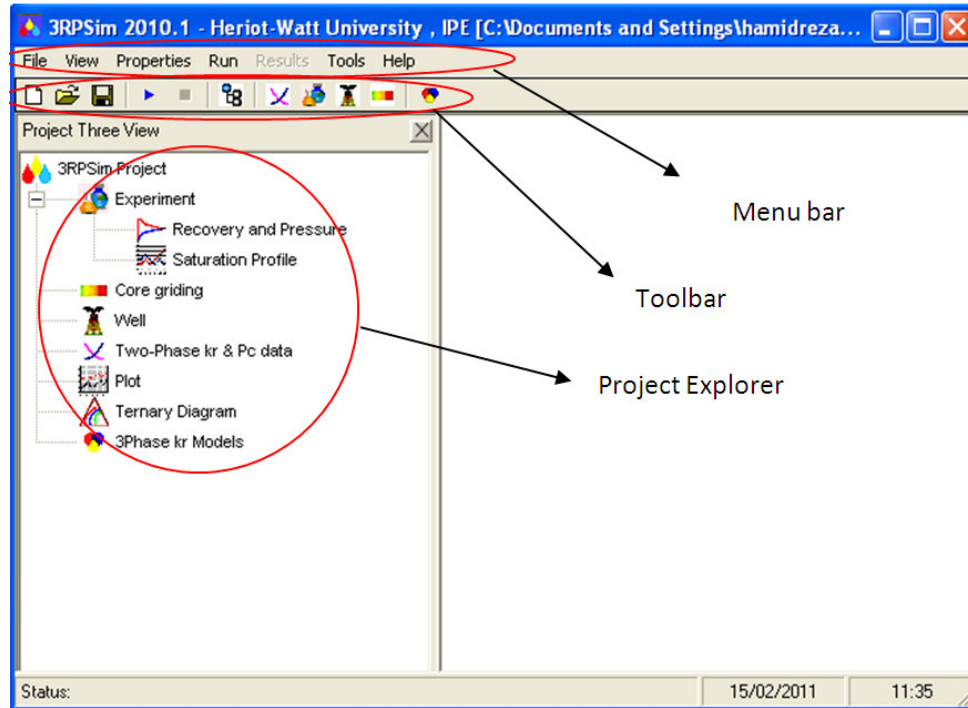


Figure A-1: Main page

A.1 Input data:

The required data for implementing coreflood simulation can be imported into 3RPSim in two ways. The first step is to create a new project by clicking on New Project located in File menu and then going step by step to import needed data and the second step is to open an existing data file, which has already been created by 3RPSim. The input data file in this computer program is saved on the Microsoft Excel format with “xls” suffix.

Figure A-2 shows the first step in creating new data file representing general description of the project like name of the project, company, well name, type of core and date, etc. The input data in this section is for introducing the project and won't be used in simulation calculation.

The second step in a new project is importing core and fluid properties including length, diameter, irreducible water saturation, initial water and gas saturation values, porosity, permeability, number of grid blocks and fluid viscosities. Unit of every piece of data can be selected from a variety of common units used in industry. By pressing “Next” button user will be taken to the third step in order to import experimental data including

oil, water and gas production and pressure drop across the core in terms of injection time obtained from unsteady state coreflood test (Figure A-4). Number of experimental data points and initial pressure of coreflood test are also specified. Moreover the unit of recovery and pressure data should be defined at the conditions in which the experiment has been carried out. The next stage in creating new project is to define inlet and outlet conditions of the core while performing flooding test (Figure A-5). In this window the values of constant injection rate and constant outlet production or constant outlet pressure are specified for the duration of the test period. At this stage the number of injection scenarios, and for each scenario the injection period and injection rate of every fluid are supplied. If at the core outlet, the production is maintained constant (variable pressure), then the pressure vs. time data are input, otherwise if the pressure is maintained constant (variable production) then the production rate vs. time is given. In the case that coreflood test has been performed under constant production rate and with the fact that all fluids are supposed to be incompressible hence production flow rate being as same as injection rate. Consequently number of production scenario must be equal to 1 and the pressure table must be left empty.

Eventually, data file containing all, but kr and P_c , data will be created for simulation, by pressing the “Finish” button.

3RPSim new project wizard

Step 1: General description
This is a brief description of 3RPSim project

Name of project :

Company:

Date: ...

Core ID :

Depth :

Field :

Formation :

Well :

Note :

< Back Next > Cancel

Figure A-2: First step of input data, general information

3RPSim new project wizard

Step 2: Core and fluid properties
This page defines core and fluid properties

Core

Length : cm

Diameter : cm

Irreducible Water Saturation (Swc): frac

Initial Water Saturation: frac

Initial Gas Saturation: frac

Porosity: frac

Permeability : mD

Number of grid:

Fluid

Oil viscosity : cP

Water viscosity : cP

Gas viscosity : cP

< Back Next > Cancel

Figure A-3: Second step of input data, core and fluid properties

3RPSim new project wizard

Step 3: Experimental Data

This page specifies experimental data including recovery and pressure drop across the core.

Number of Data : Initial Pressure : atm

Time : sec Recovery : Pore Volume

	A	B	C	D	E
1	Time	Oil Rec	Water Rec	Gas Rec	Pressure Drop
2					
3					
4					
5					
6					
7					
8					
9					
10					
11					
12					
13					
14					
15					
16					
17					
18					

< Back Next > Cancel

Figure A-4: Third step of input, experimental data

3RPSim new project wizard

Step 4: Injection - Production Constraints

This page defines injection and production constraints.

Number of Injection Scenario : Number of Production Scenario : Production Well : Constant Rate

Unit Selection

Time : sec Rate : cc/sec Pressure : atm

	A	B	C	D
1	Time	Oil Rate	Water Rate	Gas Rate
2				
3				
4				
5				
6				
7				
8				
9				
10				
11				
12				
13				
14				
15				

	A	B
1	Time	Pressure
2		
3		
4		
5		
6		
7		
8		
9		
10		
11		
12		
13		
14		
15		

< Back Finish Cancel

Figure A-5: Fourth step of input, injection and production constraints

Determination of unknown three phase or two phase flow functions, i.e. k_r , and P_c representing a particular coreflood experiment, is the main task implemented by 3RPSim. These unknown functions must be constrained within a certain criteria to produce accurate and physically sound estimation. These constrains can be imposed via “Estimation Parameter” located in “Tools” menu shown in Figure A-6. First of all the user should identify the number and kind of involved phases in the coreflood experiment and secondly type of relative permeability function of involved phased must be specified. Relative permeability of every phase can be either function of single saturation (own fluid saturation) or two other fluid saturations i.e. $k_{ri} = k_{ri}(S_i)$, or $k_{ri} = k_{ri}(S_j, S_k)$, depending on the fluid flow physics that has occurred in the core. Obviously, for a two-phase-flow experiment relative permeability is only a function of its own phase saturation whilst for a three-phase-flow both options can be applied. The end point saturation of k_r curve of a given phase can either be fixed or left to be flexible.

Three options have been considered for incorporating capillary pressure function in fluid flow simulation. First one is to ignore capillary pressure, the second one is to use measured two phase P_c curve (for two-phase experiments) and the third one is to estimate P_c curves as well as relative permeability in an iterative process (for two or three-phase experiments). For instance while using low IFT oil/gas fluid in coreflood experiment the capillary pressure between oil and gas is negligible and can be ignored. Third option is more appropriate for those experiments in which there are no measurements for P_c and in addition fluid flow is capillary dominant (high IFT).

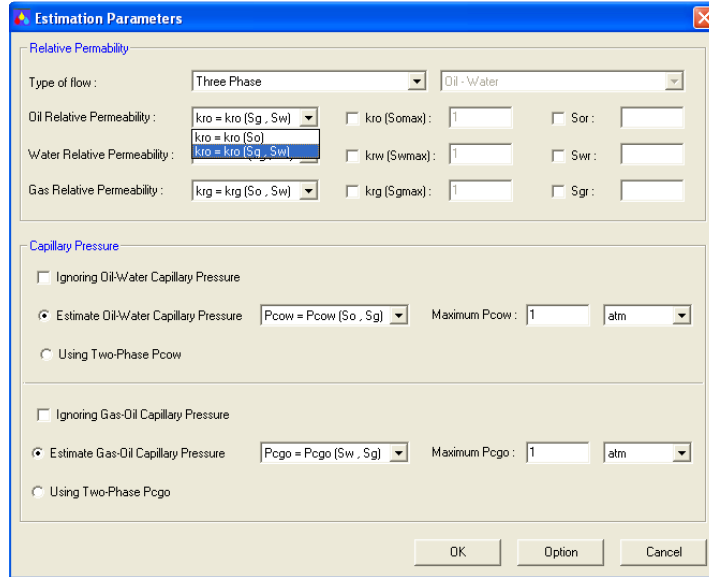


Figure A-6: Defining constraints for unknown kr and P_c

Some other parameters affecting simulation results, which are given automatically by the software can be viewed and altered by going to “Option” located in the “Tools” menu (Figure A-7). These parameters are numerical control for simulation: minimum time step, limit for the material balance error, number of iterations, minimum and maximum attainable phase saturation and objective function weight-factor for history matching.

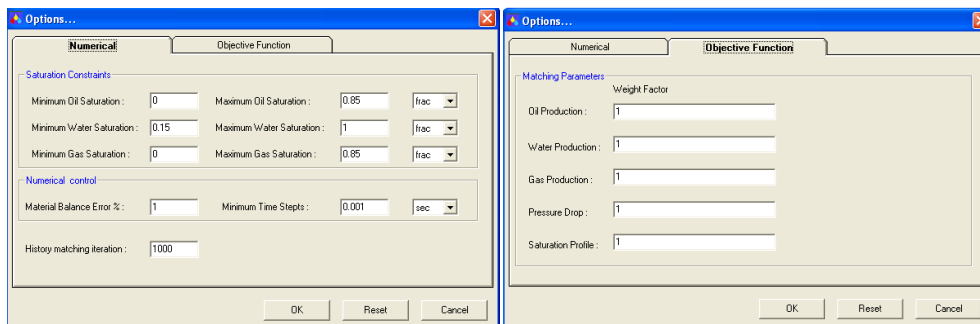


Figure A-7: Option

“Heterogeneous Core” item in “Properties” menu can be used in order to consider variation of core properties e.g. porosity, permeability along the core. Such data can be obtained from x-ray scanning.

Saturation profile along the core measured during coreflood experiment by means of x-ray can be utilized as observed data as well as recovery and pressure data in order to assist estimation process and to determine more precise k_r values.

A.2 Running simulation:

Estimation of k_r and P_c can be commenced by pressing “F5” key or “Start Estimation” located in the “Run” menu. Progress of the estimation process including current iteration number and minimum misfit value between experiment and simulation obtained so far, can be observed in “Estimation Status” in the “View” menu (Figure A-8). Meanwhile user can observe best simulation results match with experiment data including production profile, pressure drop and saturation path via “Estimation plot” in the “View” menu (Figure A-9). Moreover user would be able to stop estimation process at any iteration.

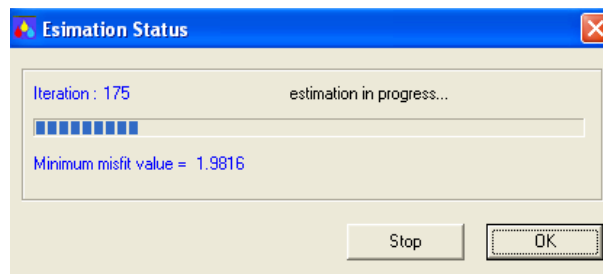


Figure A-8: Estimation status

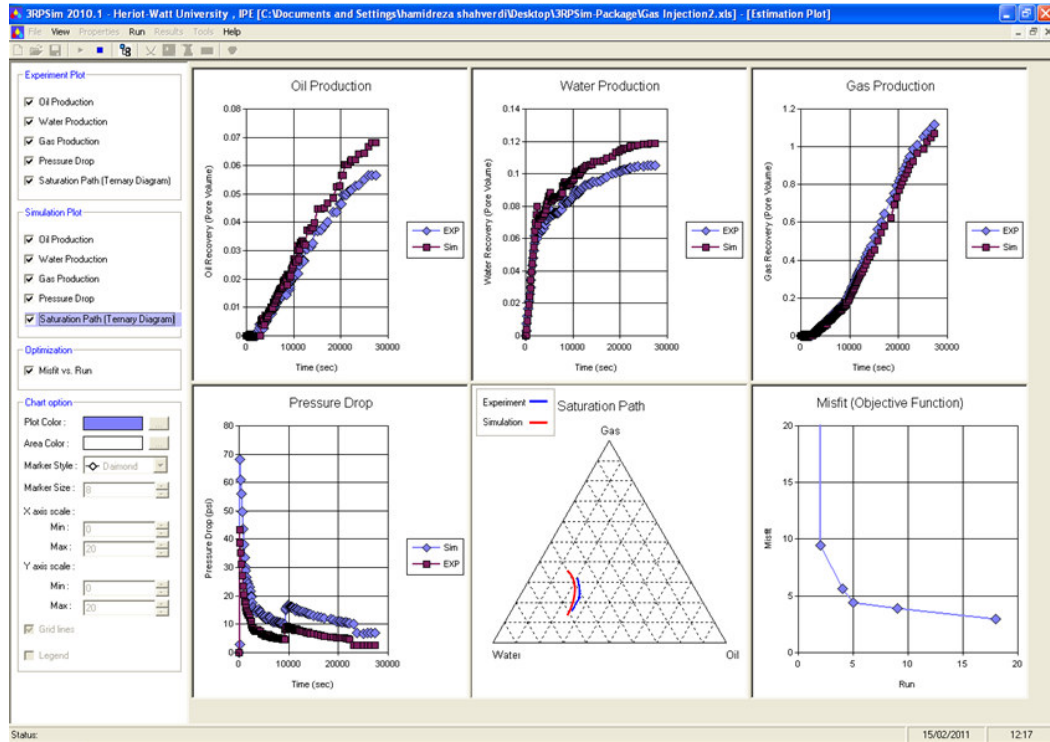


Figure A-9: Estimation plot

A.3 Results:

Having completed the estimation process, all simulation results including relative permeability, capillary pressure, oil production, water production, gas production, pressure drop and saturation profile along the core for different timesteps and the misfit (error) values (of the objective function) with corresponding estimated values of the coefficients are available in “Results” menu. Estimated k_r and P_c values can be viewed either in XY plot or isoperm curve in ternary diagram shown in Figure A-11 and Figure A-12, respectively. Also the calculated fluid recovery and pressure data compared with experimental data can be seen in XY graphs. The produced three phase k_r and P_c values can be exported into a Microsoft Excel file in form of a 2D-table as demonstrated in Figure A-10.

3phase kro		Sw										
		0.08	0.1	0.2	0.3	0.4	0.5	0.6	0.7	0.8	0.9	1
Sg	0	0.093969	0.087001	0.056222	0.032206	0.014855	0.004467	0.000743	0.00044	0.000215	6.86102E-05	0
	0.1	0.066583	0.061658	0.039896	0.02291	0.010698	0.003261	0.000598	0.000355	0.000174	0	
	0.2	0.044006	0.040763	0.026429	0.015233	0.007174	0.002253	0.000469	0.000278	0		
	0.3	0.028238	0.024316	0.015819	0.009175	0.004383	0.001442	0.000354	0			
	0.4	0.013278	0.012318	0.008088	0.004737	0.002324	0.00083	0				
	0.5	0.005128	0.004769	0.003175	0.001818	0.000988	0					
	0.6	0.001786	0.001688	0.001139	0.000719	0						
	0.7	0.000968	0.000903	0.000612	0							
	0.8	0.000389	0.000362	0								
	0.9	4.97E-05	0									
	0.92	0										

Figure A-10: 2D-table of three phase kr as function of two saturations. The shaded area represents experiment saturation path in which estimated kr is reliable

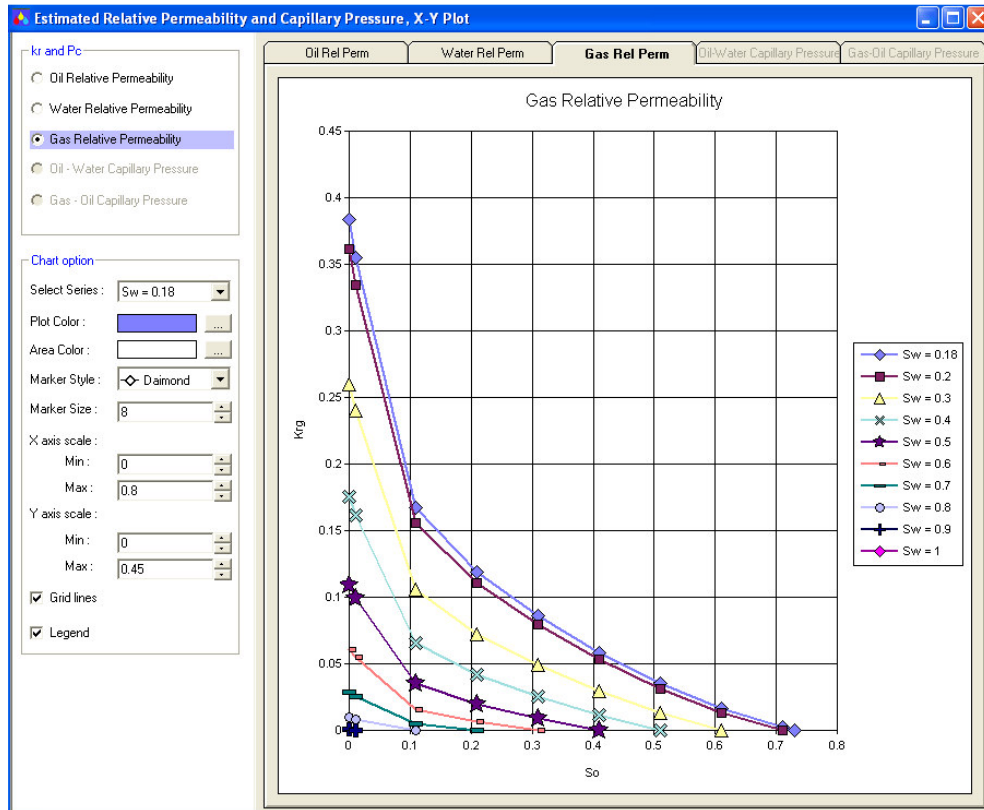


Figure A-11: XY plot of estimated kr and Pc

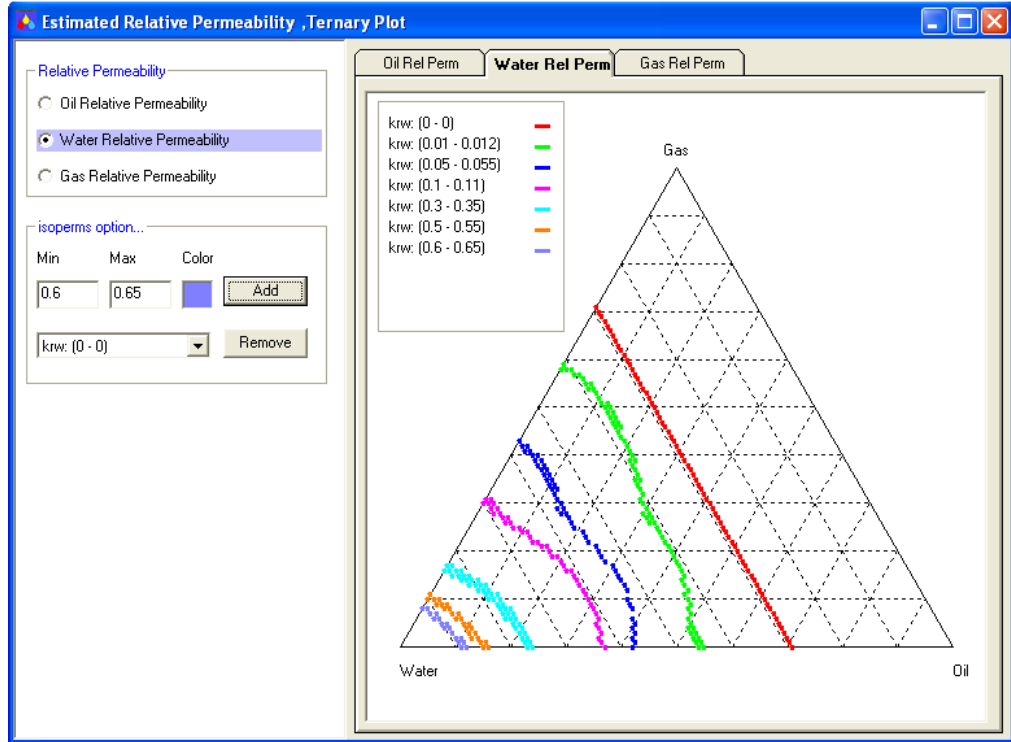


Figure A-12: An example of a ternary diagram illustrating three phase kr.

A.4 Three phase kr models:

In case there is no WAG injection type of experimental results available, from which to estimate three-phase relative permeabilities for input to a simulator, one could use an existing correlation, which can calculate three-phase kr from the two-phase data.

Although there is a relatively large number of 3-phase kr correlations and models available in the literature, only a few of them have been included in the existing commercial reservoir simulators. In commercial simulator it is not enough to specify the parameters of a given model and run the simulator in three phase without a prior simulation run to define such parameters. In other words the incorporated 3-phase models cannot be used without having to run a simulation. There is, therefore, a need for a standalone tool (Software) that practicing reservoir engineers can use to generate 3-phase kr using a comprehensive set of 3-phase kr models. In case there is no three-phase relative-permeability model verified by experimental data, the Software allows us

to make a more informed decision on the choice of one of the existing 3-phase k_r values that will then be used as input to the reservoir simulator.

A separate module was developed in 3RPSim in order to directly calculate 3-phase k_r curves using two phase k_r from a large number of published 3-phase k_r models, independently of any reservoir simulator. It also enables users to construct 2D tables of 3-phase k_r values, which can then be input to reservoir simulators (for models that are not available in the simulator). This module also includes 3-phase models, which are currently available in existing reservoir simulators. This program is accessible through “Three-Phase k_r Models” located in “Tools” menu (Figure A-13).

For generating three phase k_r by existing models there is no need of any basic coreflood data and the two-phase relative-permeability data can be directly utilised through “Properties” menu and some other essential parameters needed by the corresponding model e.g. S_{wc} , and S_{om} . The models, which have so far been included in this software, are: Stone I, Stone Exponent, Stone II, Saturation-Weighted Interpolation, IKU, Corey, Naar-Wygal and Hirasaki, Blunt and Fayers.

The results (3-phase k_r) can be shown in the form of k_r versus water and gas saturations, in a 2D Table, Figure A-10. The results can also be displayed as XY plots or in ternary diagrams as demonstrated in Figure A-11 and 13, respectively.

Existing Three-Phase kr Models

Selecting kr Model : Saturation-Weighted Interpolation (1988)

Model Parameters

krovw : Swc : Som :
Sorg : Sgro : Sorw :
SLr : Lambada : Exponent :

Blunt option

Layer Drainage krog* : krgo* : So* :
 Hysteresis Parameter Cg : Ch : Co :

Saturation Trajectory : Oil Saturation Water Saturation Gas Saturation

Initial Saturation:

Type of two phase data

(Oil - Water) Rel Perm :
(Oil - Gas) Rel Perm :
(Gas - Water) Rel Perm :

Run Model Export 2D-Table Ternary Plot X-Y Plot Cancel

Figure A-13: Three phase kr models